Photonic crystal antireflection coatings, surface modes, and impedances

Felix J. Lawrence

THE UNIVERSITY OF
SYDNEY

CUDOS and Institute of Photonics and Optical Science,
School of Physics,
The University of Sydney,
Australia.

2012

Abstract

We present a rigorous definition of a wave impedance for 2D rectangular and triangular lattice photonic crystals (PCs), in the form of a matrix. Reflection and transmission at an interface between PCs can be represented by matrices that relate the Bloch mode (eigenmode) amplitudes in the two PCs; we show that these matrices, which are multi-mode generalisations of reflection and transmission coefficients, may be calculated from the PCs' impedances that we define.

Given the impedances and Bloch factors (propagation constants) of a collection of PCs, the reflection and transmission properties of arbitrary stacks of these PCs may be calculated efficiently using a few matrix operations. Therefore our definition enables PC-based antireflection coatings to be designed efficiently: some computationally expensive simulations are required in an initial step to find a range of PCs' impedances, but then the reflectances of every coating that consists of a stack of these PCs can be calculated without any further simulations.

We first define the PC impedance from the transfer matrix of a single PC layer (i.e., a grating). Since transfer matrix methods are not especially widespread, we also present a method and associated source code to extract a PC's propagating and evanescent Bloch modes from a scattering calculation that can be performed by any off-the-shelf field solver, and to calculate impedances from the extracted modal fields.

Finally, we put our method to use. We apply it to design antireflection coatings, nearly eliminating reflection at a single frequency for one or both polarisations, or lowering it across a larger bandwidth. We use it to find surface modes at interfaces between PCs and air, and their projected band structures. We use the impedance to define effective parameters for PC homogenisation, and we briefly describe how our definition has been used to dispersion engineer a PC waveguide.

Statement of originality

Most of the work described in this thesis is my own, and has not been submitted as part of any other degree. The contributions of others are explicitly acknowledged either in the following *Statement of contribution for joint author publications* or in the main text, as are the parts of the work done in my Honours year.

Felix J. Lawrence

Statement of contribution for joint author publications

> Lawrence, F. J. *et al.* "Antireflection coatings for two-dimensional photonic crystals using a rigorous impedance definition". *Appl. Phys. Lett.* **93,** 1114 (2008)

This Letter is partially based on work done in FL's Honours year, and partially on work done during his PhD. Most of the software used was provided by KD and LB, and FL extended it in collaboration with them. In FL's PhD he extended the software implementation of the method (with help from KD and LB) to support non-normal incidence and frequencies above the first Wood anomaly. FL wrote the letter, which was heavily edited and proofread by MdS, KD, and LB.

> Lawrence, F. J. *et al.* "Impedance of square and triangular lattice photonic crystals". *Phys. Rev. A* **80,** 23826 (2009)

The suggestion of generalising the method to triangular lattices was made by FL's supervisors. LB supplied the orthogonality relations, which as noted in the paper are from previous work, and FL worked out how to use these to define the impedance for these structures. LB suggested the final notation used in the paper. Taking the Mathematica-based code used in the Letter, LB and KD extended and refined their routines that normalise and orthogonalise Bloch modes. FL then made other changes to the code and reorganised much of it, writing it in Python in an object-oriented style suited to the new type of problem to be solved. FL ran all the simulations, some coating designs were independently verified by KD. FL wrote the paper, which was edited and proofread by MdS, KD, LB and RMcP.

> Lawrence, F. J. *et al.* "Photonic-crystal surface modes found from impedances". *Phys. Rev. A* **82,** 053840 (2010)

The suggestion of considering surface modes was made by FL's supervisors. Although FL had many useful discussions with his supervisors and a lot of feedback, the method described is essentially FL's. FL wrote all the new code for this paper and ran all the simulations; the heart of this code (that finds and normalises Bloch modes) remains that provided by KD and LB. KD independently verified some of the double interface surface mode projected band structures, using a different code. FL wrote the

paper, which was edited and proofread by MdS, KD, LB and RMcP. The inclusion of the appendix was suggested by FL's supervisors in response to a reviewer's comment, and MdS and FL jointly decided the relevant quantities for the convergence tables. The error in the convergence tables that led to the Erratum was entirely FL's.

> Lawrence, F. J. *et al.* "Bloch-mode based homogenisation of photonic crystals". *Optical Fibre Technology (ACOFT), 2010 35th Australian Conference on,* 1–3 (2010)

FL decided to investigate the possibility of using our impedance definition to extract homogenised parameters for PCs. Useful discussions were had with all FL's supervisors, but in particular RMcP informed him about the presence of Wood anomalies. FL wrote the three page conference submission, which was edited and proofread by MdS.

> Lawrence, F. J. *et al.* "A flexible Bloch mode method for computing complex band structures and impedances of two-dimensional photonic crystals". *J. Appl. Phys.* **111,** 013105 (2012)

FL decided to develop a code for calculating PC impedances in the scalar limit that he would make available freely, based on an existing Bloch mode extraction method. His supervisors convinced him to extend the scope of this method to include calculation of PC impedance matrices, and to reimplement the mode extraction method himself. In particular, LB provided and/or explained the maths in Sec. II B before Eq. (11), including the new step of defining the backward mode amplitudes with respect to the end of the PC sample. The remainder of the numerical method was developed largely by FL. FL wrote the code and associated extensive documentation, and performed the simulations. FL wrote the paper, which was edited and proofread by MdS, KD, LB and RMcP.

We, the undersigned, do hereby certify the above to be an accurate reflection of Felix Lawrence's contribution to the publications submitted as part of his PhD thesis.

Prof. C. Martijn de Sterke	Prof. Lindsay C. Botten
Prof. Ross C. McPhedran	Dr. Kokou B. Dossou

Acknowledgements

First I thank my tireless supervisors, who have ploughed countless hours into my work, provided assistance whenever requested, presented me with opportunities to grow as a researcher and as a person, and have genuinely been a pleasure to work with. Martijn, I have repeatedly been stunned by your intuitive grasp of topics and your ability to communicate them. Ross, it is to the credit of neither of us that at PECS I was identified as your student by the quality of a joke I made. I thank Lindsay, a man "who breathes matrices", for sharing his wizardry with me. Thank you Kokou for your quiet support, your always bug-free code and your eye for detail.

I must also thank my family, in particular my parents and my aunt and uncle Cristine and Don Davison. Whenever I have needed help, they have stepped in, and then some.

Within CUDOS I salute the other surviving jerks, especially Stephen Dekker, a "hero of our times", and Sahand Mahmoodian, for his contributions to the English language. I tip my hat to the new breed of jerks, particularly Scott Brownless, Chad Husko, and Björn Sturmberg, for showing me a good time whenever I needed to see one. Thank you Michael Lee, my partner in procrastination, and Nadav Gutman, for your words of advice about completing this document. Thanks also to my former students Scott "worth repeating" Brownless, Caitlin Fisher, and Pat Blown—working with you guys was satisfying and fun, and the second half of Chapter 5 owes its existence to you. There are many other past and present members of CUDOS and the School of Physics who are more than worthy of my thanks, but by this point the reader is probably itching to delve into the remainder of this thesis.

List of author's publications

1. F. J. Lawrence *et al.* "Antireflection coatings for two-dimensional photonic crystals using a rigorous impedance definition". *Appl. Phys. Lett.* **93,** 121114 (2008)

2. F. J. Lawrence *et al.* "Impedance of square and triangular lattice photonic crystals". *Phys. Rev. A* **80,** 023826 (2009)

3. F. J. Lawrence *et al.* "Photonic-crystal surface modes found from impedances". *Phys. Rev. A* **82,** 053840 (2010)

4. F. J. Lawrence *et al.* "Bloch-mode based homogenisation of photonic crystals". *Optical Fibre Technology (ACOFT), 2010 35th Australian Conference on,* 1–3 (2010)

5. J. S. Brownless *et al.* "Coupled waveguide modes in hexagonal photonic crystals". *Opt. Express* **18,** 25346–25360 (2010)

6. F. J. Lawrence *et al.* "A flexible Bloch mode method for computing complex band structures and impedances of two-dimensional photonic crystals". *J. Appl. Phys.* **111,** 013105 (2012)

7. P. Blown *et al.* "Semi-analytic method for slow light photonic crystal waveguide design". *Photon. Nanostruct.: Fundam. Appl.* **10,** 478–484 (2012)

8. J. S. Brownless *et al.* "Supermodes of hexagonal lattice waveguide arrays". *J. Opt. Soc. Am. B* **29,** 1338–1346 (2012)

Contents

Chapter 1

Introduction

This thesis is about photonic crystal impedance: how it is defined, how impedances may be calculated, and what they can be used to do. The topic is inspired by conventional treatments of thin film stacks: knowing the impedance Z (or equivalently the refractive index n) and thickness d of each layer in a stack allows the efficient calculation of the reflective and transmissive properties of the stack. If it is easy enough to calculate the properties of individual stacks, then it becomes possible to design stacks with particular properties: for example, coatings may be designed that control or eliminate reflection at an interface between dielectrics.

Coupling into bulk photonic crystals (PCs) has traditionally been problematic due to interface reflections, particularly near the photonic crystal band edge where much of the interesting physics occurs. This problem could be solved by thin-film-style antireflection coatings, but practical design of such coatings requires quantification of the propagative, reflective and transmissive quantities of PCs. The propagative properties of a PC are encapsulated by its modes' Bloch factors; this is an established result. A PC's propensity to reflect or transmit light at an interface with any other PC, however, has not previously been quantified in a convenient, efficient and reliable fashion, and achieving this is the most important outcome of this thesis.

This chapter starts by giving an overview of the problem of coupling into PCs and some proposed solutions to do so more efficiently, and evaluating the potential of these solutions (Sec. 1.1). We then recap in Sec. 1.2 how this problem has been solved for uniform media—how reflection can be eliminated inside, for example, camera lenses, over a broad range of frequencies. We introduce this theory in terms of wave impedances rather than by using the standard refractive index Fresnel equations; the impedance method is more general: it does not assume that the permeability of each material $\mu = 1$, and it is more easily generalised to apply to PCs, as we do in Chapter 2.

Antireflection coatings have not only been used in thin films—they are also common in microwave networks and at junctions between microwave waveguides and transmission lines. Such structures, like PCs, can be multimoded. This adds considerable complexity to any useful model, and therefore a quite general formalism has been developed to describe reflection and transmission between components. We briefly discuss this formalism of scattering and transfer matrices in Sec. 1.3.

We then turn our attention toward modelling photonic crystals. A photonic crystal may be modelled as an infinite stack of gratings; its properties may be found from those of the gratings that comprise it. Therefore some fundamental and useful properties of gratings are discussed in Sec. 1.4. We directly consider photonic crystals in Sec. 1.5, discussing their eigenstates

and how to model light propagation and reflection in a way similar to the thin-film framework. The discussion is brought to a head in Sec. 1.6 with an overview of attempts to characterise coupling between PCs in terms of impedance, and the success (or otherwise) of applying such methods to calculate the properties of PC stacks. We conclude in Sec. 1.7 with a recapitulation of how the thin-film framework, including impedances, may be generalised to PC stacks.

1.1 Introducing photonic crystals

The defining feature of a photonic crystal is that its refractive index varies periodically. A typical example of a photonic crystal is a thin layer of silicon with a regular patterning of tiny cylindrical holes drilled through it—a PC slab. The photonic crystals considered herein are periodic in two dimensions but not in the third, the z–direction, like the Battenberg cake and lattice biscuit in Fig. 1.1. The diameters of the holes are typically smaller than the wavelengths at which the PC operates, and are usually arranged in a rectangular or triangular lattice, with lattice constant similar to the operating wavelength in the material.

When light travels along the inside of the PC slab, unusual effects can occur. Depending on the size and arrangement of the holes, and the incident light's properties, the holes might scatter the light such that the backward reflections interfere constructively, and the PC totally reflects the incident light. Or an incident beam might be refracted by an angle strongly dependent on its frequency; or it may be collimated and travel through the PC slab without angular dispersion; or it might just scatter. There is no general way to know *a priori* how incident light will interact with the PC, and its behaviour is obtained numerically by solving Maxwell's equations.

The PCs discussed herein are taken to be devices fabricated from dielectric materials. Each PC has either a rectangular or triangular lattice, but does not necessarily extend infinitely in all directions. The theory developed is for 2D PCs, which are invariant in the z–direction (an infinitely tall version of Fig. 1.1's Battenberg cake), with the aim of approximating the properties of PC slabs (the lattice biscuit in Fig. 1.1). When simulating 2D PCs, light is confined to the plane by mathematical decree; in PC slabs it is confined in the z–direction by total internal reflection.

1.1.1 Properties and applications

The property that initially propelled photonic crystals into the spotlight is the photonic crystal band gap, frequencies at which light cannot propagate inside the PC. At such frequencies, the back-scattered light off each hole interferes sufficiently constructively with the light from every other hole such that all light is reflected. Yablonovitch proposed that this property could be used to "tame" spontaneous emission, increasing the lifetime of an excited state embedded inside a PC when the emission frequency lies inside the PC's band gap: in order to decay, the atom or quantum dot needs to emit a photon, but due to the band gap it cannot [9].

Another application of the photonic band gap, one that drives much of the research today, is for guiding waves. Unlike any metallic mirror, a dielectric PC in band gap has no intrinsic loss upon reflection, and unlike a structure for total internal reflection, it reflects light from all angles in the plane: thus PCs are excellent at confining light. Meade *et al.* [10] proposed removing a row of holes from a PC slab and sending light down the line defect, i.e., the empty row. In the PC's band gap, the light is confined

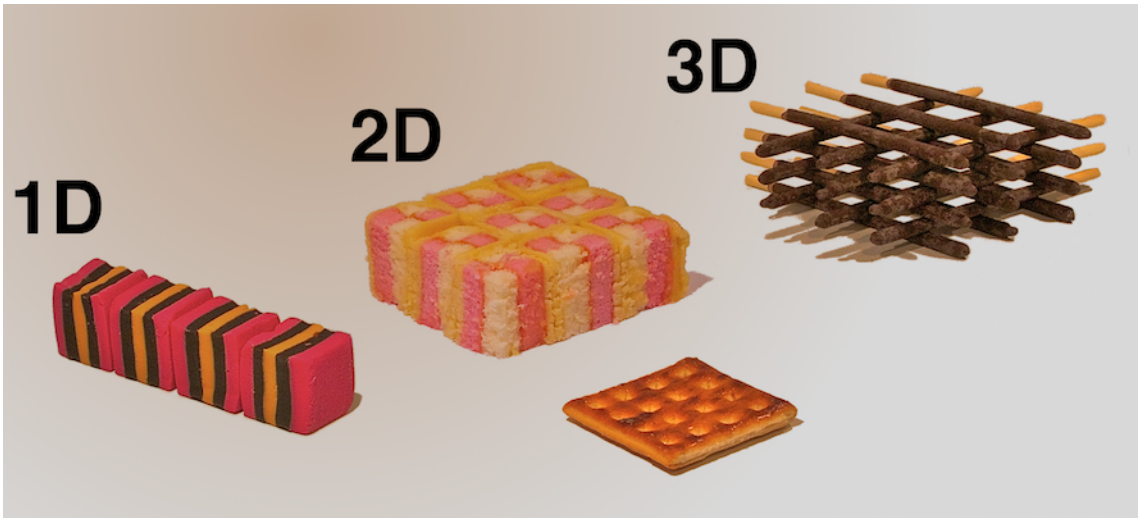

Figure 1.1: *Molding the flow of sugar...* With apologies to Joannopoulos *et al.* [18]. Each colour/material represents a medium with a different refractive index. An infinite stack of liquorice allsorts is periodic in one dimension; each allsort is a unit cell. The Battenberg cake represents 9 unit cells of a 2D photonic crystal—an ideal 2D PC is infinitely tall. 2D PCs are commonly used to model slab PCs (the lattice biscuit), which are also perodic in two dimensions but of finite extent in the third. Because slab PCs are inherently three dimensional objects, it is more difficult to compute their properties those of truly 2D PCs. Finally, the choc-pile lattice is a 3D photonic crystal, periodic in three dimensions.

on either side of the line defect by the PC, and it is confined between the top and bottom faces of the slab by total internal reflection. Such photonic crystal waveguides (PCWs) confine light in a width comparable to the optical wavelength. PC waveguides can have sharp bends with low loss [11–13], can efficiently split light at junctions [14–16], and exhibit a number of other desirable characteristics for a platform for the integration of photonic devices onto a chip, such as CMOS fabrication compatibility [17].

PCWs have a wide range of parameters that may be tuned in order to tailor their dispersion: by adjusting the width of the line defect [19] or the radii and position of holes near the line defect, it is possible to design PCWs with small group velocities and low dispersion [20, 21]. These slow light PCWs are desirable for nonlinear processes, which need the high intensity of light that accompanies the slowdown [20].

Bragg reflection is the process that is responsible for the photonic crystal band gap. It is most easily explained by analogy to a 1D PC that consists of periodically alternating slabs of dielectric materials, like the liquorice allsorts in Fig. 1.1. At each of the interfaces in the 1D PC, an incident plane wave is partially reflected and partially transmitted, in a ratio quantified by the Fresnel equations (1.9). It is possible to calculate the reflection and transmission properties of the PC's unit cell, using the standard thin film stack techniques discussed in Sec. 1.2.2. If the reflections off each unit cell interfere sufficiently constructively, then the reflectance of the 1D PC is close to unity, and the light is in the PC's band gap. If the reflectance is unity for all incident angles at a particular frequency and polarisation, then the PC is said to have a *complete* band gap at this frequency.

2D PCs are more complicated, and their band gaps generally may not be found analytically. However the basic physics remains: the backwards scattering off each row of holes interferes constructively giving a net reflectance

of close to unity. Numerical methods that can be used to calculate the band gaps and other properties of 2D PCs are outlined in Sec. 1.5.

Other useful applications of PCs do not rely on the PC band gap, and we now outline a few of these. Krauss [22] and Busch *et al.* [23] give good overviews of these applications.

Superprisms

The characteristics of a PC can vary strongly depending on the properties of the incident light. A superprism is a PC that "refracts" light in different directions depending on the light's frequency—clearly this takes place outside the PC's band gap. The term "superprism" was coined in 1998 by Kosaka *et al.* and initially referred to "extraordinary angle-sensitive light propagation" [24], i.e. strong angular dispersion, but the definition was soon modified in a followup paper [25] to refer to strong (chromatic) dispersion, i.e. frequency-sensitive light propagation. Having strong chromatic dispersion gives superprisms obvious potential applications as frequency demultiplexers and spectrometers [26], which split an input signal into separate physical channels based on frequency.

In 1999 Kosaka *et al.* experimentally demonstrated a superprism that deflects a beam of light with wavelength $\lambda = 0.99\,\mu$m by $\Delta\theta = 50°$ with respect to the deflection of a beam with $\lambda = 1.0\,\mu$m [25, 27]. This effect is 500 times stronger than that of a regular prism [27]. Since then, many other superprisms have been demonstrated experimentally, e.g. [28–30].

There have also been a number of other reported PCs with strong angular dispersion, which are superprisms by the original definition [24, 26, 31, 32]. A beam of light incident on such a PC may be refracted in strongly varying directions depending on only small changes in the angle of incidence.

Whether or not a PC has strong chromatic or angular dispersion, it can be somewhat simplistic to refer to PCs as "refracting" light [33], since refraction is a property of uniform media and there are more complicated effects at play in PCs. Nevertheless, the observed effect of a superprism is that light emerges from the PC at positions that vary strongly with frequency or incident angle, which is important for splitting light based on these properties.

Self-collimation

Self-collimation is an effect where a bulk PC guides light in a collimated beam [34]. As the beam propagates it remains collimated, despite the lack of a line defect or another feature to guide it. It does this because of unusual angular dispersion properties. For self-collimated light, in the PC the wavevector component k_y in the direction of propagation depends weakly on the incident angle. Since an incident beam consists of a superposition of plane waves with slightly different incident angles, if all components share the same propagation constant k_y inside the PC then all components of the beam acquire phase at the same rate through the PC and the beam remains collimated and does not disperse [35, 36].

Lijun Wu *et al.* [29] demonstrated a PC that self-collimates at some frequencies, and is a superprism at others. Tang *et al.* [37] presented a self-collimator, which they used to collimate light exiting a PC waveguide. Prather *et al.* [38] presented a square lattice PC that supports self-collimated beams propagating in the direction of either lattice vector. They went on to exploit this PC to build waveguides without a physical channel, optical interconnects, beam splitters, Mach-Zender interferometers, a two-bit all-optical analog-to-digital converter and more [39]—all these devices consist only of

the self-collimating PC and some mirrors constructed by locally modifying hole radii. Over time, more sophisticated examples have been proposed and demonstrated: very recently, Z. H. Wu *et al.* proposed a PC for which k_y is nearly independent of k_x over the entire Brillouin zone, leading to self-collimation for a very broad range of incident angles [40].

1.1.2 Fabrication

Photonic crystal slabs are typically fabricated from semiconductor wafers, most commonly silicon, GaAs or InP, using e-beam lithography [23]. The process has been developed over the past decade to give excellent accuracy for hole placement and good control over hole radius [41]. It is also possible, but not easy, to fabricate non-circular holes with unusual shapes and sharp corners (Fig. 1.6, [30]). In this way, any number of PCs, waveguides, and/or other devices may be written onto a silicon wafer, and elaborate multi-component devices may be created [30, 39].

A typical fabrication process (e.g. that described in Ref. [41]) begins by covering a silicon on insulator wafer with an electron beam resist. An electron beam is used to remove the resist from the desired hole locations, and then the resist is chemically developed to fix it. The structure is then etched into the silicon by a process such as reactive ion etching, which drills through any silicon not covered by the masking layer of resist. The resist is then chemically removed, and the insulator layer underneath the silicon can optionally be removed by a chemical underetching process.

Photonic crystals may also be fabricated from materials that are not semiconductors—for example, chalcogenide glasses, which have highly nonlinear properties, may also be patterned by e-beam lithography [42]. Another (somewhat unusual) platform for photonic crystals is moulded silk [43], which is biocompatible.

1.1.3 Coupling to PCs

In order to send light through a PC or PC waveguide (PCW), light must first be coupled into it. Usually there is some sort of reflection loss associated with this coupling, which is essentially due to an impedance mismatch. Such losses occur not only when coupling into a slab, but also at the front and back of each PC within the slab, in the case of a multiple PC structure. Near the band edge, where much interesting physics takes place, this reflection loss is inherently high. A small coupling loss may be overcome by boosting the input power, but if many PCs are integrated into a single device, then the interface losses quickly dominate. Not only do these coupling losses decrease the intensity of signals passing through PCs, but the reflections become *stray light*, replacing signal by noise. Reflections off the back and front interfaces can cause each PC in the system to exhibit Fabry-Pérot resonances.

Similar effects would occur inside multi-component optical and microwave systems, such as camera lenses and radar systems, had methods not been developed to eliminate these reflections. Impedance has been a critical element in these design methods, as we see in Secs. 1.2.2.

PC interface reflections could also almost be eliminated by the use of antireflection coatings, which sit between the two PCs, efficiently coupling light from one into the other. Herein we discuss PC-PC or PCW-PCW interfaces for generality: dielectric-PC and strip waveguide-PCW interfaces are special cases of these. We now explore some schemes that have been developed to reduce coupling loss between PCs.

Matching modes for low reflection

In some cases, light is transmitted into a PC with little or no reflection, even without an antireflection coating. This phenomenon is desirable for obvious reasons. It occurs when the incident and transmitted modes have similar transverse fields with similar ratios between the $\mathbf{E}_{\|}$ and $\mathbf{H}_{\|}$ field components in the interface plane. This is because the transverse components of the overall field must be continuous across the interface, and any difference between two modes' field profiles must be made up by reflected modes and other transmitted modes.

Frequently, a mode's group velocity has been used to describe its reflective character: the conventional wisdom is that modes with similar group velocities usually couple with little reflection, whereas it is harder to couple from a fast mode to a slow mode or vice-versa [44]. Following this logic, which is further discussed in Sec. 1.6.1, choosing one's PCs to have modes with similar transverse fields and group velocities can help ensure low coupling losses. For some purposes this approach is totally inapplicable: group velocity matching is useless for coupling into slow light modes due to the inherent difference in v_g between the slow light PC waveguide and the input and output waveguides.

Matching the incident and transmitted modes' v_g or even their transverse field is not a necessary condition for efficient direct coupling. White *et al.* [45] showed this by demonstrating a slow light waveguide which has intrinsically low reflection at an interface with a regular PC waveguide. In this system, the propagating modes in each waveguide have quite different field profiles, and this difference is made up by reflected and transmitted evanescent waveguide modes, which rapidly decay away from the interface. For the field to be continuous across this interface, no contribution is required from the backward propagating mode in the incident medium, and so there is no net reflection.

But ultimately, mode matching is not an especially practical solution to the coupling problem, because it places restrictions on the modes and PCs that may be used. This exhausts some of the degrees of freedom that would otherwise be available for optimising the PC's features, and thus it increases the complexity of finding a PC with the other desired properties.

Adiabatic coupling regions

The most straightforward way to reduce reflection involves replacing the sharp interface with a long adiabatic transition region between the two PCs. These structures are analogous to the bells and horns of wind and brass instruments, which match the acoustic modes of a narrow tube to those of free space. In a PC adiabatic transition region, the parameters that differ between the PCs, such as hole radius/shape, or lattice constant, slowly vary over many periods. Johnson *et al.* [46] proved that if the transition between two PC waveguides is gentle enough, then broadband coupling may be achieved. Adiabatic taper couplers for PC waveguides have been extensively studied numerically both in PC waveguides [47–49] and for bulk PCs [44, 50], and are frequently used experimentally [51–54].

The disadvantage of adiabatic coupling regions is their length: in order to be effective, they must be gentle (read: long), and thus they are hostile to miniaturisation. If m photonic crystals are to be integrated onto a chip, then there are at least $m+1$ interfaces, each of which potentially needs a coating—if adiabatic transition regions were the chosen solution to coupling losses, then much of the space on the chip would be devoted to these transition regions.

Sanchis *et al.* [55] enhanced the performance of a short (2–4 period) PC waveguide taper for a rod type PC[1] by including a defect in the taper. The defect consists of one or two rods with small radius, positioned along the centre of the taper. The position, the radii and the number of rods was varied until numerical simulations showed the structure to have low reflection; each candidate defect was evaluated by a computationally expensive FDTD (finite difference time domain) simulation. The technique was demonstrated experimentally [56], and later refined by Håkansson *et al.* [57], who employed genetic algorithms to perform the search of parameter space, before a semi-analytic method [58] was developed to make the evaluation of each set of defects more efficient. In the semi-analytic method [58], numerics are used to calculate Bloch mode transmission and reflection matrices representing the properties of each interface (between input waveguide and taper, and taper and PC waveguide); these quantities are then used in an analytic expression to calculate the reflection of the structure as a whole. As we see in Sec. 1.6, this kind of method can be far more efficient than methods such as FDTD, but an even greater computational advantage may be obtained by calculating such matrices from impedances.

Antireflection coatings

Most antireflection coatings are much shorter than adiabatic transition regions, and typically rely on resonant effects. The principle behind most antireflection coatings is to replace the interface between the PCs with a series of two or more interfaces. If the coating is designed properly, then the reflections off each of these interfaces interfere destructively, leaving little or no net reflection. In Sec. 1.2.2 we discuss how antireflection coatings for dielectric media have conventionally been designed using thin films, but here we consider a look at some coatings that have been designed for PCs.

The most common type of PC antireflection coating is obtained by modifying the radius and/or position of one or more rows of holes at the front of the PC. These coatings work in a way roughly analogous to thin film antireflection coatings. For example, the spirit of the *quarter-wave plate*[2] is captured by the design process described by Lee *et al.* [59]. The reflection coefficient of the bare interface is calculated, and a grating is found which has the same reflectance when embedded in the incident medium. This grating is placed in front of the PC (Fig. 1.2) and the phase properties of the coating are varied by moving the holes until the reflections cancel out and there is no net reflection [59]. The design procedure consists of two one-dimensional

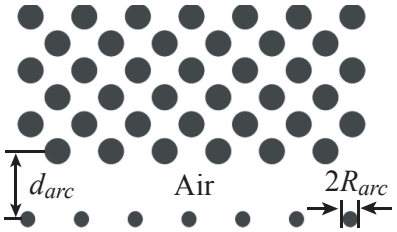

Figure 1.2: Lee *et al.'s* antireflection coating, which consists of a grating placed at a variable distance from the front of the PC [59].

[1] i.e., a PC that consists of high index rods in air

[2] Quarter-wave plates are described in Sec. 1.2.2. They consist of a film with refractive index $n = \sqrt{n_1 n_2}$ of thickness $\lambda/4n$ between two uniform dielectrics with refractive indices n_1 and n_2; the film's refractive index is such that the reflectances of its two interfaces are equal, so it acts as an on-resonance Fabry-Pérot interferometer, and therefore has zero reflectance.

searches: first they run repeated FDTD simulations to find a grating with the desired reflectance, then they run further computationally expensive FDTD simulations to calculate the separation between PC and grating that gives the lowest net reflection. This type of coating has been demonstrated both theoretically [59] and experimentally [60], but the authors acknowledge that their method works only at relatively low frequencies where only one mode is involved at the interface. By separating a two-dimensional parameter search into two one-dimensional searches, the design problem becomes feasible despite the inefficiency of the simulations. Most sets of parameters cannot be decoupled in this way, so this approach does not scale to more powerful coatings that demand additional degrees of freedom.

Another coating inspired by the quarter-wave plate was proposed by de Sterke *et al.*, in the context of coupling between PC waveguides with different widths [61]. Using transfer-matrix based methods, they found an intermediate waveguide that had equal reflectance into the input and target waveguides. They then varied the intermediate waveguide's length until the overall structure had low reflection ($R \simeq 0.002$ instead of $R = 0.59$ for the uncoated interface). Since the intermediate waveguide is a PC, they do not have continuous control over its thickness: if they truncate the PC part way through a unit cell, then its reflection properties change. Their intermediate waveguide was also relatively long: 8 periods. In order to design a perfect and compact antireflection coating, another continuous degree of freedom needs to be introduced; this brings with it another parameter space to explore.

Another design technique for a thin film-style coating was proposed by Miri *et al.* [62]. Their coating consists of two additional rows of holes in front of the target bulk PC. The radius of the holes in each row can be a variable, as is the position of each row (Fig. 1.3). Each of the rows of holes

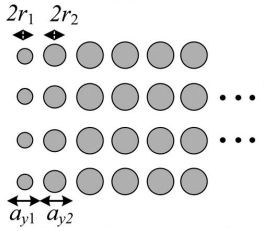

Figure 1.3: Miri *et al.'s* antireflection coating consisting of two, one-period-thick PC layers. The hole radii and layer thicknesses are variables [62].

is thought of as a one-period layer of a bulk PC, and a large number of candidate bulk PCs are auditioned for a role as a coating layer. Using only one numerically expensive simulation per candidate PC, Miri *et al.* calculate impedances and propagation constants for the candidate PCs by analogy to transmission lines—this part of their method is discussed in more detail in Sec. 1.5.3. Having thus characterised the candidate PCs' properties, they calculate the reflection of the structures with each combination of PCs in the coating. They harness the transmission line framework developed in Sec. 1.3 to exhaustively search this parameter space efficiently, analytically calculating each stack's reflection coefficient from the constituent PCs' impedances and propagation constants. The combination of PCs in the stack with the lowest reflectance becomes their coating. Their method, published after ours [1, 2], has no rigorous underpinning but nevertheless it gives correct answers at low frequencies, where only one mode is excited in each PC.

Hugonin *et al.* propose a similar style of coating for an interface between two PC waveguides, one supporting a fast mode, the other with a slow mode [63]. By exhaustively scanning a small two-dimensional param-

eter space of hole positions in two layers (Fig. 1.4), they reduce $R = 0.22$ to $R = 0.003$. They calculate the reflection coefficient of each coating stack

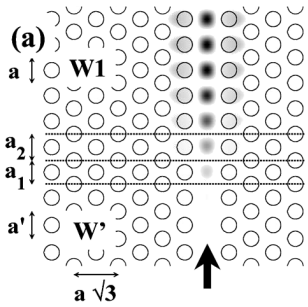

Figure 1.4: Hugonin *et al.*'s PCW antireflection coating consisting of two layers with modified lattice constant [63].

using a scattering-matrix-based mode-matching method [64], similar to that on which our method is based.

Rather than using a PC layer as a thin-film coating, Li *et al.* proposed a somewhat literal thin film antireflection coating for a square lattice photonic crystal [65]. That is, they designed a two-layer *V-coating*[3] for the PC that consists of a layer of $n = \sqrt{12}$ dielectric (the PC's background material) and an air slot (Fig. 1.5). They design their coating by calculating the PC's im-

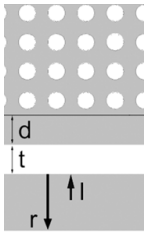

Figure 1.5: Li *et al.*'s antireflection coating, which consists of a layer of uniform dielectric and an air slot, each of variable width [65].

pedance (the manner in which they do this is described in Sec. 1.6.3), which they use in the theoretical framework for calculating reflectances of thin-film stacks, which we describe in Sec. 1.2.2. Their design method requires only one lengthy simulation to find the PC's impedance; they can then use Eq. (1.9) and the two-layer equivalent to Eq. (1.10) to efficiently calculate each candidate coating's reflection and transmission without further simulations. An inherent downside of using air slots is that light is confined in the PC slab in the vertical direction by total internal reflection, but in the air slot there is nothing to confine the light, so it can escape. The purpose of an antireflection coating is to reduce loss and stray light; an inherently lossy antireflection coating therefore is not desirable.

Matsumoto and others from the Baba group experimentally demonstrated a PC superprism with an elaborate antireflection coating consisting of a layer of teardrop-shaped projected holes [30] (Fig. 1.6). Previous numerical studies [66] of a similar coating showed that it can reduce coupling loss across the structure from $R > 0.9$ to $R < 0.2$, for a range of incident angles. The design process for this coating is quite involved, requiring lengthy FDTD simulations to evaluate each point in the two-dimensional parameter space

[3] V-coatings, discussed in Sec. 1.2.2, are a stack of two thin films that eliminate reflection at a single frequency, incident angle and polarisation. The materials may be chosen arbitrarily, and zero reflection is obtained by adjusting the layers' thicknesses.

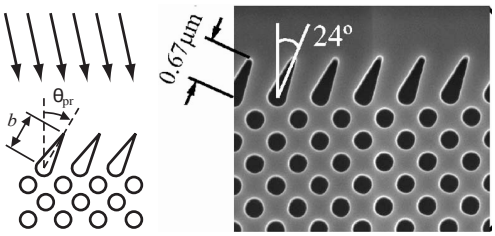

Figure 1.6: The Baba group's antireflection coating for a superprism, consisting of one layer of teardrop-shaped projected holes [30, 66].

of coatings, consisting of the projection length and angle [66, 67]. Another downside inherent to teardrop-shaped holes is that sharp corners are difficult to fabricate with e-beam lithography.

A number of researchers have found that reflections may be reduced by carefully choosing the plane in which the PC is truncated [68–74] (Fig. 1.7). Conceptually, such techniques may be considered either as mode matching

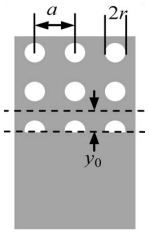

Figure 1.7: A truncated row of holes at the edge of a PC [72].

or as an antireflection coating. From the latter perspective, a row of partial holes is appended to the front of the PC, and forms an antireflection coating. From the former perspective, there is no coating—the bulk PC itself is modified: the hole moves across the edge of the unit cell such that the PC's truncated edge is the edge of a unit cell. In either case, only one degree of freedom is available—the position of the structure's edge with respect to the hole centre—and this is not always enough to eliminate reflections [74].

Truncation techniques are usually applied when coupling from a conventional dielectric waveguide (such as a strip waveguide) into a PC waveguide—cases where some choice of truncation must naturally be made. For interfaces between bulk PCs, it is not natural to drill "half a hole" in the middle of a silicon slab, and so there have been fewer reports on such methods of reducing coupling. One such structure was proposed by Zhang and Li [75], in which the holes are truncated, and additional degrees of freedom are obtained by drilling slots between the truncated holes. Given the delicacy of the resulting structure (Fig. 1.8), this method, which relied on repeated FDTD simulations to explore the parameter space, is unlikely to be demonstrated experimentally.

Śmigaj *et al.* do not use a truncated row of holes to eliminate reflection—instead they place a grating at the interface of a bulk PC and air [74, 76, 77]. Their design is extremely compact, while supporting up to four degrees of freedom (Fig. 1.9). Their design process relies on assigning a scalar impedance to the photonic crystal (calculated from the specular reflection coefficient from air onto the PC), and calculating the required quarter-wave plate to eliminate reflection at the interface. This $\lambda/4n$ layer is then replaced by a simple grating analytically calculated to have effective properties that are equivalent to the $\lambda/4n$ layer. In the final step, the properties of this

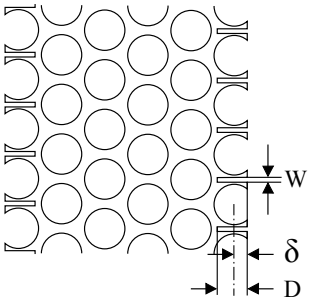

Figure 1.8: Zhang and Li's antireflection coating of truncated holes with air slots [75].

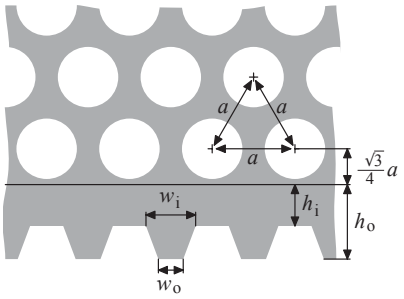

Figure 1.9: Śmigaj *et al.'s* antireflection grating [74].

layer are numerically optimised to find the best coating, a step that requires repeated numerical simulations. They present one such coating that lowers the reflectance off a PC from $R > 0.29$ for all incident angles, to an average reflectance across all angles of $R = 0.028$ [74].

Finally, Witzens *et al.* demonstrated an elegant method to match slab modes to bulk PC modes using multiple cascading gratings [78]. They present a case where their method reduces reflectance from $R = 0.91$ to $R = 0.16$, but this requires 19 layers of holes, which is as impractical for miniaturisation as an adiabatic transition. They also demonstrated a short, 3 layer structure which reduced reflectance to $R = 0.42$, which is still a worthy achievement given that they work at frequencies higher than most of the other coatings in this section; they must suppress diffraction into two modes composed of three diffraction orders.

In order to design antireflection coatings, some of the above methods require a vast amount of computationally expensive numerical simulations to explore the multidimensional parameter space of potential coatings. This includes the methods of the Baba group [30, 66, 67], Hugonin *et al.* [63], and of Zhang and Li [75]. Other methods manage to decouple the numerical search and only require exploration of one dimension at a time, such as the methods of Lee *et al.* [59] and de Sterke *et al.* [61]. Miri *et al.* [62] take this one step further, and only need to explore one or two dimensions in computationally-intensive numerical simulations: having thus evaluated many candidate PCs, the multidimensional search for a coating can be done without recourse to further numerical simulation. The method of Lee *et al.* [59] and the initial stage of Śmigaj *et al.*'s method [74, 76] are most efficient of all: they only require one numerical simulation of the PC, then coatings may be designed without further simulations (although the efficient part of Śmigaj *et al.*'s method only provides a good starting point for a computationally intensive numerical search). The efficiency of these last

two methods does come at a cost: they cannot take advantage of the many degrees of freedom that PC-like coatings offer. Our coating design process is most similar to that of Miri *et al.* [62]: we require only one dimension of parameters to be explored in a computationally intensive fashion.

Of the above methods for bulk PCs, only those of the Baba group [30, 66, 67] and Witzens *et al.* [78] have been demonstrated at frequencies where multiple diffraction orders propagate in the input medium and/or any coating layers. The other methods simply do not work at many frequencies of interest—as discussed in Sec. 1.6, these methods do not work at frequencies above the first Wood anomaly. The first Wood anomaly, a grating phenomenon discussed in Sec. 1.4, occurs at $\lambda = nd_x$, where d_x is the lattice periodicity in the interface direction, and n is the PC background's refractive index. At non-normal incidence, the anomaly occurs at even lower frequencies. For rod-type PCs in air, this frequency can be relatively high in the band structure, but for standard PCs that consist of air holes in semiconductor, at oblique incidence the first Wood anomaly often coincides with the first band gap.

It would be better for a method to exploit the framework of thin film optics like Miri *et al.*'s method [62], but to do so in a rigorous fashion that supports high frequencies and multiple diffraction orders. To begin to develop such a method, which we present in Chapter 2, we start by revisiting the framework of thin film optics.

1.2 Uniform media

The properties of light interacting with stacks of uniform media (whether dielectrics or metals) is well understood, and is treated by a range of textbooks, such as Refs. [79–84]. A powerful framework has been developed to calculate light's propagation or decay through uniform media, and its behaviour at interfaces. The framework, which we seek to emulate for photonic crystals, can easily handle a wide range of problems, including analytically modelling thin film antireflection coatings (Sec. 1.2.2), surface plasmons (Sec. 1.2.3), and slab waveguides (Sec. 1.2.4). The link between these structures is that they all consist of one or more parallel planar interfaces with uniform media on both sides (Figs. 1.11–1.14); the structures are modelled by representing the field in each medium as a superposition of its eigenmodes (plane waves), and relating the relative amplitudes of the plane waves in each medium by reflection and transmission coefficients.

If this framework could be adapted to PCs, then many complicated PC structures could be modelled semi-analytically. To take the same examples as above, if we could encapsulate the propagative qualities of PCs, and calculate the reflection and transmission at the interface between any pair of PCs, then the reflection and transmission of a stack of the PCs may be calculated in a way analogous to calculating those of a thin film stack, enabling the design of antireflection coatings (Ch. 2). The method for calculating the properties of surface plasmons at a metal-dielectric interface may similarly be adapted to a PC-PC interface, and the dispersion relation and modes of a PC waveguide or array of waveguides may be calculated based on the separate properties of the waveguide and of the mirror (Ch. 5).

Much of the material in this section will be familiar to the reader. Here we outline the thin-film framework with an eye on developing a PC framework: we introduce many of this thesis' recurring themes, techniques, quantities and notations in familiar territory before using them in the wild. The least familiar quantity here is likely the (wave) impedance Z (Eq. (1.4)), which depends on the direction of propagation. We use this quantity extensively: it

relates plane wave amplitudes to fields, and we rewrite the Fresnel equations Eq. (1.9) in terms of it. Of the many quantities described as impedances, our definition of PC impedance is most closely related to the wave impedance.

1.2.1 Propagation and reflection

In a linear uniform medium, continuous-wave light is well represented as a superposition of plane waves that either propagate or decay exponentially. Suppressing the factor $\exp(-i\omega t)$, we may write the fields as

$$\mathbf{E}(\mathbf{r}) = \sum_s \mathbf{E}_s \exp(i\,\mathbf{k}^{(s)} \cdot \mathbf{r}), \tag{1.1a}$$

$$\mathbf{H}(\mathbf{r}) = \sum_s \mathbf{H}_s \exp(i\,\mathbf{k}^{(s)} \cdot \mathbf{r}), \tag{1.1b}$$

where $\mathbf{E}_s$ and $\mathbf{H}_s$ are the amplitudes of plane wave s, and $\mathbf{k}^{(s)}$ is its wavevector. At a planar interface between two such media, incoming waves are partially transmitted and partially reflected. The properties of a planar interface between isotropic uniform *dielectrics* are often calculated using the Fresnel equations and Snell's law; we describe a different but similar approach that is more easily generalised to a method suitable for PCs. The method we describe is based on wave impedances [83] and traditional thin-film techniques. It has three steps. First, we show that we can decouple the problem into a set of independent problems, each involving only one forward and one backward plane wave in each medium. Next, we find the directions or decay rates of these waves in each medium from the wavevector of the incident wave. Finally, we use the two media's impedances to calculate reflection and transmission coefficients r and t, which relate the waves' amplitudes.

Decoupling

Across an interface between uniform media, the $\mathbf{E}_\parallel$ and $\mathbf{H}_\parallel$ field components parallel to the interface plane are continuous. We split each wavevector $\mathbf{k}$ into components $\mathbf{k}_\parallel$ parallel to the interface, and the component $k_\perp = \beta$ normal to the interface. Herein we assume that the elements of $\mathbf{k}_\parallel$ are real, namely that the wave does not decay in the interface plane. The continuity of $\mathbf{E}_\parallel$ and $\mathbf{H}_\parallel$ at every point on the interface implies that $\mathbf{k}_\parallel$ is conserved across the interface, i.e. it is the same for the incident, transmitted and reflected waves. Therefore we can consider one value of $\mathbf{k}_\parallel$ at a time, and ignore all plane waves in the system with other $\mathbf{k}_\parallel$. Similarly we separate the plane waves into two polarisation components: one with with polarisation $\mathbf{E} = \mathbf{E}_\parallel$ and another with $\mathbf{H} = \mathbf{H}_\parallel$. We choose our axes such that $\mathbf{E}_\parallel$ and $\mathbf{H}_\parallel$ may be represented by scalars $E_\parallel$ and $H_\parallel$.

Thus we can separate the terms of the summation in Eq. (1.1) into pairs of forward and backward plane waves with equal $\mathbf{k}_\parallel$ and polarisation: upon reflection at a planar interface this basis is complete as long as the surrounding media are also isotropic and uniform and all interfaces in the problem are planar and parallel. This constraint is satisfied by thin film structures. The requirement of *completeness*, i.e. that these plane waves are sufficient to represent any fields that arise in the problem, is a theme that recurs in Secs. 1.4 and 1.5—here it allows us to break up a complicated problem involving many plane waves per medium into many independent problems, each of which is easy to solve.

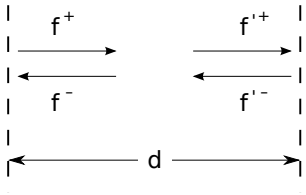

Figure 1.10: Forward and backward plane wave amplitudes defined at two phase origins separated by d.

Modes and propagation

Having shown that we can decompose a thin-film problem into a pair of waves per medium, we now find the direction of these waves from the wavevector of the incident plane wave. We know that $\mathbf{k}_\parallel$ is conserved across the system. The other wavevector component, the propagation constant $\beta = k_\perp$, is different in each medium and may be calculated from $\mathbf{k}_\parallel$ and the wavenumber $k = |\mathbf{k}| = nk_0$, which depends on the refractive index n of the medium:

$$\beta = \pm\sqrt{(nk_0)^2 - \mathbf{k}_\parallel \cdot \mathbf{k}_\parallel}. \tag{1.2}$$

The sign of β indicates the direction of propagation or decay. For evanescent waves, the propagation constant β is imaginary and determines the decay length $1/\mathrm{Im}(\beta)$. For propagating waves, the wavevector $\mathbf{k}$ points in the direction of (phase) propagation.

We may write the $E_\parallel$ and $H_\parallel$ fields in the structure in terms of the amplitudes f^+ and f^- of the forward and backward waves. But in order to write both fields in terms of one set of wave amplitudes, we must quantify the relationship between the fields. For any plane wave, the ratio between the electric and magnetic field amplitudes is given by the characteristic impedance of the medium,

$$Z_c = |\mathbf{E}|/|\mathbf{H}| = \sqrt{\mu/\epsilon}. \tag{1.3}$$

A more useful quantity for us is the ratio

$$Z = \frac{E_\parallel}{H_\parallel}, \tag{1.4}$$

which is the *wave impedance* [83] and depends on the direction of the wave relative to the interface. Equivalently, the wave admittance $Y = 1/Z$ may be used instead. For light polarised with the E field parallel to the interface, the wave impedance is $Z = Z_c k/k_\perp$. It is important to note that the $\mathbf{E}$ and $\mathbf{H}$ fields in Eqs. (1.3) and (1.4) are those due to a single plane wave, rather than an arbitrary superposition of forward and backward plane waves—some attempts to calculate PC impedances do not make this distinction.

Using the wave impedance we can write the field at any point in each medium in terms of amplitudes f^+ and f^- of the forward and backward plane waves, the conserved wavevector components $\mathbf{k}_\parallel$, and the propagation constants $\pm\beta$:

$$E_\parallel(\mathbf{r}) = \left(f^+ e^{i\beta r_\perp} + f^- e^{-i\beta r_\perp}\right) e^{i\mathbf{k}_\parallel \cdot \mathbf{r}} \sqrt{Z}, \tag{1.5a}$$

$$H_\parallel(\mathbf{r}) = \left(f^+ e^{i\beta r_\perp} - f^- e^{-i\beta r_\perp}\right) e^{i\mathbf{k}_\parallel \cdot \mathbf{r}} / \sqrt{Z}. \tag{1.5b}$$

In particular, we can relate the amplitudes on opposite sides of a slab of uniform media (Fig. (1.10)) with thickness d:

$$f'^+ = \exp(+i\beta d) f^+, \tag{1.6a}$$

$$f'^- = \exp(-i\beta d) f^-. \tag{1.6b}$$

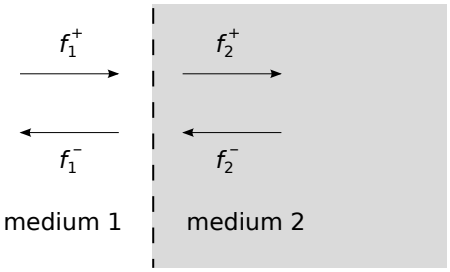

Figure 1.11: Incoming (f_1^+ and f_2^-) and scattered (f_2^+ and f_1^-) plane wave amplitudes at the interface between two isotropic uniform media.

We now investigate how to find f^+ and f^- for each slab in a stack of uniform media.

Reflection & transmission

At a planar interface between uniform dielectrics (Fig. 1.11), the amplitudes f_2^+ and f_1^- of the outgoing plane waves are related to the amplitudes f_1^+ and f_2^- of the incoming waves:

$$f_1^- = r_{12} f_1^+ + t_{21} f_2^- \tag{1.7a}$$

$$f_2^+ = t_{12} f_1^+ + r_{21} f_2^- . \tag{1.7b}$$

The transmission and reflection coefficients may be calculated by imposing the continuity of $E_\parallel$ and $H_\parallel$ across the interface plane. Specifically, using Eqs. (1.5), field continuity may be enforced for all $\mathbf{r}$ in the interface plane ($r_\perp = 0$) by setting

$$(f_1^+ + f_1^-)\sqrt{Z}_1 = E_\parallel = (f_2^+ + f_2^-)\sqrt{Z}_2, \tag{1.8a}$$

$$(f_1^+ - f_1^-)/\sqrt{Z}_1 = H_\parallel = (f_2^+ - f_2^-)/\sqrt{Z}_2. \tag{1.8b}$$

For uniform dielectrics, this condition is rarely used directly to calculate r and t: from it, the Fresnel equations have been derived, which relate r and t to the incident angle and the media's refractive indices.

The transmission and reflection coefficients may also be calculated from the media's wave impedances [83]—in fact this method is more general than the Fresnel equations: it does not assume the relative permeability of each medium to be $\mu_r = 1$, and so also applies to metals [85, 86]. The resulting expressions for r and t, which are valid in both polarisations and include the effect of incident angle, are

$$r_{12} = \frac{Z_2 - Z_1}{Z_2 + Z_1} \tag{1.9a}$$

$$t_{12} = \frac{2\sqrt{Z_1 Z_2}}{Z_2 + Z_1}. \tag{1.9b}$$

Note that in Eq. (1.5), we normalise the field amplitudes $f^\pm$ with a factor $\sqrt{Z}$; if we did not do this, and let f^+ and f^- be electric field amplitudes, as is commonly done, then the transmission coefficient t_{12} given by Eq. (1.9b) would have the denominator $2Z_2$, which perhaps is a more familiar result. Wave impedances encapsulate all the information about the wave and medium that is necessary to calculate the reflection and transmission at interfaces; it is therefore the tool of choice to calculate reflection and transmission, and in Chapter 2 we generalise the concept to PCs. Herein we refer to the wave impedance simply as the impedance.

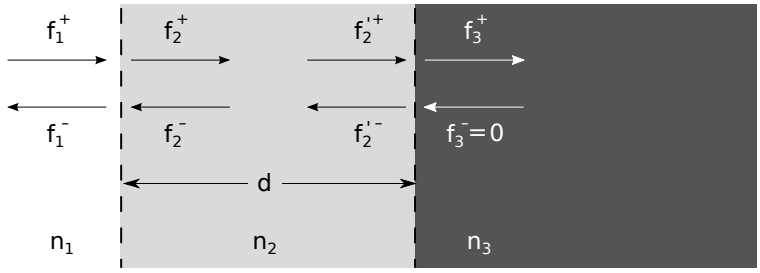

Figure 1.12: A one layer coating consisting of a slab of material 2 with thickness d inserted between semi-infinite media 1 and 3.

1.2.2 Thin films and antireflection coatings

The reflective and transmissive properties of a stack of uniform media may be calculated from the reflection and transmission coefficients of each interface, which are encapsulated by the materials' impedances Z, and the propagation qualities of each layer, which are encapsulated by the propagation constant β in each layer. Consider a system consisting of an incident medium 1, a thin film 2, and a semi-infinite target medium 3 (Fig. 1.12).

For light of a given frequency, incident angle and polarisation, the outgoing waves at each interface are related to the incoming waves by Eq. (1.7), and the amplitudes on either side of material 2 are related by Eq. (1.6). Fixing $f_3^- = 0$, the system of equations may be solved for r_{net} and t_{net} by finding f_1^- and f_3^+ in terms of f_1^+:

$$r_{\text{net}} = \frac{r_{12} + r_{23}\exp(2i\beta d)}{1 + r_{12}r_{23}\exp(2i\beta d)}, \tag{1.10a}$$

$$t_{\text{net}} = \frac{t_{12}t_{23}\exp(i\beta d)}{1 + r_{12}r_{23}\exp(2i\beta d)}, \tag{1.10b}$$

where we have used the results $r_{ij} = -r_{ji}$ and $r_{ij}^2 + t_{ij}t_{ji} = 1$ [79].

More complicated systems consisting of several layers can be solved recursively, using Rouard's method [79, 87]. Other methods of calculating stack reflectances include the transfer matrix method discussed in Sec. 1.3.2, and an approximate but elegant geometric method of adding reflection vectors, which ignores resonance inside the layers [79].

A thin-film antireflection coating is a thin film stack with a reflectance much lower than that at a direct interface between the input and output materials. If we can efficiently evaluate the reflectances of many thin film stacks involving a given pair of input and output media, then we can sift through these to find an antireflection coating.

The simplest antireflection coating is the single-layer *quarter-wave plate*, which is a one layer coating (Fig. 1.12). Inspecting Eq. (1.10a), we see that $r_{\text{net}} = 0$ when $r_{12} = r_{23}$ and $\beta d = \pi/2$. At normal incidence, this corresponds to $n_2 = \sqrt{n_1 n_3}$, and $d = \lambda/4n_2$, hence the name. Generally a material with an exact refractive index of $\sqrt{n_1 n_3}$ would not be available; a suitable material with a refractive index that is near-enough may be chosen from a catalogue of material properties such as Ref. [88]. If the coating layer's refractive index is not exactly $\sqrt{n_1 n_3}$, then the coating does not entirely eliminate reflection.

Ultimately, an antireflection coating needs to match the phase and amplitude of the reflected waves to cancel, and therefore two continuous degrees of freedom are required for successful design of a coating. One way to get two degrees of freedom and eliminate reflection entirely at the target frequency is to use two layers. A common two-layer antireflection coating is

the *V-coating* [89]. The dielectrics in the coating may be chosen somewhat arbitrarily—the only restriction being that the reflectance at each interface is sufficiently large. Once the materials have been chosen, the thicknesses of the two coating layers are adjusted to give zero reflection; the thicknesses for $r_{\text{net}} = 0$ may be analytically calculated by solving a two-layer version of Eq. (1.10a) [89]. The PC antireflection coatings presented later in this thesis take inspiration from V-coatings in that the length of each layer is fixed "somewhat arbitrarily", and the PC comprising the layer is varied.

More complicated coatings with additional layers also exist, and equivalents to Eq. (1.10) may be derived for them. Simple antireflection coatings such as those so far described are fully effective only at a single frequency, incident angle, and polarisation. More complicated coatings, such as those inside camera lenses, may involve many layers in order to be broadband, multi-angle and polarisation insensitive. These may be designed methodically by approximate methods [79], some of which are quite elegant [90], or more commonly by numerical optimisers or brute force computation: by computing reflectances off many structures and choosing the one with the best reflection properties.

Using the above methods to calculate the reflectance off a thin film stack, it is efficient and relatively straightforward to find antireflection coatings. If the thin-film framework were generalised to PCs, then it would become feasible to adapt the above antireflection coating design techniques to PCs.

1.2.3 Surface plasmons

A thin-film like formalism for photonic crystals would enable modelling photonic crystal surface modes, in analogy to the well-studied phenomenon of surface plasmons. Surface plasmons are confined to a metal/dielectric interface, along which they propagate. They decay exponentially in both directions away from the interface plane. In the metal, the field of a surface plasmon decays because the real part of the metal's permittivity is negative. On the dielectric side of the interface, they decay due to an effect similar to total internal refraction: the in-plane components $\mathbf{k}_{\|}$ of the wavevector $\mathbf{k}$ are so large that the out of plane component $k_{\perp}$ must be imaginary to satisfy $nk_0 = |\mathbf{k}|$ for the fixed free space wavenumber k_0.

The dispersion relation for a surface mode may be derived using the thin-film framework introduced in Sec. 1.2.1. In Eq. (1.7), the amplitudes of the outgoing plane waves are written in terms of the incoming plane waves. As before, the reflection and transmission coefficients r_{ij} and t_{ij} may be calculated analytically using the impedance equations (1.9). A surface plasmon exists when the outgoing amplitudes f_1^- and f_2^+ are non-zero, without any incoming waves; i.e., a surface plasmon's existence requires r_{ij} and/or t_{ij} to diverge. By fixing frequency and solving for the k_x at which these quantities

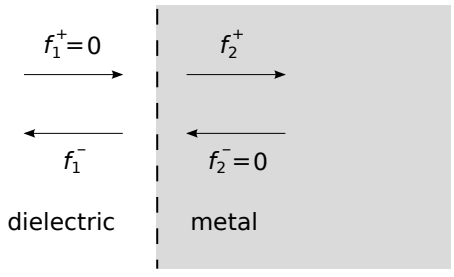

Figure 1.13: A dielectric-metal interface supporting a surface mode. Only the outgoing waves have non-zero amplitude (cf. Fig. 1.11).

diverge, it is possible to build up the dispersion relation for surface plasmons at a particular interface.

Surface modes have been observed on photonic crystals, both experimentally [91–94] and theoretically [95–97]. Here, the metal is replaced by a dielectric-based band gap PC, but the effect is similar: light is confined to the PC's surface, and decays exponentially away from the interface plane. An important difference between surface plasmons and PC surface modes is that surface plasmons require metals for the negative permittivity, and metals are lossy. PCs may be constructed entirely from dielectric materials, which in principle have much lower loss.

With a reflection and transmission framework for photonic crystals, it is possible to calculate the dispersion relation for PC surface modes semi-analytically in a way analogous to that explained above—based on poles in the reflection or transmission operators. This is done in Chapter 5.

1.2.4 Slab Waveguides

Using the same framework, it is possible to derive the dispersion relation and modes of a slab waveguide, a 2D object that confines light in one dimension. It consists of a slab of dielectric material, sandwiched between two semi-infinite dielectric media with lower refractive index (Fig. 1.14). Due to total internal reflection, the outer materials act like dielectric mirrors. Like a surface plasmon, the condition for a guided mode is

$$f_1^+ = f_3^- = 0, \tag{1.11}$$

or equivalently, that light reflected off both mirrors interferes constructively,

$$f_2^+ = r_{21} \exp(i\beta d)\, r_{21} \exp(i\beta d)\, f_2^+ = \pm f_2'^-. \tag{1.12}$$

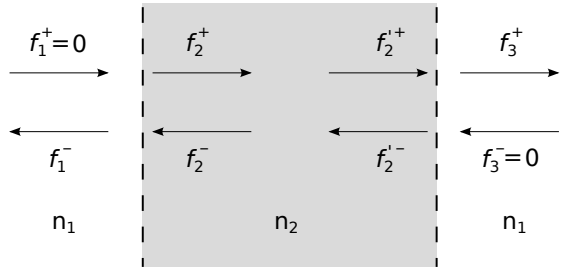

Figure 1.14: A slab waveguide, if $n_2 > n_1$. Like a surface plasmon (Fig. 1.13), the waveguide mode exists if there are outgoing waves in the absence of incident waves normal to the interface.

Much of the interest in photonic crystals involves photonic crystal waveguides, which guide light in a dielectric region that sits between two bandgap PCs. With the ability to mathematically represent the reflection off PCs, it is easy to extend the theory for dielectric slab modes to find the dispersion relations and modes of PC slab waveguides. As we discuss in Sec. 5.2, this allows efficient dispersion engineering of PC slab waveguides.

1.3 Equivalent circuits

Electrical engineers have developed a number of techniques analogous to the thin-film techniques described above [83, 98]. Some of these techniques have

been adapted to model doubly-periodic grids [99, 100], which have the same class of periodicity as 2D PCs. However, in microwave engineering, a number of structures of interest are multi-moded, necessitating the development of more powerful techniques than required for thin-film optics [101]. As we see in Chapter 2, the ability to model multiple modes in each material is critical for an accurate description of photonic crystal properties, even in some cases where the PC has only one propagating mode. A number of engineering techniques have been adapted to describe stacks of PCs and PC waveguides.

We start in Sec. 1.3.1 by describing the methods for modelling transmission line junctions. These methods are directly analogous to thin film techniques—in fact, thin films may be modelled as transmission lines. In Sec. 1.3.2 we show another way to represent the properties of an interface between transmission lines—as a two-port network. These networks can be generalised to N-port networks, which are sufficiently powerful to model interfaces between multimoded waveguides, or, potentially, PCs.

1.3.1 Transmission lines

Most transmission lines consist of two conductors: a standard example of a transmission line is a coaxial cable. An AC signal (a voltage wave) propagates down the line at a particular frequency, and may be characterised by its propagation constant[4] β and its characteristic impedance Z_c. With a similar form to Eq. (1.5), the voltage V and current I along the line due to a pair of forward and backward waves are

$$V(y) = (f^+ e^{i\beta y} + f^- e^{-i\beta y}) \sqrt{Z_c} \tag{1.13a}$$

$$I(y) = (f^+ e^{i\beta y} - f^- e^{-i\beta y}) / \sqrt{Z_c} \tag{1.13b}$$

where as usual we have omitted the factor $\exp(-i\omega t)$. β plays the same role as in optical systems. The transmission line's characteristic impedance Z_c is defined as the ratio of voltage V and current I for any wave on the line:

$$Z_c = \frac{V}{I}. \tag{1.14}$$

When comparing this definition to Eq. (1.4) for uniform media, recall that

$$V = \int_A \mathbf{E} \cdot d\mathbf{l}, \tag{1.15a}$$

$$I = \oint_C \mathbf{H} \cdot d\mathbf{l}, \tag{1.15b}$$

where A is any path between the conductors, and the C is a closed path around one of the conductors.

At the interface between a pair of transmission lines, or between a transmission line and a circuit element, an incident wave is partially reflected and partially transmitted, in ratios given by

$$r_{12} = \frac{Z_{c2} - Z_{c1}}{Z_{c2} + Z_{c1}}, \tag{1.16a}$$

$$t_{12} = \frac{2\sqrt{Z_{c1} Z_{c2}}}{Z_{c2} + Z_{c1}}, \tag{1.16b}$$

[4] In this section we do not always follow standard engineering notation—for consistency with the rest of the thesis we use optics-style notation wherever possible. So here, a wave with propagation constant β travels along an infinite transmission line as $V(y) = V_0 \exp(i\beta y)$, and decay is given by $\mathrm{Im}(\beta)$.

which is the same as Eq. (1.9) for an interface between uniform media [83, 98]. Thus the characteristic impedance of a transmission line plays the same role as the wave impedance of a uniform medium.

A number of methods have been developed to eliminate the reflection due to the impedance mismatch at a junction between a pair of transmission lines. Several of these techniques may easily be adapted to the design of thin film coatings, and potentially also photonic crystal AR coatings. For example the quarter wave transformer is directly analogous to the quarter wave plate discussed in Sec. 1.2.2: an intermediate transmission line with $Z_c = \sqrt{Z_{c1} Z_{c2}}$ is introduced between transmission lines 1 and 2 [98]. Design techniques have also been developed for broadband impedance matching. For example, Chebyshev multisection matching transformers can achieve low but non-uniform reflection over a wide bandwidth [98].

In fact, the analogy between transmission lines and dielectric slab waveguides may be formalised [83], as may an analogy between transmission lines and thin films. An effective voltage and current can be ascribed to the medium, and transmission line techniques may be used. Multimoded reciprocal media, such as photonic crystals, cannot be modelled by a single transmission line, but may be modelled by multiconductor transmission lines. But rather than representing dielectrics by transmission lines, or vice versa, it is easier to write them in a common language, using the powerful formalism of network analysis.

1.3.2 Multi-port networks

In network analysis, the circuit under consideration may be divided into a number of N-port networks. An N-port network has N input modes and N output modes, which are related in some linear way. The most common structure considered is a two-port network, which might consist of the junction between two transmission lines, each of which supports an incoming and an outgoing mode. The interface between two multimode waveguides may be modelled as an $(M_1 + M_2)$-port network, where M_1 and M_2 are the number of propagating and evanescent modes considered in waveguides 1 and 2 respectively [101].

This formalism is very general, and many structures may be modelled in this way: a length of transmission line; junctions between transmission lines; lumped circuit elements; interfaces between metallic microwave waveguides; interfaces between uniform media, slabs of uniform media, and stacks of uniform media; and even doubly-periodic grids [99]. In each case, as long as the media are reciprocal and linear, the structure can be represented by an intersection between N transmission lines, each of which represents a mode of the structure's input or output medium. In Sec. 1.5.2, we describe modelling a PC as a semi-infinite stack of identical N-port networks representing a single layer of the PC, and use network analysis techniques to find the N-port networks that represent finite stacks of arbitrary length.

The properties of a N-port network are characterised by any one of five related matrices:

- By its scattering matrix $\mathbf{S}$, which relates the incoming amplitudes to the outgoing amplitudes,
- By its transmission/chain/$ABCD$ matrix, which relates the (generalised) voltage and current across/through some ports to the (generalised) voltage and current across/through the others,
- By its transfer matrix $\mathcal{T}$, which relates the incoming and outgoing amplitudes in some ports to the incoming and outgoing amplitudes in

the other ports,

- By its impedance matrix (known as the $\mathcal{R}$–matrix [102] in the gratings community)...
- ...or admittance matrix, which relate the (generalised) voltage across each port to the (generalised) current through every other.

Any one of these five matrices may be found from any of the others, and so each matrix fully characterises the reflection and transmission properties of the network at a given frequency (and incident angle and polarisation, if applicable to the system). Scattering matrix, R–matrix and transfer matrix approaches are also commonly used to model PCs, as described in Sec. 1.5. The impedance and admittance matrices mentioned above are not defined with respect to PC eigenmodes, and may not be used directly in a thin-film-like framework to describe PC propagation. They are unrelated to those we define in Chapter 2 and use throughout this thesis.

For those with an optics background, the scattering matrix is perhaps the most intuitive of these matrices. For an interface between two single-moded media (e.g. Fig. 1.11),

$$\begin{pmatrix} f_2^+ \\ f_1^- \end{pmatrix} = \mathbf{S} \begin{pmatrix} f_1^+ \\ f_2^- \end{pmatrix}, \tag{1.17}$$

where

$$\mathbf{S} = \begin{pmatrix} t_{12} & r_{21} \\ r_{12} & t_{21} \end{pmatrix} \tag{1.18}$$

is the scattering matrix. For multimoded systems, where $f^{\pm}$ are vectors, the r and t coefficients are replaced by matrices $\mathbf{R}$ and $\mathbf{T}$. Rouard's method [79, 87] may straightforwardly be generalised and applied to determine the characteristics of a network of several such components.

But there is a more direct way to calculate the properties of a network of N-port components from the properties of the individual components. The transfer matrix $\mathcal{T}$ is ideally suited to concatenating components and finding the properties of the resultant stack. The transfer matrix is defined such that

$$\begin{pmatrix} f_2^+ \\ f_2^- \end{pmatrix} = \mathcal{T} \begin{pmatrix} f_1^+ \\ f_1^- \end{pmatrix}, \tag{1.19}$$

and [103]

$$\mathcal{T} = \begin{pmatrix} \mathbf{T}_{12} - \mathbf{R}_{21}\mathbf{T}_{21}^{-1}\mathbf{R}_{12} & \mathbf{R}_{21}\mathbf{T}_{21}^{-1} \\ -\mathbf{T}_{21}^{-1}\mathbf{R}_{12} & \mathbf{T}_{21}^{-1} \end{pmatrix}, \tag{1.20}$$

where in the two-port case the matrices $\mathbf{R}$ and $\mathbf{T}$ reduce to scalars r and t. Given the transfer matrices $\mathcal{T}_1, \mathcal{T}_2, \ldots$ of N-port networks in series, the transfer matrix of the total structure is the product,

$$\mathcal{T}_{\text{net}} = \ldots \mathcal{T}_2 \, \mathcal{T}_1. \tag{1.21}$$

The $ABCD$ matrix fulfils the same role as $\mathcal{T}$, but relates $V = (f^+ + f^-)\sqrt{Z_c}$ and $I = (f^+ - f^-)/\sqrt{Z_c}$ between two sets of ports [98]:

$$\begin{pmatrix} V_2 \\ I_2 \end{pmatrix} = [ABCD] \begin{pmatrix} V_1 \\ I_1 \end{pmatrix}. \tag{1.22}$$

It is related to $\mathcal{T}$ by the similarity transformation

$$[ABCD] = \left[\begin{pmatrix} \mathbf{Z}_c^{1/2} & \mathbf{0} \\ \mathbf{0} & \mathbf{Z}_c^{-1/2} \end{pmatrix} \mathcal{I} \right] \mathcal{T} \left[\begin{pmatrix} \mathbf{Z}_c^{1/2} & \mathbf{0} \\ \mathbf{0} & \mathbf{Z}_c^{-1/2} \end{pmatrix} \mathcal{I} \right]^{-1}, \tag{1.23}$$

where $\mathbf{Z}_c = \text{diag}(Z_c)$, $\mathcal{I} = 1/\sqrt{2} \begin{pmatrix} \mathbf{I} & \mathbf{I} \\ \mathbf{I} & -\mathbf{I} \end{pmatrix}$ and $\mathbf{I}$ is the identity matrix.

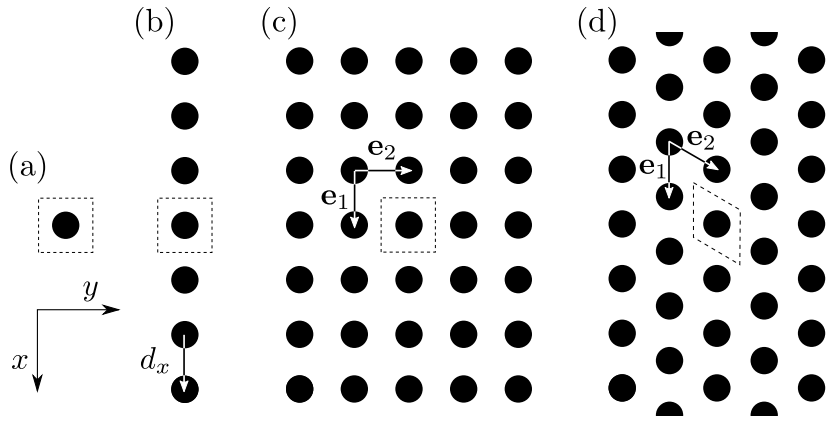

Figure 1.15: (a) A square unit cell, (b) A grating constructed from this unit cell, (c) a square-lattice PC constructed from this grating, and (d) A triangular lattice PC constructed from a parallelogram unit cell.

We can model each layer in a stack of PCs by a transfer matrix if we define a common basis of input and output modes. In fact, a number of methods exist to do this, as discussed in Sec. 1.5.2. But such methods are not as physically enlightening as a method that gives the amplitudes of each PC's eigenmodes, and reflection coefficients/matrices in the style of the thin-film framework. Using such an approach, the modes in each N-port network would be the eigenstates of the relevant PC, and we would calculate transfer or scattering matrices for propagation through each PC section, and transfer or scattering matrices for crossing the interface between each pair of PCs. This is the technique described in Chapter 2.

1.4 Gratings

A photonic crystal may be thought of as a stack of gratings. This provides a convenient way to model a PC: the properties of an individual grating can be found numerically and summarised as a transfer matrix, written in a basis we define shortly. Knowing the transfer matrix of an individual grating, we can raise it to integer powers (applying Eq. (1.21)) to calculate the transfer matrix of a stack of the gratings, i.e., the PC. This is the basis of a number of efficient and highly accurate numerical methods to model PCs [33, 103–108], including the method upon which ours is based, and we describe this approach in Sec. 1.5. But before we consider stacked gratings, it is important to consider the properties of individual gratings. Grating theory is quite mature, and can not only help us numerically model PCs, but also shed insights into some of their properties.

Introducing gratings

The gratings we consider are 2D objects, periodic in one direction and finitely thick in the other (Fig. 1.15(b)). We only consider gratings that consist of a periodic row of inclusions embedded in a background dielectric, i.e. we ignore reflection gratings such as periodic grooves on a metal surface. The unit cell of the PC we want to model can be used to define the grating (Fig. 1.15). The unit cell may be thought of as the "atom", and is reproduced infinitely along a line to form the grating, the "molecule". The grating may then be reproduced in another direction, to form the photonic crystal, the "bulk material".

The key property of a grating is that it diffracts an incident plane wave into a countably infinite set of diffracted waves. A few of the diffracted orders are propagating plane waves; the rest decay evanescently. The directions and decay rates of the diffracted orders are determined by the grating equation: for each diffraction order $s = 0, \pm 1, \pm 2, \ldots$, the wavevector component $k_x^{(s)}$ (along the grating) is

$$k_x^{(s)} = k_x + \frac{2\pi s}{d_x}, \tag{1.24}$$

where k_x is the incident wave's wavevector component and d_x is the grating's period [80, 109]. Eq. (1.24) and Eq. (1.2) fully determine the wavevectors of the reflected and the transmitted diffraction orders: $k_y^{(s)}$ may be derived from $k_x^{(s)}$ and the wavenumber $k = nk_0$:

$$k_y^{(s)} = \pm\sqrt{k^2 - {k_x^{(s)}}^2}, \tag{1.25}$$

where the sign depends on whether the diffracted order is reflected or transmitted. A diffracted order s propagates if its propagation constant $k_y^{(s)}$ is real, and decays if it is imaginary.

Simulating gratings

Thus the directions and decay rates of all diffracted grating orders are determined by the k and k_x of the incident wave (just like at an interface between uniform media) and the grating period—the contents of the unit cell are irrelevant so far. The difficult part of a grating problem is calculating the amplitudes of each of the diffracted orders; these amplitudes depend strongly on the contents of the unit cell. These scattering amplitudes can be found numerically in a number of ways, as briefly discussed by Gralak *et al.* [106], and earlier by Petit [109]. The two that we use are the finite element method (FEM) and a combination of the multipole method and lattice sums.

FEM is a general tool that may be used to solve continuous wave scattering problems under various boundary conditions. By setting periodic boundary conditions on two sides of the grating's unit cell, the infinite grating may be simulated using a finite computation domain. In some FEM implementations, including the in-house code [110] used in Chapter 2 and the commercial package COMSOL used in Chapter 3, it is possible to set the other boundaries to be transparent to specified grating orders (so that the grating is effectively surrounded by an infinite uniform dielectric), and calculate the scattering into these from the incident grating order.

Alternatively, for the common case of a unit cell consisting of a central circular inclusion in a uniform background, the amplitudes of the diffracted orders can be calculated in a highly efficient and accurate manner by using multipole techniques to find the properties of a single unit cell, combined with lattice sums to find the properties of the array [111].

We can write the amplitude of each diffracted order into a vector to quantify how the grating diffracts the incident wave. If the incident wave is set to unit amplitude, then the grating's reflectance is the sum of the squared moduli of the propagating reflected orders' amplitudes, and its transmittance is the sum of the squared moduli of the amplitudes of the propagating transmitted waves. Diffraction into evanescent orders does not directly affect the grating's reflectance and transmittance, because the evanescent orders do not carry energy, except by "tunnelling" through a thin layer into a propagating wave. However, the number of propagating orders is not a continuous function of k_x and k: as frequency increases, previously evanescent orders

become propagating. This can cause discontinuities in the slope of the reflectance spectrum of the grating and of a photonic crystal constructed from the grating, so we now briefly discuss the phenomenon.

Wood anomalies

Using Eqs. (1.24) and (1.25), there is a change in the number of propagating orders at the values of k_x and k that satisfy

$$k = k_x + \frac{2\pi s}{d_x} \tag{1.26}$$

for some integer s. Such points are Wood anomalies, first observed by R.W. Wood in 1902 [112]. They were explained as above by Lord Rayleigh in 1907 [113], and so such wavelengths are also known as Rayleigh wavelengths [114]. Note that k in Eq. (1.26) is that in the medium in which the grating is embedded: it is the refractive indices of the incident and final media that dictate the number of supported propagating grating orders.

Even more important than the discontinuity in the slope of the grating's reflectance, crossing a Wood anomaly demands a change in the way that the field is represented far from the grating. At a large enough distance from the grating, the amplitudes of the scattered evanescent orders decay to be negligible compared to the amplitudes of the propagating orders. Therefore the field away from the grating can be accurately represented as a superposition of only the propagating diffraction orders, and only these need to be included in an N-port representation of the grating[5]. At frequencies below the first Wood anomaly, the light scattered by a grating or stack of gratings can be represented accurately as a single reflected and a single transmitted plane wave, i.e. only the specular order needs to be considered. The first Wood anomaly is the frequency at which any such treatment becomes manifestly incorrect.

Modelling gratings

So the grating's reflectance and transmittance do not tell the whole story—it is usually useful to know into which orders the incident light has been diffracted, so that the field at any position outside the grating may be determined. As mentioned above, diffracted light from a single incident plane wave can be written as an infinitely long vector, which includes the amplitudes of all excited diffraction orders. If the grating is represented as an N-port network, where each port is a forward or backward diffraction order, then this vector is a column of the grating's scattering matrix $\mathbf{S}$.

Before we can usefully define this scattering matrix, we must note two important facts. The first is that the basis of diffraction orders is complete. This property follows simply from the grating equation (1.24): every one of the diffracted orders, if reflected back onto the original grating, diffracts only into the same set of diffraction orders. The basis of diffraction orders is complete for the modelling of stacks of parallel gratings with the same period d_x, and so it is complete for modelling of PCs and stacks of PCs. The second point, which we elaborate on in the following paragraphs, is that the scattering matrix can be truncated. Combined, these facts mean that it is possible to set each of these orders incident onto the grating, calculate the scattering amplitudes from the grating, and build up a scattering matrix $\mathbf{S}$. As noted in Sec. 1.3.2, the scattering matrix encapsulates the grating's

[5]This assumes that the terminal planes/phase origins are not close to the grating's surface, i.e. that enough space for the evanescent orders to decay has been included in the network. A choice of smooth grating profile, as here, helps the assumption.

reflection and transmission properties, and may be used to calculate the transfer matrix for the grating.

The set of diffraction orders excited by an incident plane wave is of countably infinite length, so to be complete, a grating's scattering matrix should be of infinite dimension. It is not feasible to compute the scattering amplitudes into an infinite number of plane waves, so in practice this set is truncated to the propagating and weakly evanescent orders, by ignoring those with $|k_x^{(s)}| \gg k$ and large $|\mathrm{Im}(k_y^{(s)})|\Delta y$, where Δy is the distance between the grating's surface and the reference point/phase origin. The justification for this is that even a short distance away from the grating's surface, all but the weakest evanescent orders have decayed to a negligible field strength, and so their contribution to the superposition of fields is dwarfed by the propagating and weakly evanescent orders. An inspection of Eqs. (1.24) and (1.25) shows that in most situations the inclusion of a few evanescent modes is sufficient to describe scattering accurately. Indeed, for the gratings that constitute the photonic crystals in this thesis, 5 forward and 5 backward diffracted orders are sufficient to give accurate results.

The diffraction orders are also orthogonal, satisfying

$$A\delta_{ss'} = \int_{-d_x/2}^{d_x/2} E_s(x) E_{s'}^*(x)\,\mathrm{d}x, \tag{1.27}$$

where $E_s(x)$ is any non-zero component of the E field of grating order s on the edge of the grating, A is the product of the two orders' amplitudes (i.e. an arbitrary non-zero real constant), and $\delta_{ss'}$ is the Kronecker delta.

Therefore a truncated basis that consists of the propagating grating orders and a few weakly evanescent orders is suitable for modelling the scattering from an ideal grating. A scattering matrix may be calculated as described above, and from it the transfer matrix may be calculated. From the transfer matrix, it is easy to calculate the properties of stacks of gratings using Eq. (1.21), and this class of structures includes finite thicknesses of photonic crystals.

Although we are on the cusp of describing the techniques we use to model PCs, we will pause here and approach the problem from one more direction before we go into detail about PC modelling techniques.

1.5 Photonic crystals

In Secs. 1.2 and 1.4 we went to lengths to write the electric and magnetic field as a superposition of a few plane waves, instead of representing the fields directly. Even in Sec. 1.3.1 we wrote the voltage and current in terms of a superposition of travelling waves. Writing the field in this way allows us to write down analytic expressions for $\mathbf{E}(\mathbf{r})$ and $\mathbf{H}(\mathbf{r})$, rather than having to solve Maxwell's equations numerically to compute the fields over a discretised domain of many $\mathbf{r}$ values. Instead of having to calculate and store the field throughout the structure, by representing the field using a small basis we need only store a handful of plane wave amplitudes, which can be related to each other analytically to solve for the properties of stacks (Sec. 1.2.1).

The most common method of simulating PC scattering is to define a structure, e.g. a finite thickness of PC embedded in a uniform dielectric, and numerically solve Maxwell's equations to find $\mathbf{E}(\mathbf{r})$ and $\mathbf{H}(\mathbf{r})$ throughout the structure. Several numerical methods exist to do this, including FDTD and FEM. Producing such data is computationally expensive, and the results are opaque and single purpose: these methods find the field in a particular (and finite) length of PC, or a particular stack of PCs, and this data is not easily

adapted to give information about other related stacks of PCs. Furthermore, such methods offer limited physical insight into why the field is as it is.

Many PC scattering problems of practical significance, including the design of PC antireflection coatings, require the evaluation of large numbers of PC structures. Specifically, the parameter space to be explored when designing a p-layer PC antireflection coating, considering m candidate PCs for each layer, contains m^p possible coatings. Exhaustively searching this parameter space by directly using FDTD or FEM simulations requires one computationally-expensive simulation for each of the m^p structures—even for two-layer coatings this process can be prohibitively slow. More sophisticated search algorithms can reduce the number of required simulations, but since the evaluation of each coating is so computationally expensive, and the parameter space necessarily so large, the design process is still very slow. If the thin-film methods from Sec. 1.2 were adapted to PCs, then the scattering properties of the m^p coatings could be analytically calculated from the propagation constants of the m PCs and the reflection and transmission coefficients of the $\binom{m}{2} \sim m^2$ interfaces. That is, in principle $O(m^2)$ computationally expensive simulations would be needed to calculate the propagation constants of each PC and the reflection and transmission coefficients of each interface, followed by m^p very fast analytical calculations to explore the parameter space fully—this process scales much better than a search that uses FDTD or FEM simulations directly.

A further efficiency gain is possible if the reflection and transmission coefficients are calculated analytically using numerically-determined PC impedances: if each PC's impedance and propagation constant are calculated from one computationally intensive simulation, then fully exploring the parameter space of coatings requires m slow simulations, followed by m^p fast analytic calculations. This further efficiency is the subject of Sec. 1.6 and leads to the definition of PC impedance in Chapter 2. However, all of these efficiencies require the adaptation of the thin film framework to PCs, and throughout this section we begin to do this, by defining a basis for PC modes and exploring how to quantify propagation, reflection and transmission.

We started our description of thin film framework of Sec. 1.2 by defining a basis of eigenmodes: the plane waves that propagate/decay through the medium unchanged but for a phase/decay factor, the eigenvalue $e^{i\mathbf{k}\cdot\mathbf{r}}$. We saw that this basis was determined by the frequency and direction of the incident plane wave, and the refractive index of each medium. In order to make sense of light propagation through photonic crystals, it would be wise to start by writing the field in each PC as the superposition of a handful of eigenmodes.

The PC's eigenmodes are Bloch modes, and satisfy Bloch's theorem,

$$\mathbf{\Psi}_{m,\mathbf{k}}(\mathbf{r}) = \mathbf{u}_{m,\mathbf{k}}(\mathbf{r})\, e^{i\mathbf{k}\cdot\mathbf{r}}, \tag{1.28}$$

where $\mathbf{u}_{m,\mathbf{k}}(\mathbf{r})$ is a periodic function that shares the lattice periodicity, i.e. $\mathbf{u}_{m,\mathbf{k}}(\mathbf{r}) = \mathbf{u}_{m,\mathbf{k}}(\mathbf{r}+\mathbf{R})$ for any lattice vector $\mathbf{R}$ [115, 116]. Each Bloch mode $\mathbf{\Psi}_{m,\mathbf{k}}(\mathbf{r})$ may be identified by its wavevector $\mathbf{k}$ and an integer index m that distinguishes modes of different frequency. In a 2D band structure (Fig. 1.16), each line represents a mode with a different m.

In Eq. (1.28) $\mathbf{k}$ only appears in the exponential term; for a given m, the wavevector $\mathbf{k}$ is only a unique label for the mode up to a reciprocal lattice vector.[6] By convention $\mathbf{k}$ is taken to be in the first Brillouin zone (BZ). It may be real or complex; in Sec. 1.5.1 we consider only modes with real $\mathbf{k}$, and in Sec. 1.5.2 we broaden our view and consider modes with complex $\mathbf{k}$.

[6]Note that the wavevectors of a set of grating orders differ by reciprocal lattice vectors—therefore they may be expected to be related to Bloch modes in some way.

For photonic crystals, $\mathbf{\Psi}_{m,\mathbf{k}}(\mathbf{r})$ describes the electric and/or magnetic field. If we restrict our attention to points separated by any lattice vector $\mathbf{R}$, then the Bloch mode propagates like a plane wave in a uniform medium, i.e. as $e^{i\mathbf{k}\cdot\mathbf{R}}$. This insight has led to a number of attempts to represent PCs by an effective uniform medium; we discuss the viability of such homogenisation approaches in Chapter 4.

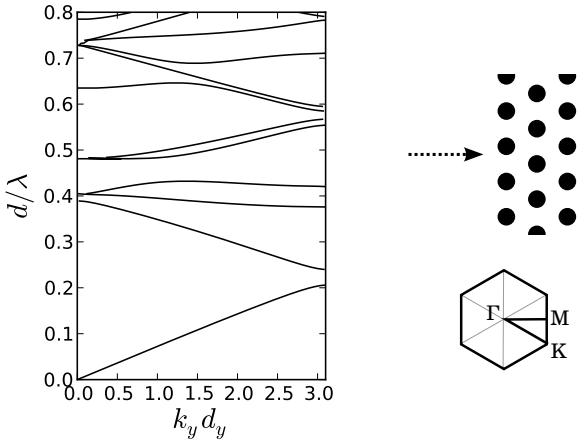

Figure 1.16: Part of a PC band structure, which relates normalised frequency d/λ to the propagation constant k_y. This band structure is for a triangular lattice PC with air holes of radius $r = 0.3$ in an $n = 3$ background dielectric, for normally incident light (i.e. along $\Gamma - M$ in the BZ). This band structure was generated using the multipole method with lattice sums [111] and the transfer matrix method [108]

.

1.5.1 Basis of propagating Bloch modes

In a PC of infinite extent, only propagating Bloch modes exist, since evanescent modes would diverge in one direction. Therefore many treatments of in-band PCs or solid state crystals (e.g. [18, 115]) only consider propagating modes, which have real $\mathbf{k}$ and carry energy through an infinite PC.

Propagating Bloch modes are typically found numerically by the plane wave expansion method, in which $\mathbf{k}$ is specified and an eigenvalue equation is solved for the frequencies ω at which modes exist. The solutions $\mathbf{\Psi}_{m,\mathbf{k}}(\mathbf{r})$ are enumerated by the index m. In this way a band structure or dispersion relation may be calculated, which relates the ω and $\mathbf{k}$ at which propagating Bloch modes exist for the studied PC (Fig. 1.16). The band structure gives insight into the propagative qualities of modes, including their phase and group velocities. It also maps the location of band gaps.

The basis of propagating Bloch modes for dielectric PCs is complete: just as an arbitrary field distribution in a uniform medium may be represented by a superposition of propagating plane waves using a Fourier transform, a field in a PC may be represented by a superposition of propagating Bloch modes [116]. But in the thin film framework of Sec. 1.2, we did not use a basis of all propagating plane waves to model thin films: there, we used Snell's law (conservation of $\mathbf{k}_{\|}$) and frequency conservation to define a minimal basis. Sometimes this basis had to include evanescent waves (Secs. 1.2.3 and 1.2.4). We now generalise this minimal basis to PCs.

1.5.2 Basis of propagating and evanescent Bloch modes

We are finally in a position to start developing a thin-film-like framework for PCs. Much of the work has already been done in the literature: in this section, which runs parallel to the development of the thin-film framework in Sec. 1.2.1, we describe the relevant basis of Bloch modes and briefly explain how it may be calculated. This basis includes evanescent Bloch modes, which have been studied less than propagating Bloch modes but nevertheless are a well-established concept [117–119]. We now see the form that a framework for PC stacks should take, and this helps us to evaluate the potential of each proposed PC impedance definition in Sec. 1.6.

Decoupling

As in Sec. 1.2.1, the first step is to decouple general scattering problems into smaller ones that depend on different sets of Bloch modes. Like thin film stacks, frequency, polarisation and $\mathbf{k}_\parallel$ are conserved across parallel interfaces between PCs—but with the catch that for each Bloch mode $\mathbf{k}_\parallel$ is only determined up to a reciprocal lattice vector. This is because in thin films, the structure is invariant under a translation by any vector in the interface plane, whereas in one direction a PC interface is only invariant under translation by a lattice vector in the interface plane. This proviso means that the minimal basis of Bloch modes is larger than just one forward and one backward mode per PC: in principle scattering occurs between a countably infinite set of Bloch modes. Like the infinite set of grating diffraction orders (in which $\mathbf{k}_\parallel$ is also fixed modulo a reciprocal lattice vector), the set of Bloch modes may be truncated to the propagating modes and a handful of evanescent modes. The degree of truncation, i.e. the number of evanescent modes required for accurate modelling of the system, is a point to which we repeatedly return throughout this thesis.

Modes and propagation

It is clumsy to compute this basis of Bloch modes using plane wave expansion techniques, which fix $\mathbf{k}$ and solve for ω. Although doing so is possible [120], it is more natural to use a method that uses the boundary conditions that define our basis, ω and $\mathbf{k}_\parallel$. The grating methods of Sec. 1.4 use exactly these boundary conditions, and in that section we saw that the set of grating orders is closed under scattering by all gratings with a given period. The grating orders of course are not usually Bloch modes, but since this set is closed under repeated grating scatterings, it is sufficient to describe PC scattering and therefore it is a sufficient basis to describe Bloch modes between the grating layers.[7] We can use the set of grating orders and how they scatter to construct a set of Bloch modes—a popular procedure, [33, 103, 106, 108, 121] which we now briefly outline.

The defining characteristic of a PC's Bloch modes is that they travel through the PC unchanged except for multiplication by a Bloch factor; they are the PC's eigenstates. Scattering across one layer of PC is represented in the basis of grating orders by multiplying a vector of plane wave amplitudes on one side of the PC by a transfer matrix $\mathcal{T}$. Scattering across many

[7] Alternatively, the basis for representing the field at a unit cell edge may be arrived at by another argument: due to the PC's periodicity, at fixed ω and $k_\parallel$ the field in the neighbourhood of a line parallel to the interface may be represented by a Fourier *series*. Each plane wave s in this series has $k_\parallel^{(s)} = k_\parallel + 2\pi s/d_\parallel$; i.e. they are the grating orders (cf. (1.24)). This approach is useful when simulating PCs that are not naturally described as a stack of gratings—such as when the unit cell edge cuts through an inclusion, the case for many triangular lattice PC waveguide supercells.

(ℓ) layers of PC, i.e. multiplying the vector of grating order amplitudes by $\mathcal{T}^\ell$, is most efficiently done by diagonalising $\mathcal{T}$ to find its eigenvectors. By definition, the eigenvectors of $\mathcal{T}$ are unchanged when multiplying by $\mathcal{T}$ (i.e. travelling across a layer), except for multiplication by an eigenvalue. The PC's Bloch modes may be represented by the eigenvectors of the transfer matrix $\mathcal{T}$, and the Bloch factors are its eigenvalues. Each eigenvector contains the grating order amplitudes at the edge of the grating's unit cell that are associated with the Bloch mode—the actual field of the Bloch mode $\mathbf{\Psi}_{n,\mathbf{k}}(\mathbf{r})$ inside the unit cell may be calculated numerically by setting the grating orders incident upon the grating with amplitudes given by the eigenvector.

The eigensystem of the transfer matrix is

$$\mathcal{T} = \mathcal{F}\mathcal{L}\,\mathcal{F}^{-1}, \tag{1.29}$$

where $\mathcal{L}$ is a diagonal matrix of Bloch factors/eigenvalues $e^{i\mathbf{k}\cdot\mathbf{e}_2}$, with $\mathbf{e}_2$ the PC lattice vector that does not run along the grating. $\mathcal{F}$ is a matrix of eigenvectors that each represent a Bloch mode in terms of the grating orders. If $\mathcal{F}$ is square and has an inverse, the completeness of the Bloch mode basis follows from the completeness of the grating orders. Columns of $\mathcal{F}$ may be removed, projecting the field onto a smaller basis of Bloch modes. Mode orthogonality relations may be derived from energy conservation or from reciprocity [108].

The unknown component of the wavevector, $k_\perp$, describes how the mode propagates or decays and may be calculated from the mode's Bloch factor. For evanescent modes, $k_\perp$ is complex, and to represent the dispersion properties of these modes, the band structure (Fig. 1.16) is generalised to a three-dimensional *complex band structure* (Fig. 1.17).

Therefore we can represent the field in each PC in a way amenable to providing physical insight: as a few Bloch mode amplitudes in a vector $\mathbf{c}$. Calculating propagation through ℓ periods of PC is as simple as multiplying $\mathbf{c}$ by $\mathcal{L}^\ell$. The mode amplitudes $\mathbf{c}$ can be partitioned into vectors $\mathbf{c}^+$ and $\mathbf{c}^-$ which respectively contain the amplitudes of forward and backward propagating/decaying modes [108]. Likewise, $\mathcal{L}$ may be partitioned into two diagonal matrices $\mathbf{\Lambda}^+$ and $\mathbf{\Lambda}'^-$. Similarly to Eqs. (1.6), amplitude vectors at positions separated by $\ell\,\mathbf{e}_2$ (Fig. 1.18) are related by

$$\mathbf{c}'^+ = \mathbf{\Lambda}^+\mathbf{c}^+, \tag{1.30a}$$

$$\mathbf{c}'^- = \mathbf{\Lambda}'^-\mathbf{c}^-. \tag{1.30b}$$

Reflection & transmission

The remaining pillar of the thin-film framework is a quantification of reflection and transmission at interfaces. Since the field in the PC is represented as vectors $\mathbf{c}^\pm$ of amplitudes rather than scalar amplitudes $f^\pm$, reflections and transmissions generally must be represented by matrices. Since matrices do not commute, the PC equivalents to the expressions from Sec. 1.2 are often substantially more complicated, but nevertheless many may be generalised to PCs. The eigensystem (1.29) contains most of the information needed to calculate reflection and transmission matrices. We use it to do so in Chapter 2, which is the key result of this thesis and enables a range of thin-film techniques to be applied to PC stacks, including efficient design of antireflection coatings.

Discussion

This method requires few Bloch modes to represent a scattering problem, and due to the restrictions on ω and $\mathbf{k}_\parallel$ imposed by the grating equation,

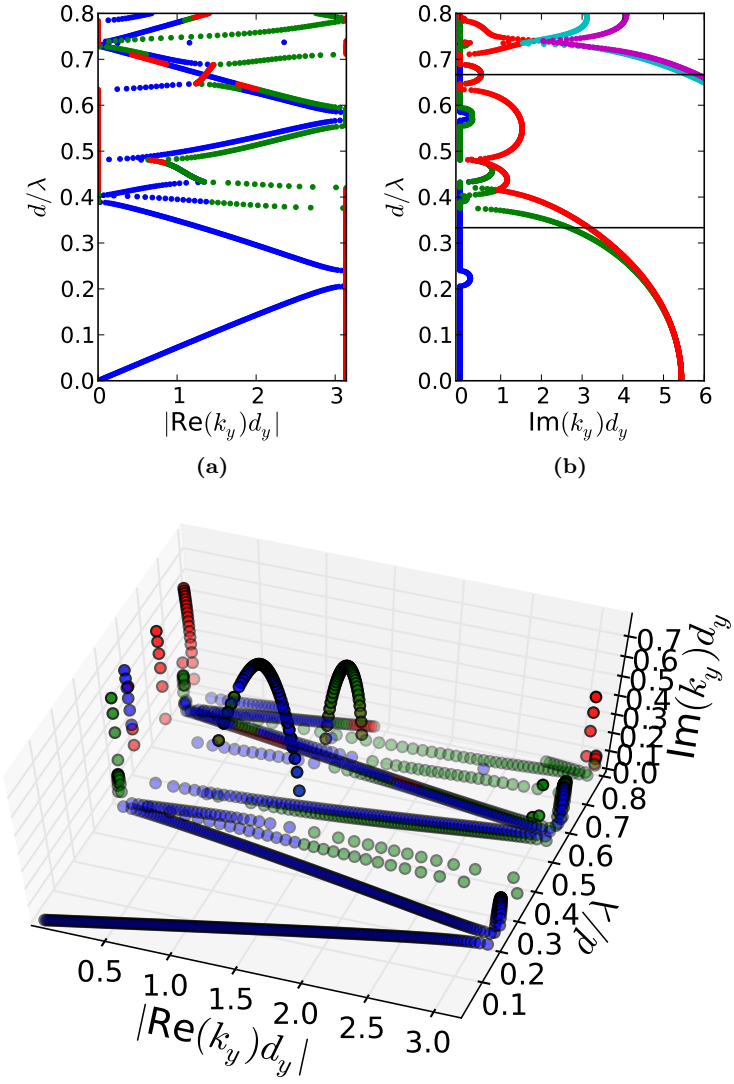

(a) **(b)** **(c)**

Figure 1.17: Two representations of a PC's complex band structure, which encapsulates how its Bloch modes propagate or decay. The band structure is for the same PC and normally incident light as in Fig. 1.16, and is calculated by the same technique. (a) and (b) respectively show the real and imaginary parts of the wavevector component k_y, relative to normalised frequency d/λ. (c) shows the complex band structure in one figure. The colour of each point is somewhat arbitrary; the only purpose of using multiple colours is to link the value of $\mathrm{Re}(k_y)$ in (a) to $\mathrm{Im}(k_y)$ in (b) at each frequency. For clarity, the magenta and cyan k_y values are not shown in (a) or (c). The two black lines in (b) mark Wood anomalies.

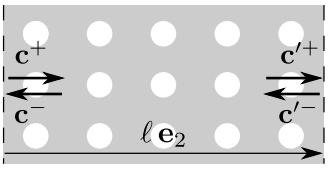

Figure 1.18: Forward and backward Bloch mode amplitude vectors defined at two phase origins separated by $\ell\,\mathbf{e}_2$. Here, $\ell = 5$.

these are precisely the Bloch modes that the incident wave scatters into. Typically, a bulk PC can be modelled in this way using only the propagating grating orders and a few evanescent orders—however many are necessary to describe grating scattering at the unit cell's edge. Many of the calculations in later chapters use 5 forward and 5 backward plane waves; a convergence table is provided in Chapter 5.

Importantly, if too few modes or grating orders are used, then inaccurate results are obtained. In our experience, the minimum number of Bloch modes for reasonable results is the number of propagating grating orders, therefore at frequencies above the first Wood anomaly it is essential to consider multiple Bloch modes. At these frequencies, a N-port network is required to describe the PC, generally with $N > 2$. As we see in Chapter 2, failure to represent enough modes leads to manifestly incorrect results. I stress this point because many of the methods highlighted in the remainder of this chapter approximate the field by a single pair of modes and therefore are only valid at low frequency.

1.5.3 Extracting modal information from field solvers

If the PC framework of Sec. 1.5.2 were complete and included a way to calculate reflection and transmission matrices from PC impedances, then the problem discussed at the start of this section, evaluating the m^p coatings, would require $O(m)$ slow numerical simulations followed by m^p fast matrix calculations. However the framework as developed depends on transfer-matrix methods, which are not as widely available as other numerical methods. In this section we briefly point out various methods to calculate reflection, transmission and/or propagation quantities from field scattering data produced by other numerical methods. The definition of impedance for summarising the reflection and transmission properties is a theme central to this thesis and is discussed separately in Sec. 1.6.

A number of attempts have been made to measure PC propagation constants and reflection and transmission coefficients at dielectric-PC interfaces. The majority of these are Nicholson-Ross-Weir (NRW) extraction techniques [122], which implicitly or explicitly assume that only one forward and one backward mode are present in the structure and its surrounds. They work by simulating a finite thickness of PC surrounded by the incident dielectric—such methods are incapable of directly simulating a PC structure with a single interface, because it would require an infinite computational domain.[8] The PC layer's reflection and transmission coefficients r_{net} and t_{net} are measured, then Eq. (1.10) (r_{net} and t_{net} for a one-layer thin film) is inverted to

[8]For uniform media, perfectly matched layers (PMLs) have been developed; these act like a matched terminating load on a transmission line. PMLs absorb plane waves from a uniform dielectric without reflection; thus the PML makes the uniform dielectric appear to be infinite. Since each unit cell of a PC scatters light, Bloch modes have forward and backward plane wave components, so a PML for PCs would need to emit light back into the PC as well as absorb the incoming light; due to these difficulties a PML for PCs is yet to be developed, although Fallahi and Hafner [123] present a related boundary condition.

find the reflection and transmission coefficients r and t of the dielectric-PC interface and the propagation constant $k_\perp$ for the PC. The procedure may equivalently be done either in the language of thin films, or using an equivalent circuit model. Crucially, this method may not be directly applied to calculate reflection at PC-PC interfaces, which would require the simulation of semi-infinite PCs. In Sec. 1.6.3 we list some authors who have applied this method to PCs and who have gone on to extract "PC impedances" from the reflection coefficients.

NRW techniques only work when a single pair of forward and backward Bloch modes is involved, i.e. at low frequency, below the first Wood anomaly.[9] With multiple modes, Eq. (1.10) must be replaced by a matrix equation and the inversion procedure becomes quite difficult. To my knowledge no-one has presented such a matrix version; all have assumed that only one pair of modes is important.

Another way that r has been calculated for a uniform-medium/PC interface is using FDTD with an incident pulse [65, 124]. The idea here is that the reflection coefficient is calculated after the back end of the pulse has reached the front surface of the PC, but before it has had time to reflect off the back surface of the PC. This method does not allow calculation of t, the propagation constant, or the modal field, but it was successfully applied to design the air-slot antireflection coating described in Sec. 1.1.3 [65].

Śmigaj *et al.* show that r and t between the modes of two media may be calculated from overlap integrals between their modal fields [125]. However, this approach assumes that the PCs are geometrically similar and that one pair of forward/backward Bloch modes per PC dominates.

Ha *et al.* presented a method of extracting multiple Bloch modes and their propagation constants from the scattered field inside a PC [126–128]; Fan *et al.* did this earlier but only for a single Bloch mode [129]. Ha *et al.* applied their method to PC waveguides, using numerically generated field data [126, 127], and also fields measured experimentally in a SNOM [128]. Briefly, they numerically fit a superposition of Bloch modes to the scattered field, using numerical optimisers and least squares techniques. They impose a symmetry relationship between the Bloch factors of forward and backward modes, and in a later paper they include in their fit the dispersion relation at multiple frequencies, to gain numerical stability [128]. Their method can find any propagating or evanescent mode that is present with sufficient amplitude in the field data, and calculate the PC's complex band structure. In Chapter 3 we extend Ha *et al.*'s method to find PC impedances and improve its stability and accuracy by imposing additional symmetry relationships.

Any method that relies on using scattered field data from a PC stack suffers a number of disadvantages compared to the transfer matrix methods outlined in Sec. 1.5.2, the biggest of which are inefficiency and inaccuracy. Transfer matrix methods need only analyse a single unit cell in order to obtain the results needed to model the PC; using most techniques described above, the computational domain must be larger. If periodic boundary conditions are enforced in the FEM or FDTD simulations, then only one period is needed in the transverse direction; otherwise the simulated PC needs to be sufficiently wide as to avoid edge effects, which drastically increases the computational domain. In the other direction, the entire structure must be simulated, i.e. every row of holes in the structure of interest must be included in the computational domain. Therefore, for such problems, transfer-matrix methods are usually to be preferred over other methods.

[9] Indeed, these techniques are mainly used for metamaterials, which by definition lie well below the first Wood anomaly, since a periodic structure is only a metamaterial if the periodicity $d \ll \lambda/n$. Photonic crystals are often used at higher frequencies, near and above the first Wood anomaly, so this extraction technique is of less use.

1.6 Characterising reflection: PC impedance

Calculating reflection and transmission at PC interfaces using any of the above methods is computationally expensive. When designing a p layer antireflection coating from m candidate PCs, there are m^p potential coatings to evaluate. As discussed at the start of Sec. 1.5, a thin-film-like framework can be used to evaluate these coatings using only $O(m^2)$ lengthy simulations, to characterise the $\binom{m}{2}$ interfaces. If the reflection and transmission coefficients are calculated from impedances using an equation like (1.4), then one could run $O(m)$ slow simulations to find the impedance and propagation constants of each PC, before calculating the m^p stacks' properties analytically and efficiently.

Because of this, there has been considerable interest in encapsulating the reflection and transmission properties of each individual PC into a single quantity, an impedance. Ideally, only one computation would be required per PC to find its impedance and propagation constants, and then the reflection and transmission between pairs of PCs could be calculated directly from the two PCs' impedances. Many definitions of impedance for PCs have been offered, but most are *ad hoc*. Few have been demonstrated to have any predictive power. We now consider the most significant of these proposed impedance definitions.

1.6.1 Group velocity as impedance

A qualitative connection was made between reflection and group velocity mismatch by a number of authors, including Refs. [12, 46, 50, 69, 130]. Momeni and Adibi went further [44], claiming that if the field profile in both media is similar, then the inverse of the group velocity (i.e. the group index $n_g = c/v_g$) in each medium can be used in place of the materials' impedances in Eq. (1.9). While this definition is simple, easy to calculate and intuitively desirable because of analogies with uniform media, more often than not it gives incorrect results, e.g. [45, 63].

1.6.2 Field-based definitions

The next common class of impedance definitions attempt to define each PC's impedance in terms of $E_\parallel$ and $H_\parallel$, the electric and magnetic field components parallel to the interface, which are used to define the wave impedance for uniform media (1.4). As for uniform media, it is important that these fields are due to a single mode, rather than a superposition of forward and backward modes, which restricts the choice of numerical method. A critical difference between PCs and uniform media is that for PCs the ratio $E_\parallel/H_\parallel$ is not uniform—it varies throughout the unit cell and along its edge. If the photonic crystal is periodic in the $x-y$ plane, then this ratio is a function of x and y. Our convention is that all interfaces lie parallel to the $x-z$ plane (Fig. 1.15). For clarity, in the following discussion we have modified other authors' notations to fit our choice of axes.

Boscolo *et al.* [130] took a weighted average of $E_\parallel/H_\parallel$ along the unit cell edge of the PC's dominant Bloch mode. They define a quantity that we will refer to as the local impedance,

$$\eta(x,y) = E_\parallel(x,y)/H_\parallel(x,y). \tag{1.31}$$

They average η along the unit cell edge, $y=0$, weighted by the real part of the y component of the Poynting vector at these points, $\mathrm{Re}(P_\perp(x,0))$:

$$Z_{\text{Boscolo}} = \frac{\int \eta(x,0)\,\mathrm{Re}(P_\perp(x,0))\,\mathrm{d}x}{\int \mathrm{Re}(P_\perp(x,0))\,\mathrm{d}x}. \tag{1.32}$$

The choice of the weighting factor $\mathrm{Re}(P_\perp(x,0))$ makes sense—one would expect regions with high field intensity to be more important in a field-matching calculation—but the specific choice of factor is only justified empirically. They write that "Compared to all of the alternatives we could think of, this one gave the results that best match those for well known periodic devices for microwave frequencies".

Ushida *et al.* [69] show that $\eta(x,y)$ is real for symmetric values of y, such as at the edge or centre of an up-down symmetric unit cell. When proposing a method to design a quarter-wave-type one-layer antireflection coating for normal incidence, they use the local impedance at the centre of the unit cell edge,

$$Y_{\mathrm{Ushida}} = 1/Z_{\mathrm{Ushida}} = 1/\eta(0,0). \tag{1.33}$$

Their method does not appear to be particularly accurate: they describe it as "qualitative" and do not apply it to design antireflection coatings or even present any reflection or transmission coefficients calculated by it.

Lu and Prather take a slightly different approach to Boscolo's—rather than calculating $\eta(x,0) = E_\parallel(x,0)/H_\parallel(x,0)$ at each point and taking a weighted spatial average of the results, they instead take separate spatial averages of $E_\parallel(x,0)$ and $H_\parallel(x,0)$ along a unit cell edge, and define impedance in terms of these quantities [131]. Working with light polarised such that $\mathbf{E} = (0,0,E_z)$ (E_z polarisation), they define

$$Z_{\mathrm{Lu}} = -\frac{\int E_z(x,0)\,\mathrm{d}x}{\int H_x(x,0)\,\mathrm{d}x}, \tag{1.34}$$

where the integration is along the unit cell edge. Again, this definition is empirical, and no theoretical justification is given as to why Z_{Lu} may be used in Eq. (1.9) to give reflection and transmission coefficients. However, the theoretical justification was later provided, along with the necessary assumptions, by Śmigaj and Gralak [132]—we discuss this below.

Also for light in E_z polarisation, Biswas *et al.* [133] multiply the numerator and denominator of $\eta = E_z/H_x$ by E_z^*,

$$\eta = \frac{|E_z|^2}{E_z^* H_x}, \tag{1.35}$$

and note that the numerator is associated with an energy density and the denominator with a flux. Inspired by this, they define

$$Z_{\mathrm{Biswas}} = \frac{\iint |\mathbf{E}_\parallel|^2\,\mathrm{d}x\,\mathrm{d}z}{\iint \mathbf{E}_\parallel^* \times \mathbf{H}_\parallel\,\mathrm{d}x\,\mathrm{d}z} = \frac{\iint |E_z|^2 + |E_x|^2\,\mathrm{d}x\,\mathrm{d}z}{\iint E_z^* H_x - E_x^* H_z\,\mathrm{d}x\,\mathrm{d}z} = \frac{U}{S}, \tag{1.36}$$

where ϵU is the field energy and S is the complex conjugate of the y component of the energy flux vector.[10] This definition is physically desirable, as the energy flux divided by the energy density is the group velocity [134], which links Z_{Biswas} to Sec. 1.6.1. Although this definition is still *ad hoc*, Biswas *et al.* demonstrate that it can accurately calculate reflection coefficients in 2D: between air and a rod-type bulk square lattice PC, and at the exit of a rod-type square lattice waveguide.

Momeni *et al.* [72, 135] propose a definition similar to Z_{Biswas}. By "analogy with homogeneous bulk media", they define

$$Z_{\mathrm{Momeni}} = \frac{|\langle \mathbf{E}_\parallel \rangle|^2}{2P_\perp}, \tag{1.37}$$

[10] In Ref. [133], the complex conjugate symbol * was missing from $\mathbf{E}_\parallel^*$ in the denominator but included on E_z^* and E_x^*.

where the numerator is the square modulus of the spatially averaged $\mathbf{E}$ field components parallel to the interface, where the averaging takes place along the interface. The denominator $2P_\perp = \mathrm{Re}(\mathbf{E} \times \mathbf{H}^*)_\perp$ is the component of the Poynting vector that is perpendicular to the interface, calculated using Bloch modal amplitudes instead of spatially varying fields. They offer an alternative form of Eq. (1.37) using $P_\perp = W_E v_{g\perp}$, in terms of the average energy density W_E and the group velocity perpendicular to the interface $v_{g\perp}$, which also harks back to the connection between group velocity mismatches and impedance mismatches (Sec. 1.6.1). Momeni *et al.* numerically demonstrate that their method can accurately calculate reflection coefficients at frequencies below the Wood anomaly, and that it fails at higher frequencies where multiple diffracting orders propagate.

The main difference between the definitions of Biswas *et al.* and Momeni *et al.* is that the former use $\langle |\mathbf{E}_\parallel|^2 \rangle$, a quantity related to the field energy, while the latter use $|\langle \mathbf{E}_\parallel \rangle|^2$. Across the interface, $\mathbf{E}_\parallel$ is continuous in both its amplitude and phase, which is presumably why Momeni *et al.* do not use the field energy and instead take the average of the electric field itself.

In the single mode approximation, it is also possible to take the field in a metamaterial and calculate the effective power, voltage and current of its equivalent transmission line model. Caloz and Itoh [136] use pairs of these quantities to define three different expressions for the impedance in analogy to the voltage-current, power-voltage, and power-current definitions of the equivalent transmission lines [137].

Simovski and Tretyakov [138] defined an impedance based on field averaging across the entire unit cell, before acknowledging that it is not related to the reflection at interfaces [139]. In the latter paper Simovski offers an alternate definition, equivalent to Lu and Prather's [131], (Eq. (1.34)), where the field is averaged across the interface plane only. Unlike Lu and Prather, Simovski mathematically relates this impedance to the reflection at an interface, although to do so they approximate each Bloch mode to a pair of forward and backward plane waves.

Śmigaj and Gralak [132] agree that the definition (1.34) of Lu and Prather [131] is rigorously correct, explicitly making the same single-mode, single-plane-wave assumptions. Paul *et al.* extend this work to consider interfaces between homogeneous dielectrics and metamaterials [140].

All the other field-based definitions of impedance presented above empirically associate the define impedance with reflection coefficients, and are theoretically justified only by analogy to uniform media or transmission lines. Furthermore, all are fundamentally rooted in the idea of each PC supporting only one Bloch mode, an assumption that is incorrect at frequencies above the first Wood anomaly. Therefore there appears no clear path to extend such definitions to work at the higher frequencies of interest.

1.6.3 Scattering-based definitions

In Sec. 1.5.3 we discussed methods to calculate reflection coefficients between PCs and uniform dielectrics. One of these, the NRW method, involves calculating the reflection coefficient from the reflection and transmission through a finite slab of PC in free space, either by inverting Eq. (1.10) or using the transmission line scattering/transfer matrix framework. Since the vacuum impedance Z_0 is a known quantity, it is possible to use the resulting single-interface air/PC reflection coefficient r in the impedance mismatch equation (1.9) to define an impedance for the PC,

$$Z_{\mathrm{NRW}} = Z_0 \frac{1+r}{1-r}. \tag{1.38}$$

Simovski *et al.* [122] give a good overview of this method, which is followed by many authors to define and calculate impedances for PCs [62, 65, 141, 142], and for metamaterials [138, 139, 143–146].

If a well-defined PC impedance can exist, satisfy Eq. (1.9) and reduce to the standard definition (1.4) for uniform dielectrics, then this "reverse engineering" process calculates it correctly. By finding the impedance, reflection coefficients can easily be calculated for other interfaces involving the PC. If no consistent impedance exists with these conditions, then the calculated impedance (trivially) gives the correct results at the interface from which it was calculated, but may give incorrect results for interfaces between the PC and other media.

Many of the above authors go one step further than finding Z_{NRW}: they calculate effective n, ϵ and/or μ of a homogeneous medium with equivalent reflection/transmission and propagation properties to the metamaterial. In Chapter 4 we discuss such methods and their appropriateness to PCs.

Of the authors cited above, only Miri *et al.* use their method "in anger", demonstrating that it is accurate and powerful enough to use for practical purposes, at frequencies below the Wood anomaly [62]. Miri *et al.* applied their method to design a PC antireflection coating, searching a similar parameter space and designing a similar coating to that found in one of my papers [1]. This coating was designed at a frequency below the first Wood anomaly, where scalar impedances can give good results.

Most authors acknowledge that impedances "reverse-engineered" from reflection and transmission coefficients only work in the single-mode, single-plane-wave approximation, i.e. at frequencies below the first Wood anomaly. While this is an appropriate assumption for metamaterials, which by definition have lattice constants much smaller than the operating wavelength, many PC applications are at frequencies above the Wood anomaly and so these definitions are not sufficiently powerful. An example for which such definitions must fail, even with PCs supporting only one propagating mode, is given in Chapter 2.

1.6.4 Multiconductor transmission line definition

Only Fallahi and Hafner [123] present an impedance method general enough to work beyond the single-mode approximation, but they present it as a boundary condition and not as part of a thin-film-like framework. They first represent one layer of a PC using the multiconductor transmission line framework, using the Fourier Modal Method to calculate the $\mathcal{R}$ matrix of the layer, which relates the voltage V (or $E_{\|}$ field [102, 123]), to the current I (or $H_{\|}$), on both sides (1 and 2) of the PC layer:

$$\begin{pmatrix}\mathbf{V}_2(0)\\ \mathbf{V}_1(0)\end{pmatrix} = \mathcal{R}\begin{pmatrix}\mathbf{I}_2(0)\\ \mathbf{I}_1(0)\end{pmatrix}, \tag{1.39}$$

where $\mathbf{V}_\ell(0)$ and $\mathbf{I}_\ell(0)$ are related to the wave amplitudes $\mathbf{f}_\ell^{\pm}$ by Eq. (1.13).

The matrix $\mathbf{Z}_{\mathrm{Fallahi}}$ that Fallahi and Hafner call their impedance matrix has half the dimensions of $\mathcal{R}$. It is defined such that

$$\mathbf{V}_1(0) = \mathbf{Z}_{\mathrm{Fallahi}}\mathbf{I}_1(0), \tag{1.40}$$

for $\mathbf{V}$ and $\mathbf{I}$ (i.e. vectors of $E_{\|}$ and $H_{\|}$ grating order amplitudes) due to only forward modes in a semi-infinite PC. It is argued that the same matrix $\mathbf{Z}_{\mathrm{Fallahi}}$ may be used to relate $\mathbf{V}_\ell(0)$ and $\mathbf{I}_\ell(0)$ at arbitrary numbers of layers ℓ into the semi-infinite PC. This matrix $\mathbf{Z}_{\mathrm{Fallahi}}$ is calculated from the aforementioned $\mathcal{R}$ matrix for a PC layer, so once it is calculated it can be used to define boundary conditions that allow the simulation of a semi-infinite

PC. The matrix dimension is the number of basis functions; in the given examples it is as high as 50 without demonstrating convergence at frequencies near the second Wood anomaly [123]. We further discuss their impedance definition, and how it relates to our own, after Paper 2.1.

1.7 Thesis outline

Directly evaluating the scattering properties of PC stacks is computationally expensive, so it is not practical to directly compute the properties of a large parameter space of PC stacks. This makes it slow and computationally-intensive to design thin-film antireflection coatings, or to dispersion-engineer waveguides. It would be good to have a thin-film like framework for analysing transmission and reflection properties of PC stacks, which would allow efficient design of antireflection coatings and dispersion engineering of PC surface modes and waveguide modes.

To develop such a framework, a basis must be chosen and propagation and reflection/transmission at PC interfaces must be quantified. The propagating and evanescent Bloch modes at fixed $\omega, \mathbf{k}_\parallel$ are the natural basis, as these quantities are conserved in PC scattering. A PC's propagative properties are summarised by its complex band structure, which may be calculated in a number of ways.

Transmission and reflection between Bloch modes can be represented by scalar coefficients only at low frequency, below the first Wood anomaly: at many frequencies of interest they must take the form of matrices. Reflection and transmission matrices for each interface may be calculated by transfer-matrix methods, but it would be good to have an efficient way to store each PC's reflective properties concisely, as an impedance independent of the other PC at the interface—this would allow m small matrices to be stored instead of $\binom{m}{2}$ reflection and $\binom{m}{2}$ transmission matrices, or m large transfer matrices. Ideally there would also be a way to calculate these matrices that did not require transfer-matrix methods, which are less widespread than other numerical techniques.

Many definitions of impedance have been proposed for PCs. Not all of them have been proven to be related to reflection or transmission coefficients. Of the definitions that may be used rigorously to calculate reflection and transmission coefficients, the vast majority are scalars and so do not work at many frequencies of interest, including the operating frequencies of the majority of PC waveguides, or superprisms like the one described by Matsumoto *et al.* [30]. Of the impedance definitions, only the definition of Fallahi and Hafner [123] is capable of modelling PCs at frequencies above the first Wood anomaly, but their impedance matrices are large, thus computationally intensive, and they report that their results converge slowly even as further modes are added.

Propagation through stacks of PCs can be efficiently modelled by transfer-matrices in the basis of grating diffraction orders. But for many physicists, the thin-film framework of Sec. 1.2.2 is more familiar and intuitive than the transfer matrix methods of Sec. 1.3—physical insight may be gained by representing fields in terms of Bloch mode amplitudes instead of the transfer matrix's basis of diffraction orders. Furthermore, transfer matrices become ill-conditioned when strongly evanescent modes are included. Scattering matrices are usually more stable [108], but the scattering matrix of a surface plasmon interface diverges, so it may not be feasible to model PC surface modes using such an approach.

Of those canvassed, the best solution would be to calculate a small impedance matrix for each PC, as well as its Bloch factors. Given a pair of

PC's impedances at the given frequency, incident angle and polarisation, we would be able to calculate the Bloch mode reflection and transmission matrices between them. To design a coating or dispersion engineer a waveguide with m candidate PCs, we would calculate the impedances and propagation constants/Bloch factors of the PCs in m computationally expensive simulations. Then the reflection and transmission properties of arbitrary stacks of the PCs could be calculated efficiently and accurately from these quantities, with no need for further computationally expensive processes. We present such a method in Chapter 2, with impedances calculated from transfer-matrix simulations.

In Chapter 3 we calculate the same impedance matrices without the need for a specialised field solver. Using widely available software, we simulate the field scattered in a length of PC, and present a technique to extract the Bloch modes and the PC's impedance from the scattering data.

At low frequencies, the field in each PC may be represented by a single pair of Bloch modes, and the impedance matrix may be truncated to a scalar. This opens a door to physical intuition: scalars are easier to represent than matrices, and so in Chapter 4 we inspect some PC impedances and Bloch factors. We also discuss the possibility and the relevance of homogenising PCs, representing them by a homogenous effective medium.

In Chapters 2 and 3 we prove the worth of our method by applying it to design antireflection coatings. We explore some other applications of our method in Chapter 5. We show that impedances can be used to find surface modes of PCs, which are analogous to surface plasmons but are not intrinsically lossy. Finally, we briefly describe how the PC framework is very useful for dispersion engineering PC waveguides, as it allows efficient calculation of the modes of different PC waveguides on an industrial scale.

We conclude in Chapter 6 with a brief discussion of the key results of this thesis, and the scope for future work.

Chapter 2

Impedance and antireflection coatings

In Chapter 1 we sketched the desired qualities of a framework for describing transmission and reflection through PC stacks. This framework, modelled on the thin film framework (Sec. 1.2), describes the field in each PC by the amplitudes of the PC's eigenmodes. Mode amplitudes in different unit cells of one PC are related by any of three equivalent quantities: propagation constants, eigenvalues, or Bloch factors; and at interfaces the amplitudes are related by reflection and transmission quantities.

In Sec. 1.5.2 we saw that Bloch modes scatter into one another at PC interfaces, so to represent the field in a PC we generally need to consider multiple Bloch modes, sometimes including evanescent modes. Therefore the forward and backward plane wave amplitudes f_i^+ and f_i^- that represent the field in layer i of a thin film stack (Fig. 1.12) must be replaced in the PC framework by vectors $\mathbf{c}_i^+$ and $\mathbf{c}_i^-$ of forward and backward Bloch mode amplitudes (Fig. 1.18).

Since the Bloch modes are PC eigenstates, propagation through the PC is represented by multiplying $\mathbf{c}_i^+$ and $\mathbf{c}_i^-$ by diagonal matrices of Bloch factors (Eqs. (1.30)). Each PC's Bloch factors can be found by diagonalising its transfer matrix, as discussed briefly in Sec. 1.5.2. The Bloch factors provide a compact and efficient quantification of a PC's propagation properties.

But can we also efficiently quantify a PC's interface scattering properties? Reflection and transmission at an interface between PCs, or between a uniform medium and a PC, are most intuitively represented by matrices in the Bloch bases of the two media. The following Letter 2.1 shows that we can calculate these matrices efficiently, for square lattice PCs, from one impedance matrix per PC. In the Letter, the formulation of the impedance definition is somewhat abbreviated—a fuller treatment is given in Paper 2.3, which follows the Letter. PC impedances are defined with respect to a reference medium, which throughout this thesis is chosen to be vacuum.

Reflection and transmission matrices at an interface between PCs 1 and 2 are defined to satisfy

$$\mathbf{c}_1^- = \mathbf{R}_{12}\mathbf{c}_1^+ + \mathbf{T}_{21}\mathbf{c}_2^- \tag{2.1a}$$

$$\mathbf{c}_2^+ = \mathbf{T}_{12}\mathbf{c}_1^+ + \mathbf{R}_{21}\mathbf{c}_2^-, \tag{2.1b}$$

which is a vector version of Eqs. (1.7), in a fundamentally different basis. The matrices $\mathbf{R}_{12}$, $\mathbf{T}_{12}$, $\mathbf{R}_{21}$ and $\mathbf{T}_{21}$ can be calculated by enforcing field continuity across the interface (*à la* Eqs. (1.8)), which is done in the basis of grating diffraction orders. Briefly, each grating order has a distinct $\mathbf{k}_\parallel$, so if the field is written in the basis of grating orders then field continuity can

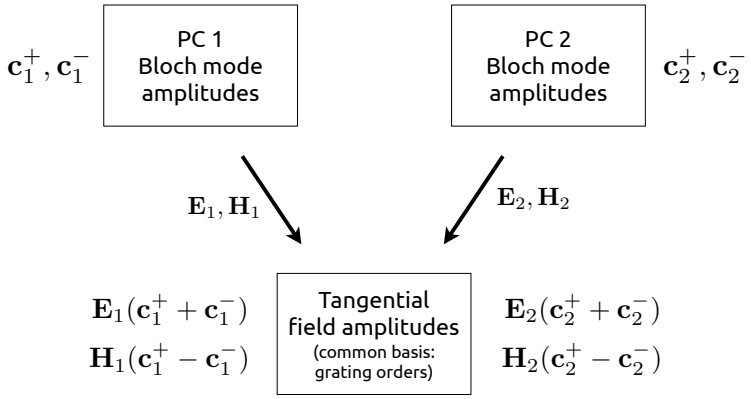

Figure 2.1: The $\mathbf{E}$ and $\mathbf{H}$ matrix for each PC maps the vectors of forward/backward Bloch mode amplitudes $\mathbf{c}^{\pm}$ to vectors that may be equated across a PC/PC interface, as long as the PCs share a periodicity.

be decoupled into a set of independent linear equations as in Sec. 1.2.1—simultaneously applying Eqs. (1.8) to each grating order—this derivation is detailed in the discussion following Paper 2.1.[1] We seek to be able to write each of $\mathbf{R}_{12}$, $\mathbf{T}_{12}$, $\mathbf{R}_{21}$ and $\mathbf{T}_{21}$ in terms of one matrix that depends only on PC 1, and another that depends only on PC 2. These two matrices are what we call the PC's impedances.

In our method, impedance matrices are defined in terms of matrices $\mathbf{E}$ and $\mathbf{H}$ for each PC. A detailed definition of $\mathbf{E}$ and $\mathbf{H}$ is provided in Paper 2.3, and analytic expressions are given in Appendix A for uniform dielectrics; here we briefly describe their function and their ingredients. $\mathbf{E}$ and $\mathbf{H}$ map Bloch mode amplitude vectors $\mathbf{c}^{\pm}$ to vectors of the field quantities that are continuous across the interface: the $E_{\parallel}$ and $H_{\parallel}$ field amplitudes appearing in Eqs. (1.8) that are associated with superpositions of forward and backward plane waves in each grating order (Fig. 2.1). These field vectors may be equated across the interface, doing so is equivalent to applying Eqs. (1.8) to all grating orders simultaneously. $\mathbf{E}$ and $\mathbf{H}$ are defined in terms of two quantities: the matrix $\mathcal{F}$ that diagonalises the PC's transfer matrix $\mathcal{T}$ (Eq. (1.29)), and the background dielectric's wave impedance Z or admittance Y.

In Letter 2.1 only, ζ denotes the PC impedance. In the remainder of this thesis, the PC impedance is denoted $\mathcal{Z}$.

[1] Many PC interfaces do not involve a change in the background dielectric. In such cases, there is no Fresnel reflection, so field continuity can be enforced in any common basis, not just the basis of grating diffraction orders. Use of a basis other than diffraction orders may be more convenient when the Bloch modes are very different to plane waves; for example, to calculate reflections between PC waveguides it might be more efficient to equate fields in the basis of a reference PC waveguide.

Antireflection coatings for two-dimensional photonic crystals using a rigorous impedance definition

Felix J. Lawrence,[1,a)] Lindsay C. Botten,[2] Kokou B. Dossou,[2] and C. Martijn de Sterke[1]
[1]*Centre for Ultrahigh-bandwidth Devices for Optical Systems (CUDOS) and School of Physics, University of Sydney, New South Wales 2006, Australia*
[2]*CUDOS and Department of Mathematical Sciences, University of Technology, Sydney, New South Wales 2007, Australia*

(Received 12 August 2008; accepted 10 September 2008; published online 26 September 2008)

We show that no consistent scalar definition of impedance is generally possible for photonic crystals. Instead, we present a rigorous semianalytic matrix definition of impedance for square lattice photonic crystals, defined in terms of Bloch modes. We then apply our definition to design a range of multilayer photonic crystal antireflection coatings efficiently. © *2008 American Institute of Physics*. [DOI: 10.1063/1.2992066]

Photonic crystals (PCs) are useful in two regimes: band gap applications, such as waveguides and Bragg reflectors, and in-band applications such as supercollimation and superprisms. In-band applications require light to be coupled into the PC, and therefore suffer insertion losses that lead to noise. At frequencies near band gaps, where the most interesting effects occur, coupling losses are especially high. These can be alleviated by long mode matching structures[1,2] or by shorter and thus more practical antireflection coatings.

Currently not enough is known about coupling losses to design PC antireflection coatings efficiently—any design process is limited to trial and error, each trial involving its own numerical simulation.[3,4] However, if we know the *impedances* of the PCs concerned, each trial is reduced to a few straightforward calculations. The problem becomes of similar difficulty to designing thin film coatings. We present a rigorous semianalytic definition of impedance for square lattice PCs and apply it to design antireflection coatings for square lattices at different frequencies and incident angles.

In many fields, impedance is a long-established concept and a useful engineering tool. Impedance is an intrinsic property of a substance, and given the impedances of two adjacent materials, the reflection and transmission coefficients at their interface can be easily calculated. The use of impedance dramatically simplifies the study of reflections as finding all $\binom{p}{2}=(p^2-p)/2$ reflection coefficients between p materials requires only p impedances.

In uniform dielectrics, the (wave) impedance Z, which generally depends on incident angle and polarization, is

$$Z = E_{\parallel}/H_{\parallel}, \tag{1}$$

where $E_{\parallel}$ and $H_{\parallel}$ are electric and magnetic fields components parallel to the reflection interface. The reflection at the interface between two dielectrics is then

$$r_{12} = \frac{Z_2/Z_1 - 1}{Z_2/Z_1 + 1}, \tag{2}$$

where $Z_{1,2}$ are the impedances of media 1 and 2, respectively. Equation (2) appears in many fields of physics, such as transmission lines, electronics, and acoustics. At normal incidence in nonmagnetic dielectric media, Z is inversely proportional to its refractive index n. The constant of proportionality is the vacuum impedance Z_0.

The extension of the concept of impedance to PCs is difficult. Bulk PCs naturally scatter light in multiple directions, and it is hard to separate interface reflections from internal scattering so as to derive Eq. (2). Another approach to impedance is required. A few *ad hoc* impedance definitions[5–9] have been proposed to satisfy Eq. (2), but all such "impedances" are scalar, and below we show that, in general, no consistent scalar impedance can be defined.

To be useful in the design of thin-film-like coatings, any impedance should be:

(1) *uniquely defined* for each PC at any frequency, incident angle and polarization,
(2) *sufficient* to find the reflection and transmission between two PCs,
(3) *economical.*

The first two points, satisfied for uniform media by Eqs. (1) and (2), respectively, express the fundamental impedance functionality that is required to design complicated thin film coatings. The third criterion prescribes practicality—we use impedance to simplify problems, so an unwieldy impedance is less useful.

In our treatment of PCs, at each frequency the field inside each PC is represented as a superposition of propagating and evanescent Bloch modes, its quasiperiodic eigenmodes. This is the natural basis in the sense that a PC's Bloch mode travels through the PC's interior without reflection. Considering each PC as a stack of gratings, its Bloch modes are represented as a superposition of propagating and evanescent plane wave solutions to the grating equation, $\sin\theta_s - \sin\theta_0 = s\lambda/d$, where θ_0 is the incident angle and integer s is the plane wave order. The Bloch basis is countably infinite, so to make calculations manageable, we project the field onto a truncated but sufficiently complete set of $2m$ propagating and slowly evanescent Bloch modes—a least square approximation that balances satisfaction of the first two criteria against the third. We partition this set into m forward traveling/decaying modes and m backward modes. Interface reflection and transmission coefficients thus become $m \times m$ matrices mapping between truncated Bloch sets, as must the impedances. The plane wave basis is also truncated, but it need not

a)Electronic mail: felix@physics.usyd.edu.au.

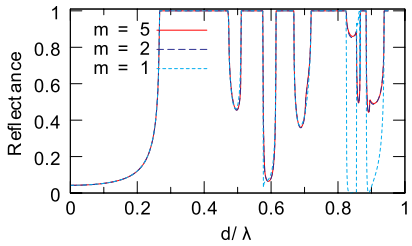

FIG. 1. (Color online) Reflections from free space at $\theta_0=25^\circ$ off the bulk PC, as calculated by impedances of dimension m.

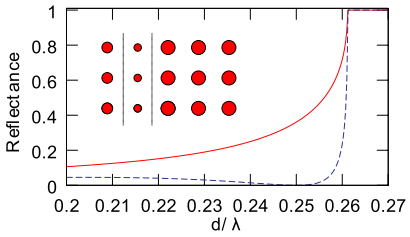

FIG. 2. (Color online) Reflectances for $\theta_0=0^\circ$ off the uncoated (solid) and coated (dashed) PCs. Inset: Schematic of a coated PC.

be truncated as strongly as it does not affect the dimension of impedances. Larger m gives more accurate results, but in this letter, we find that square lattice PC interface reflectances are predicted accurately as long as $m \geqslant p$, where p is the number of propagating plane wave solutions to the grating equation.

To define impedance, we first take the procedure for calculating the reflection at an interface between uniform dielectrics, and generalize it to work with Bloch modes. We map the Bloch modes in each PC to plane wave field amplitudes and use these to compare fields across the interface and find the reflection. The matrix that maps PC i's forward Bloch modes to plane wave field strength coefficients, found numerically via the transfer matrix,[10] is denoted $\mathbf{E}_i$ or $\mathbf{H}_i$ for the E or H field components, respectively.[11] The columns of $\mathbf{E}$ and $\mathbf{H}$ are the sums and differences of forward and backward plane wave expansions of Bloch modes. As we consider many more orders of plane waves than Bloch modes, these matrices are not square in practice, and we cannot find their inverses directly. Instead it can be shown by reciprocity that the transfer matrix is symplectic, from which the orthogonality relation $\mathbf{E}_i^T\mathbf{H}_i=\mathbf{I}$ follows. For the interface between PC1 and PC2, we can equate the plane wave field strength coefficients in a least squares sense and project onto the Bloch bases to derive

$$\mathbf{R}_{12} = (\mathbf{A}_{12}\mathbf{A}_{12}^T + \mathbf{I})^{-1}(\mathbf{A}_{12}\mathbf{A}_{12}^T - \mathbf{I}), \tag{3a}$$

$$\mathbf{T}_{12} = \mathbf{T}_{21}^T = 2\mathbf{A}_{12}^T(\mathbf{A}_{12}\mathbf{A}_{12}^T + \mathbf{I})^{-1}, \tag{3b}$$

$$\mathbf{R}_{21} = (\mathbf{I} + \mathbf{A}_{12}^T\mathbf{A}_{12})^{-1}(\mathbf{I} - \mathbf{A}_{12}^T\mathbf{A}_{12}), \tag{3c}$$

where $\mathbf{A}_{12}=\mathbf{H}_1^T\mathbf{E}_2$ maps PC2's Bloch modes to PC1's via plane wave field strength coefficients, and the reflection and transmission matrices $\mathbf{R}_{ij}$ and $\mathbf{T}_{ij}$ operate in the relevant Bloch bases. Comparing Eqs. (3) to (2), $\mathbf{A}_{12}$ plays the role of $\sqrt{Z_2/Z_1}$. If we could separate $\mathbf{A}_{12}$ into a ζ_1 and a ζ_2, then these ζ_i would satisfy criterion 2. To satisfy criterion 1, ζ_1 and ζ_2 must be independent of PC2 and PC1 respectively. We now define such ζ_i.

When projecting onto a complete basis of Bloch modes, inverses exist and $\mathbf{A}_{01}^{-1}\mathbf{A}_{02}=\mathbf{A}_{12}$ exactly. For a truncated basis, this is an approximation equivalent to calculating $\mathbf{R}_{12}$ and $\mathbf{T}_{12}$ from $\mathbf{R}_{10}$, $\mathbf{R}_{01}$, $\mathbf{T}_{10}$, $\mathbf{T}_{01}$, $\mathbf{R}_{02}$, and $\mathbf{T}_{02}$ by assuming there was an infinitesimally thin sliver of PC0 between PC1 and PC2. The relation means that we can define the impedance of each medium i as $\zeta_i=\mathbf{A}_{0i}$, where 0 is a suitable reference medium, e.g. free space. This satisfies criterion 1. As dim $(\zeta)=m$, criterion 3 is satisfied by using a truncated Bloch basis.

Figure 1 shows the reflection of light from free space off a square lattice PC, calculated using impedances of various dimension m. The PC, with lattice constant d, consists of cylindrical rods of $n=3.4$ and radius $r=0.18\,d$ on a free space background. The light is polarized with E parallel to the cylinder axes and is incident from $\theta_0=25^\circ$. Figure 1 shows that at low frequencies, $m=1$ is sufficient to calculate reflectances accurately, however, especially above $d/\lambda=0.703$, where $p=2$ (the grating equation has a second propagating solution), $m=2$ is required for accurate calculation, and there is no discernible difference between results using $m \geqslant 5$.

Having defined impedance for PCs, we now apply our definition by designing two antireflection coatings for a square lattice PC: one at normal incidence and low frequency and one at higher frequency and non-normal incidence. Designing an antireflection coating is a thorough test of any impedance definition. If the impedances are wrong, then the coating does not work.

Antireflection coatings, commonplace in thin-film optics, consist of one or more thin layers placed in front of the bulk material (Fig. 2 inset). The layer materials and widths must be carefully chosen so that all interface reflections cancel—since a PC's width cannot be varied continuously, a perfect antireflection coating needs two layers in general. The net reflection is easily derived from the interface reflections and the phase changes across the layers, for example, in the scalar case $m=1$, appropriate for low frequencies, a two layer coating has net reflection coefficient[12]

$$\rho = \frac{R_{12} + \Lambda_2^2 R_{23} + \Lambda_2^2\Lambda_3^2 R_{34} + \Lambda_3^2 R_{12}R_{23}R_{34}}{1 + \Lambda_2^2 R_{12}R_{23} + \Lambda_2^2\Lambda_3^2 R_{12}R_{34} + \Lambda_3^2 R_{23}R_{34}}, \tag{4}$$

where the phase change across a layer is $\Lambda_i=\mu_i^{d_i}$, with μ_i the layer's Bloch factor and d_i its width in periods. Equation (4) can easily be generalized for coatings with larger m and/or more layers.

Finding a two-layer antireflection coating is equivalent to solving Eq. (4) for $\rho=0$. For PCs, there is no simple link between Bloch factor μ and impedance ζ, so we solve the equation by numerical search—we try many different PCs as the coating layers until we find a combination for which $|\rho|^2 \simeq 0$. This requires calculating all $\mathbf{R}_{ij}$ between the PCs considered. For a set of n PCs, doing this directly takes n^2-n simulations, which is impractical as n is large. However, it takes only n simulations to find all PC impedances, from which we can easily calculate the $\mathbf{R}_{ij}$ using Eqs. (3a)–(3c).

Our first coating is for the PC of Fig. 1, for normally incident light of frequency $d/\lambda=0.25$. Without a coating, the bulk PC has reflectance $R=0.36$. The reflectances at surrounding frequencies are shown in Fig. 2. We aim to design a two-layer coating where the layers, PCs 1 and 2, differ

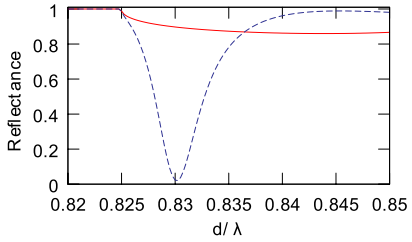

FIG. 3. (Color online) Reflectances for $\theta_0=25^\circ$ off the uncoated (solid) and coated (dashed) structures.

from the bulk PC only in their rod radii r_1 and r_2. At this low frequency, $p=1$ so we choose $m=1$ to reduce ζ, $\mathbf{R}$, $\mathbf{T}$, and μ to scalars.

To design a coating, we first generate a database of $\zeta(r)$ and $\mu(r)$ at this frequency and incident angle, analogous to the tables of refractive indices used in the design of thin film coatings. This is the most computationally intensive step of the coating design, involving finite element transfer matrix analysis of each PC to find its Bloch modes and $\mathbf{E}$. We then use $\zeta(r)$ and $\mu(r)$ in Eq. (4) to find $R(r_1,r_2)=|\rho(r_1,r_2)|^2$ numerically, assuming each layer is one period thick.

We find that $R\simeq 0$ when $r_1=0.137\ d$ and $r_2=0.156\ d$. A more rigorous calculation with larger m confirms that $R\simeq 10^{-6}$—we have indeed designed an antireflection coating. Figure 2 shows that the coating has a wide bandwidth. This unintentional but desirable result may be enhanced by explicitly designing a broadband coating with more layers.

So far, a scalar impedance has yielded results sufficiently accurate to design coatings. We now develop a coating for the same bulk PC under circumstances in which $p=2$, where matrix impedances are required. We choose $d/\lambda=0.83$ and $\theta_0=25^\circ$. At this frequency and incident angle, there is only one propagating Bloch mode in the bulk PC. The part of the beam reflected off the PC is scattered into two propagating plane waves. We take R to be the sum of the two plane wave reflectances, shown for a range of frequencies in Fig. 3. At the target frequency, $R=0.897$.

As $p=2$, we choose $m=\dim(\zeta)=2$, and again we generate a database of $\zeta(r)$ and $\mu(r)$. Using a matrix generalization of Eq. (4), we find a two-layer coating for which $R=0.023$—the layers have widths $d_1=1$ and $d_2=2$, and rod radii $r_1=0.102$ and $r_2=0.217$. Accurate reflectances ($m=5$) at other d/λ are shown in Fig. 3. Note that the minimum R does not quite occur at the target frequency—this indicates that we have insufficient degrees of freedom to suppress both of the reflected plane waves simultaneously. To design a coating with $R=0$, we would need to add more degrees of freedom, e.g., by using more layers or rectangular lattices.

We saw in Fig. 1 that scalar versions of our impedance do not work in general. In fact, any scalar impedance or treatment of reflections is doomed to inconsistency if there are multiple propagating plane waves, i.e., if $p\geqslant 2$. To show this, we consider as an example reflections between PC1, PC2 and PC3 with radii 0.08 d, 0.12 d, and 0.18 d, respectively. At $\theta_0=25^\circ$ and $d/\lambda=0.83$, $p=2$, and each of these PCs has one propagating Bloch mode. We first rigorously calculate r_{ij} and t_{ij} for each pair of PCs. These are the mappings between propagating modes that any correct scalar impedance method must predict. We note that $|r_{23}|^2=0.8053$. We now recalculate $|r_{23}|^2$ indirectly, using r_{12}, r_{21}, t_{12}, t_{21}, r_{13}, and t_{13} and considering there to be an infinitesimal sliver of PC1 between PC2 and PC3 (cf. derivation of $\mathbf{A}_{01}^{-1}\mathbf{A}_{02}=\mathbf{A}_{12}$). If we were willing to assume that $r_{ij}=-r_{ji}$, we could have derived an equivalent expression for $|r_{23}|^2$ from Eq. (2), independent of the definition of Z. We find that $|r_{23}|^2=0.1886$, nowhere near the correct value. Repeating this calculation with larger $\mathbf{R}_{ij}$ and $\mathbf{T}_{ij}$ matrices, we find $|r_{23}|^2=0.8067$ for $m=2$ and $|r_{23}|^2=0.8054$ for $m=3$, much closer to the correct result. Therefore scalars are not powerful enough to represent reflection fully, and no consistent scalar Z can be defined for these PCs.

We have rigorously defined an impedance-like matrix ζ that can be used for accurate calculation of coupling losses in up-down symmetric PCs and have presented a least square approximation to control its dimension. Furthermore, we have demonstrated the utility of this impedance by applying it to design antireflection coatings for a PC. Our definition of PC impedance should also enable the design of other simple coatings inspired by thin film optics.

This work was produced with the assistance of the Australian Research Council (ARC). CUDOS (the Centre for Ultrahigh-bandwidth Devices for Optical Systems) is an ARC Centre of Excellence.

[1] B. Momeni and A. Adibi, Appl. Phys. Lett. **87**, 171104 (2005).
[2] J. Witzens, M. Hochberg, T. Baehr-Jones, and A. Scherer, Phys. Rev. E **69**, 046609 (2004).
[3] T. Baba and D. Ohsaki, Jpn. J. Appl. Phys., Part 1 **40**, 5920 (2001).
[4] T. Baba, T. Matsumoto, and M. Echizen, Opt. Express **12**, 4608 (2004).
[5] S. Boscolo, C. Conti, M. Midrio, and C. G. Someda, J. Lightwave Technol. **20**, 304 (2002).
[6] J. Ushida, M. Tokushima, M. Shirane, A. Gomyo, and H. Yamada, Phys. Rev. B **68**, 155115 (2003).
[7] R. Biswas, Z. Y. Li, and K. M. Ho, Appl. Phys. Lett. **84**, 1254 (2004).
[8] M. Mazilu and K. Dholakia, Opt. Express **14**, 7709 (2006).
[9] B. Momeni, A. A. Eftekhar, and A. Adibi, Opt. Lett. **32**, 778 (2007).
[10] L. C. Botten, T. P. White, A. A. Asatryan, T. N. Langtry, C. M. de Sterke, and R. C. McPhedran, Phys. Rev. E **70**, 056606 (2004).
[11] G. Y. Vahn, T. P. White, M. J. Steel, C. M. de Sterke, K. Dossou, and L. C. Botten, J. Appl. Phys. **102**, 053103 (2007).
[12] O. S. Heavens, *Optical Properties of Thin Solid Films* (Dover, London, 1991).

One of the key results of Letter 2.1 is that for certain frequencies and PCs, no scalar impedance that satisfies Eq. (2) (Eq. (1.9) in the main text of this thesis) can be defined. The three PCs used to demonstrate this each support only one pair of propagating modes at the operating frequency. The three interfaces presented are each between semi-infinite media, so the evanescent modes do not carry energy here. Nevertheless they clearly play enough of a role in the coupling between propagating modes that they may not be neglected. For this example, which was not hard to find, none of the impedance definitions from Secs. 1.6.1–1.6.3 could give correct answers in all three cases.

Our impedances ζ_1 and ζ_2 are defined such that

$$\mathbf{R}_{12} = (\mathbf{Z}_{12} + \mathbf{I})^{-1}(\mathbf{Z}_{12} - \mathbf{I}), \tag{2.2}$$

where

$$\mathbf{Z}_{12} = (\zeta_1^{-1}\zeta_2)(\zeta_1^{-1}\zeta_2)^T = \mathbf{H}_1^T\mathbf{E}_2\mathbf{E}_2^T\mathbf{H}_1. \tag{2.3}$$

$\mathbf{R}_{12}$ is in the Bloch basis: from a vector $\mathbf{c}_1^+$ of incident Bloch mode amplitudes it gives the reflected Bloch mode amplitudes $\mathbf{c}_1^-$. For square lattices, $\mathbf{Z}_{12}$ was initially derived by setting $\mathbf{c}_2^- = \mathbf{0}$ and manipulating the resulting equations into the form

$$\mathbf{c}_1^+ + \mathbf{c}_1^- = \mathbf{Z}_{12}(\mathbf{c}_1^+ - \mathbf{c}_1^-). \tag{2.4}$$

Using the mode orthogonality relation for square lattice PCs, i.e.

$$\mathbf{E}^T\mathbf{H} = \mathbf{H}^T\mathbf{E} = \mathbf{I}, \tag{2.5}$$

if all matrices are square and have inverses then we can rewrite Eq. (2.3) as

$$\mathbf{Z}_{12} = {\mathbf{E}_1}^{-1}\mathbf{E}_2{\mathbf{H}_2}^{-1}\mathbf{H}_1. \tag{2.6}$$

As we discuss in Sec. IV. of Paper 2.3, this has the same form as a ratio of wave impedances

$$Z_{12} = Z_2/Z_1 = E_2/H_2\ H_1/E_1, \tag{2.7}$$

the obvious difference being that Eq. (2.6) is a matrix equation, while Eq. (2.7) is a scalar equation. The order of factors is fixed in Eq. (2.6) because matrices do not commute—they may not be rearranged to separate $\mathbf{Z}_{12}$ into one matrix that depends on PC 1 and another for PC 2. To escape this entanglement, we separate $\mathbf{Z}_{12}$ into two factors, writing each factor as the product of two impedance matrices ζ_1^{-1} and ζ_2 (Eq. (2.3)), each of which are defined with respect to a common reference medium (vacuum, in all examples in this thesis). These impedance matrices can be used to calculate $\mathbf{R}_{12}$ as we have just shown, as well as $\mathbf{T}_{12}$, $\mathbf{R}_{21}$ and $\mathbf{T}_{21}$, all of which work in the relevant bases of Bloch modes.

Comparison to $\mathbf{Z}_{\text{Fallahi}}$

It is interesting to compare our impedance matrix to that of Fallahi and Hafner [123], discussed in Sec. 1.6.4. In contrast to ours, Fallahi and Hafner's definition is not related to the Bloch modes of either PC: its domain is a common basis. In their paper they use the basis of grating orders (Eq. (9) in Ref. [123]), making comparison with our work easy. Considering only the field from a superposition of forward Bloch modes, they define

$$\begin{pmatrix}\tilde{\mathbf{E}}_z\\ \tilde{\mathbf{E}}_x\end{pmatrix} = \mathbf{Z}_{\text{Fallahi}}\begin{pmatrix}\tilde{\mathbf{H}}_x\\ -\tilde{\mathbf{H}}_z\end{pmatrix}, \tag{2.8}$$

where $\tilde{\mathbf{E}}_z$ is a vector of the E_z amplitudes of the grating diffraction orders, the $E_{\parallel}(\mathbf{0})$ from Eq. (1.5) in the E_z polarisation; the other field amplitude vectors are similarly defined. We have relabelled the axes to be consistent with our treatment. In our method, the two polarisations are treated separately, so for the purpose of comparison we restrict our attention to the E_z polarisation, offering a simplified version of Fallahi and Hafner's definition,

$$\tilde{\mathbf{E}}_z = \mathbf{Z}_{\mathrm{F}} \tilde{\mathbf{H}}_x. \tag{2.9}$$

The fields $\tilde{\mathbf{E}}_z$ and $\tilde{\mathbf{H}}_x$ are some arbitrary superposition of only forward Bloch modes. For any superposition of modes $\mathbf{c}^+$, we can write these fields using the quantities from our framework,

$$\tilde{\mathbf{E}}_z = \mathbf{E}\,\mathbf{c}^+ \tag{2.10a}$$

$$\tilde{\mathbf{H}}_z = \mathbf{H}\,\mathbf{c}^+. \tag{2.10b}$$

Inserting Eqs. (2.10) into (2.9), multiplying by $\mathbf{H}^T$ and applying the mode orthogonality relation Eq. (2.14), we see that for any $\mathbf{c}^+$,

$$\mathbf{c}^+ = \mathbf{H}^T \mathbf{Z}_{\mathrm{F}} \mathbf{H}\,\mathbf{c}^+. \tag{2.11}$$

By the mode orthogonality relation, this equality always holds when

$$\mathbf{Z}_{\mathrm{F}} = \mathbf{E}\mathbf{E}^T. \tag{2.12}$$

Comparing this to our impedance matrix ζ, we find

$$\zeta\zeta^T = \mathbf{H}_0^T \mathbf{Z}_{\mathrm{F}} \mathbf{H}_0. \tag{2.13}$$

2.2 Triangular lattice PCs

In the Letter we do not explicitly derive its Eqs. (3), the expressions for $\mathbf{R}$ and $\mathbf{T}$ in terms of impedances. We do so in the next paper, and extend the impedance definition to triangular lattice PCs, in which the lattice vectors are not orthogonal. This fact complicates the up-down symmetry used to relate forward and backward modes. For square and rectangular lattice PCs with up-down symmetric unit cells, the matrix $\mathbf{E}$ may be applied to vectors $\mathbf{c}^+$ of forward Bloch modes as well as to vectors $\mathbf{c}^-$ of backward modes, to find the field amplitude $E_{\parallel}$ in each grating order.

For triangular lattices, in which each grating is displaced by $d_x/2$ from the prior, the matrices $\mathbf{QE}$ and $\mathbf{QH}$ must instead be used for backward modes $\mathbf{c}^-$. The matrix $\mathbf{Q}$ is diagonal, consisting of alternating ± 1 entries—it represents the relative phase change between grating diffraction orders associated with shifting the phase origin by $d_x/2$.

This change complicates many things, including the mode orthogonality relations Eq. (2.5), which for triangular lattices become

$$\mathbf{E}^T\mathbf{H} + \mathbf{H}^T\mathbf{E} = \mathbf{I} \tag{2.14a}$$

$$\mathbf{E}^T\mathbf{Q}\mathbf{H} - \mathbf{H}^T\mathbf{Q}\mathbf{E} = \mathbf{0}. \tag{2.14b}$$

Note that relations for square or rectangular lattices may be retrieved from Eqs. 2.14 by setting $\mathbf{Q} = \mathbf{I}$, although the implied normalisation of $\mathbf{E}$ and $\mathbf{H}$ has changed by a factor $1/\sqrt{2}$ each. We use this new normalisation in Paper 2.3 and the remainder of this thesis, so that the orthogonality relations for square and triangular lattices have similar forms.

As for the square case, the impedance is defined by semi-analytically calculating the reflection and transmission at a PC-PC interface, then writing

the resulting equation in terms of one matrix per PC, which is the PC's impedance. These two steps each pose challenges. The first step is not entirely new—a method was presented for square lattice PCs that share a background refractive index by Botten *et al.* [108]. In Sec. II B of the next paper we present both steps but focus on the second, using a compact notation that abstracts away some of the physics of the first step. Therefore we now present a less abbreviated version of the first step, finding $\mathbf{R}$ and $\mathbf{T}$ matrices.

2.2.1 Derivation of $\mathbf{R}_{12}$ and $\mathbf{T}_{12}$

The reflection and transmission at an interface between PCs, i.e. the relatationship between incoming and outgoing Bloch modes in the two PCs, can be found directly by equating the tangential field components across the interface. The interface between PCs is slightly nebulous: if the PCs share a background medium then there is no physical interface, only an imaginary line across which it makes more sense to represent the field by the other PC's Bloch modes. If the PCs do not share a background medium, then there is also a dielectric interface. It is convenient to enforce field continuity across the interface in the basis of grating orders: once in this basis the problem may be decoupled into a set of problems that each only involve the forward and backward plane waves associated with one diffraction order (Sec. 1.2.1).

We consider two adjacent PCs, with light incident from PC 1, i.e., we fix $\mathbf{c}_2^- = \mathbf{0}$. Enforcing field continuity across the interface, we obtain

$$\mathbf{E}_1\mathbf{c}_1^+ + \mathbf{Q}\mathbf{E}_1\mathbf{c}_1^- = \mathbf{E}_2\mathbf{c}_2^+ \tag{2.15a}$$

$$\mathbf{H}_1\mathbf{c}_1^+ - \mathbf{Q}\mathbf{H}_1\mathbf{c}_1^- = \mathbf{H}_2\mathbf{c}_2^+. \tag{2.15b}$$

From these equations we can find $\mathbf{R}_{12}$ and $\mathbf{T}_{12}$. First we find $\mathbf{c}_2^+$ in terms of $\mathbf{c}_1^+$, by calculating ${\mathbf{E}_1}^T$(2.15b)+${\mathbf{H}_1}^T$(2.15a), then applying the orthogonality relations (2.14) to obtain

$$\mathbf{c}_1^+ = ({\mathbf{H}_1}^T\mathbf{E}_2 + {\mathbf{E}_1}^T\mathbf{H}_2)\mathbf{c}_2^+. \tag{2.16}$$

Therefore,

$$\mathbf{T}_{12} = ({\mathbf{H}_1}^T\mathbf{E}_2 + {\mathbf{E}_1}^T\mathbf{H}_2)^{-1}. \tag{2.17}$$

Similarly, to find $\mathbf{R}_{12}$ we seek an expression for $\mathbf{c}_1^-$ in terms of $\mathbf{c}_1^+$, by calculating ${\mathbf{E}_2}^T\mathbf{Q}$(2.15b)−${\mathbf{H}_2}^T\mathbf{Q}$(2.15a):

$$({\mathbf{H}_2}^T\mathbf{Q}\mathbf{E}_1 - {\mathbf{E}_2}^T\mathbf{Q}\mathbf{H}_1)\mathbf{c}_1^+ + ({\mathbf{H}_2}^T\mathbf{E}_1 + {\mathbf{E}_2}^T\mathbf{H}_1)\mathbf{c}_1^- = \mathbf{0}. \tag{2.18}$$

Rearranging, we see that

$$\mathbf{R}_{12} = ({\mathbf{H}_2}^T\mathbf{E}_1 + {\mathbf{E}_2}^T\mathbf{H}_1)^{-1}({\mathbf{H}_2}^T\mathbf{Q}\mathbf{E}_1 - {\mathbf{E}_2}^T\mathbf{Q}\mathbf{H}_1). \tag{2.19}$$

Here we derived expressions for $\mathbf{R}_{12}$ and $\mathbf{T}_{12}$ that require two matrices per PC: $\mathbf{E}$ and $\mathbf{H}$. Each of these matrices is half the original dimension of the transfer matrix, so we have gained some efficiency by enforcing symmetry between forward and backward modes. The framework is also more amenable to physical insight than transfer or scattering matrices, as the amplitude of each Bloch mode in the system is readily apparent and it is easy to enforce conditions such as $\mathbf{c}_2^- = \mathbf{0}$. But in order to obtain an impedance, we must find a single matrix per PC to do this job. We do this in Paper 2.3, which follows.

A point of notational difference between this paper and the remainder of the thesis is that for consistency with [108], in this paper we use $\alpha \equiv k_x = k_\parallel$ and $\chi \equiv k_y = k_\perp$.

Impedance of square and triangular lattice photonic crystals

Felix J. Lawrence,[1,*] Lindsay C. Botten,[2] Kokou B. Dossou,[2] C. Martijn de Sterke,[1] and R. C. McPhedran[1]
[1]*Centre for Ultrahigh-bandwidth Devices for Optical Systems (CUDOS) and School of Physics, University of Sydney, New South Wales 2006, Australia*
[2]*Department of Mathematical Sciences and CUDOS, University of Technology, Sydney, New South Wales 2007, Australia*
(Received 15 June 2009; published 31 August 2009)

We give a rigorous semianalytical definition of impedance for square and triangular (hexagonal) lattice two-dimensional photonic crystals (PCs). Our impedance is a small matrix, derived from transfer matrices, which stores the information required to calculate the reflection and the transmission between PCs. We apply our definition to design PC antireflection coatings efficiently. This task is $O(n)$ with the number of candidate PCs as only one simulation per PC is required to find the impedances; the reflection and the transmission properties of a large number of coatings may then be evaluated quickly using the impedances in a simple matrix equation, in a way similar to the design of thin-film coatings. This is much faster than directly finding the reflections and the transmissions between pairs of candidate PCs, which requires one simulation per pair, a task that is $O(n^2)$.

DOI: 10.1103/PhysRevA.80.023826 PACS number(s): 42.70.Qs, 42.79.Wc

I. INTRODUCTION

Bulk two-dimensional photonic crystals (PCs) have several in-band applications, including the use as superprisms [1] and supercollimators [2]. In the photonic band gap, where no light can propagate, bulk PCs are used as mirrors for solar cells [3]. Unfortunately the interesting in-band properties of bulk PCs often occur close to a band edge, and so are plagued by large insertion loss. This not only degrades the signal but also leads to stray light, thwarting the integration of several such components into a device. The losses can be reduced by adiabatic mode matching structures, which by nature must be long, and therefore are unfriendly to miniaturization. Alternatively the insertion loss may be reduced by shorter (and thus more practical) antireflection coatings (Fig. 1). These coatings work by introducing additional PC-PC interfaces, carefully chosen to create additional reflections that interfere destructively with the other reflections, leaving zero or low net reflectance. In this paper we provide the tools to find such coatings and demonstrate their utility by designing three antireflection coatings.

If we aim to find a two-layer PC antireflection coating like Fig. 1, considering m candidate PCs for each layer, then there are m^2 possible such coatings. Therefore, it is important to be able to find the reflection and the transmission at PC-PC interfaces quickly and efficiently. For uniform dielectrics, thin-film antireflection coatings are commonplace and the essential tool in their design is *impedance*, or more specifically *wave impedance*, defined to be

$$Z_w = E_\parallel / H_\parallel, \tag{1}$$

where $E_\parallel$ and $H_\parallel$ are the field components tangential to the interface. For isotropic nonmagnetic materials, Z_w is inversely proportional to the refractive index n at normal incidence; for the incident angle θ it is proportional to either $n\cos(\theta)$ or $n/\cos(\theta)$ depending on polarization, with the vacuum impedance Z_0 as the constant of proportionality. Impedance is also defined for transmission lines and acoustics, and in all these fields the reflection at an interface between two media, traveling from medium 1 toward medium 2, is

$$r_{12} = \frac{Z_2/Z_1 - 1}{Z_2/Z_1 + 1}, \tag{2}$$

where Z_i is the wave impedance of medium i. Equation (2) is equivalent to the Fresnel reflection coefficient.

An equivalent definition of impedance for photonic crystals has not been forthcoming. There is one rigorous definition of scalar PC impedance [4], but it is valid only at low frequencies. In our previous work [5] we gave a rigorous semianalytical matrix definition of impedance that is valid at all frequencies and incident angles, but only for square lattices. Here, we elaborate on our method and extend it to treat triangular lattices and 45° rotated square lattices.

Previously [5] we set down three criteria for a useful impedance—a PC's impedance must:

(i) *incorporate sufficient information* about the PC to yield the reflection and the transmission between it and any other PC;

(ii) *be uniquely defined* for a PC at a given frequency, incident angle, and polarization; and

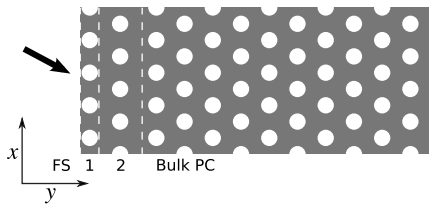

FIG. 1. A PC with a two-layer coating. Light, represented by the arrow, is incident from free space (FS) on the left. The first layer's PC is derived from the bulk PC by compressing its unit cell in the y direction; the second layer's PC is derived by stretching the unit cell.

*felix@physics.usyd.edu.au

(iii) be as *compact* as possible, i.e., easy to store.

When considering propagation in PCs, the Bloch (eigenmode) basis is the natural choice. Since each PC has a different set of propagating and evanescent Bloch modes, and each mode in one PC may couple to several modes in another PC, we need to consider several Bloch modes simultaneously for each PC. Therefore, transmission coefficients must be replaced with transmission matrices mapping the incident PC's Bloch basis to the receiving PC's basis, and reflection coefficients should also be replaced with reflection matrices, which change the basis from forward to backward propagation or vice versa. As reflections and transmissions are best represented by matrices, it is sensible to look for matrix representations of the impedance.

Section II of this paper presents our definition of impedance. In Sec. II A we define $\mathcal{E}$, a matrix that maps Bloch mode amplitudes to electric and magnetic field amplitudes in the plane-wave basis and give reciprocity-based mode orthogonality relations for $\mathcal{E}$. We derive impedance matrices in Sec. II B by considering a PC-PC interface and deriving expressions for the reflection and the transmission matrices in either direction, using the PCs' $\mathcal{E}$ matrices to enforce field continuity. From these expressions we eventually obtain impedance matrices for each PC. In Sec. III we apply our definition to design antireflection coatings for two PCs. We design single-frequency V coatings that reduce near-unit reflectance to 10^{-3}, as well as multifrequency antireflection coatings that reduce reflections over a chosen frequency range. We conclude in Sec. IV by interpreting our impedance and discussing its similarities and differences to conventional wave impedance.

II. THEORY

Our approach is a semianalytical least-squares based method. The basis change matrix between each PC's Bloch basis and the plane-wave basis, found numerically using a transfer-matrix method [6], is used analytically to solve for reflections and transmissions and find an impedance. In practice we work with a truncated set of modes and a less strongly truncated set of plane waves, so the basis change matrix is actually a projection and our results are least-squares approximations that exploit the orthogonality of modes.

Our conventions are that the z axis points out of the plane in which dielectric constant varies with position, and the x axis is parallel to the interface between PCs (Fig. 1). In each instance we consider incident light propagating at a given frequency and incident angle (to the y axis) and polarized with either the **E** or the **H** field pointing out of the lattice plane.

We consider the photonic crystal to be a stack of gratings, each of which scatters light into a countably infinite set of plane-wave diffraction orders s, which are given by the grating equation

$$\alpha_s = \alpha_0 + \frac{2\pi s}{d}, \quad s = 0, \pm 1, \pm 2, \ldots, \tag{3}$$

where d is the period along the grating and $\alpha_s = (\mathbf{k}_s)_x = k \sin \theta_s$ with k as the wave number in the background medium and θ_s as the diffraction angle (when real). Note that, for incident angle θ_i, the zeroth diffracted order has $\alpha_0 = k \sin \theta_i$.

To find the quantities needed for the impedance definition, we use a numerical transfer-matrix method [7]. The transfer matrix $\mathcal{T}$ encapsulates the scattering properties of a grating—a one-period layer of the PC. It maps a vector of incident and outgoing plane-wave coefficients on one side of a PC's unit cell to the corresponding vector on the other side of the unit cell. The plane waves represented in this vector are the propagating and the evanescent grating diffraction orders. For perfect accuracy, $\dim(\mathcal{T})$ must be infinite; however, in practice we truncate $\mathcal{T}$ to consider only the propagating and slowly evanescent plane waves—we ignore any that decay across the unit cell by more than a factor of 10^5. The transfer matrix $\mathcal{T}$ is diagonalized to give a diagonal matrix of Bloch factors and a matrix of eigenvectors $\mathcal{F}$ in which each column represents a Bloch mode and each row represents a plane wave. In Secs. II A and II B, the impedance matrix $\mathcal{Z}$ is defined from $\mathcal{F}$. We may optionally make a second truncation, removing the columns of $\mathcal{F}$ that correspond to the most strongly evanescent modes—this approximation reduces the dimension of the impedance matrix $\mathcal{Z}$, which is a square matrix with dimension equal to half the number of columns in $\mathcal{F}$. We now explain this procedure more fully.

A. Nomenclature and orthogonality

We expand the field in each PC in terms of its propagating and evanescent Bloch modes. Following Botten *et al.* [6], we partition the modes into forward and backward sets by the direction of energy transport (for propagating modes) or decay (for evanescent modes). At any given frequency, incident angle, and polarization, there is a countable infinity of modes, but in most circumstances only a handful propagate. We truncate the set of Bloch modes to the propagating and most slowly evanescent modes, as the strongly evanescent modes are not important.

Each Bloch mode can be expanded in the plane-wave basis of grating diffraction orders s. In the E_z polarization where the **E** field is out of plane, the field E_z about the interface due to a given mode m is

$$E_{zm}(\mathbf{r}) = \sum_{s=-\infty}^{\infty} Y_s^{-1/2} (f_{m,s}^{+} e^{i\chi_s y} + f_{m,s}^{-} e^{-i\chi_s y}) e^{i\alpha_s x}, \tag{4}$$

where $f_{m,s}^{+}$ and $f_{m,s}^{-}$ are the coefficients of the plane waves of diffraction order s, respectively, in the $+y$ and the $-y$ directions; $\chi_s = (\mathbf{k}_s)_y = \sqrt{k^2 - \alpha_s^2}$; and $Y_s = \chi_s/(\omega\mu_0)$ is the *wave admittance* for plane-wave order s, i.e., $Y_s = \sqrt{\epsilon/\mu_0}\cos(\theta_s)$, where the possibly complex θ_s is found from α_s, determined by the grating equation (3). For propagating diffraction orders, Y_s is the ratio of field components in the grating plane, $H_\parallel/E_\parallel$. The coefficient $Y_s^{-1/2}$ was chosen so that for the propagating orders, $f_{m,s}^{\pm}$ are normalized to unit flux with a comparable normalization for the contrapropagating evanescent modes [7].

From Maxwell's equations we can derive

$$H_{xm}(\mathbf{r}) = \sum_{s=-\infty}^{\infty} Y_s^{+1/2}(f_{m,s}^{+}e^{i\chi_s y} - f_{m,s}^{-}e^{-i\chi_s y})e^{i\alpha_s x}, \tag{5}$$

where we use the relation $\chi_s/(\omega\mu_0)=Y_s$. For the other polarization H_z, an expression for $H_{zm}(\mathbf{r})$ may be obtained from the right-hand side (RHS) of Eq. (4) by replacing Y_s with the wave impedance $Z_s=\sqrt{\mu_0/\epsilon}\cos(\theta_s)$, and $E_{xm}(\mathbf{r})$ can be found from the RHS of Eq. (5) by replacing $Y_s^{+1/2}$ with $-Z_s^{+1/2}$.

For the forward modes, we write down $\mathbf{F}_+$, the matrix of coefficients $f_{m,s}^{+}$ that maps forward Bloch mode amplitudes to forward plane-wave amplitudes. Similarly, to map forward Bloch mode amplitudes to backward plane-wave amplitudes, we write down $\mathbf{F}_-$ from $f_{m,s}^{-}$. We denote the corresponding matrices for backward modes with a prime: $\mathbf{F}'_+$ and $\mathbf{F}'_-$. Combining these into the matrix

$$\mathcal{F}=\begin{pmatrix}\mathbf{F}_+ & \mathbf{F}'_+\\ \mathbf{F}_- & \mathbf{F}'_-\end{pmatrix}, \tag{6}$$

we have the matrix of eigenvectors for the transfer matrix $\mathcal{T}$ of a single grating layer, i.e., $\mathcal{T}=\mathcal{F}\mathcal{L}\mathcal{F}^{-1}$, where $\mathcal{L}$ is a diagonal matrix of Bloch factors [7]. In practice $\mathcal{F}$ is found by diagonalizing the transfer matrix $\mathcal{T}$ using standard eigenvalue methods.

For a square or a triangular lattice photonic crystal with a 180° rotationally symmetric unit cell, the backward modes are related to the forward modes as follows:

$$\mathcal{F}=\begin{pmatrix}\mathbf{F}_+ & \mathbf{Q}\mathbf{F}_-\\ \mathbf{F}_- & \mathbf{Q}\mathbf{F}_+\end{pmatrix}, \tag{7}$$

where $\mathbf{Q}$ is a diagonal matrix of plane-wave phase factors that encapsulates the deviation from a rectangular lattice. For a square or a rectangular lattice $\mathbf{Q}=\mathbf{I}$, and for triangular and 45° rotated square lattices, or indeed any case in which every grating is displaced by half a period from the preceding grating, $\mathbf{Q}=\mathrm{diag}(e^{is\pi})$. The mode orthogonality relations that we use here are based on reciprocity, which manifests itself in the symplectic nature of the transfer matrix [7]. The orthogonality relations yield

$$\mathcal{F}^T\mathbf{K}_Q\mathcal{F}=\mathbf{K}_I, \tag{8}$$

where $\mathbf{K}_Q=\left(\begin{smallmatrix}\mathbf{0} & \mathbf{Q}\\ -\mathbf{Q} & \mathbf{0}\end{smallmatrix}\right)$ and $\mathbf{K}_I=\left(\begin{smallmatrix}\mathbf{0} & \mathbf{I}\\ -\mathbf{I} & \mathbf{0}\end{smallmatrix}\right)$. One can also derive orthogonality relations based on energy conservation that involve Hermitian transposes, but we use reciprocity-based relations because they are more general, i.e., applicable to both lossy and lossless media.

To map Bloch mode amplitudes to plane-wave field components, we introduce a matrix inspired by Eqs. (4) and (5) at $y=0$ (the interface between layers), with the x factor left out and the terms in the sum for Bloch mode m separated into a vector. These vectors for the various Bloch modes are assembled into a matrix that maps Bloch modes to plane waves, which for the E_z polarization takes the form

$$\mathcal{E}_i=\begin{pmatrix}\mathbf{E}_i & \mathbf{Q}\mathbf{E}_i\\ \mathbf{H}_i & -\mathbf{Q}\mathbf{H}_i\end{pmatrix}=\begin{pmatrix}\mathbf{Y}^{-1/2} & \mathbf{0}\\ \mathbf{0} & \mathbf{Y}^{+1/2}\end{pmatrix}\mathcal{I}\mathcal{F}, \tag{9}$$

where $\mathcal{I}=1/\sqrt{2}\left(\begin{smallmatrix}\mathbf{I} & \mathbf{I}\\ \mathbf{I} & -\mathbf{I}\end{smallmatrix}\right)$ and $\mathbf{Y}=\mathrm{diag}(Y_s)$. $\mathbf{E}_i$ and $\mathbf{H}_i$, respectively, map PC i's forward Bloch mode amplitudes to vectors of E_z and H_x field components, where each element of the vector is a field component for a different diffraction order. These tangential field components are continuous across PC interfaces: $\mathcal{E}_i$ maps PC i's forward and backward Bloch mode amplitudes to the plane-wave diffraction order field components that we equate when calculating reflections and transmissions.

For H_z polarization, where impedances $\mathbf{Z}=\mathrm{diag}(Z_s)$ replace admittances $\mathbf{Y}$, we similarly define

$$\mathcal{E}_i=\begin{pmatrix}\mathbf{H}_i & \mathbf{Q}\mathbf{H}_i\\ -\mathbf{E}_i & \mathbf{Q}\mathbf{E}_i\end{pmatrix}=\begin{pmatrix}\mathbf{Z}^{-1/2} & 0\\ 0 & \mathbf{Z}^{+1/2}\end{pmatrix}\mathcal{I}\mathcal{F}. \tag{10}$$

In either polarization, the Bloch mode orthogonality relations (8) can be rewritten as

$$\mathbf{K}_I\mathcal{E}^T\mathbf{K}_Q\mathcal{E}=\mathbf{I}. \tag{11}$$

As the set of Bloch modes is truncated to a greater extent than the set of plane waves, $\mathcal{E}$ is generally not square, so Eq. (11) provides a left inverse for $\mathcal{E}$.

To find an approximate right inverse for $\mathcal{E}$, we invert the full rank $\mathcal{E}_F=[\mathcal{E}|\mathcal{E}_D]$, where $\mathcal{E}_D$ are columns corresponding to the modes dropped from the truncated set. Using Eq. (11) it can be shown that

$$\mathcal{E}\mathbf{K}_I\mathcal{E}^T\mathbf{K}_Q=\mathbf{I}-\mathcal{E}_D\mathbf{K}_I\mathcal{E}_D^T\mathbf{K}_Q. \tag{12}$$

Our impedance definition neglects terms involving the dropped modes $\mathcal{E}_D$; we include them here, so that we can check the validity of this approximation in Sec. III. We are now suitably equipped to calculate interface reflections and search for an impedance.

B. Impedance derivation

We specify the field in each PC as vectors of Bloch mode amplitudes, e.g., $\mathbf{c}_1=\left(\begin{smallmatrix}\mathbf{c}_1^{+}\\ \mathbf{c}_1^{-}\end{smallmatrix}\right)$, in which $\mathbf{c}_1^{+}$ and $\mathbf{c}_1^{-}$, respectively, contain the forward and the backward Bloch mode amplitudes in PC 1. The reflection and the transmission matrices at an interface between PC 1 and PC 2, for light incident from PC 1, are $\mathbf{R}_{12}$ and $\mathbf{T}_{12}$, respectively. Note that $\mathbf{R}_{12}\neq\mathbf{R}_{21}$; indeed, these matrices are not even comparable as they operate on different Bloch bases. By definition of $\mathbf{R}_{ij}$ and $\mathbf{T}_{ij}$,

$$\mathbf{c}_1^{-}=\mathbf{R}_{12}\mathbf{c}_1^{+}+\mathbf{T}_{21}\mathbf{c}_2^{-}, \tag{13a}$$

$$\mathbf{c}_2^{+}=\mathbf{R}_{21}\mathbf{c}_2^{-}+\mathbf{T}_{12}\mathbf{c}_1^{+}. \tag{13b}$$

We want to find expressions for $\mathbf{R}_{12}$ and $\mathbf{T}_{12}$ in terms of separate "impedance" matrices for the general PC 1 and PC 2. We start by equating the tangential field components, which are continuous across the interface, to find the outgoing modes $\mathbf{c}_1^{-}$ and $\mathbf{c}_1^{+}$ from the incident modes $\mathbf{c}_1^{+}$ and $\mathbf{c}_2^{-}$. Formally, we set

$$\mathcal{E}_1\mathbf{c}_1=\mathcal{E}_2\mathbf{c}_2, \tag{14}$$

where $\mathcal{E}$ for each region was defined in Eqs. (9) and (10) for the E_z and the H_z polarizations, respectively. Since Eq. (14) is exact only at full rank, we proceed in a least-squares sense, projecting Eq. (14) onto the basis of modes for either PC 1 or

2. Using the orthogonality relations (11), we may isolate $\mathcal{I}\mathbf{c}_1$ and $\mathcal{I}\mathbf{c}_2$ that contain symmetrized and antisymmetrized forms

$$\mathcal{I}\mathbf{c}_1 = \mathcal{I}\mathbf{K}_I\mathcal{E}_1^T\mathbf{K}_Q\mathcal{E}_2\mathbf{c}_2 = \begin{pmatrix} \mathbf{A}_{12} & \mathbf{0} \\ \mathbf{0} & \mathbf{B}_{12} \end{pmatrix}\mathcal{I}\mathbf{c}_2, \tag{15a}$$

$$\mathcal{I}\mathbf{c}_2 = \mathcal{I}\mathbf{K}_I\mathcal{E}_2^T\mathbf{K}_Q\mathcal{E}_1\mathbf{c}_1 = \begin{pmatrix} \mathbf{A}_{21} & \mathbf{0} \\ \mathbf{0} & \mathbf{B}_{21} \end{pmatrix}\mathcal{I}\mathbf{c}_1. \tag{15b}$$

Respectively, these may be written as

$$\mathbf{c}_1^+ + \mathbf{c}_1^- = \mathbf{A}_{12}(\mathbf{c}_2^+ + \mathbf{c}_2^-), \tag{16a}$$

$$\mathbf{c}_1^+ - \mathbf{c}_1^- = \mathbf{B}_{12}(\mathbf{c}_2^+ - \mathbf{c}_2^-), \tag{16b}$$

and

$$\mathbf{c}_2^+ + \mathbf{c}_2^- = \mathbf{A}_{21}(\mathbf{c}_1^+ + \mathbf{c}_1^-) \tag{17a}$$

$$\mathbf{c}_2^+ - \mathbf{c}_2^- = \mathbf{B}_{21}(\mathbf{c}_1^+ - \mathbf{c}_1^-), \tag{17b}$$

where in E_z polarization

$$\mathbf{A}_{ij} = \mathbf{H}_i^T(\mathbf{I}+\mathbf{Q})\mathbf{E}_j + \mathbf{E}_i^T(\mathbf{I}-\mathbf{Q})\mathbf{H}_j, \tag{18a}$$

$$\mathbf{B}_{ij} = \mathbf{H}_i^T(\mathbf{I}-\mathbf{Q})\mathbf{E}_j + \mathbf{E}_i^T(\mathbf{I}+\mathbf{Q})\mathbf{H}_j. \tag{18b}$$

For H_z polarization the definitions of $\mathbf{A}_{ij}$ and $\mathbf{B}_{ij}$ are swapped and of opposite sign. A quick inspection yields the useful relation

$$\mathbf{A}_{ij} = \mathbf{B}_{ji}^T, \tag{19}$$

which allows us to rewrite Eqs. (17a) and (16b) in terms of $\mathbf{B}_{12}^T$ and $\mathbf{A}_{12}^T$, respectively.

At full rank, Eqs. (15) hold simultaneously. Substituting Eq. (15b) into Eq. (15a) and using Eq. (19), we see that $\mathbf{A}_{12}\mathbf{B}_{12}^T=\mathbf{I}$. However, when the mode bases have been truncated, generally at most two of Eqs. (16) and (17) may hold simultaneously. To find the impedance in terms of $\mathbf{A}_{12}$, we adopt a hybrid scheme, which analytically preserves energy conservation, and use Eqs. (16a) and (17b).

Substituting Eqs. (13) into Eqs. (16a) and (17b) and rearranging, we find the reflection and the transmission matrices as

$$\mathbf{T}_{12} = 2\mathbf{A}_{12}^T(\mathbf{A}_{12}\mathbf{A}_{12}^T + \mathbf{I})^{-1}, \tag{20a}$$

$$\mathbf{R}_{12} = (\mathbf{A}_{12}\mathbf{A}_{12}^T - \mathbf{I})(\mathbf{A}_{12}\mathbf{A}_{12}^T + \mathbf{I})^{-1}. \tag{20b}$$

Similar expressions involving $\mathbf{B}_{12}$ may be found using Eqs. (16b) and (17a):

$$\mathbf{T}_{12} = 2\mathbf{B}_{12}^T(\mathbf{I} + \mathbf{B}_{12}\mathbf{B}_{12}^T)^{-1}, \tag{21a}$$

$$\mathbf{R}_{12} = (\mathbf{I} - \mathbf{B}_{12}\mathbf{B}_{12}^T)(\mathbf{I} + \mathbf{B}_{12}\mathbf{B}_{12}^T)^{-1}. \tag{21b}$$

Looking at our expressions for $\mathbf{R}_{12}$ and comparing them to Eq. (2), we would like to write $\mathbf{A}_{12}\mathbf{A}_{12}^T=\mathcal{Z}_1\mathcal{Z}_2^{-1}$ or $\mathbf{B}_{12}\mathbf{B}_{12}^T=\mathcal{Z}_2\mathcal{Z}_1^{-1}$ for some impedance matrices $\mathcal{Z}_1$ and $\mathcal{Z}_2$. However, by inspection of the structures of $\mathbf{A}_{12}$ and $\mathbf{B}_{12}$ it is clear that this is generally not possible because the matrices from PC 1 and PC 2 are entangled, i.e., they do not commute. This is further discussed in Sec. IV.

Instead, we separate $\mathbf{A}_{12}$ into a $\mathcal{Z}_1$ and a $\mathcal{Z}_2$ by deriving a transitivity property and choosing a reference PC. Consider the interface between some PC j and the reference PC 0. If we imagine there to be a null sliver of another PC, PC i, at this interface, then like Eq. (14) we may equate $\mathcal{E}_0\mathbf{c}_0=\mathcal{E}_i\mathbf{c}_i$ and $\mathcal{E}_i\mathbf{c}_i=\mathcal{E}_j\mathbf{c}_j$ and write, in analog to Eq. (16a),

$$\mathbf{c}_0^+ + \mathbf{c}_0^- = \mathbf{A}_{0i}(\mathbf{c}_i^+ + \mathbf{c}_i^-), \tag{22a}$$

$$\mathbf{c}_i^+ + \mathbf{c}_i^- = \mathbf{A}_{ij}(\mathbf{c}_j^+ + \mathbf{c}_j^-). \tag{22b}$$

Substituting Eq. (22b) into Eq. (22a) and comparing the result to Eq. (16a), we hypothesize that $\mathbf{A}_{0j}=\mathbf{A}_{0i}\mathbf{A}_{ij}$. This relation may be shown more rigorously by considering the matrix

$$\begin{pmatrix} \mathbf{A}_{0i}\mathbf{A}_{ij} & \mathbf{0} \\ \mathbf{0} & \mathbf{B}_{0i}\mathbf{B}_{ij} \end{pmatrix} = \mathcal{I}(\mathbf{K}_I\mathcal{E}_0^T\mathbf{K}_Q\mathcal{E}_i)(\mathbf{K}_I\mathcal{E}_i^T\mathbf{K}_Q\mathcal{E}_j)\mathcal{I}. \tag{23}$$

Applying Eq. (12), we see that the RHS of Eq. (23) collapses to

$$\mathcal{I}(\mathbf{K}_I\mathcal{E}_0^T\mathbf{K}_Q\mathcal{E}_j)\mathcal{I} = \begin{pmatrix} \mathbf{A}_{0j} & \mathbf{0} \\ \mathbf{0} & \mathbf{B}_{0j} \end{pmatrix} \tag{24}$$

when $\mathcal{E}_0^T\mathbf{K}_Q\mathcal{E}_{Di}\mathbf{K}_I\mathcal{E}_{Di}^T\mathbf{K}_Q\mathcal{E}_j=\mathbf{0}$, i.e., at the full rank. For truncated mode sets, this error term is small when the modes of PC 0 and/or PC j are well represented by the modes of PC i. In practice $\mathcal{E}_0^T\mathbf{K}_Q\mathcal{E}_{Di}\simeq 0$ is an easily calculated sufficient condition for Eq. (24) to hold. We conclude by equating Eqs. (23) and (24) and rearranging to define

$$\mathbf{A}_{ij} \coloneqq \mathbf{A}_{0i}^{-1}\mathbf{A}_{0j}, \tag{25a}$$

$$\mathbf{B}_{ij} \coloneqq \mathbf{B}_{0i}^{-1}\mathbf{B}_{0j}. \tag{25b}$$

As $\mathbf{A}_{0i}$ is independent of PC j and depends only on the fixed reference PC 0, we may rigorously define the impedance of PC i to be $\mathcal{Z}_i=\mathbf{A}_{0i}$ and its admittance to be $\mathcal{Y}_i=\mathbf{B}_{0i}$, i.e.,

$$\mathcal{Z}_i = \mathbf{H}_0^T(\mathbf{I}+\mathbf{Q})\mathbf{E}_i + \mathbf{E}_0^T(\mathbf{I}-\mathbf{Q})\mathbf{H}_i, \tag{26a}$$

$$\mathcal{Y}_i = \mathbf{H}_0^T(\mathbf{I}-\mathbf{Q})\mathbf{E}_i + \mathbf{E}_0^T(\mathbf{I}+\mathbf{Q})\mathbf{H}_i. \tag{26b}$$

Using Eqs. (20a), (20b), and (25a) we find that when light is incident from some PC i onto some PC j the reflection and the transmission matrices in terms of impedance are

$$\mathbf{T}_{ij} = 2(\mathcal{Z}_i^{-1}\mathcal{Z}_j)^T[(\mathcal{Z}_i^{-1}\mathcal{Z}_j)(\mathcal{Z}_i^{-1}\mathcal{Z}_j)^T + \mathbf{I}]^{-1}, \tag{27a}$$

$$\mathbf{R}_{ij} = [(\mathcal{Z}_i^{-1}\mathcal{Z}_j)(\mathcal{Z}_i^{-1}\mathcal{Z}_j)^T - \mathbf{I}][(\mathcal{Z}_i^{-1}\mathcal{Z}_j)(\mathcal{Z}_i^{-1}\mathcal{Z}_j)^T + \mathbf{I}]^{-1}. \tag{27b}$$

Similar equations in terms of admittances are also easy to derive from Eqs. (20a) and (20b) using the $\mathbf{B}_{ij}$ version. We have found no reason, theoretical or numerical, to prefer the use of $\mathcal{Z}$ over $\mathcal{Y}$ or vice versa.

The impedance $\mathcal{Z}_i$ is *sufficient* to find reflection and transmission. For fixed PC 0 it is *defined uniquely*, and its dimen-

sion is equal to the size of the truncated Bloch basis, which (for the PC structures considered here) is usually less than five modes in each direction, so it is also *compact*. Therefore, this definition fulfills all three criteria to be a useful impedance.

III. APPLICATION

To show the utility of our definition, we use it to design antireflection coatings for PCs. This is a practical test for the impedance definition; if the impedance definition was incorrect, then the coatings designed using this formulation would not work. Any incorrectly calculated reflection coefficient invalidates the net reflection off the coated structure. We use our impedance definition to design a coating consisting of two thin PC layers such that the overall structure (Fig. 1) has near-zero net reflectance at a target frequency, incident angle, and polarization. We aim to emulate a two-layer thin-film *V coating*. Such a coating is usually found by fixing the layers' refractive indices and continuously varying their thicknesses until the reflections off each interface cancel, leaving zero net reflection over a narrow frequency range. Two degrees of freedom (i.e., two layers) are required as both the phases and the amplitudes of the reflections must be controlled. For thin films, the reflection off a dielectric with an arbitrary two-layer coating is

$$\rho = \frac{r_{12} + \Lambda_2^2 r_{23} + \Lambda_2^2 \Lambda_3^2 r_{34} + \Lambda_3^2 r_{12} r_{23} r_{34}}{1 + \Lambda_2^2 r_{12} r_{23} + \Lambda_2^2 \Lambda_3^2 r_{12} r_{34} + \Lambda_3^2 r_{23} r_{34}}, \tag{28}$$

where r_{ij} is the reflection in layer i off layer j; and $\Lambda_i = e^{i\phi_i}$, where ϕ_i is the phase change across layer i [8]. For fixed r_{ij}, i.e., fixed n_i, a V coating may be found analytically by solving $\rho = 0$ for ϕ_1 and ϕ_2. The layer thicknesses may easily be found from ϕ_i.

Equation (28) does not generally apply to PCs as they have multiple modes, so require matrix rather than scalar representations of reflection and transmission quantities. A matrix equation analogous to Eq. (28) may be derived for PCs, and we use it to find antireflection coatings, i.e., coatings that have low reflection into propagating plane waves. A PC layer's thickness may not be varied continuously without changing the PC's impedance; any PC must be an integer number of unit cells thick. Therefore we cannot solve the equation solely by manipulating phase factors as is done for thin films. So, instead of fixing the layer materials and solving for the thicknesses, we set the layers to be a fixed number of unit cells thick (e.g., both layers in Fig. 1 are one unit cell thick) and solve for the PC in each layer.

There are many useful continuous degrees of freedom for the PC: the radius, the shape, or the refractive index of the inclusion or the thickness of the unit cell. We choose the last option: leaving the shape of the inclusions unchanged, we vary one lattice vector while holding the transverse lattice vector constant. This degree of freedom was chosen because, experimentally, the hole position is easier to control than the hole size or shape.

Both $\mathbf{R}_{ij}$ and Λ_i depend on the choice of PC i, so it is hard to solve for zero reflection analytically. Any attempt would involve solving a transcendental matrix equation to find the required impedances, followed by the inverse problem of finding PCs that have the required impedances. Instead we use our method's advantage: once we know each PC's impedance, it is easy to find the reflection and the transmission matrices. We therefore generate a database of impedances and Bloch factors for many PCs, which we use to do an exhaustive search over all coatings made from PCs in the database and choose the coating with the lowest reflection.

Without the impedance database, at best we would have to calculate the reflection between each pair of PCs individually before starting the search—with m PCs, this requires $m(m-1)$ simulations so it is a computationally intensive task. Generating the database however takes only m simulations, one per PC. Once we have the database, we can calculate the $m(m-1)$ reflection and transmission matrices using Eqs. (27), which are almost instantaneous compared to a simulation. Using the database, these equations, and the matrix version of Eq. (28), a search over a large number of possible coatings for low reflection is easily performed.

A. V coating

The first PC that we coat is a triangular lattice of cylindrical air holes, with the interface in the Γ-K direction. Its background index is 2.86 and it has a hole radius of $0.25d$, where d is the lattice constant. We coat it for E_z polarized light with frequency $d/\lambda = 0.38$, incident from free space (FS) with angle 30°. Under these conditions the uncoated reflectance is $R = 0.94$. We consider unit cells up to 1.8 times as thick as the regular lattice.

Before generating a database of PC impedances, it remains to choose the impedance matrix dimension. In the PC's background material there are two propagating plane-wave solutions to the grating equation, both of which are generally involved in propagating Bloch modes, so scalar impedances are grossly insufficient. Indeed, for scalar impedances the error term $\mathcal{E}_{D0}^T \mathbf{K}_Q \mathcal{E}_t$ (where t denotes the target PC) has an element of unit magnitude, so this level of approximation is likely unacceptable. For 2×2 impedance matrices, an element of $\mathcal{E}_{D0}^T \mathbf{K}_Q \mathcal{E}_t$ has a magnitude of 0.27, which is also too large. Instead, we use $\mathcal{Z}$ matrices of dimension 3, for which the largest element in $\mathcal{E}_{D0}^T \mathbf{K}_Q \mathcal{E}_t$ is less than 0.03.

We perform an exhaustive search over 15 129 different two-layer coatings with both coating layers arbitrarily chosen to be one unit cell wide (like Fig. 1). This search took less than 1 min on a desktop computer, including database computation. We find that for a coating with layer cell thicknesses $d_1 = 1.52(\sqrt{3}/2)d$ and $d_2 = 0.67(\sqrt{3}/2)d$ [the regular triangular lattice cell thickness is $(\sqrt{3}/2)d$], the net reflection at the target frequency is virtually eliminated: $R \simeq 10^{-3}$. Fields in the structure for the target wavelength are given in Fig. 2, and the coating's antireflection property is confirmed by calculations at full rank (Fig. 3).

If we try this with scalar impedances, ignoring the large error term $\mathcal{E}_{D0}^T \mathbf{K}_Q \mathcal{E}_t$, then we obtain manifestly incorrect reflection coefficients and no valid coating is found due to inaccuracies arising from dropped modes. With 2×2 $\mathcal{Z}$ matrices we find a useful but imperfect coating.

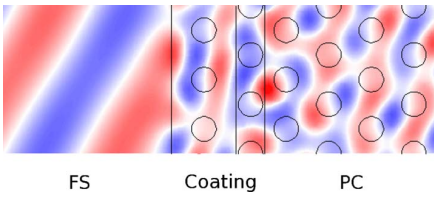

FIG. 2. (Color online) Re(E_z) for PC with antireflection coating. E_z polarized light at $d/\lambda=0.38$ is incident at $\theta_i=30°$ from FS onto the structure. The flat wave fronts in free space indicate low reflectance.

B. Multifrequency coating

Next, we coat the PC from Sec. III A to have low reflectance across the range of frequencies $d/\lambda \in (0.37, 0.39)$. Our algorithm is simple: we choose m candidate PCs and consider a large number of coatings at multiple frequencies across the desired range. We choose the coating that most consistently minimizes the net reflection at each frequency, i.e., the coating that has the lowest maximum reflectance at the frequencies considered.

We consider $m=72$ candidate layer PCs, which are the same as the bulk PC except for the length of one lattice vector, as in Sec. III A. Each PC layer is chosen to be one unit cell wide. We work at 11 different frequencies, evenly spaced across the range $d/\lambda \in (0.37, 0.39)$. As designing a broadband coating is harder than designing a coating for a single frequency, in order to get satisfactory results we use an extra degree of freedom: a third coating layer. This increases the number of possible coatings by a factor m to a total of $11m^3=4\ 105\ 728$ reflectance calculations. With this many calculations, our fast impedance method for calculating coating reflectances is essential.

First, we generate a database of the $11m=792$ impedances. We could build on the impedance database of Sec. III A if we wished, but generating this database from scratch takes about 1 min on a desktop computer. Calculating all the reflectances takes a considerably longer time, 4.6 h (4.1 ms per coating per frequency), and we find that the optimal coating for our above criterion has cell thicknesses d_1 $=1.09(\sqrt{3}/2)d$, $d_2=0.62(\sqrt{3}/2)d$, and $d_3=0.81(\sqrt{3}/2)d$. The maximum reflectance among the 11 frequencies is 0.12. The coating's reflection spectrum calculated at full rank (Fig. 4) confirms that we have found a broadband antireflection coating.

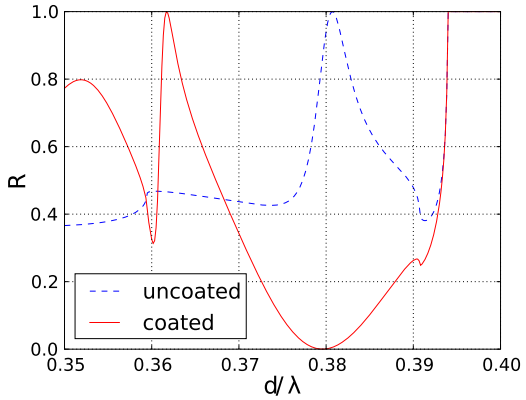

FIG. 3. (Color online) Reflection spectrum of a PC with (solid line) and without (dashed line) a two-layer coating designed for $d/\lambda=0.38$ and $\theta_i=30°$.

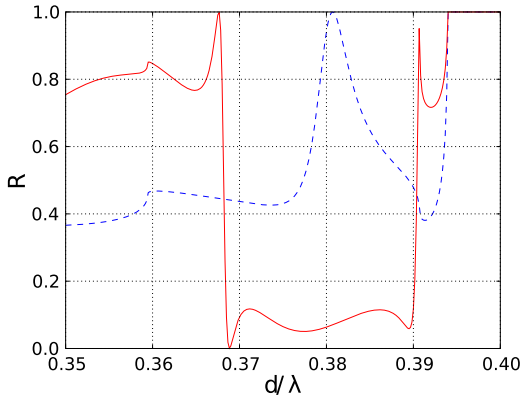

FIG. 4. (Color online) Reflection spectrum of a PC with (solid line) and without (dashed line) a three-layer coating designed to minimize the maximum reflectance over the frequency range $d/\lambda \in (0.37, 0.39)$ with $\theta_i=30°$.

C. Superprism V coating 1

Our next coating is for a superprism presented by Matsumoto *et al.* [1], which consists of air holes in a square lattice rotated by 45°. Considering this lattice as a stack of gratings, every second grating is shifted by $d/2$, so $\mathbf{Q}=\mathrm{diag}(e^{is\pi})$ as for a triangular lattice. The background index is 2.963, and the hole radius is $0.312d$. The light is incident in H_z polarization from the background material at an incident angle of 10° to the normal. The PC acts as a superprism for frequencies $d/\lambda \in (0.295, 0.315)$, and we choose $d/\lambda=0.31$ as our target. At this frequency there are three propagating modes in the incident dielectric and one in the superprism itself. It is noted in the original paper that without an antireflection structure virtually no light couples into the PC—we find that for the uncoated structure $R=0.93$.

Following the same procedure as above, again choosing $\dim(\mathcal{Z})=3$, we search over 48 841 two-layer coatings with each layer one unit cell wide, taking 2.5 min on a desktop computer. The lowest reflectance we find in this set of coatings is $R=0.43$; the phase change across each layer is not enough to control the net reflection adequately. Instead, we search for a coating with an outer layer two unit cells wide and an inner layer one unit cell wide. Naturally this step does not require us to recalculate our database of impedances. We find a coating with $R=0.05$ at the target frequency (Fig. 5). The coating has cell thicknesses $d_1=(2.65/\sqrt{2})d$ and d_2 $=(3.04/\sqrt{2})d$, compared to the regular lattice with $(1/\sqrt{2})d$. The feature around $d/\lambda=0.31$ is due to a Fabry-Perot-like resonance inside the coating.

D. Superprism V coating 2

The coating in Sec. III C is not as successful as that in Sec. III A. This is because there are three propagating dif-

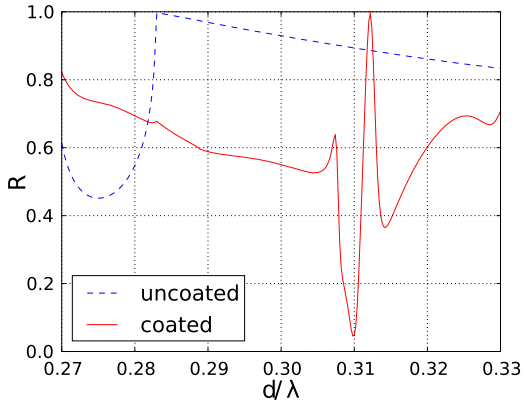

FIG. 5. (Color online) Reflection spectrum of the Matsumoto superprism [1] with (solid line) and without (dashed line) a two layer coating, incident from $n=2.963$ dielectric. R is reduced from 0.90 to 0.05 at $d/\lambda=0.31$.

fraction orders in the incident medium at $d/\lambda=0.31$ and $\theta_i=10°$, and an antireflection coating must suppress the reflections into each of these channels. Individually, each order requires two degrees of freedom for reflections to be eliminated. To show that there is nothing intrinsically difficult about coating the superprism itself for a single frequency, we now find a coating for an incident medium with $n=1$, which only has a single propagating diffraction order. We set $\theta_i=30.97$ to keep α_0, the quantity conserved by Snell's law, the same as in Sec. III C. We may use the impedance database generated in Sec. III C; the only new impedance we must calculate is that of free space, the new incident medium—an easy task.

Searching for a two-layer coating with layers a single unit cell thick and $\dim(\mathcal{Z})=3$, we find that for a coating with cell thicknesses $d_1=(1.43/\sqrt{2})d$ and $d_2=(1.83/\sqrt{2})d$ the reflectivity drops from $R=0.996$ (compared to $R=0.93$ in Sec. III C for the same PC incident from a $n=2.963$ dielectric) to $R=0.001$. Figure 6, generated at full rank, confirms that this coating not only provides a deeper reflection minimum than that in Sec. III C, but also one with a larger bandwidth.

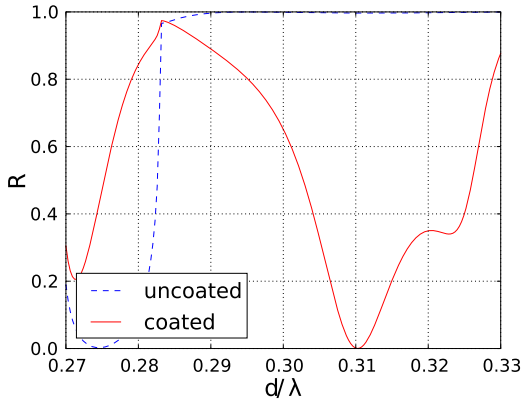

FIG. 6. (Color online) Reflection spectrum of the Matsumoto superprism [1] with (solid line) and without (dashed line) a two layer coating for $d/\lambda=0.31$, incident from $n=1$ dielectric. R is reduced from 0.996 to 0.001.

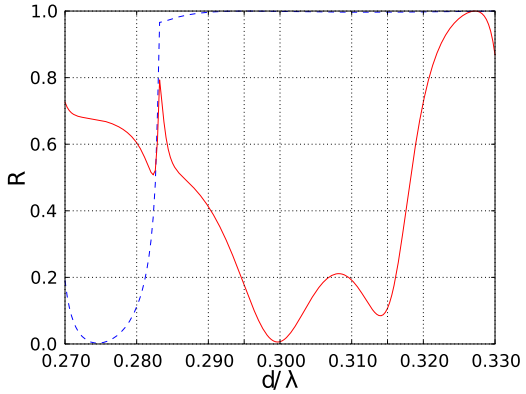

FIG. 7. (Color online) Reflection spectrum of the Matsumoto superprism [1] with (solid line) and without (dashed line) a three layer coating, incident from $n=1$ dielectric. R is minimized over the range $d/\lambda \in (0.295, 0.315)$.

E. Superprism multifrequency coating

Now we design a three-layer multifrequency coating the PC from Secs. III C and III D for light incident from free space. We follow the procedure from Sec. III B, minimizing the reflectance at 15 evenly spaced frequencies in $d/\lambda \in (0.295, 0.315)$, the range in which the PC acts as a superprism [1].

After 2 min to generate the impedance database, and a further 2 h to evaluate all 125 000 coatings at the 15 frequencies (3.7 ms per coating per frequency), we find a coating that reduces the reflection to a maximum of $R=0.194$ at the frequencies sampled. This coating has $d_1=(1.62/\sqrt{2})d$, $d_2=(1.32/\sqrt{2})d$, and $d_3=(2.07/\sqrt{2})d$, and its reflection spectrum calculated at full rank is plotted in Fig. 7. The $\dim(\mathcal{Z})=3$ results deviate slightly from the full rank results, so potentially one might find a marginally better coating using larger impedance matrices; but in the interests of computational efficiency, $\dim(\mathcal{Z})=3$ impedances are adequate.

F. Confirmation of results

Our impedance is rigorously defined using quantities found by a Bloch mode transfer-matrix method [7] that has previously been shown to be accurate [9]. It is also of interest to be able to compare its results with those from a purely numerical and general purpose commercial package, such as COMSOL MULTIPHYSICS. It is difficult to simulate semi-infinite PCs in COMSOL, since a perfectly matched layer for a PC must emit backward-scattered plane waves in order to absorb the forward traveling Bloch modes without reflection. Therefore, we simulate a different structure based on that in Sec. III D.

We consider a thick (14 period) layer of the superprism in Sec. III D, surrounded by FS, and design antireflection coatings at $d/\lambda=0.31$ for the front and the back interfaces. For the front FS-PC interface, we use the coating from Sec. III D, which has $d_1=(1.43/\sqrt{2})d$ and $d_2=(1.83/\sqrt{2})d$. For the PC-FS interface, the optimal coating is found to have $d_1=(1.83/\sqrt{2})d$ and $d_2=(1.43/\sqrt{2})d$, which is the reverse of the FS-PC coating. This symmetry follows from reciprocity in

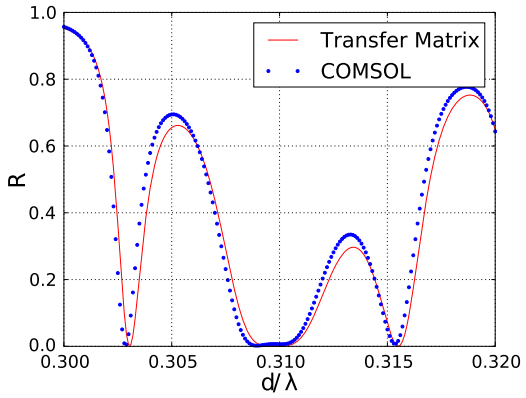

FIG. 8. (Color online) Reflectance of a 14-period layer of Matsumoto superprism [1], incident from and transmitting into $n=1$ dielectric, and coated on both sides to minimize R for $d/\lambda=0.31$. There is a good agreement between our method's results and those from COMSOL MULTIPHYSICS.

cases such as this, where the PC only supports one propagating mode. Note that the coatings are independent of the thickness of the superprism layer.

Since both interfaces have antireflection coatings for $d/\lambda=0.31$, we expect the overall structure to have near-zero reflectance at this frequency. The reflectance spectrum of the structure, as calculated using our transfer-matrix method and also by the commercial package COMSOL MULTIPHYSICS, is presented in Fig. 8. The COMSOL results are less accurate, being generated by a method not specifically developed for structures like those considered here. Nevertheless they agree well with the Bloch method, and in particular both methods show near-zero reflectance at $d/\lambda=0.31$, demonstrating that the antireflection coatings work, and that both computational methods are functioning to a good accuracy.

IV. DISCUSSION AND CONCLUSION

In Sec. III we successfully used our impedance to design antireflection coatings. Impedance may also be used to design coatings with other reflective properties—instead of selecting the coating with lowest reflection, if we wanted to we could select the coating that best reflects or transmits into a particular mode, or the coating that acts most like a beam splitter. With additional degrees of freedom, we could not only design broadband antireflection coatings, but also polarization filters. We could also design a coating for a PC mirror in a solar cell [3], so that it reflects the majority of light into the most effectively absorbed modes. The impedance definition's great benefit is that it allows a fast calculation of reflection and transmission matrices for large numbers of PC coatings—this collection of coating properties can then be searched for whatever behavior is desired.

The coatings in Secs. III D and III E, where light was incident from free space, were more successful at coating the superprism than the coating in Sec. III C, in which light was incident from a high index dielectric. In Sec. III D we attribute this difference in coating quality to the number of propagating modes in the incident medium (one in free space and three in the high index background) and note that, whenever practicable, the incident medium should be chosen to have as few propagating modes as possible at the operating frequency. This does not preclude the presence of a high index dielectric layer in front of the coating (although if this layer were thick it might limit the coating's bandwidth), but crucially this high index region must be considered to be part of the coating, not the input medium.

Our impedance definition makes two restrictions on PC properties. First, it applies only to PCs with a lattice that can be considered a stack of gratings with each grating either unshifted or shifted by half a period with respect to its predecessor. Such lattices have the property that $\mathbf{Q}^2=\mathbf{I}$, which is necessary to derive the impedance in a relatively simple form. In Sec. III we applied the definition to coating PCs that were distortions of the regular triangular lattice, but maintained the half-period grating shift.

The second restriction is that the PC's unit cell must be symmetric under 180° rotation, so that the backward modes are related to the forward modes, i.e., $\mathbf{F}'_+=\mathbf{Q}\mathbf{F}_-$ and $\mathbf{F}'_-=\mathbf{Q}\mathbf{F}_+$. In Sec. III we only considered circular inclusions, but the definition is valid for unit cells with any pattern or shape of inclusions as long as the symmetry condition is met. Using supercells, PC waveguides would satisfy both restrictions.

Defining each PC's impedance with respect to a fixed PC 0 may seem awkward, but it parallels how a dielectric's refractive index n is defined as the ratio of the admittances of the dielectric and free space. However, using such relative impedances does introduce another approximation when the mode set is truncated, because an extra set of projections needs to be made. The modes of free space are simply plane waves, so when free space is our reference medium we project each PC's modes onto a truncated set of plane waves, which effectively limits the number of plane waves in the calculation to the size of the truncated Bloch set. This suggests that free space or a uniform dielectric might not be a practical reference medium for problems where there are few propagating Bloch modes but the modes consist of many plane-wave orders—in these cases one of the candidate PCs for the coating might be a more suitable reference.

The key difference between our matrix impedance and the conventional scalar impedance comes from noncommutativity: for square lattices, in which $\mathbf{Q}=\mathbf{I}$ and $\mathcal{Z}_i$ simplifies to $2\mathbf{H}_0^T\mathbf{E}_i$, one can use the mode orthogonality relations (11) to show that, at full rank, $\mathcal{Z}_i=\mathbf{E}_0^{-1}\mathbf{E}_i$, $\mathcal{Y}_i=\mathbf{H}_0^{-1}\mathbf{H}_i$, and

$$(\mathcal{Z}_i^{-1}\mathcal{Z}_j)(\mathcal{Z}_i^{-1}\mathcal{Z}_j)^T=(\mathbf{E}_i^{-1}\mathbf{E}_j)(\mathbf{H}_j^{-1}\mathbf{H}_i). \tag{29}$$

Due to noncommutativity, this matrix product from Eqs. (27) cannot be written as a simple product of two impedances like its scalar counterpart Z_j/Z_i from Eq. (2). This noncommutativity is understandable because R_{ij} maps PC i's Bloch modes to themselves, whereas R_{ji} operates on PC j's modes. Written in terms of fields, the scalar counterpart of Eq. (29) is

$$Z_j/Z_i=(E_j/H_j)(H_i/E_i), \tag{30}$$

where the $\|$ subscripts are omitted for clarity. Comparing Eqs. (29) and (30) suggests that the ratios E_i/E_j and H_i/H_j,

both dimensionless quantities, are more general than the traditional impedances $Z_i = E_i / H_i$; for dielectrics we can only define the dimensional impedance Z_i because the field scalars in Eq. (29) commute to give Eq. (30).

The Bloch modes of uniform dielectrics are simply plane waves, so $\mathbf{F}_+$ is a permutation of the identity matrix and $\mathbf{F}_- = \mathbf{0}$. In this case, $\mathbf{E}_i$ and $\mathbf{H}_i$ may be written as diagonal matrices of square roots and reciprocal square roots of wave impedances. These diagonal matrices commute, which explains why such matrix impedances are not required for uniform dielectrics.

In conclusion we have rigorously defined both an impedance $\mathcal{Z}$ and an admittance $\mathcal{Y}$ for square and triangular lattice photonic crystals. This matrix impedance plays the same role as a conventional scalar wave impedance, in that it may be used to calculate the reflection at an impedance mismatch. It even plays this role in an analogous way to the scalar impedance—the impedance mismatch equation (27b) is similar to the scalar impedance mismatch equation (2). We successfully applied our definition to design antireflection coatings for photonic crystals efficiently, which demonstrates the utility of our definition.

ACKNOWLEDGMENTS

This work was produced with the assistance of the Australian Research Council (ARC). CUDOS (the Centre for Ultrahigh-bandwidth Devices for Optical Systems) is an ARC Centre of Excellence. We thank Alessandro Tuniz for his assistance with producing results in COMSOL.

[1] T. Matsumoto, T. Asatsuma, and T. Baba, Appl. Phys. Lett. **91**, 091117 (2007).
[2] D. W. Prather, S. Shi, D. M. Pustai, C. Chen, S. Venkataraman, A. Sharkawy, G. J. Schneider, and J. Murakowski, Opt. Lett. **29**, 50 (2004).
[3] P. Bermel, C. Luo, L. Zeng, L. C. Kimerling, and J. D. Joannopoulos, Opt. Express **15**, 16986 (2007).
[4] W. Śmigaj and B. Gralak, Phys. Rev. B **77**, 235445 (2008).
[5] F. J. Lawrence, L. C. Botten, K. B. Dossou, and C. M. de Sterke, Appl. Phys. Lett. **93**, 121114 (2008).
[6] L. C. Botten, N. A. Nicorovici, R. C. McPhedran, C. M. de Sterke, and A. A. Asatryan, Phys. Rev. E **64**, 046603 (2001).
[7] L. C. Botten, T. P. White, A. A. Asatryan, T. N. Langtry, C. M. de Sterke, and R. C. McPhedran, Phys. Rev. E **70**, 056606 (2004).
[8] O. S. Heavens, *Optical Properties of Thin Solid Films* (Dover Publications, London, 1991).
[9] K. Dossou, M. A. Byrne, and L. C. Botten, J. Comput. Phys. **219**, 120 (2006).

In Letter 2.1 and Paper 2.3 we not only show that our impedance method can calculate reflection and transmission matrices, but we also demonstrate a practical application for the method: the design of antireflection coatings. The impedance method accurately and efficiently calculates the reflectance of the coated structures, which can include one-period-thick PC layers and semi-infinite PCs. One of the designed coatings was verified by an independent method using commercial software. The only other PC impedance that has been used "in anger" without a separate optimisation step is that of Miri *et al.* [62], who also verified one of our coatings to within round-off of our parameter space. However, their method only works at frequencies below the first Wood anomaly.

Since the publication of Letter 2.1 and Paper 2.3, we noticed that at normal incidence, Bloch modes consisting of odd superpositions of grating orders are weakly coupled to. These modes are *uncoupled*-to for symmetry reasons: given a normally incident plane wave the entire system is symmetric about the y axis. This is not a new observation [147–149], but is a useful one: uncoupled modes may be truncated from $\mathbf{E}$ and $\mathbf{H}$, reducing the dimension of the impedance matrix with minimal penalty to accuracy.[2]

In Letter 2.1, the degree of freedom used in both coatings was the hole radius r. In Paper 2.3, we turned our attention to hole shifting, modifying the lattice vector $\mathbf{e}_2$ to build our cast of candidate PCs, and we ran separate multipole simulations for each candidate PC to find its Bloch factors and impedance. We later realised that it is unnecessary to run separate simulations for coating layers that differ only in their lattice vector $\mathbf{e}_2$: instead, we can simulate only the PC with the shortest $\mathbf{e}_2$, place lengths of uniform dielectric between the PC layers, and vary the dielectric's length, which can be done analytically—a trick discussed in Paper 3.1. In this way, a coating may be designed that only requires one computationally expensive simulation to evaluate all the coating PCs. There is a choice between two concepts here: the layers in a coating can be thought of as one-period layers of different candidate PCs, or they can be thought of as identical gratings separated by different thicknesses of dielectric, a multilayer generalisation of the coating design of Lee *et al.* [59] (Fig. 1.2). If the first paradigm is preferred, then it would also be possible to calculate the impedances of each of the candidate PCs from the transfer matrix $\mathcal{T}$ of one grating, by analytically adding phase to either side of the grating before diagonalising $\mathcal{T}$ to find $\mathcal{F}$, $\mathbf{E}$, $\mathbf{H}$, the impedance $\mathcal{Z}$ and the Bloch factors.

In Sec. III C of Paper 2.3, we attempted to design an antireflection coating at a frequency above the first Wood anomaly in the incident medium, where light was reflected into three grating orders. We found a narrowband coating that reduced reflection but did not eliminate it, and instead set ourselves the easier task in Sec. III D of designing a coating for the same PC, incident from air, where there is only one reflected order. At this frequency, it is easier to design an effective coating when incident from air, because fewer reflections need to be suppressed. Because multiple grating orders propagate inside the PC, the problem still requires impedance matrices rather than scalars. Our impedance method is capable of designing antireflection coatings that suppress reflection into more than one diffraction order—although such coatings require more degrees of freedom. We present such a coating in Sec. IV C of Paper 3.1, which we now introduce.

[2] A note of caution: the $\mathbf{E}_0$ and $\mathbf{H}_0$ matrices of the reference medium must also be truncated, removing the odd modes. If the reference medium is free space, then this requires writing $\mathbf{E}_0$ and $\mathbf{H}_0$ not as diagonal matrices of grating orders, but as matrices of odd and even superpositions of the degenerate grating orders, as discussed in Appendix A.

Chapter 3

Impedance extraction from field scattering data

So far, we have defined impedance in terms of the transfer matrix $\mathcal{T}$ of a grating. We have calculated $\mathcal{T}$ using in-house code that is not publically available: either by finite element methods [110] or using the multipole method and lattice sums [111]. Implementing such methods requires a substantial investment of time and expertise, which presents a significant barrier to adoption of PC impedances. Indeed, since publication of Papers 2.1 and 2.3, a number of scalar impedance definitions and coating design techniques have been proposed or applied that are less powerful than ours, but that are easier to calculate with generic tools [62, 150].

Therefore, I developed a method to calculate PC impedances from the scattered field in a finite length of PC. As noted in Paper 3.1, this field data can be produced by widely available FDTD or FEM software, or even measured experimentally with a SNOM. We embrace and extend a method developed by Ha *et al.* [126], whereby the scattered field is represented as a superposition of several unknown forward and backward Bloch modes, and the modes and their Bloch factors are extracted from the field data using numerical optimisers and least squares techniques. In the second part of the method, we extract the $\mathbf{E}$ and $\mathbf{H}$ matrices from the modal fields, and use these to calculate the PC impedances.

To encourage adoption of our impedance method, we have released our source code freely on the internet, in the hope that other researchers might find it useful to design antireflection coatings, or explore some of the other applications of PC impedances. It may be downloaded from https://launchpad.net/blochcode.

A flexible Bloch mode method for computing complex band structures and impedances of two-dimensional photonic crystals

Felix J. Lawrence,[1,a)] Lindsay C. Botten,[2] Kokou B. Dossou,[2] R. C. McPhedran,[1] and C. Martijn de Sterke[1]
[1]*CUDOS and Institute of Photonics and Optical Science (IPOS), School of Physics, University of Sydney, NSW 2006, Australia*
[2]*CUDOS and Department of Mathematical Sciences, University of Technology, Sydney, NSW 2007, Australia*

(Received 10 October 2011; accepted 3 December 2011; published online 11 January 2012)

We present a flexible method that can calculate Bloch modes, complex band structures, and impedances of two-dimensional photonic crystals from scattering data produced by widely available numerical tools. The method generalizes previous work which relied on specialized multipole and finite element method (FEM) techniques underpinning transfer matrix methods. We describe the numerical technique for mode extraction, and apply it to calculate a complex band structure and to design two photonic crystal antireflection coatings. We do this for frequencies at which other methods fail, but which nevertheless are of significant practical interest. © *2012 American Institute of Physics*. [doi:10.1063/1.3674281]

I. INTRODUCTION

When modeling photonic crystals (PCs), it is important to consider all the relevant Bloch modes. Light at a fixed frequency, polarization, and incident angle exists in a PC as a superposition of a set of propagating and evanescent Bloch modes, the PC's eigenstates. At low frequencies, only one mode generally needs to be considered. For light at frequencies above the first Wood anomaly,[1] each row of holes in the PC diffracts light into several propagating orders, so the PC may support multiple propagating Bloch modes. At the PC's front and back interfaces, some of its modes couple via reflection, affecting the overall reflection and transmission through the PC, so it is important to model all relevant modes.

It is often important to include evanescent modes.[2] If the PC is not long—for example, if it is a layer in a thin antireflection coating—then evanescent modes can play a role in energy transport.[3] Evanescent modes can also play a role in field matching across an interface between PCs[4] or PC waveguides.[5] The propagative qualities of an evanescent mode are well-represented by its complex band structure,[6] which augments the traditional band structure, conveying information about the rate at which the mode accumulates phase together with information about the mode's decay rate.

There have been a number of studies seeking to derive impedance-like quantities to characterize reflection at PC interfaces by a scalar.[7,8] Furthermore, a number of studies have adapted metamaterial parameter extraction techniques[9] to photonic crystals, and used them to design antireflection coatings.[10,11] However, since these techniques characterize reflection and transmission by a single complex number each, they cannot handle problems involving multiple modes, where every mode reflects into every other mode. Scalar-based methods generally give manifestly incorrect results for light at frequencies above the first Wood anomaly, which ranges from $a_x/\lambda = 1/n$ for normally incident light to $a_x/\lambda = 1/2n$ for light at the Brillouin-zone edge, where a_x is the length of the lattice vector parallel to the interface, λ is the free space wavelength and n is the PC's background index. Above this frequency, generally several Bloch modes must be simultaneously considered in each PC, regardless of whether these modes are propagating or evanescent. Reflection at a PC/PC interface is well-described by a matrix that maps incident modes to reflected modes, as we have shown previously.[4,12] In our experience, the minimum acceptable dimension of this reflection matrix, as argued in Sec. II A, is usually

$$M_{\min} = \left\lfloor \frac{a_x}{n\lambda}(1+\sin\theta_i) \right\rfloor + \left\lfloor \frac{a_x}{n\lambda}(1-\sin\theta_i) \right\rfloor + 1, \qquad (1)$$

where θ_i is the incident angle from a uniform dielectric with the PC's background index, and $\lfloor x \rfloor$ denotes the *floor* of x. We have previously achieved accurate results modeling PC stacks using impedance matrices of this dimension and higher.[4,12,13]

A number of methods for finding multiple Bloch modes and complex band structures have been demonstrated. Transfer-matrix[14] and scattering-matrix[15] based methods were developed to derive a PC's Bloch modes from the properties of a single grating layer. The plane wave expansion method has also been extended to include evanescent modes.[16] Finally, Ha *et al.* presented a method for extracting Bloch modes from the output of an electromagnetic field (EM) solver,[17] or even near-field measurements.[18,19] We improve the accuracy, stability, and efficiency of Ha *et al.*'s method and extend it to calculate PC impedances for two-dimensional (2D) PCs, which can be used to calculate reflection and transmission at interfaces.[4,12] These PC impedances and the reflection and transmission operators are represented by matrices; our method supports the presence and interaction of multiple Bloch modes and so it can work well both above and below the first Wood anomaly.

We have made software available that uses the method described in this paper to calculate PCs' Bloch modes,

a)Electronic mail: felix@physics.usyd.edu.au.

complex band structures, and impedances. The software, called BlochCode, can then use these complex band structures and impedances to calculate reflection and transmission matrices and coefficients for arbitrary stacks of PCs. BlochCode is open-source and is available on the Internet.[20]

In Sec. II, we present our method for finding Bloch modes from the electric field E and the magnetic field H in a PC structure. Section II A recaps some useful results from our previous work[12] and provides some background theory. Section II B details our improvements to Ha *et al.*'s method[17] of finding Bloch factors and modal fields, and Sec. III outlines our procedure for successfully applying this method to minimize the residual derived in Sec. II B. Section II C explains how we calculate PC impedance matrices from the modal fields. In Sec. IV, we apply our method to demonstrate its utility. In Sec. IV A, we calculate the complex band structure for light normally incident on a triangular lattice PC. In Sec. IV B, we reproduce the design process of a known antireflection coating for a PC, at a frequency and incident angle for which it is critical to include at least two Bloch modes in the calculations. Finally, in Sec. IV C, we use our method to design an all-polarization antireflection coating for a square lattice self-collimating PC, at a high frequency where a scalar method cannot find a coating for the PC.[21]

II. THEORY

Our method uses a two-step process to extract a PC's modes and impedance from the field in a finite length of the PC. The PC is assumed to be two-dimensional, lossless, and to have relative permeability $\mu_r = 1$. Like Ha *et al.*'s method,[17] we could use data generated by finite element method (FEM) or finite difference time domain (FDTD) simulations, or even experimentally measured by a near-field probe such as a scanning near-field optical microscopy (SNOM),[19] although the impedance part of our method is not valid for SNOM data, which is derived from a 3D object. First, the Bloch factors and the Bloch modal fields are found (Sec. II B), then these modes are analyzed to calculate the PC's impedance (Sec. II C).

A. Background theory

Two-dimensional PCs in the x-y plane may be described as a stack of gratings parallel to the x axis,[22] each of which diffracts incident light into an infinite set of grating orders. At the edge of each unit cell, the PC's Bloch modes may be written as a superposition of the underlying grating orders.[15] Their directions are given by the grating equation

$$k_x^{(p)} = k_x + \frac{2\pi p}{a_x} = k\sin\theta_i + \frac{2\pi p}{a_x}, \tag{2}$$

where k_x is the x component of the incident plane wave's wavevector, $k_x^{(p)}$ is that of the pth diffraction order, and a_x is the length of the lattice vector parallel to the x axis. The wavevector component in the direction perpendicular to the grating is $k_y^{(p)} = \sqrt{k^2 - k_x^{(p)^2}}$ where k is the wavenumber in the medium. Evanescent grating orders have imaginary $k_y^{(p)}$, so for a given k and $k_x^{(p)}$, the number of propagating grating orders is the number of solutions to Eq. (2) with real $k_y^{(p)}$, or $M_{\min}$ in Eq. (1). In our experience, $M_{\min}$ also provides an upper bound on the number of propagating Bloch modes, and at non-normal incidence is a lower bound on the number of Bloch modes required to model a PC accurately. At normal incidence, symmetry allows odd modes to be ignored, so in this case good results may be obtained with fewer than $M_{\min}$ modes—see Sec. IV C. Using Bloch modes found from accurate multipole and FEM transfer matrix methods,[23,24] we have consistently had success modeling PCs with no more than $M_{\min} + 2$ Bloch modes.

Bloch's theorem relates the electric and magnetic fields associated with each mode at equivalent points in different unit cells of a PC. The ratio of each mode's field at points separated by the lattice vector $\mathbf{e}_1 = (a_x, 0)$ is $e^{ik_x a_x}$. For the PC's other lattice vector $\mathbf{e}_2$, this ratio is different for each mode and is the mode's Bloch factor, denoted by μ. Calculating μ for each mode is the goal of Sec. II B. For square and rectangular lattices, $\mathbf{e}_2 = (0, a_y)$ and $\mu = e^{ik_y a_y}$, where k_y is the y component of the mode's wavevector. For triangular lattices, the lattice vector $\mathbf{e}_2$ is $(a_x/2, a_y)$ and so the Bloch factor may be written $\mu = e^{i(k_x a_x/2 + k_y a_y)}$.

Bloch modes come in forward/backward pairs. Popov *et al.* provide a useful discussion of symmetry properties.[25] We assume mirror symmetry in each unit cell, which means that each backward mode's field profile in a unit cell is the reflection on the x axis of its forward partner's. The Bloch factors of a pair are related because of this: for square and rectangular lattices, $\mu_b = 1/\mu_f$, where μ_f and μ_b are, respectively, the Bloch factors of the forward and backward modes. For triangular-like lattices, the symmetry is more complicated since the reflection of $\mathbf{e}_2$ is not $-\mathbf{e}_2$, the translation corresponding to the field ratio $1/\mu_f$, but $(a_x/2, -a_y)$; these vectors differ by $-\mathbf{e}_1$. Accounting for this discrepancy, we find $\mu_b = e^{-ik_x a_x}/\mu_f$ for triangular lattices.

A PC's impedance is defined in terms of two matrices, $\mathbf{E}$ and $\mathbf{H}$.[12] For $E = E_z$ polarized light, each matrix maps a vector of forward Bloch mode amplitudes $\mathbf{c}_+$ to a vector of the E_z or H_x fields associated with each grating diffraction order. Specifically, $E_{p,m}$, the (p,m)th element of $\mathbf{E}$, is the E_z field of normalized mode m due to forward and backward plane waves in grating order p, at the center $(x = 0)$ of a unit cell's edge. Thus, for a set of forward propagating/decaying Bloch modes $\mathbf{c}_+$, the field components along the edge of the unit cell, i.e., the quantities that are continuous across an interface between PCs or dielectrics, are

$$E_z(x) = \sum_p \mathbf{E}_p \mathbf{c}_+ e^{ik_x^{(p)} x}, \quad H_x(x) = \sum_p \mathbf{H}_p \mathbf{c}_+ e^{ik_x^{(p)} x}, \tag{3}$$

where $\mathbf{E}_p$ and $\mathbf{H}_p$ are the rows of $\mathbf{E}$ and $\mathbf{H}$ corresponding to grating order p. In the $H = H_z$ polarization, $\mathbf{E}$ and $\mathbf{H}$ map to E_x and H_z fields, and these quantities replace E_z and H_x in Eq. (3).

Previously,[12] we defined PC impedances in terms of these matrices. For E_z polarized light, the impedance of a PC is

$$\mathcal{Z} = \mathbf{H}_0^T(\mathbf{I} + \mathbf{Q})\mathbf{E} + \mathbf{E}_0^T(\mathbf{I} - \mathbf{Q})\mathbf{H}, \tag{4}$$

and for H_z polarized light it is

$$\mathcal{Z} = -\left[\mathbf{H}_0^T(\mathbf{I}-\mathbf{Q})\mathbf{E} + \mathbf{E}_0^T(\mathbf{I}+\mathbf{Q})\mathbf{H}\right], \tag{5}$$

where $\mathbf{E}$ and $\mathbf{H}$ are calculated for the PC, and $\mathbf{E}_0$ and $\mathbf{H}_0$ are calculated for a reference material, usually free space. $\mathbf{Q}$ is a diagonal matrix that takes into account the half-period shift of gratings in triangular lattice PCs: for square lattices $\mathbf{Q}=\mathbf{I}$, and for triangular lattices $\mathbf{Q}=\text{diag}\,[(-1)^p]$, where p is the grating order.

Given impedances $\mathcal{Z}_1$ and $\mathcal{Z}_2$ for two PCs, it is simple to calculate the reflection and transmission matrices across their interface[12]

$$\mathbf{T}_{12} = (\mathbf{A}_{12}^T\mathbf{A}_{12} + \mathbf{I})^{-1}2\mathbf{A}_{12}^T, \tag{6a}$$

$$\mathbf{R}_{12} = (\mathbf{A}_{12}\mathbf{A}_{12}^T + \mathbf{I})^{-1}(\mathbf{A}_{12}\mathbf{A}_{12}^T - \mathbf{I}), \tag{6b}$$

where $\mathbf{A}_{12}=\mathcal{Z}_1^{-1}\mathcal{Z}_2$.

B. Finding modes

Our method of finding the Bloch modes and Bloch factors is based on the method presented by Ha *et al.*,[17] although our method offers some significant improvements in accuracy and efficiency. We take field data for several unit cells of a PC, and try to write it as a superposition of Bloch modes, thus finding the modal fields and Bloch factors. The final steps of our mode-finding method impose symmetry relationships between forward and backward modal fields, increasing accuracy by almost halving the number of unknowns in the problem. We now outline our method.

In an EM solver, we simulate a section of 2D PC with Bloch-Floquet periodic boundary conditions on two boundaries, and uniform dielectric on the others (Fig. 1). We sample the E_z or E_x (depending on polarization) field component at many (N_p) points in unit cell $\ell=0$, and then at the equivalent points in each of the other unit cells. If desired, E_y, H_x, H_y, or H_z may be used in place of or in addition to E_z and E_x. For triangular lattice PCs, we use the field in the simulated unit

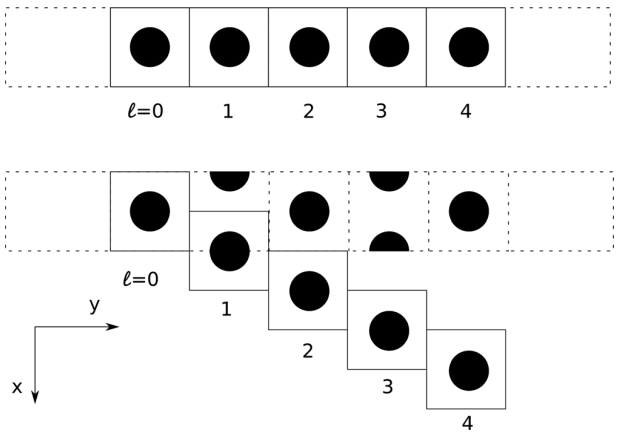

FIG. 1. Schematic of $L=5$ PC structures for a square and a triangular PC lattice. The squares with solid edges are the unit cells used by our method. For the triangular lattice PC, the field in the solid-edge unit cells are calculated from the unit cells of the simulated structure (dashed edges) using Bloch's theorem, with the ratio $e^{ik_x a_x}$ between adjacent cells' fields.

cells (dashed edges in Fig. 1) to calculate the field in the unit cells separated by a lattice vector (solid edges): we apply Bloch's theorem with integer multiples of the lattice vector $(a_x, 0)$.

We seek to write these electric field components as a superposition of forward and backward Bloch modes. So we want to express every $U_\ell(\mathbf{r})$, i.e., the E_z or E_x field component for sampled point $\mathbf{r}$ in unit cell ℓ, as

$$U_\ell(\mathbf{r}) = \sum_m \mu_m^\ell A_m(\mathbf{r}) + \sum_{m'}(1/\mu_{m'}^{L-1-\ell})A_{m'}(\mathbf{r}) + w(\ell,\mathbf{r}), \tag{7}$$

where $A_m(\mathbf{r})$ and μ_m are, respectively, the modal field and the Bloch factor of forward mode m; m' denotes backward modes, and $w(\ell,\mathbf{r})$ is the residual error. More specifically, for forward modes, $A_m(\mathbf{r})$ is the field component of mode m at point $\mathbf{r}$ of the first unit cell, $\ell=0$. The Bloch factor μ_m is the ratio of the field in cells $\ell+1$ and ℓ, so $\mu_m^\ell A_m(\mathbf{r})$ is the field component of forward mode m at point $\mathbf{r}$ of unit cell ℓ. To avoid ill-conditioning, the field $A_{m'}(\mathbf{r})$ at point $\mathbf{r}$ of each backward mode m' is defined in the last unit cell, $\ell=L-1$. This means that the coefficients of $A_m(\mathbf{r})$ and $A_{m'}(\mathbf{r})$ in Eq. (7) have moduli no greater than 1. As noted in Sec. II A, the Bloch factor $\mu_{m'}$ of each backward mode is related to that of its forward partner; we enforce this relationship in practice, thereby halving the number of Bloch factors that must be found.

Equation (7) for all ℓ and all sampled $\mathbf{r}$ may be written in matrix form as

$$\mathbf{U} = \mathbf{C}\mathbf{A} + \mathbf{W}, \tag{8}$$

where $\mathbf{U}$ contains the E_z or E_x field components from the EM solver, $\mathbf{A}$ is a matrix of modal fields, $\mathbf{C}$ is a matrix constructed from Bloch factors, and $\mathbf{W}$ is a matrix of residuals $w(\ell,\mathbf{r})$ that must be minimized. $\mathbf{U}$ is a $L\times N_p$ matrix: the field in its ℓth row and rth column is $U_{\ell,r}=U_\ell(\mathbf{r})$, the field component at point $\mathbf{r}$ in unit cell ℓ. Similarly, $\mathbf{A}$ is a $M\times N_p$ matrix; the field in its mth row and rth column is $A_{m,r}=A_m(\mathbf{r})$, the field of mode m at point $\mathbf{r}$ in cell $\ell=0$ for forward modes, or cell $\ell=L-1$ for backward modes. $\mathbf{C}$ is a $L\times M$ matrix. For a forward mode m, the (ℓ,m)th element of $\mathbf{C}$ is μ_m^ℓ, and for a backward mode m', the (ℓ,m')th element is $1/\mu_{m'}^{L-1-\ell}$. If multiple field components (e.g., E_z, H_x, and $H_{y)}$ are to be used to find the modes, then the additional data can be added as extra columns in $\mathbf{U}$.

We start the optimization process knowing $\mathbf{U}$, and with information about the structure of $\mathbf{C}$, and no direct information about $\mathbf{A}$. In our method, we first find the Bloch factors that determine $\mathbf{C}$, a relatively difficult problem. Once $\mathbf{C}$ is known, solving Eq. (8) for the modal fields $\mathbf{A}$ becomes a pure least-squares problem that can be solved accurately and efficiently using standard techniques.

To find the modes, we seek to minimize the difference between the observed field $\mathbf{U}$ and the superposition of Bloch mode fields $\mathbf{CA}$. That is, we seek to minimize $\|\mathbf{W}\|_F^2$ in Eq. (8), the sum of squared moduli of the elements of $\mathbf{W}$. Constraining the problem by dividing by the squared Frobenius norm $\|\mathbf{U}\|_F^2$ of $\mathbf{U}$, the quantity we minimize is

$$w^2 = \frac{||\mathbf{U} - \mathbf{CA}||_F^2}{||\mathbf{U}||_F^2}, \tag{9}$$

where $w^2 = \|\mathbf{W}\|_F^2/\|\mathbf{U}\|_F^2$. First we eliminate $\mathbf{A}$ from Eq. (9) in order to find $\mathbf{C}$ with a numerical minimizer. We use an alternative representation of the Frobenius norm, $||\mathbf{U}||_F = \sqrt{\mathrm{tr}(\mathbf{U}^H\mathbf{U})}$, to write

$$w^2 = \frac{\mathrm{tr}\Big((\mathbf{U}^H - \mathbf{A}^H\mathbf{C}^H)(\mathbf{U} - \mathbf{CA})\Big)}{||\mathbf{U}||_F^2}. \tag{10}$$

Finding $\mathbf{A}$ for arbitrary $\mathbf{C}$ is a standard least-squares problem; the optimal $\mathbf{A}$ satisfies $\mathbf{C}^H\mathbf{CA} = \mathbf{C}^H\mathbf{U}$. We expand Eq. (10), twice apply this relation, and rearrange to get

$$w^2 = 1 - \frac{\mathrm{tr}(\mathbf{U}^H\mathbf{C}\mathbf{C}^+\mathbf{U})}{||\mathbf{U}||_F^2}, \tag{11}$$

where $\mathbf{C}^+ = (\mathbf{C}^H\mathbf{C})^{-1}\mathbf{C}^H$ is the Moore-Penrose pseudo-inverse of $\mathbf{C}$.

Using Eq. (11) and a numerical minimizer, the Bloch factors that determine $\mathbf{C}$ may often be found to a useful level of accuracy (see Sec. III for implementation details). In order to improve the accuracy and reliability of the results, we impose further physical constraints.

The PC impedance method[4,12] assumes the unit cell to be up-down symmetric, which causes the forward and backward modes to be related. So far, we have only imposed a relationship between the forward and backward Bloch factors, not the modal fields within each unit cell. We can halve the number of unknowns in $\mathbf{A}$ and strongly improve the quality of our results by enforcing this relationship in the minimization process.

We commence by partitioning the forward (f) and backward (b) modes, and the points in the left (L; $y \le a_y/2$) and right (R; $y \ge a_y/2$) halves of the unit cell:

$$\mathbf{U} = (\mathbf{U}_L, \mathbf{U}_R), \quad \mathbf{C} = \big(\mathbf{C}_f, \mathbf{C}_b\big), \tag{12a}$$

$$\mathbf{A} = \begin{pmatrix} \mathbf{A}_{L,f} & \mathbf{A}_{R,f} \\ \mathbf{A}_{L,b} & \mathbf{A}_{R,b} \end{pmatrix}. \tag{12b}$$

After normalization, the field of a backward mode is the field of its forward partner reflected about the x axis, thus

$$\big(\mathbf{A}_{L,b}, \mathbf{A}_{R,b}\big) = \big(\gamma\mathbf{A}_{R,f}\mathbf{P}, \gamma\mathbf{A}_{L,f}\mathbf{P}^{-1}\big), \tag{13}$$

where $\mathbf{P}$ is the permutation matrix that maps points $(x, a_y - y)$ to (x, y), and γ is a normalizing diagonal matrix whose elements are the ratios of backward and forward mode amplitudes. The columns of $\mathbf{A}_{R,f}$ and $\mathbf{A}_{R,b}$, corresponding to points in the right half of the unit cell, can easily be ordered so that $\mathbf{P} = \mathbf{I}$; from now on we assume this ordering. Equation (8) can now be written with roughly half as many unknowns,

$$(\mathbf{U}_L, \mathbf{U}_R) = \big(\mathbf{C}_f, \mathbf{C}_b\gamma\big)\begin{pmatrix} \mathbf{A}_{L,f} & \mathbf{A}_{R,f} \\ \mathbf{A}_{R,f} & \mathbf{A}_{L,f} \end{pmatrix} + \mathbf{W}. \tag{14}$$

$\mathbf{C}_b\gamma$ represents each backward mode's amplitude in each cell, relative to that of the corresponding forward mode in cell 0.

The constraints on $\mathbf{A}$ [Eq. (13)] mean that Eq. (14) does not have a least-squares form, so may not be immediately simplified in the way that Eq. (9) led to Eq. (11). To transform Eq. (14) into a more useful form, we block-diagonalize $\mathbf{A}$ and right-multiply by the matrix $\left(\begin{smallmatrix} \mathbf{I} & \mathbf{I} \\ \mathbf{I} & -\mathbf{I} \end{smallmatrix}\right)$, to show

$$(\mathbf{U}_+, \mathbf{U}_-) = (\mathbf{C}_+\mathbf{A}_+, \mathbf{C}_-\mathbf{A}_-) + \mathbf{W}'. \tag{15}$$

Here we have introduced the symmetric and antisymmetric forms $\mathbf{U}_\pm = \mathbf{U}_L \pm \mathbf{U}_R$, $\mathbf{C}_\pm = \mathbf{C}_f \pm \mathbf{C}_b\gamma$, and $\mathbf{A}_\pm = \mathbf{A}_{L,f} \pm \mathbf{A}_{R,f}$.

Equation (15) takes the form of two independent least-squares equations, each with half the dimension of Eq. (14). The two equations must be satisfied simultaneously, so to find the Bloch factors we can minimize

$$w^2 = \frac{||\mathbf{U}_+ - \mathbf{C}_+\mathbf{A}_+||_F^2 + ||\mathbf{U}_- - \mathbf{C}_-\mathbf{A}_-||_F^2}{||\mathbf{U}_+||_F^2 + ||\mathbf{U}_-||_F^2}, \tag{16}$$

or equivalently

$$w^2 = 1 - \frac{\mathrm{tr}(\mathbf{U}_+^H\mathbf{C}_+\mathbf{C}_+^+\mathbf{U}_+) + \mathrm{tr}(\mathbf{U}_-^H\mathbf{C}_-\mathbf{C}_-^+\mathbf{U}_-)}{||\mathbf{U}_+||_F^2 + ||\mathbf{U}_-||_F^2}. \tag{17}$$

Again, this quantity may be minimized by a numerical optimizer. The residual w^2 for any solution to Eq. (17) is equal to the residual obtained by inserting the solution into Eq. (11): the two equations differ only in the symmetry constraint on backward modal fields [Eq. (13)]. Compared to Eq. (11), we have removed N_pM unknowns from $\mathbf{A}$ (where $N_p \gg M$ is the number of sampled points in each unit cell), halving its dimension at the cost of adding M unknowns to $\mathbf{C}_\pm$ as γ. These new unknowns must be found simultaneously with the Bloch factors using a numerical minimizer, so it is important to supply a good starting estimate; our method for doing so is detailed in Sec. III.

C. Calculating impedance

Once the Bloch factors and γ are known, the modal fields can be reconstructed and analyzed to determine the PC's impedance. The essential quantities for this calculation are the E and H field components in the plane of the PC interface (i.e., E_z and H_x, or E_x and H_z, depending on polarization) of each Bloch mode m along the left edge ($y = 0$) of a unit cell (see Fig. 1). These quantities, $E_m(x)$ and $H_m(x)$, may be found from Eq. (15) using the known values for $\mathbf{C}_+$ and $\mathbf{C}_-$ and inserting the appropriate E or H fields into $\mathbf{U}_+$ and $\mathbf{U}_-$.

To calculate the impedance, we find the $\mathbf{E}$ and $\mathbf{H}$ matrices for the PC, as defined in Sec. II A. Inserting multiples of unit vectors $\mathbf{c}_+$ into Eq. (3), we can show that

$$E_m(x) = \mathcal{A}_m \sum_p E_{p,m} e^{ik_x^{(p)}x}, \tag{18a}$$

$$H_m(x) = \mathcal{A}_m \sum_p H_{p,m} e^{ik_x^{(p)}x}, \tag{18b}$$

where $\mathcal{A}_m$ is the amplitude of the normalized mode m, and $E_{p,m}$ and $H_{p,m}$ are the elements of $\mathbf{E}$ and $\mathbf{H}$. It is straightforward to exploit the orthogonality of the plane wave grating diffraction orders to show that

$$\mathcal{A}_m E_{p,m} = 1/a_x \int_{-a_x/2}^{a_x/2} E_m(x) e^{-ik_x^{(p)} x} dx, \tag{19a}$$

$$\mathcal{A}_m H_{p,m} = 1/a_x \int_{-a_x/2}^{a_x/2} H_m(x) e^{-ik_x^{(p)} x} dx. \tag{19b}$$

Equations (19) let us calculate each element of the $\mathbf{E}$ and $\mathbf{H}$ matrices, up to a normalization constant $\mathcal{A}_m$ per column. We remove the constants by calculating the PC's impedance [Eq. (4) or (5)] with the PC itself as the reference material: by reciprocity-derived Bloch mode orthogonality relations,[12] this quantity should be the identity matrix. The diagonal entries of this matrix are the $\mathcal{A}_m^2$; the off-diagonal terms, which should be zero, provide an error estimate. After normalizing the $\mathbf{E}$ and $\mathbf{H}$ matrices for the PC, we calculate its impedance matrix $\mathcal{Z}$ from Eq. (4) or (5) using a reference medium such as free space.

III. NUMERICAL PROCEDURE

Having outlined the theoretical basis of our method for finding the Bloch factors and impedance of a PC at a given frequency, incident angle, and polarization, we now provide some practical detail about our implementation of the method. We outline the procedure for $M = 3$ pairs of Bloch modes.

In COMSOL Multiphysics 4.2, we simulate a 1×8 unit cell sample of PC, embedded in its background dielectric, with Bloch-Floquet periodic boundary conditions along the two long boundaries (Fig. 1 shows a 1×5 structure). Equation (15) is a set of LN_p equations, with $2M$ and MN_p unknowns in $\mathbf{C}_\pm$ and $\mathbf{A}_\pm$, respectively. To be overspecified, the method requires $LN_p > MN_p + 2M$; thus $L = 8$ periods and a large N_p is sufficient to find $M = 3$ modes. A deeper structure with more unit cells does not necessarily provide useful information about additional evanescent modes, as their amplitude deep inside the structure may be negligible. From COMSOL we export the relevant E and H field components in the $L = 8$ unit cells, sampled over a $101 \times (50L + 1)$ grid.

In order to compute a mode, it must be present in the structure with sufficient amplitude to be detected. Light at normal incidence often fails to excite odd Bloch modes; these *uncoupled modes*[26] consequently cannot be found by an optimization, which loses accuracy in searching for modes that are not present. At frequencies above the first Wood anomaly, the frequencies at which the higher order modes are most important, this problem may be avoided by exciting the PC slab not with a normally incident plane wave, but with the first grating diffraction order. This technique is used in Secs. IV A and IV C. If the uncoupled mode is not relevant to a particular problem, it may instead be ignored.

If we seek to find $M = 3$ Bloch modes, then finding a global minimum of Eq. (17) involves searching for $2M = 6$ complex numbers. This is a hard problem if attacked directly, but we use an algorithm that gives more consistent success by providing a good starting estimate. We start by minimizing the residual w^2 in Eq. (11), which forces a relationship between forward and backward Bloch factors but not the modal fields. This involves finding only M complex numbers. As a starting estimate for the forward Bloch factors, we either take the result of a neighboring simulation, or the analytically calculated Bloch factors for the dielectric background of the PC. At every step of the minimization, evanescent modes are sorted into forward and backward decaying modes, based on the moduli of their Bloch factors. The minimization can be done by any standard numerical minimizer, such as SciPy's[27] fmin, which is a modified Nelder-Mead optimization.[28] At this point, the results are equivalent to those from the method of Ha *et al.*,[17] except that we have lessened the likelihood of $\mathbf{C}$ being ill-conditioned by renormalizing the backward Bloch factors $\mu_{m'}$ in Eq. (7) and setting their phase origin to the end of the PC.

Occasionally, we encounter an instability in which a pair of modes have very large equal and opposite field amplitudes and very small Bloch factors. When this occurs, we follow a Gram-Schmidt-like process: we subtract the field of non-problematic modes (i.e., modes with $|\mu| > 10^{-3}$) from $\mathbf{U}$ and repeatedly minimize Eq. (11) to find each of the remaining modes individually.

Using the solution to Eq. (11) as our estimate for the Bloch factors, the modal fields may be found with a least-squares optimization. The average field ratio of each pair of backward and forward modes gives us an estimate for γ. We now have a plausible estimate for γ and the Bloch factors, which we can use as a starting estimate to minimize Eq. (17).

To further refine the estimates, we repeatedly iterate through the modes, fixing all but one μ and the corresponding element of γ, minimizing Eq. (17) to find the two variables. After this process, we finally minimize Eq. (17) across all 6 complex dimensions simultaneously to obtain the correct Bloch factors and modal fields from which we calculate impedances. Forward and backward propagating modes are sorted based on their flux,[15] before impedances are calculated as outlined in Sec. II C.

IV. APPLICATIONS

We now apply our method to a range of typical problems. Each of these problems involves frequencies above the first or second Wood anomaly—frequencies at which scalar methods fail and multiple modes are required to describe the system. BlochCode, software that implements our method in Python, using SciPy[27] and Sage,[29] is freely available on the Internet;[20] we use it here.

A. Complex band structure

The first application of our method is to calculate the complex band structure of a PC. The PC is a triangular lattice of circular air holes with radius $r = 0.3\ a$ and lattice constant $a_x = a$ in a dielectric background with $n = 3$. We calculate the band structure for light polarized with the $\mathbf{H}$ field out of the PC plane (H_z polarization) at frequencies $a/\lambda \in (0, 0.5)$ in the $\Gamma - M$ direction, i.e., at normal incidence. Using

COMSOL, we calculate the field in an 8 period slab of the PC, and we apply our method to find the largest three Bloch factors. w^2 varies: it is less than 10^{-8} at low frequencies and less than 10^{-4} at high frequencies.

Figure 2 summarizes the propagation properties of the two/three most dominant modes. The moduli of the Bloch factors $|\mu|$, which quantify how the modes' amplitudes vary with propagation, are shown in Figs. 2(a) and 2(b). Below the Wood anomaly, an inspection of $\mathbf{A}$ and γ shows that the third mode is barely excited by the normally incident plane wave, and this reduces the accuracy of the results [Fig. 2(a)]. Ignoring the uncoupled mode at low frequencies (where the $p=1$ grating order is evanescent and so may not be used to excite the structure, as mentioned in Sec. III) increases the accuracy of the other two modes [Fig. 2(b)]. The complex arguments of the Bloch factors, which quantify how phase is acquired through propagation, are shown in Fig. 2(c), and the information about amplitude and phase is summarized in a single plot in Fig. 2(d). Aside from slight errors in the phase of strongly evanescent modes in Fig. 2(c), there is good agreement between Fig. 2 and Bloch factors calculated by highly accurate multipole techniques.

Figure 2 shows that at frequencies below the Wood anomaly there is at most one propagating Bloch mode, which becomes evanescent in the first bandgap with a decay factor $|\mu|$ of no less than 0.5; it still decays far more slowly than the other evanescent Bloch modes at that frequency. Figure 2(c) shows that for the evanescent modes, either 0 or π phase is acquired across each unit cell.

B. Antireflection coating

Our next application is to reproduce the design of an antireflection coating we presented previously,[12] found using PC impedances calculated with a specialized transfer-matrix method.[24] As in this previous paper, our design strategy is to try out a very large number of potential coatings, and choose the coating that gives the lowest reflectance off the coated structure. The use of PC impedances makes this a feasible problem, as the evaluation of each coating is quick, involving a few operations on $M \times M$ (here 3×3) matrices.

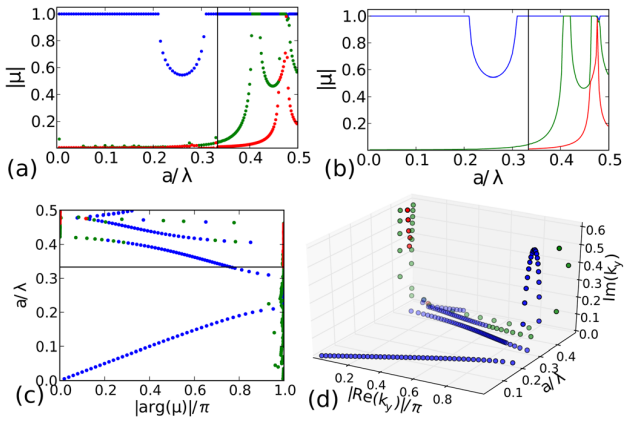

FIG. 2. (Color online) Complex band structure for the PC. The Wood anomaly ($a/\lambda = 0.333$) is marked. The modes are sorted into colors by $|\mu|$; where two modes are propagating (i.e., have $|\mu| = 1$), they are sorted by $|\arg(\mu)|$. (a) Magnitude of Bloch factors $|\mu|$, with three Bloch modes found at all frequencies. (b) $|\mu|$ with two Bloch modes found below the Wood anomaly, three above. (c) Argument of Bloch factors. (d) Complex band structure in 3D.

The target PC is a triangular lattice with lattice constant $a_x = a$, consisting of air holes in a dielectric background with $n = 2.86$. The holes are cylinders with radius $r = 0.25\ a$. We seek to coat the PC to minimize reflection for light with frequency $a/\lambda = 0.38$, incident from air at an angle of 30° in the E_z polarization. At this frequency and incident angle, $M_{\min} = 2$; we consider a total of 3 modes to ensure accuracy. As in our previous work,[12] we seek a two-layer coating, where the degree of freedom is a_y, the lattice vector component perpendicular to the air/PC interface. For a regular triangular lattice, $a_y = (\sqrt{3}/2)a$.

We choose 121 candidate PCs with $a_y \in [0.6, 1.8]$ $(\sqrt{3}/2a)$ and simulate 8 periods of each in COMSOL. We apply our method to the resulting data, using the Bloch factors of the previous PC as the starting estimate for the next. BlochCode processes the 121 PCs in approximately 13 mins on a 3.06 GHz Intel Core 2 Duo desktop computer. An equivalent approach that only requires one PC to be evaluated is detailed in Sec. IV C; we do not use it here since the purpose of this section is to demonstrate the reliability and consistency of the optimization procedure.

We then calculate the reflectances off the $121^2 = 14\,641$ coated stacks (Fig. 3), which takes 34 s on a single core of the desktop computer. The optimal coating is found to have thicknesses $a_{y1} = 1.53(\sqrt{3}/2)a$ and $a_{y2} = 0.65(\sqrt{3}/2)a$, and reduces the reflectance of the structure from $R = 0.945$ to $R = 1.96 \times 10^{-4}$. The results in Fig. 3 agree well with data calculated by a highly accurate multipole scattering matrix method: the RMS difference is 3.4×10^{-3}, and the only noticeable differences occur on the two sharp resonant features near the lower edge of the figure. Specifically, the multipole-based calculations show that the coating reduces the PC's reflectance from $R = 0.943$ to $R = 4.29 \times 10^{-4}$.

C. All-polarization antireflection coating

Finally, we apply our methods to find an all-polarization antireflection coating for a silicon-based self-collimating

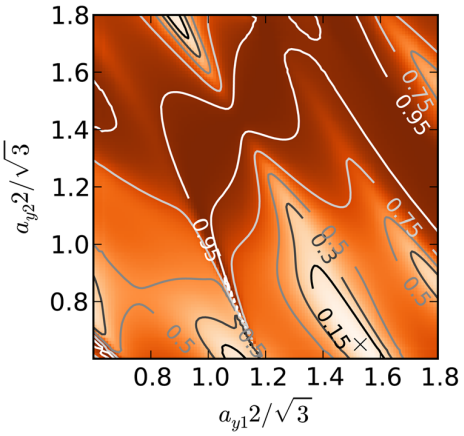

FIG. 3. (Color online) Reflectance of the coated PC as a function of a_{y1} and a_{y2}, the relative thicknesses of the two coating layers, calculated using PC impedances from BlochCode. The minimum reflectance is marked.

square-lattice photonic crystal presented by Park *et al.*[21] They investigated this class of structures using a scalar treatment of reflections, and were able to design an all-polarization coating at $a/\lambda = 0.28$, below the first Wood anomaly. Since their scalar treatment does not support multiple propagating or evanescent Bloch modes, it generally does not work above the Wood anomaly. Our method does not have this limitation and we demonstrate this by designing an antireflection coating for both polarizations at a frequency well above the Wood anomaly, using more than one Bloch mode.

Park *et al.*[21] showed that at $a/\lambda = 0.368$, a 2D silicon ($n = 3.518$) PC with $r = 0.45\ a$ is self-collimating for both polarizations at normal incidence. The large radius is an extreme case that is challenging to simulate accurately. At this frequency $M_{\min} = 3$, so for E_z polarized light we include $M = 3$ modes in our calculations, with light incident from the $p = 1$ grating order so that the otherwise uncoupled mode is excited. For H_z light, this procedure does not yield accurate results—Bloch factors are calculated accurately, but the calculated reflection coefficients differ from those calculated directly in COMSOL. The calculated impedances prove sufficiently accurate to design an effective antireflection coating, but the inaccuracies mean that the coating is not optimal.

To avoid these inaccuracies in H_z polarization, we exploit the symmetry that causes the uncoupled mode. The physical structure and normally incident field are both symmetric about the y-axis, and so modes without even symmetry are not coupled to. Therefore, we formally ignore the uncoupled odd mode, in each PC and in the reference medium, setting $M = 2$. In our H_z COMSOL simulations for this structure, light is normally incident.

In Fig. 2 of Park *et al.*'s paper,[21] they state that $R \simeq 0.28$ for E_z polarized light, and $R \simeq 0.35$ for H_z light. We calculate with BlochCode that a semi-infinite slab of the PC has $R = 0.284$ for E_z, and $R = 0.354$ for H_z polarized light at this frequency, when incident from silicon. Specialized FEM-based transfer-matrix calculations agree, showing $R = 0.284$ for E_z polarization, and $R = 0.357$ for H_z polarization.

At $a/\lambda = 0.368$, normally incident light is reflected by the PC into three propagating diffraction orders. Due to the symmetries of the problem, the ± 1 orders are only excited in an even superposition, so light is reflected into two modes. A successful coating needs to suppress reflection into both these modes simultaneously, and so must balance two modes' amplitudes and two modes' phases simultaneously for each polarization. Thus the design of a perfect all-polarization coating requires eight continuous degrees of freedom. Rather than trying to search an 8-dimensional parameter space, which is computationally expensive even when the evaluation of each point is efficient, we consider coatings with four degrees of freedom and accept that we are unlikely to find an all-polarization coating with zero reflectance.

Nevertheless, this is a particularly difficult problem: not only do we need many degrees of freedom to find a satisfactory coating, but if either of the Bloch factors in a PC is incorrect or any element of the PC's impedance matrix is wrong, then the calculated net reflection off the structure is incorrect as well.

To limit the coating's thickness, we embed the four degrees of freedom into two rows of holes by varying both the hole radii, r_1 and r_2, and the space after the layers, d_1 and d_2 (Fig. 4). Increasing d_1 and d_2 is similar to increasing a_y, as in Sec. IV B, but because the candidate PCs are independent of d, only one PC per radius needs to be simulated in COMSOL. Furthermore, the properties of the layers of silicon with thickness d_i may be calculated analytically. We consider 36 possible hole radii in the range $r_i \in [0.10, 0.45]a$ and 99 values of $d_i \in (0, 1)a$. To allow a thin coating, we set $a_y = 2r + 0.1a$ for each PC. If necessary, additional degrees of freedom could be added to find a coating with even lower reflectances.

On a single core of a 16×2.4 GHz Intel Xeon-Quad workstation, it took a total of 15 mins to find the modes of the 36 PCs in the two polarizations. For E_z polarization, $w^2 \simeq 10^{-5}$ for most radii, and for H_z polarization w^2 ranged roughly from 3×10^{-3} for thin unit cells to 10^{-7} for the thicker cells with larger radius. Due to the large number of candidate coatings ($\sim 1.3 \times 10^7$), the embarrassingly parallel problem was split over 16 cores of the workstation, taking approximately 80 mins per polarization.

The best E_z coating reduces R from 0.284 to 9.56×10^{-5}, and the best H_z coating reduces R from 0.354 to 3.33×10^{-4}. The best all-round coating is taken to be the one with the lowest total reflection in the two polarizations. This coating has $r_1 = 0.13\ a$, $d_1 = 0.89\ a$, $r_2 = 0.17\ a$, and $d_2 = 0.90\ a$ (Fig. 4). In E_z it reduces R to 0.0141, and in H_z it reduces R to 0.0197. Calculations from a specialized transfer matrix method[24] agree with these results, giving $R = 0.0142$ in E_z polarization and $R = 0.0211$ in H_z.

To verify these results without the aid of our specialized methods, implementations of which are not publicly available, we simulate the structure using COMSOL Multiphysics. Since COMSOL cannot directly calculate reflection coefficients off semi-infinite PCs, we simulate a 20-period section of the uncoated PC surrounded by the background dielectric, and compare the results to a simulation with the antireflection coating on both sides of the PC section. BlochCode calculates the reflectance of the uncoated and coated structures to be 0.407 and 0.0124, respectively, in the E_z polarization, and 0.574 and 0.0074 in the H_z polarization. The COMSOL simulations agree with these results, showing that the coating reduces R from 0.407 to 0.0129 in the E_z polarization, and from 0.585 to 0.0055 in the H_z polarization.

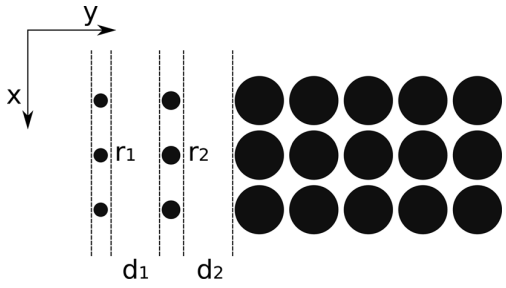

FIG. 4. Schematic of the all-polarization antireflection coating. r_1 and r_2 are the radii of the holes in the first two layers, and d_1 and d_2 are the thicknesses of the extra silicon background layers between the first few rows of holes. For this coating, $r_1 = 0.13\ a$, $d_1 = 0.89\ a$, $r_2 = 0.17\ a$, and $d_2 = 0.9\ a$.

V. DISCUSSION AND CONCLUSION

We have detailed a method for calculating the complex band structure and impedance of PCs. The method takes into account structural symmetries in the PC, and enforces relationships between the fields of forward and backward modes, thus improving the method's accuracy by eliminating ill-conditioning and constraining modal fields. We have applied the method to three cases, and have demonstrated that it works for a variety of square and triangular lattice 2D photonic crystals, for light in both polarizations and at different incident angles. We have demonstrated that our method works at frequencies both above and below the first Wood anomaly, the frequency above which scalar methods cannot adequately describe light propagation and reflection in PCs.

The stronger the excitation of a Bloch mode, the more accurately our method calculates its properties. Thus, the method is well-suited to calculating reflection and transmission through arbitrary PC stacks, where the most important modes are those that are strongly excited. Since PC impedances make it so easy to calculate the reflection and transmission properties of many combinations of PCs in a stack, it is feasible to search large parameter spaces of PC stacks for particular reflective properties over a range of frequencies, incident angles and polarizations. The method can be used to design not only all-polarization antireflection coatings, but also broadband antireflection coatings,[12] polarization filters, angular filters, and other devices.

Ha *et al*. have applied their method to slab PC waveguides.[19] We have not yet applied our method to any 3D structure. As long as the *x*-*z* plane mirror symmetry is present, our method for finding the complex band structure remains valid. The field of a slab waveguide might be sampled only over the PC's surface (as in a SNOM experiment[19]) or throughout the entire volume of the structure (as in a simulation); either case provides sufficient information to determine the modal fields within the sampled region and the associated complex band structure. However, the impedance formalism is yet to be developed for 3D structures.

Our method is also valid for finding modes of PC waveguides, using supercells. Calculation of reflection and transmission matrices between PC waveguides is yet to be demonstrated using impedances, but they have previously been calculated directly from the supercell's **E** and **H** matrices.[5]

Bloch mode analysis is a valuable tool in understanding light's interactions with PCs. Using an EM solver and our method, for which source code is available,[20] it is straightforward to find a PC's complex band structure and its impedance. Respectively, these quantities dictate how the Bloch modes travel through the PC, and which modes they couple with at a PC interface. If these quantities are known for a set of PCs, then it is fast and efficient to calculate how light travels through arbitrary stacks of the PCs.

ACKNOWLEDGMENTS

This research was conducted by the Australian Research Council Centre of Excellence for Ultrahigh bandwidth Devices for Optical Systems (Project No. CE110001018).

[1]R. W. Wood, Philos. Mag. **4**, 396 (1902).
[2]R. Smaâli, D. Felbacq, and G. Granet, Physica E **18**, 443 (2003).
[3]N. Stefanou, V. Karathanos, and A. Modinos, J. Phys. Condens. Matter **4**, 7389 (1992).
[4]F. J. Lawrence, L. C. Botten, K. B. Dossou, and C. M. de Sterke, Appl. Phys. Lett. **93**, 1114 (2008).
[5]C. M. de Sterke, K. B. Dossou, T. P. White, L. C. Botten, and R. C. McPhedran, Opt. Express **17**, 17338 (2009).
[6]V. Heine, Surf. Sci. **2**, 1 (1964).
[7]R. Biswas, Z.-Y. Li, and K. M. Ho, Appl. Phys. Lett. **84**, 1254 (2004).
[8]W. Smigaj, P. Lalanne, J. Yang, T. Paul, C. Rockstuhl, and F. Lederer, Appl. Phys. Lett. **98**, 111107 (2011).
[9]C. R. Simovski, Metamaterials **1**, 62 (2007).
[10]M. Miri, A. Khavasi, K. Mehrany, and B. Rashidian, Opt. Lett. **35**, 115 (2010).
[11]T.-T. Kim, S.-G. Lee, M.-W. Kim, H. Y. Park, and J.-E. Kim, Appl. Phys. Lett. **95**, 011119 (2009).
[12]F. J. Lawrence, L. C. Botten, K. B. Dossou, C. M. de Sterke, and R. C. McPhedran, Phys. Rev. A **80**, 23826 (2009).
[13]F. J. Lawrence, L. C. Botten, K. B. Dossou, R. C. McPhedran, and C. M. de Sterke, Phys. Rev. A **82**, 053840 (2010).
[14]B. Gralak, S. Enoch, and G. Tayeb, J. Opt. Soc. Am. A **17**, 1012 (2000).
[15]L. C. Botten, N.-A. P. Nicorovici, R. C. McPhedran, C. M. de Sterke, and A. A. Asatryan, Phys. Rev. E **64**, 046603 (2001).
[16]Y.-C. Hsue and T.-J. Yang, Phys. Rev. E **70**, 016706 (2004).
[17]S. Ha, A. A. Sukhorukov, K. B. Dossou, L. C. Botten, C. M. de Sterke, and Y. S. Kivshar, Opt. Lett. **34**, 3776 (2009).
[18]A. A. Sukhorukov, S. Ha, I. V. Shadrivov, D. A. Powell, and Y. S. Kivshar, Opt. Express **17**, 3716 (2009).
[19]S. Ha, M. Spasenović, A. A. Sukhorukov, T. P. White, C. M. de Sterke, L. K. Kuipers, T. F. Krauss, and Y. S. Kivshar, J. Opt. Soc. Am. B **28**, 955 (2011).
[20]https://launchpad.net/blochcode for BlochCode homepage, with source code.
[21]J. Park, S.-G. Lee, H. Park, and M. Lee, Opt. Express **18**, 13083 (2010).
[22]L. C. Botten, N.-A. P. Nicorovici, A. A. Asatryan, R. C. McPhedran, C. M. de Sterke, and P. A. Robinson, J. Opt. Soc. Am. A **17**, 2165 (2000).
[23]R. C. McPhedran, N.-A. P. Nicorovici, L. C. Botten, and K. A. Grubits, J. Math. Phys. **41**, 7808 (2000).
[24]L. C. Botten, T. P. White, A. A. Asatryan, T. N. Langtry, C. M. de Sterke, and R. C. McPhedran, Phys. Rev. E **70**, 56606 (2004).
[25]E. Popov, L. Mashev, and D. Maystre, J. Mod. Opt. **33**, 607 (1986).
[26]K. Sakoda, Phys. Rev. B **52**, 7982 (1995).
[27]E. Jones, T. Oliphant, P. Peterson *et al*., *SciPy: Open source scientific tools for Python* (2001-), http://www.scipy.org/.
[28]M. H. Wright, in *Numerical Analysis 1995*, Proceedings of the 16th Dundee Conference, edited by D. F. Griffiths and G. A. Watson (Addison-Wesley Longman, Harlow, 1996), *Pitman Research Notes in Mathematics*, Vol. 344, pp. 191–208.
[29]W. Stein *et al*., *Sage Mathematics Software (Version 4.7)*, The Sage Development Team (2011), http://www.sagemath.org.

In Paper 3.1 we develop methods to use a widely available commercial field solver to calculate PC impedances, Bloch factors, and antireflection coatings, in place of our specialised in-house code. The process described is slower and less reliable than the specialised multipole and FEM codes, but if the specialised code is not available, then the described method is certainly faster than directly designing an antireflection coating by independently evaluating each member of the combinatorial explosion of coatings with the commercial field solver.

The design of an antireflection coating has two steps: calculating impedances and Bloch factors, and calculating stack reflectances. Both of these tasks are *embarrassingly parallel*: both consist of many small problems, each one totally independent of the others. In principle, these small problems could be divided among the available cores of the computer: using this approach, a workstation with 16 cores can finish a step containing many of these problems in almost 1/16th of the time a non-parallel computation would take.

In practice, it is not possible to parallelise the first step: and not for any worthwhile reason. Using the method described in Paper 3.1, each of the small problems in this step requires a separate instance of the commercial field solver. If this field solver is Comsol Multiphysics, as in Paper 3.1, then each instance requires a separate licence—which costs several thousand Australian dollars. Even our in-house code may not be run in parallel: part of it is written in Mathematica, which also requires a separate licence per process. Thus, parallelising this step is not feasible purely due to the revenue models of the software providers. Thankfully, the PC impedance formalism drastically cuts the number of expensive (computationally and otherwise) numerical simulations required to design a coating.

The second step of a coating design, exploring the coating parameter space, involves many calculations with 3×3 or 5×5 matrices. As this step is also embarrassingly parallel—each stack's reflectance can be calculated independently of the others—and does not require commercial software, it may easily be parallelised. In fact, using the free and open source Sage software, which is based on NumPy and Python, parallelising my algorithm required only four additional lines of code. In the example given in Paper 3.1, this reduced the time taken to explore the parameter space by a factor of 16, to 80 minutes per polarisation.

3.2 Impedance matrices as overlap integrals

So far, we have defined PC impedance using the matrices $\mathbf{E}$ and $\mathbf{H}$, which map Bloch mode amplitudes to plane wave field amplitudes. The matrices $\mathbf{E}$ and $\mathbf{H}$ are new, so it might be helpful to provide an equivalent definition for the impedance in terms of quantities with which most readers are already familiar: the modal fields themselves. In this section, we show that each element of a PC's impedance matrix is essentially an overlap integral between a PC Bloch mode and a mode of the reference material, before discussing the significance of this result. We now derive this relation explicitly.

For simplicity, we work with square lattice PCs, which in E_z polarisation have impedance $\mathcal{Z} = 2\mathbf{H}_0^T\mathbf{E}$. The i,jth element of this matrix is

$$\mathcal{Z}_{i,j} = 2\sum_p \mathbf{H}^{(0)}_{p,i}\,\mathbf{E}_{p,j}, \tag{3.1}$$

where $\mathbf{H}^{(0)}_{p,i}$ is the p,ith element of $\mathbf{H}_0$ in reference medium 0, and $\mathbf{E}_{p,j}$ is the p,jth element of the $\mathbf{E}$ matrix in the PC that $\mathcal{Z}$ represents. The summation

occurs over the grating orders p. We seek to write each impedance matrix element $\mathcal{Z}_{i,j}$ directly in terms of the fields of Bloch modes in the PC and the reference medium.

Our reciprocity-based orthogonality and normalisation relation for the Bloch modes of a square or rectangular lattice PC is $2\,\mathbf{H}^T\mathbf{E} = \mathbf{I}$. It can be written in overlap integral form as

$$\delta_{ij} = \frac{1}{a_x}\int_{-a_x/2}^{a_x/2} E_i(x)\,H_j'(x) + H_j(x)\,E_i'(x)\,dx = \frac{2}{a_x}\int_{-a_x/2}^{a_x/2} H_j(x)\,E_i'(x)\,dx, \tag{3.2}$$

where in the E_z polarisation E and H refer to the E_z and H_x field components of modes i and j with wavevector x–component k_x, and E' and H' refer to the field of the reciprocal Bloch modes with wavevector x–component $-k_x$. If the unit cell is up-down symmetric, then along the unit cell edge $y = 0$ each reciprocal mode is related to its regular equivalent by $E_i'(x) = E_i(-x)$ and $H_i'(x) = H_i(-x)$. Using this property, we can rewrite Eq. (3.2) as

$$\delta_{ij} = \frac{2}{a_x}\int_{-a_x/2}^{a_x/2} H_j(x)\,E_i(-x)\,dx. \tag{3.3}$$

Eq. (3.3) can be used to normalise Bloch modes, as well as to orthogonalise pairs of degenerate Bloch modes. This orthogonality relation is based on mode reciprocity, and so it applies to lossless media as well as lossy media.

If the modes are normalised using Eq. (3.3), then from Eqs. (18) in Paper 3.1 the field of Bloch mode m along the front edge of a PC unit cell may be written as a superposition of grating orders with amplitudes given by the elements of $\mathbf{E}$ and $\mathbf{H}$,

$$E_m(x) = \sum_p E_{p,m}\,e^{ik_x^{(p)}x}, \tag{3.4a}$$

$$H_m(x) = \sum_p H_{p,m}\,e^{ik_x^{(p)}x}. \tag{3.4b}$$

The Bloch modes of another PC have the same form (provided the lattice constant a_x and wavevector $k_x^{(0)}$ are the same), differing only in the values of $E_{p,m}$ and $H_{p,m}$, i.e. for different PCs, the $\mathbf{E}$ and $\mathbf{H}$ matrices are different but the underlying bases of grating orders are the same.

Given the fields of Bloch modes i and j of PC 1 and 2 respectively, we calculate

$$2/a_x\int_{-a_x/2}^{a_x/2} H_i^{(1)}(x)\,E_j^{(2)}(-x)\,dx. \tag{3.5}$$

Using Eqs. (3.4), this is equal to

$$\frac{2}{a_x}\int_{-a_x/2}^{a_x/2}\left[\sum_p H_{p,i}^{(1)}\,e^{ik_x^{(p)}x}\right]\left[\sum_p E_{p,j}^{(2)}\,e^{-ik_x^{(p)}x}\right]dx. \tag{3.6}$$

Now, the grating equation (1.24) states that the various wavevector components $k_x^{(p)}$ differ by integer multiples of $2\pi/a_x$, and hence

$$\frac{1}{a_x}\int_{-a_x/2}^{a_x/2} e^{ik_x^{(p)}x}e^{-ik_x^{(q)}x}\,dx = \delta_{pq}, \tag{3.7}$$

where δ_{pq} is the Kronecker delta—this is a restatement of grating orthogonality (Eq. (1.27)). This relation means that the cross terms of the product

in Eq. (3.6) vanish under integration, and so we may rewrite (3.6) as a single summation,

$$\frac{2}{a_x}\int_{-a_x/2}^{a_x/2}\left[\sum_p H_{p,i}^{(1)}\, e^{ik_x^{(p)}x}\, E_{p,j}^{(2)}\, e^{-ik_x^{(p)}x}\right] dx = 2\sum_p H_{p,i}^{(1)} E_{p,j}^{(2)}, \tag{3.8}$$

which is the i,jth element of $\mathbf{A}_{12} = 2\mathbf{H}_1^T\mathbf{E}_2$.

If the modes are normalised using Eq. (3.3), then the i,jth element of a PC's impedance matrix $\mathcal{Z}$ is

$$\mathcal{Z}_{i,j} = \frac{2}{a_x}\int_{-a_x/2}^{a_x/2} H_i^{(0)}(x)\, E_j(-x)\, dx, \tag{3.9a}$$

$$\mathcal{Z}_{i,j} = -\frac{2}{a_x}\int_{-a_x/2}^{a_x/2} E_i^{(0)}(x)\, H_j(-x)\, dx, \tag{3.9b}$$

where Eq. (3.9a) is for E_z polarised light, Eq. (3.9b) is for H_z polarised light, $E_j(x)$ is the jth Bloch mode of the PC, and $H_i^{(0)}$ is the ith Bloch mode of the reference medium 0.

Even for the element $\mathcal{Z}_{1,1}$, Eqs. (3.9) have a rather different form to any field-based impedance definition discussed in Sec. 1.6.2, as they use the field of a PC's Bloch mode as well as the mode of a reference medium. Eqs. (3.9) also rely on the fields being normalised in a particular way (Eq. (3.3)).

In the derivation of (3.9), we expand the modal fields in the basis of grating orders, but we never truncate the set of grating orders. This contrasts with the matrix-based impedance definition (Eq. (26a) in Paper 2.3), where this set must be truncated so that $\mathbf{E}$, $\mathbf{H}$ and $\mathbf{Q}$ are of finite dimension. Therefore, in principle, Eqs. (3.9) can give more accurate results than a matrix-based method to calculate impedance, if truncation is an issue and the modes are not calculated using transfer-matrix methods that represent the modes by a truncated set of P diffraction orders.

3.3 Outlook for PC waveguide impedances

In the work presented in this thesis, truncation is not an issue: $P = 5$ grating orders are sufficient for accuracy, as demonstrated in the Erratum to Paper 5.1. But beyond this thesis's direct purview, there exist related problems for which a large number of grating orders must be considered.

One such problem is the simulation of PC waveguides using a supercell approach. In supercell methods, a structure that is not periodic in the x–direction is approximated by one that is. The simulation's accuracy scales with the chosen size of the supercell in the x–direction: if the supercell is too small then adjacent supercells couple, distorting the results. Unfortunately, if a larger supercell period is taken, the feature to be studied (the waveguiding region) is smaller with respect to the supercell period, and so the number of supercell grating orders $P_{\min}$ required to resolve the waveguiding region scales with the supercell size. Therefore such problems require consideration of many grating orders, even if the number of physically important Bloch modes $M_{\min}$ (which should not scale with supercell size) is small: for such problems, $P_{\min} \gg M_{\min}$. Thus the $\mathbf{E}$ and $\mathbf{H}$ matrices for such PC supercells, which have dimension $P \times M$, are potentially large and unwieldy. Therefore it would be advantageous to calculate the smaller $M \times M$ impedance matrix $\mathcal{Z}$ directly using Eqs. (3.9) and PC waveguide Bloch modes calculated by the methods of Paper 3.1.

However, a subtlety arises: the reference material should be chosen carefully—using vacuum as a reference material (as we do successfully in

all examples given in this thesis, and is discussed in Appendix B) implicitly truncates the set of grating orders to the number of Bloch modes considered (see Appendix A), and so using a P such that $P > M$ is meaningless; to obtain accurate results with such a reference material, M must be as large as P_{min}, which scales with the supercell size. Another problem with using a uniform medium as a reference PC for supercell calculations is that the front and back supercell edges often cut across the cylindrical holes of the PC; the plane wave diffraction orders of a uniform dielectric are ill-suited to describing the field across a dielectric discontinuity. An impedance matrix $\mathcal{Z}$ consists of overlap integrals between the Bloch modes of a PC and the reference medium; if the modes of the reference medium cannot represent the PC's modes then information is lost. By Bloch's theorem, it *is* always possible to describe fields of such structures by the Fourier series corresponding to grating orders, but there is no guarantee that P_{min} is not very large.

These two problems, which might frustrate the practical implementation of PC impedance methods for PC waveguide supercells, perhaps might be overcome by carefully choosing a reference medium that has modes similar to those of all structures to be simulated. Ideally the set of Bloch modes of this reference medium could accurately represent all the relevant Bloch modes of every simulated structure; if such a reference medium is found then accurate results might be obtained using a small $M_{\text{min}} \times M_{\text{min}}$ impedance matrix $\mathcal{Z}$.

If I were to tackle such a problem, my first candidate for a reference material would be one of the PCs in the problem, such as the target PC waveguide. If it turns out that a heavily truncated (i.e. small M) set of this PC's Bloch modes is insufficient to represent the important modes of the other PCs, then I would hold little hope that *any* reference material could represent the modes of all PCs in the problem with such a value of M.

Chapter 4

Characterisation by effective parameters

In recent years there has been much debate regarding the homogenisation of metamaterials, and to a lesser extent, the homogenisation of PCs. Homogenisation entails calculating effective parameters that characterise a metamaterial or PC—most commonly, an effective relative permittivity ϵ and an effective relative permeability μ.[1] Simovski *et al.* [122] give a good overview of the state of homogenisation techniques. Typically, effective ϵ and μ are calculated from a PC or metamaterial's propagation constant $k_\perp = k_y$ (or equivalently its effective refractive index n_{eff}), together with its wave impedance Z. Ideally, the PC or metamaterial can then be replaced in calculations by a homogenous medium with relative permittivity ϵ and relative permeability μ. The general consensus is that such approaches for 2D materials are strictly valid only in the long wavelength limit ($n\lambda > 100\,d$), are potentially useful but somewhat dubious at frequencies below the first Wood anomaly ($n\lambda > d$) where the single-mode approximation holds, and are manifestly incorrect at frequencies above the Wood anomaly, where we saw in Paper 2.1 that matrices are required [122]. Most recent interest is focussed on the middle wavelength range $100\,d > n\lambda > d$, where devices can be fabricated for optical wavelengths.

The most common homogenisation method, the NRW method, is largely described in Sec. 1.6.3, and comprises two steps. First, a finite length of PC or metamaterial is either simulated or experimentally measured to find that length of PC's reflection and transmission coefficients; from these two complex quantities the bulk PC's propagation constant and wave impedance (which Simovski *et al.* call the surface impedance) are found. The propagation constant k_y may be related to an effective refractive index n_{eff}, and the wave impedance Z is related to the characteristic impedance by Eq. (1.3) (at normal incidence, $Z = Z_c$). In the second step, effective parameters ϵ and μ are calculated by asserting that the usual relations between n, Z_c, ϵ and μ apply, as for homogenous media. There are issues with both steps of this approach; we detail these in the next paragraphs.

In the first step of the NRW method, a branch ambiguity arises: the propagation constant k_y is calculated from the total phase accumuluated across the length of PC, which is only known modulo 2π. Hence k_y is only determined modulo $2\pi/(\ell d_y)$, where ℓd_y is the length of the simulated PC or metamaterial, an integer ℓ multiple of the unit cell length d_y [151, 152]. This ambiguity can play havoc with the effective parameters derived from k_y. It

[1] Nomenclature: in this chapter alone, μ represents a PC's effective relative permeability, not its Bloch factor, which is instead represented by η.

can be lessened by varying the integer ℓ and calculating the reflection and transmission coefficients of several different lengths of the PC. We find the PC's propagation constant as the phase accumulated across a single unit cell ($\ell = 1$), so it is known modulo $2\pi/d_y$, i.e. up to a reciprocal lattice vector, which is the best the lattice allows.

Potential ambiguities regarding the reflection at a single interface can be eliminated by directly simulating a semi-infinite structure [153], of which our method is also capable. In fact, by applying the single-mode approximation and truncating our impedance matrix to a scalar, we can calculate the wave impedance directly rather than from a reflection coefficient.[2] Doing so sidesteps another problem of the NRW method, highlighted by Simovski *et al.* [122]: that changing the media either side of the length of PC can change its impedance (the same phenomenon as the example in Paper 2.1 that demonstrates that scalar impedances fail above the Wood anomaly). A key feature of our impedance method is that the impedance $\mathcal{Z}$ depends only on the PC and a reference material, and not on the other media in the stack: when the single-mode approximation holds, the impedance is well-defined.

The problem with the second step of standard homogenisation processes is a more fundamental one: away from the long wavelength limit no theoretical link has been established for the values of the propagation constants, impedances, or other related quantities as they vary with frequency, incident angle or polarisation. That is, not all quantities in a homogenisation procedure can be assumed to vary in a predictable way with frequency, incident angle or polarisation. Thus ϵ and μ, which are derived from these parameters, cannot be expected to represent PC properties for light at any frequency, polarisation or incident angle other than that for which the parameters were calculated. Even at a single frequency, PCs' properties generally may not be summarised by one pair of ϵ and μ tensors. For this reason Simovski *et al.* [122] stress that in most cases, homogenisation procedures do not result in *characteristic* material parameters, they only give *effective* material parameters, valid in the circumstance for which they were calculated.

Use of the NRW method to derive effective material parameters has been less common for photonic crystals, and seems mostly restricted to attempts to derive impedances as discussed in Sec. 1.6.3, although there are exceptions, such as Refs. [132, 142, 145, 152], which explicitly derive ϵ and μ parameters. For photonic crystals, more attention has been paid to characterising propagative qualities by inspecting band surfaces, either as band structures (Figs. 1.16 and 1.17) or as a set of equifrequency contours. The isotropy (or otherwise) of a PC may be determined by inspecting its equifrequency contours, which show the relationship between k_x and k_y for modes at fixed frequencies. At any given frequency, an isotropic medium has constant $k_x^2 + k_y^2 = nk_0$, and so circular equifrequency contours need to be used to ascribe an effective refractive index n, which summarises its propagation properties across all angles at that frequency. Crucially, this refractive index is not an impedance and does not generally predict reflection coefficients via the Fresnel equations [154]. If a Bloch mode's equifrequency contour is elliptical or hyperbolic, then diagonal ϵ and μ tensors can describe it at the fixed frequency [132]. But if the equifrequency contour is not elliptical or hyperbolic, then the PC cannot be characterised at that frequency even by a uniaxial optical crystal [155]. Generally, k_x and k_y are only related at a given frequency by lattice symmetries. For square lattices and regular triangular lattices, these symmetries eliminate the possibility of elliptical equifrequency

[2] From the definition of the impedance matrix $\mathcal{Z}$, if the reference medium is a uniform dielectric then the single mode approximation implicitly involves representing the field at the interface by a single grating order: it is therefore also a single plane wave approximation.

contours, so such PCs either have circular equifrequency contours and are homogenisable to an isotropic medium with an effective index n, or they cannot be represented for all propagation directions by diagonal ϵ and μ tensors.

In this chapter we show how our impedance framework may be adapted to homogenise PCs, discuss where homogenised effective parameters are valid, give a few examples, and ask whether anything is gained by doing so. We show how our impedance formalism can be used to describe PCs using two complex numbers: a propagation constant and an impedance, which may be transformed to effective ϵ and μ parameters that are valid only at one frequency, incident angle and polarisation. In Paper 4.1 we discuss the domain of applicability of these parameters, showing how they fail at frequencies above the first Wood anomaly, as well as showing an exception to this rule. To gain intuition, we plot the effective parameters for a square lattice PC (Paper 4.1) and a triangular lattice PC (Sec. 4.2) over a range of frequencies and k_x; in Sec. 4.2 we give a more detailed discussion of our homogenisation procedure. The figures presented in these sections contain the information required to generate equifrequency contours: in Sec. 4.3 we apply our method from Chapter 3 and a commercial field solver to calculate an equifrequency contour for a self-collimating PC presented by Tang *et al.* [37]. We conclude in Sec. 4.4 by assessing what might be gained by homogenising PCs.

Bloch-mode Based Homogenisation of Photonic Crystals

Felix J. Lawrence[1], Kokou B. Dossou[2], Lindsay C. Botten[2], R. C. McPhedran[1], and C. Martijn de Sterke[1]
[1]Centre for Ultrahigh-bandwidth Devices for Optical Systems (CUDOS), Institute for Photonics and Optical Sciences (IPOS) and School of Physics, University of Sydney, NSW 2006, Australia
[2]CUDOS and Department of Mathematical Sciences, University of Technology, Sydney NSW 2007, Australia

Abstract Summary

We propose a method for photonic crystal (PC) homogenisation based on the PC's Bloch modes. The resulting quantities may be used in Snell's law; to calculate reflections, transmissions, and propagation; and to locate surface modes.

Photonic crystals; homogenisation; impedance

I. Introduction

Light propagation in 2D photonic crystals (PCs) is complicated, and resists analytic treatment. Therefore many researchers are interested in the homogenisation of PCs and metamaterials [1–3], where a PC or metamaterial may be approximated by a uniform medium with some effective properties. Such effective properties may include refractive index, impedance, permittivity, and permeability. If the homogenisation is valid, then these quantities may be used in standard equations, for example the effective index may be used in the Fresnel equations to calculate reflection coefficients.

In the long wavelength limit, where $\lambda \gg d$, effective parameters for PCs may be derived analytically [4]. However, most interesting properties of PCs occur in or close to PC band gaps, which occur at higher frequencies far from this limit. At such frequencies effective parameters may only be found empirically from simulation or experiment, and there is no guarantee that the resulting quantities are useful or consistent. For example, the effective index calculated from reflections at a PC-air interface may differ from that calculated from reflections at a PC-glass interface, or from the effective index calculated by applying Snell's law.

When considering light propagation in PCs, the natural basis to consider is the set of the PC's Bloch modes (its eigenstates). The complication is that at an interface, each Bloch mode reflects and transmits into many other Bloch modes. Therefore the problem is akin to that of multiconductor transmission lines [5]: in general several modes must be considered simultaneously, and reflections and transmissions are described by matrices rather than scalar coefficients. We previously derived a Bloch-mode based method for calculating reflection and transmission matrices for PC interfaces, from an impedance-like matrix [6, 7]. The dimension of the matrices is the number of Bloch modes in the calculation. When considering all Bloch modes (a countably infinite set) the method is exact, but in practice strongly evanescent modes are neglected as they do not affect energy flow.

Our homogenisation procedure therefore consists of calculating the PC impedance using only one Bloch mode, either a propagating mode (in band) or the most slowly evanescent mode (in gap). With the field projected onto a basis of one mode, the reflection and transmission and impedance-like matrices become scalars. Scalars commute, and the impedance matrix equations [7] for the reflection and transmission at the interface between PC 1 and PC 2 may be rearranged to the familiar expressions

$$Z = E_{\parallel}/H_{\parallel},$$
$$r_{12} = \frac{Z_2/Z_1 - 1}{Z_2/Z_1 + 1}, \quad \text{and} \quad t_{12} = \frac{2\sqrt{Z_2/Z_1}}{Z_2/Z_1 + 1}, \qquad (1)$$

where $E_{\parallel}$ and $H_{\parallel}$ are the field components parallel to the plane of the interface, as measured at the phase origin (the centre of the PC unit cell's front edge). The transverse or wave impedance Z is related to the PC impedance-like matrix $\mathcal{Z}_i$ by $\mathcal{Z}_i^2 = Z_i/Z_0$, with Z_0 the wave impedance in free space [7]. The PC's propagative properties are given by the mode's Bloch factor η, which is the phase or decay factor across one period of the PC; for free space, if the interface lies in the x–z plane, $\eta = e^{ik_y d_0}$ where d_0 is some arbitrary period and k_y is the wave vector component perpendicular to the interface.

In Sec. II, we discuss where this single mode approximation yields acceptable results, and in Sec. III we use PC impedance and Bloch factor to derive common effective quantities.

II. Where is homogenisation possible?

Since our homogenisation approximation consists of discarding all Bloch modes bar one from a calculation, the approximation only works in circumstances dominated by a single Bloch mode—other homogenisation procedures are also limited to this regime [1]. When multiple propagating Bloch modes are involved, an effective index generally compatible with the Fresnel equations cannot be consistently defined [6].

This work was produced with the assistance of the Australian Research Council (ARC). CUDOS (the Centre for Ultrahigh-bandwidth Devices for Optical Systems) is an ARC Centre of Excellence.

For a given frequency, incident angle and polarisation, one can roughly see whether a Bloch mode is important by looking at the modulus of its Bloch factor $|\eta|$. The moduli of the largest two Bloch factors are shown in Fig. 1 for the E out of plane polarisation of a square lattice PC with air holes of radius 0.35 d in a $n = 3.5$ dielectric background.

Roughly speaking, the second mode becomes non-negligible above the first Wood anomaly [8] (dashed line in Fig. 1); a PC can be seen as a stack of gratings, and for a given incident angle or k_x (wave vector component along the grating), the first Wood anomaly occurs at the frequency

$$d/\lambda = |(k_x d/2 - 1)/n|, \qquad (2)$$

the lowest frequency at which the grating diffracts an incident plane wave into a second propagating order.

At frequencies well below the Wood anomaly, one Bloch mode dominates and our homogenised calculations yield accurate reflection coefficients. We now investigate the accuracy of these calculations near the Wood anomaly. Reflection coefficients are shown in Fig. 2(a) and 2(b) for a three layer section of the PC from Fig. 1, embedded in background dielectrics of $n = 2.5$ and $n = 3.5$, for frequencies and incident angles given by the red curve in Fig. 1.

Even below the Wood anomaly, the reflection coefficient calculated by the homogenised treatment starts to deviate from the correct result. In Fig. 2(b), the discontinuity in slope at the Wood anomaly of the accurate reflectance occurs because above that frequency the PC reflects light into two propagating plane wave orders.

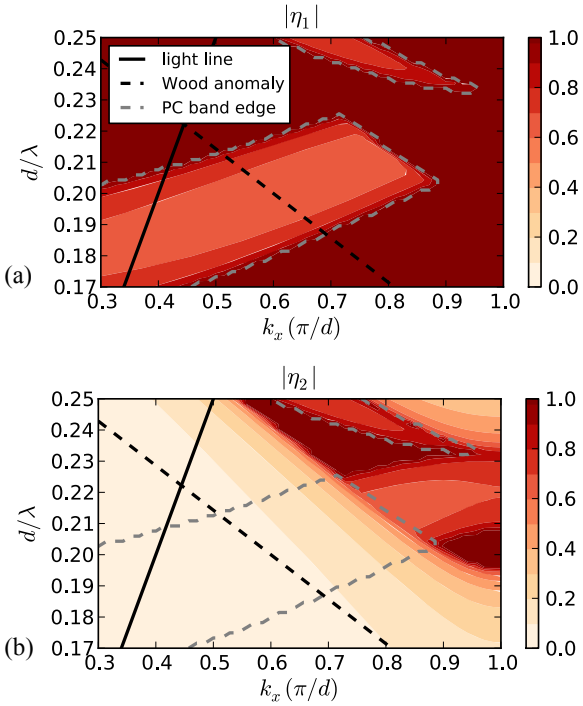

FIG. 1: Modulus of (a) η_1, the largest Bloch factor and (b) η_2 the second largest Bloch factor. Our homogenised treatment considers only the mode with the largest Bloch factor and ignores all others.

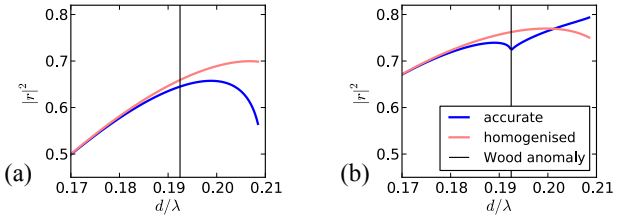

FIG. 2: Reflectances for a 3d thick layer of PC embedded in a background dielectric of (a) $n = 2.5$ and (b) $n = 3.5$, calculated accurately using five Bloch modes (blue) and with a homogenised treatment (red). Note that k_x is varied with d/λ so as to follow the red curve in Fig. 3.

In some situations, the homogenised treatment can give accurate results well above the Wood anomaly. PC surface modes, electromagnetic states that decay in both directions away from an air/PC or PC/PC interface, may be found from poles of the reflection matrix [9], in a manner similar to how surface plasmons may be found from poles of the reflection coefficient. Fig. 3 shows a surface mode for which the homogenised treatment (red) agrees with the accurate treatment (blue) both below and above the first Wood anomaly (dashed line).

Above the Wood anomaly, the dispersion relations start to diverge slightly, but still substantially agree. In this surface mode the field is concentrated in the most slowly evanescent Bloch mode, which has an amplitude at the interface over 20 times larger than that of the next most important Bloch mode. The other surface mode, in the higher frequency partial band gap, is not found by the homogenised treatment, as it is essentially a superposition of two Bloch modes and so cannot be meaningfully represented by a homogenised method.

III. Derivation of Effective Quantities

Having proposed a homogenisation method that provides an impedance Z that determines reflections and a Bloch factor η that determines propagation, and having explored the circumstances under which this approximation provides good results, we now consider the calculation of other effective parameters from Z and η. This procedure offers no new information about the PC but serves to highlight some

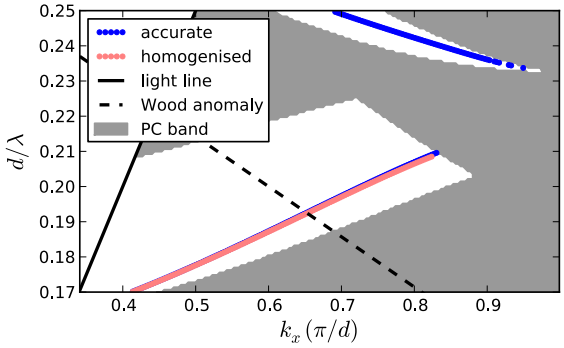

FIG. 3: Projected band structure of surface modes at an air/PC interface, below the light line (solid) and around the first Wood anomaly (dashed line). The red (lighter) points are surface modes found from homogenised impedances, and the blue (darker) points, many of which are obscured by the red points, are surface modes found with an accurate method [9].

counterintuitive results that raise questions about the physical relevance of such effective parameters.

First we calculate an effective k_y from the Bloch factor η. Approximating the Bloch mode by a plane wave we write $\eta^l = e^{ik_y ld}$. By Bloch's theorem, this approximation is valid at positions y that are integer multiples l of the lattice constant d (N.B. for a non-square lattice this d may differ from that in (2)). k_y and Z are shown in Fig. 4 for the PC from Sec. II.

From k_y and the transverse impedance Z we can calculate the PC's effective ε and μ, using equations valid for plane waves in the $|\boldsymbol{E}| = E_z$ polarisation: $\mu = Zk_y/\omega$ and $\varepsilon = |\boldsymbol{k}|^2/k_y Z\omega$. Then we can calculate the PC's effective characteristic impedance $Z_c = \sqrt{\mu}/\sqrt{\epsilon}$ and effective index $n = \sqrt{\epsilon}\sqrt{\mu}$. These quantities are shown in Fig. 5.

Note that all quantities vary strongly with both frequency and k_x; the PC is highly isotropic. The PC has a varying μ despite consisting of dielectrics. There is a small negative index region, however as this is near the Wood anomaly the validity of the single mode approximation is unclear.

Otherwise, they behave as expected: in the single mode approximation n may be used in Snell's law to find the relationship between k_x and k_y, but may not be used in the Fresnel equations since $\mu \neq 1$ generally. Reflection coefficients can be found using Z in (1), and k_y describes propagation at points differing from the phase origin by integer multiples of lattice vectors. These effective quantities are no more powerful than the Z and η from which they were derived, but are more widely used and understood.

IV. Conclusion

We have explored the approximation of our PC impedance method [6, 7] where only one Bloch mode is considered. This approximation is usually valid beneath the first Wood anomally. Under this approximation PC impedance matrices are reduced to scalars, which introduces commutativity, allowing simplification of equations. We investigate the regime in which this approximation is valid, finding that in certain circumstances the approximation can predict surface modes even at frequencies too high for it to calculate reflectances. Our homogenised quantities may be applied to Snell's law, used to calculate reflection and transmission coefficients, and used to find surface modes.

References

[1] W. Smigaj and B. Gralak, Physical Review B **77**, 235445 (2008).

[2] B. Momeni, A. Eftekhar, and A. Adibi, Optics Letters **32**, 778 (2007).

[3] G. Sun and A. G. Kirk, Opt. Express **15**, 13149 (2007).

[4] R. C. McPhedran, C. G. Poulton, N. A. Nicorovici, and A. B. Movchan, Physica A Statistical Mechanics and its Applications **241**, 179 (1997).

[5] M. Miri, A. Khavasi, K. Mehrany, and B. Rashidian, Opt. Lett. **35**, 115 (2010).

[6] F. J. Lawrence, L. C. Botten, K. B. Dossou, and C. M. de Sterke, Applied Physics Letters **93**, 121114 (2008).

[7] F. J. Lawrence, L. C. Botten, K. B. Dossou, C. M. de Sterke, and R. C. McPhedran, Physical Review A **80**, 23826 (2009).

[8] R. Wood, Philos. Mag **4**, 396 (1902).

[9] F. J. Lawrence, L. C. Botten, K. B. Dossou, R. C. McPhedran, and C. M. de Sterke, Physical Review A (submitted)

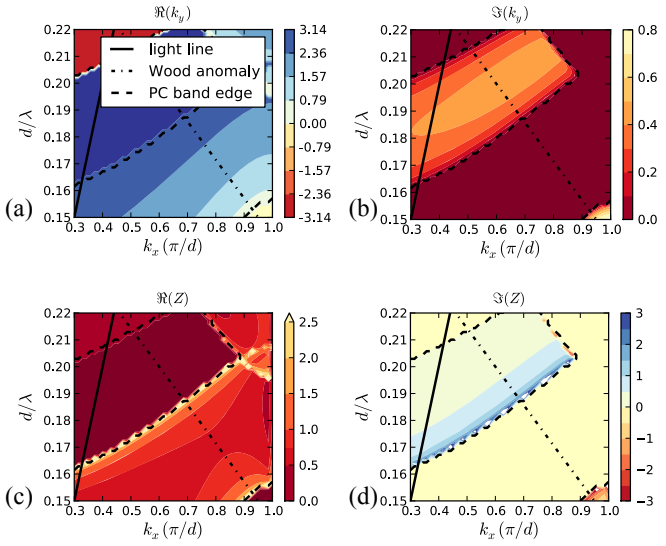

FIG. 4: Real and imaginary parts of wave vector component k_y ((a) and (b)), and transverse impedance Z ((c) and (d)). In band, k_y and Z are both real; in the band gap Z is imaginary and k_y has a real component of 0 or π.

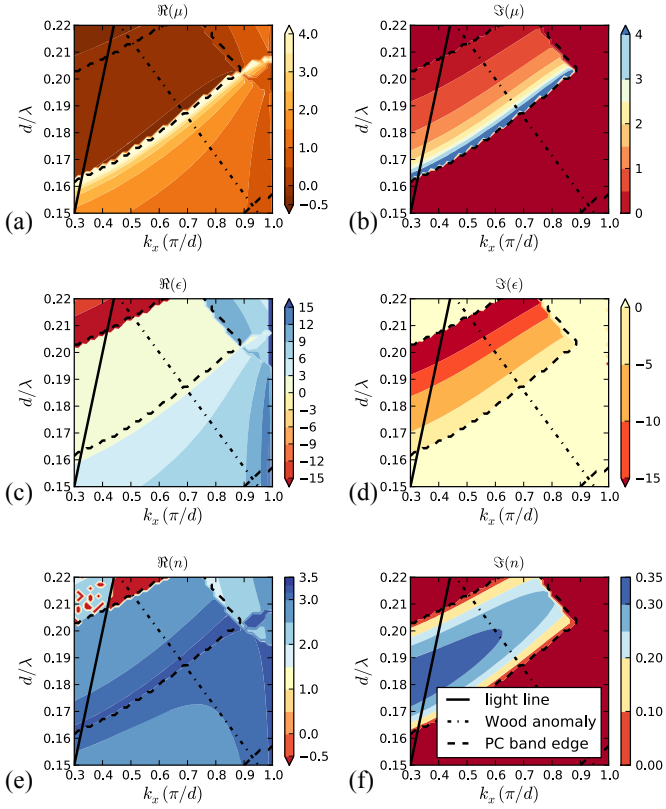

FIG. 5: Real and imaginary parts of effective permeability μ ((a) and (b)); permittivity ε, ((c) and (d)); and refractive index n ((e) and (f)). All quantities vary with both frequency and k_x: an effective index is valid only at one incident angle. μ^2 and ε^2 are always real.

4.2 Homogenisation of triangular lattice PCs

In Paper 4.1 we only consider a square-lattice PC. Here, we extend the technique to triangular lattice PCs and then apply it. But first we examine the quantities from which we calculate our effective parameters.

In this section we consider a triangular lattice PC that consists of air holes with radius $r = 0.35\,d$ in a background dielectric with $n = 3.5$. As required by our method, the PC's unit cell is up-down symmetric. We consider light incident in the H_z polarisation with a range of 50 $k_x\,d \in [0.01, \pi]$ (corresponding to different incident angles) and 50 frequencies $d/\lambda \in [0.01, 0.36]$. Multipole simulations are performed to find the Bloch factors and impedances for each frequency and k_x.

The magnitudes of the largest two Bloch factors, $|\eta_1|$ and $|\eta_2|$, are shown in Fig. 4.1. $|\eta| = 1$ for a propagating mode. Figure 4.1a shows that the PC has a complete bandgap that includes the frequency $d/\lambda = 1/3.5 \simeq 0.29$, which is the first (and second) Wood anomaly at normal incidence. As expected, no modes propagate below the light line of the PC's background material. There is a partial bandgap just above the light line—this indicates that the first band of the PC may not be coupled into at near-grazing incidence from the background dielectric. At all frequencies below the first Wood anomaly, the second mode is strongly evanescent. In the large k_x, high frequency corner of the bandgap, which is well above the Wood anomaly, $|\eta_1| = |\eta_2|$ and so this PC is likely to exhibit the braiding effects noted by Brownless *et al.* [5]. In the braided region the modes come as a pair, so homogenisation attempts are especially unlikely to succeed as they require one of the modes to be neglected. If we truncate and consider only two modes, then $\mathcal{Z}$ is a 2×2 matrix. The moduli of its four elements are shown in Fig. 4.2. If only one mode were to be considered in the PC, then $\mathcal{Z}_{11}$ (Fig. 4.2a) would be unchanged but would be the only element of $\mathcal{Z}$: this element of the 2×2 matrix encapsulates the PC's reflective properties in the single-mode approximation. Below the Wood anomaly, the varying magnitude of $\mathcal{Z}_{11}$ in Fig. 4.2a shows the existence of a "Brewster's angle" for this PC: where $\mathcal{Z}_{11}^2 = 1$ there is no reflection when coupling into the PC from the reference material (air).

Triangular lattices have non-orthogonal lattice vectors, so the Bloch factor

$$\eta = e^{i\mathbf{k}\cdot\mathbf{e}_2} = e^{i(k_x d/2 + k_y d_y)} \tag{4.1}$$

contains a k_x factor, which must removed in order to find the propagation constant k_y. The incident angle determines k_x, so Eq. (4.1) can be rearranged to find the propagation constant k_y, modulo $2\pi/d_y$. The ambiguity associated with choosing a branch can play havoc with effective parameters derived from k_y—but finding it modulo $2\pi/d_y$ is less ambiguous than finding it modulo $2\pi/(\ell d_y)$ as in the NRW method, and probably is the best that can be done given the PC's periodicity.

In the single-mode, single-plane wave approximation, there is no difference between impedance definitions for square and triangular lattices. In the definition of impedance, Eqs. (26) in Paper 2.3, $\mathbf{Q} = \mathbf{I}$ for square lattices and $\mathbf{Q} = \mathrm{diag}(e^{is\pi})$ for triangular lattices. When truncating the plane wave basis to a single grating order, these matrices become scalars. The specular grating order is $s = 0$, and so for both square and triangular lattices, $Q = 1$, and the PC impedance product $\mathcal{Z}\mathcal{Z}^T$ simplifies to

$$\mathcal{Z}\mathcal{Z}^T = (E/H)/(E_0/H_0). \tag{4.2}$$

From this quantity, the wave impedance of the PC $Z = E/H$ may easily be

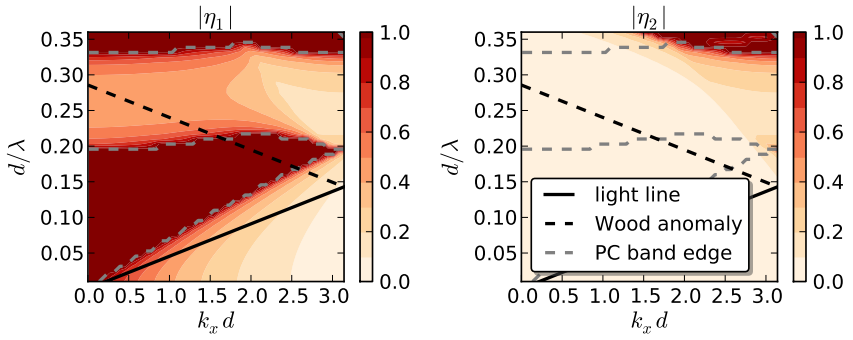

(a) **(b)**

Figure 4.1: Moduli of the largest two Bloch factors for forward modes of the triangular lattice PC.

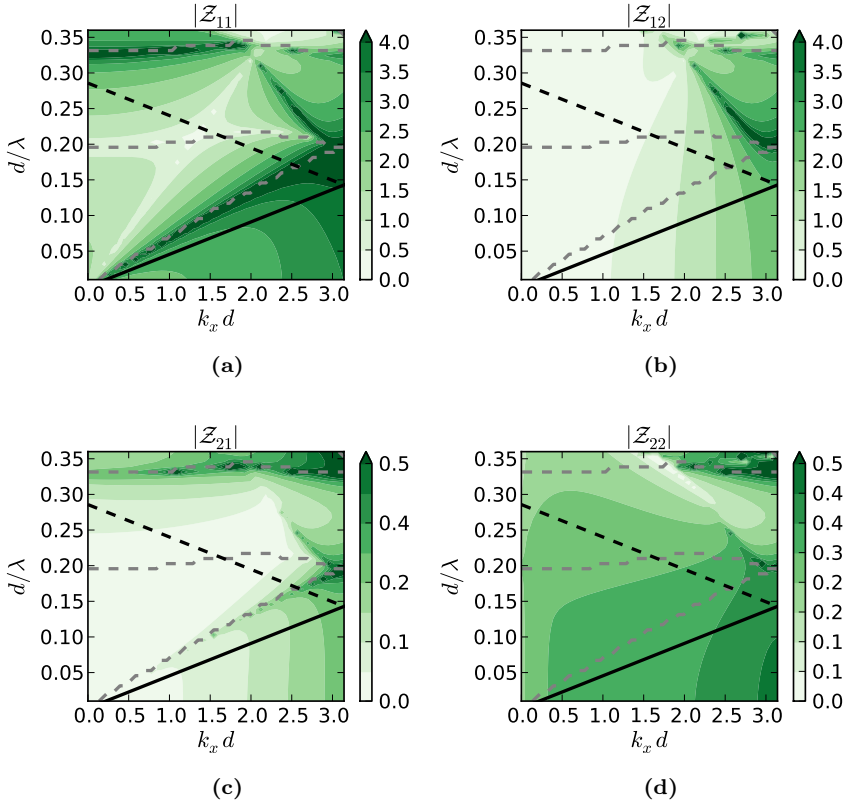

(a) **(b)**

(c) **(d)**

Figure 4.2: Moduli of each element of $\mathcal{Z}$ when two Bloch modes are considered.

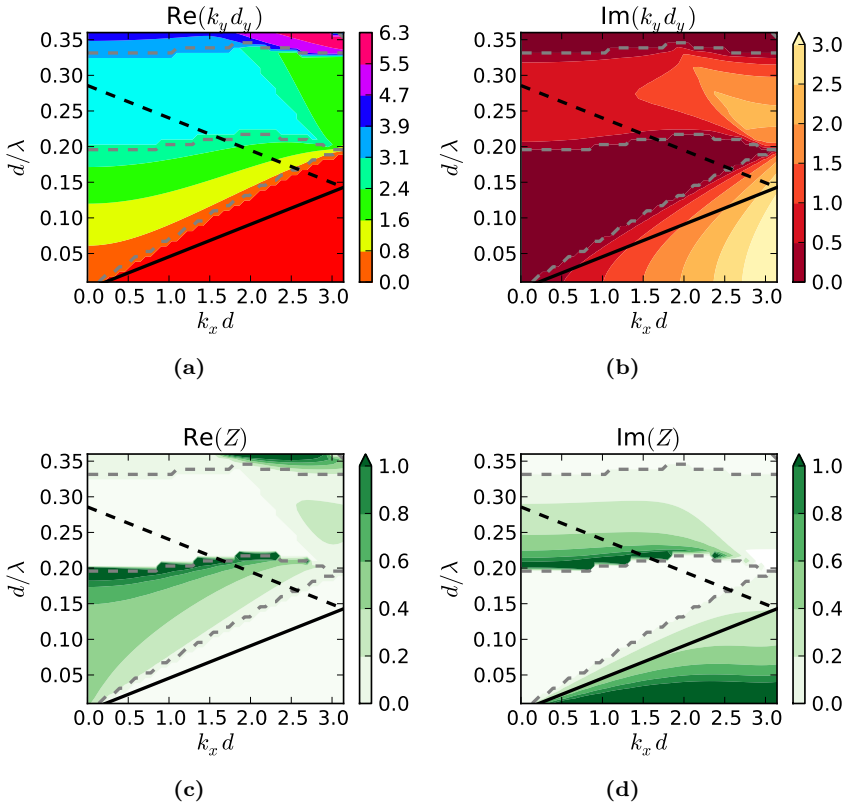

Figure 4.3: The two critical quantities, the propagation constant k_y and the wave impedance Z, that are needed to describe propagation and reflection through a homogenised PC.

calculated:

$$Z = \mathcal{Z}^2 Z_{w0}, \tag{4.3}$$

as in Paper 4.1. Z_{w0} is the wave impedance of the reference medium, free space.

By Bloch's theorem, the wavevector components k_x and k_y determine the Bloch mode's propagation through the lattice. k_x and k_y determine the phase and amplitude difference between points separated by lattice vectors, exactly as if the mode was a plane wave. In the single mode approximation, the wave impedances Z of two PCs determine the reflection and transmission coefficients between the two PCs' Bloch modes. Where the single mode approximation is valid, our modal parameters k_y and Z encapsulate the propagation and reflective properties of the Bloch modes in the system. The homogenisation step then entails representing the Bloch modes by plane waves: this may be done exactly for one point in each unit cell, due to the quasiperiodicity of Bloch modes.

Figure 4.3 shows the real and imaginary parts of the propagation constant k_y and the wave impedance Z for the PC. As expected, k_y is real in band, increases with frequency, decreases with k_x, and is imaginary below the light line. It is also imaginary in the low frequency partial band gap just above the light line. In most of the complete band gap, $\mathrm{Re}(k_y) = \pi/d_y$, indicating that the mode amplitude swaps sign across each PC period. The exception is in this band gap's braided region, where there is another mode with equal $|\eta|$ [5].

The wave impedance Z is well-behaved below the Wood anomaly in Fig. 4.3. In band, it is purely real, and out of band and below the light line it is purely imaginary, ensuring a reflectance of unity. Approaching the band's edge, Z either approaches 0 or diverges, leading to a reflectance that approaches unity. In the braided region of the band gap, $\mathrm{Re}(Z) \neq 0$, but the scalar Z is not sufficient to describe the properties of this region, where it is critical to include both modes: Z is based on only one element of $\mathcal{Z}$, which must be at least 2×2 to describe the PC.

The quantities η and $\mathcal{Z}$, or equivalently the more commonly-used quantities k_y and Z, are sufficient to characterise the propagation and reflection properties of a PC at a single frequency, incident angle, and polarisation. These quantities can either be used with the thin film framework or an equivalent transmission line model in order to calculate the reflection and transmission coefficients for a length of the PC, no matter what materials are either side of it. Uniform media are more commonly characterised by refractive index n and characteristic impedance Z_c, or by relative permittivity ϵ and relative permeability μ. For isotropic media these latter quantities are independent of k_x and vary weakly with frequency. As such, fewer numbers are required to characterise each medium: this is compounded by the fact that for lossless dielectrics $\mathrm{Im}(\epsilon) = 0$ and $\mu = 1$, so for lossless isotropic dielectrics only one real number is required to characterise the medium at each frequency.

These simplifications generally do not apply to PCs—even the PCs composed of lossless dielectrics that we consider. From k_y and Z it is possible to define effective parameters n, Z_c, ϵ and μ for a PC, using relations valid for isotropic media. For H_z polarised light, these relations take the form

$$n = k/(2\pi d/\lambda) \tag{4.4a}$$

$$Z_c = Z\ k/k_y \tag{4.4b}$$

$$\epsilon = n/Z_c \tag{4.4c}$$

$$\mu = nZ_c, \tag{4.4d}$$

where

$$k = \sqrt{k_x^2 + k_y^2} \tag{4.5}$$

is the effective wavenumber in the medium. Where k is imaginary, we take the root with $\mathrm{Im}(k) > 0$, as $\mathrm{Im}(k_y) < 0$ corresponds to evanescent growth (i.e. the backward wave, which decays in the opposite direction to the forward wave). There is some possible ambiguity in the definition of these parameters, which we discuss shortly.

Effective parameters calculated for the PC using Eqs. (4.4) are shown in Fig. 4.4. In the PC band below the Wood anomaly, the refractive index n is nearly independent of k_x, varying with frequency between $n = 2.35$ to $n = 2.6$ (Fig. 4.4a). Therefore the PC may be considered to be nearly isotropic in this regime, from a propagation perspective—its equifrequency contours are nearly circular.

However, the PC's reflective properties do not permit angle-independent characterisation: Z_c, which is k_x–invariant for all isotropic media, depends on k_x at most in-band frequencies (Fig. 4.4c). Therefore both ϵ and μ vary with k_x (Figs. 4.4e–4.4h), and the PC may not be characterised by a homogenous isotropic dispersive medium.

Below the complete band gap, ϵ and μ are real. This suggests that the partial band gap next to the light line is not a true band gap effect, but is more akin to total internal reflection. The PC's behaviour in this region is qualitatively consistent with that of a dispersive homogenous medium with $n(\omega)$ varying between 2.3 and 2.5: light cannot propagate in this medium

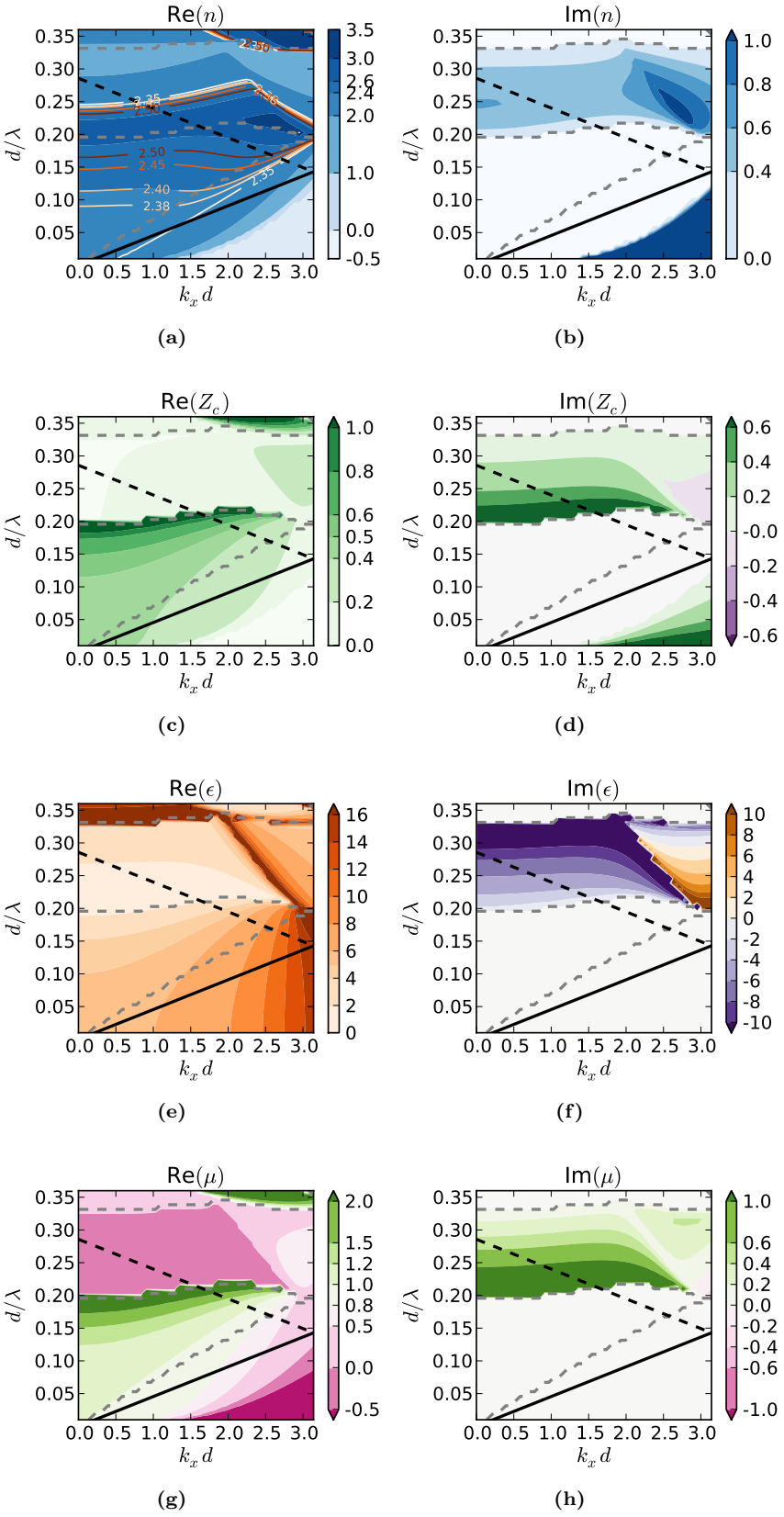

Figure 4.4: Effective parameters for the homogenised PC.

below its light line. This hypothesis is corroborated by the behaviour of Z_c, which does not diverge or vanish at this band edge (Fig. 4.4c).

Plausible variations on Eqs. (4.4) give effective parameters with entirely different properties. For example, it could be argued that the k and k_y in Eq. (4.4b) should be k and k_y in the PC's background material rather than the effective k and k_y for the PC—because the wave impedance is defined on the surface of the unit cell, which is surrounded by the background material. If this alternative definition is used, then the resulting Z_c vanishes at the edge of the partial band gap and becomes imaginary inside it. Additionally, ϵ is imaginary in the partial band gap and at some points below the light line, and μ is complex at these points. We prefer the original definition because it treats the PC as a self-contained material rather than needing extra information about the PC's background dielectric; additionally the obtained homogenised parameters are better behaved, in our opinion.

Well below the light line, where plane waves do not propagate in the PC's background dielectric, $\mathrm{Im}(n)$ and $\mathrm{Im}(Z_c)$ significantly increase in magnitude. This is because at low frequencies in this PC, $\mathrm{Im}(k_y)$ increases faster than k_x (Fig. 4.3b). This would seem to violate the principle that PCs are homogenisable and isotropic in the long wavelength limit. However, this only happens with evanescent waves, which are known to be able to resolve features smaller than their wavelength; in this example $\mathrm{Im}(k_y)$ starts to increase faster than k_x when the $1/e$ decay length of the evanescent wave becomes shorter than the unit cell length d_y. For larger k_x, and therefore even shorter decay lengths, the rapidly decaying evanescent wave only has appreciable field amplitude in a fraction of the unit cell and so it is unsurprising that the PC's effective parameters vary with k_x.

The pairs of derived parameters (n, Z_c) and (ϵ, μ) may each be used to calculate k_y and Z and through them the PC's propagative and reflective properties at the frequency, incident angle and polarisation. But as such, they carry no more information than the parameters k_y and Z from which they were derived. In the absence of k_x or frequency invariance, there is little point in working with the derived parameters, as they must be converted back to k_y and Z in order to use them. The sole practical advantage of the so-called material parameters is that ϵ and μ are real below the complete band gap, requiring half as much information to be stored.

4.3 Calculation of an equifrequency countour

Figure 4.3a shows the relationship between $\mathrm{Re}(k_y)$ and k_x at each frequency d/λ, for a particular PC's least-evanescent mode. For propagating modes, this information is more commonly represented as a set of equifrequency contours, which give information about the direction that an incident wave is "refracted" [18]. We now demonstrate that our method—in particular, the freely-available method of Chapter 3—may be applied to find an equifrequency contour, and that the results are consistent with others'.

In Fig. 4.5a we plot the $d/\lambda = 0.5765$ equifrequency contour for a self-collimating PC presented by Tang *et al.* [37]. This square lattice PC consists of $n = 2.9$ dielectric cylinders with radius $r = 0.15\ d$ in an air background, and light is incident in the E_z polarisation. The data was generated using my freely available BlochCode software, with field scattering data produced by Comsol Multiphysics. The equifrequency contour in Fig. 4.5a agrees well with that in Ref. [37]: crucially, it shares the distinctive flat sides that indicate that k_y is invariant over a domain of k_x, and therefore that the PC self-collimates light. Given that the equifrequency contour is not circular, an angle-independent set of effective parameters may not be obtained for this

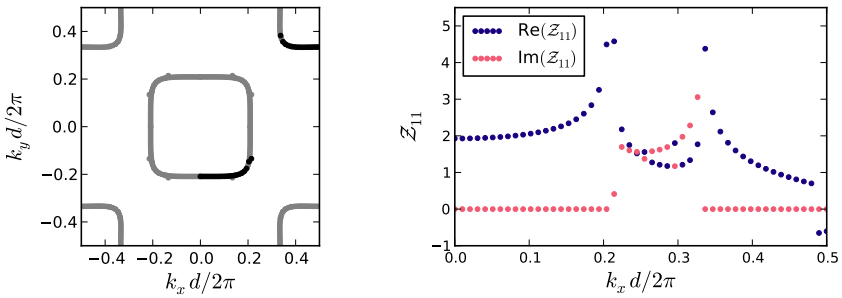

(a) **(b)**

Figure 4.5: (a) Equifrequency contour and (b) PC impedance scalar at fixed frequency for a self-collimating square lattice PC. The black points in (a) are directly obtained; the grey points are obtained from the black points by exploiting lattice symmetries.

PC. Furthermore at this frequency the second Wood anomaly lies at approximately $k_x d/2\pi = 0.42$; at least two Bloch modes need to be considered for modelling the PC with larger k_x.

Figure 4.5b shows the PC impedance scalar $\mathcal{Z}$ at this frequency. No mode propagates between $0.22 < k_x d/2\pi < 0.33$, which can be seen by the fact that $\mathrm{Im}(\mathcal{Z}) \neq 0$ at these k_x. The relatively flat $\mathcal{Z}$ curve for $|k_x d/2\pi| < 0.2$ implies that most beam components with $|k_x d/2\pi| < 0.2$ couple into the PC with similar efficiency. If this were not the case, then the beam would be distorted by the resultant filtering of its spatial components—a multi-angle antireflection coating might then be necessary to rectify this.

4.4 To what end?

It is all very well to ascribe effective parameters to a PC, but does it serve any practical purpose? In the metamaterials community, a number of working devices have been designed using transformation optics, which relies on homogenising metamaterials, or rather, the inverse problem of finding metamaterials with a particular set of characteristic parameters. Metamaterial devices based on negative index materials, such as cloaking devices [156] and superlenses [157], as well as devices not requiring negative indices, such as carpet cloaks [158, 159] and nanolenses [160] are all typically designed by calculating a required spatial distribution of effective $\epsilon(\mathbf{r}, \mathbf{k})$ and $\mu(\mathbf{r}, \mathbf{k})$, then finding a distribution of metamaterials that give $\epsilon(\mathbf{r}, \mathbf{k})$ and $\mu(\mathbf{r}, \mathbf{k})$. Rigourous or not, metamaterial homogenisation is a part of a process that has sucessfully been used to design devices, and without this process researchers would struggle to explore the vast parameter spaces to discover such devices.

In the photonic crystals community, equifrequency contours have long been put to work in the design of superprisms and supercollimators [25, 32], strongly dispersive devices which are inherently inhospitable to isotropic homogenisation. Some metamaterial techniques and applications are now spreading to the photonic crystals community [152]. Ergin *et al.* [161] used transformation optics to design a 3D carpet cloak, based on a set of 3D woodpile PCs that have spherical equifrequency contours and therefore isotropic effective indices n. Urzhumov and Smith [162] also applied transformation optics with the goal of designing a PC cloak; they needed spatially disper-

sive media so represented each PC by a spatially dispersive effective index $n(\mathbf{k})$. While the performance of their cloak is not perfect, it still demonstrates that PC effective parameters can be used with transformation optics to locate a region in parameter space with the desired properties. Both groups opted not to calculate effective impedances and tailor the reflective properties of their devices. Liang and Li [163] applied transformation optics to bend a square lattice PC into a horseshoe shape along with its guidance properties—this did not involve a homogenisation step, instead they scaled each unit cell's geometry and permittivity using transformation optics theory. I am unaware of effective ϵ and μ parameters (as opposed to effective n) for PCs being applied to design a device.

Ultimately, PCs are inherently discrete periodic media, and homogenisation methods hide this. For example, the reflection of a PC often depends on the position within the unit cell of the interface plane, but this is not represented by a homogenous effective medium. In my opinion, outside the long-wavelength limit it is safer *not* to calculate effective parameters such as n: instead light should always be modelled as a set of Bloch modes with $k_y(\omega, k_x)$ and $Z(k_x)$. While the two methods give identical results (if the homogenisation procedure in Sec. 4.2 is followed), when the PC's Bloch modes are used explicitly then the PC's discreteness is less likely to be forgotten and the parameters are less likely to be used invalidly.[3] The single mode approximation, which is necessary for all the above homogenisation methods, remains a powerful approximation because it allows PC properties to be encapsulated by scalars, which commute.

[3]Note that the PC impedance framework discussed in this thesis only applies to *stacks* of PCs, which are periodic in one dimension. Non-spatially-uniform devices, such as 2D cloaks, vary in two directions: e.g., the period might vary radially [162]. The PC impedance framework does not support such structures, as the modes of such structures are not the Bloch modes we calculate. Speculatively, if adjacent unit cells are sufficiently similar, then perhaps the structure may be considered "locally periodic": the field in each unit cell of the mosaic would be represented by the Bloch mode of a PC generated by that unit cell, and the amplitudes of the modes in a pair of adjacent cells would be related by the average of their (similar) wavevectors.

Chapter 5

Surface modes and other applications

To this point, the only application of PC impedance that we have demonstrated is the design of single frequency and broadband antireflection coatings. Other types coatings should also be possible, such as polarisation filters and band pass filters: if a PC stack with the desired properties exists, then our method can efficiently sort through the possible PC stacks to find it. But in this chapter we step away from such problems and turn our attention to some other applications of our PC impedance framework.

The first of these applications is to find the surface modes at a PC/air interface. As discussed in Sec. 1.2.3, the thin-film framework can be used to derive a condition for the existence of surface plasmons, and calculate their propagation constants and field distribution on either side of the interface. In Paper 5.1 we ape this thin-film-style treatment of surface plasmons with a matrix version for PC surface modes based on PC impedances. Surface plasmons exist where the reflection coefficients r_{12} and r_{21} diverge; we show that PC surface modes exist when the inverses of the reflection matrices $\mathbf{R}_{12}^{-1}$ and $\mathbf{R}_{21}^{-1}$ each have a zero eigenvalue. We provide an equivalent condition for this in terms of the PC impedances, which does not require numerical inversion of ill-conditioned matrices. The Bloch mode amplitudes of the surface modes are given by the matrices' null vectors.

In Section IV. of Paper 5.1 we explore the phenomenon of double interface surface modes. The studied configuration, shown in Fig. 7(c) of Paper 5.1, is the inverse of a conventional PC waveguide: the mirrors, normally PCs in bandgap, are replaced by air, and the dielectric waveguiding region is replaced by a PC. In the PC's bandgap, surface modes exist on the PC's two interfaces and they couple. In band, more conventional waveguiding occurs, with the modes propagating along the PC strip.

In the remainder of this chapter, we briefly discuss the related work of students whom I have co-supervised. In Section 5.2 we discuss a paper in which our impedances are applied to calculate the dispersion relations of conventional PC waveguides in an efficient manner, and to find PC waveguides with slow light and little dispersion. Finally, in Sec. 5.3 we discuss work where our impedances are used to find the dispersion relations of a large array of coupled PC waveguides, and model the resulting discrete diffraction.

Throughout this chapter, the propagation constants k_y of the Bloch modes in bulk PCs are de-emphasised, as we focus on the propagation constants k_x of the surface and waveguide modes, which propagate along the $\mathbf{e}_1$ lattice vector.

Photonic-crystal surface modes found from impedances

Felix J. Lawrence,[1,*] Lindsay C. Botten,[2] Kokou B. Dossou,[2] R. C. McPhedran,[1] and C. Martijn de Sterke[1]

[1]*Centre for Ultrahigh-bandwidth Devices for Optical Systems (CUDOS), Institute for Photonics and Optical Sciences (IPOS) and School of Physics, University of Sydney, New South Wales 2006, Australia*

[2]*CUDOS and Department of Mathematical Sciences, University of Technology, Sydney, New South Wales 2007, Australia*

(Received 26 June 2010; published 30 November 2010)

We present a method for finding surface modes at interfaces between two-dimensional photonic crystals (PCs), in which the surface modes are represented as superpositions of the PCs' propagating and evanescent Bloch modes. We derive an existence condition for surface modes at an air-PC interface in terms of numerically calculated PC impedance matrices, and use the condition to find surface modes in the partial band gap of a PC. We also derive a condition for modes of a three-layer structure with two interfaces, and find both coupled surface modes and waveguide modes. We show that some waveguide modes cross the band edge and become coupled surface modes.

DOI: 10.1103/PhysRevA.82.053840 PACS number(s): 42.70.Qs, 73.20.At, 42.79.Gn, 41.20.Jb

I. INTRODUCTION

Electromagnetic surface modes have long been studied for their rich and interesting physics [1]. They are confined to an interface, in the sense that the field decays exponentially away from the interface in both directions. The most widely studied example is the surface plasmon or surface plasmon polariton, which arises at the interface between a metal and a dielectric, but these have very short propagation lengths due to loss in the metal. They have been experimentally demonstrated [2], and may even be seen with the naked eye if elastically scattered on the surface of a diffraction grating [3].

Surface states may also arise at the boundaries of two-dimensional photonic crystals (PCs), which are defined as having a periodic variation in refractive index [4]. In this paper "surface mode" refers to this variety of PC surface state, while "surface plasmon" refers exclusively to a state at the interface between a metal and a dielectric. For a surface mode at an interface between air and a PC, the field decays into the PC because of the PC's band gap, and it decays on the air side of the interface due to an effect related to total internal reflection. Since the entire structure may be made from lossless materials, surface modes can have much longer propagation lengths than surface plasmons.

PC surface modes have been experimentally demonstrated [5–8], and have been found by two general numerical approaches. The most common technique is to use a supercell [4] and directly compute the modes. With the supercell approach, the PC cannot be infinitely thick and so, in principle, there is always some coupling between surface modes on the front and back of the PC. The other widely used technique involves separately finding the modes of the two materials and calculating the surface modes from these by matching them at the interface [9–11]. This allows surface modes to be calculated for interfaces between semi-infinite structures. We take the latter approach, expressing it in terms of PC impedances [12], and generalize it to work also with structures that have a material of finite thickness sandwiched between two semi-infinite media.

*felix@physics.usyd.edu.au

Surface plasmons may be found from the poles of the transmission coefficient or of the reflection coefficient

$$r_{12} = \frac{Z_2/Z_1 - 1}{Z_2/Z_1 + 1}, \tag{1}$$

where $Z = E_\parallel/H_\parallel$ is the *wave impedance*, with $E_\parallel$ and $H_\parallel$ the field components parallel to the interface. So the condition for a surface mode to exist is that the denominator of Eq. (1) vanishes. For transverse magnetic (TM) polarization ($\mathbf{H} = H_\parallel \hat{\tau}$ with $\hat{\tau}$ parallel to the interface), for which surface plasmons may exist at an air-metal interface $Z_i = -k_{\perp i}/\omega\epsilon_i$ and so by this condition surface plasmons exist when

$$\frac{k_{\perp 1}}{\epsilon_1} = -\frac{k_{\perp 2}}{\epsilon_2}, \tag{2}$$

where $k_\perp$ is the component of the wave vector perpendicular to the interface.

In this paper we generalize the procedure for finding surface plasmons to apply to dielectric PCs and their impedances. The procedure involves finding poles of the PC analog of Eq. (1), which uses semi-analytically defined PC impedances that are generally matrices [13]. This allows us to find a condition for the existence of a PC surface mode. Section II defines our nomenclature and introduces the quantities needed to describe PCs, before the surface mode existence condition is derived in Sec. III. This is then applied to give the dispersion relation of a PC surface mode. In Sec. IV we derive a condition and give examples for the case with three media and two interfaces (e.g., a strip of PC surrounded by air on either side). We conclude in Sec. V by commenting on the usefulness of our method. The Appendix presents a convergence analysis in a typical case, illustrating the accuracy and reliability of our technique.

II. BACKGROUND THEORY AND NOMENCLATURE

We write the field in each PC in its basis of Bloch modes (including propagating and evanescent modes); this is the natural basis in which to consider transmission and reflection since each Bloch mode travels independently through its PC without scattering into other modes. Our method for finding Bloch modes is based on the semi-analytical least-squares-based method of Botten *et al.* [14] and is briefly outlined

in the following. In its present form, the method applies to two-dimensional (2D) square or triangular lattice PCs with unit cells that are up-down symmetric, which precludes the study of PCs with arbitrarily truncated unit cells. For generality we treat all media as PCs (see Fig. 1): for homogeneous dielectrics such as air, a periodicity is imposed and the material's Bloch modes are simply plane waves.

Our axes are chosen such that all PC interfaces are parallel to the x-z plane, and each PC's refractive index varies periodically in the x-y plane. We assume that both the PC structure and the electromagnetic (EM) field are invariant in the z direction; this is thus a 2D problem. In any single simulation we consider one polarization, one frequency, and one Bloch vector component k_x, the component parallel to the interface. Since the EM field components parallel to a dielectric interface are continuous across it, fixing k_x across all media ensures that we have a closed set of Bloch modes under reflection and transmission at all PC interfaces. A surface mode with propagation constant k_x may therefore be represented in each medium as a superposition of these Bloch modes.

We find the Bloch modes of each PC by diagonalizing the plane-wave transfer matrix [14], which, in turn, is found using the multipole method [15]. The transfer matrix may alternatively be found with the finite element method (FEM) [16]. The dimension of the plane-wave transfer matrix is made sufficiently large that it includes all relevant plane waves, which are the grating diffraction orders excited by the rows of holes comprising the PC. In this paper's examples, five plane-wave orders were considered in each direction in each medium; this means that the calculations typically include all relevant plane waves that decay in amplitude across a PC's unit cell by a factor of 10^6 or less. In the Appendix we give criteria illustrating how the required number of plane waves is determined and show that for our calculations five plane-wave orders are sufficient to determine surface modes accurately.

We partition the Bloch modes of each PC into modes that propagate or decay in the forward $(+y)$ direction and those that propagate or decay in the backward $(-y)$ direction. The field in a PC i is represented by a vector of forward Bloch mode amplitudes $\mathbf{c}_i^+$ and a vector of backward Bloch mode amplitudes $\mathbf{c}_i^-$ (Fig. 1).

At an interface between two PCs, each incident Bloch mode may be reflected and transmitted into many modes. Reflection and transmission coefficients must therefore become nondiagonal reflection and transmission matrices. In our previous work [12] we showed that these may be written in terms of the impedance-like matrices $\mathcal{Z}_1$ and $\mathcal{Z}_2$ of PC 1 and PC 2 [cf. Eq. (1)]

$$\mathbf{T}_{12} = \left(\mathbf{A}_{12}^T\mathbf{A}_{12} + \mathbf{I}\right)^{-1} 2\mathbf{A}_{12}^T, \tag{3a}$$

$$\mathbf{R}_{12} = \left(\mathbf{A}_{12}\mathbf{A}_{12}^T + \mathbf{I}\right)^{-1}\left(\mathbf{A}_{12}\mathbf{A}_{12}^T - \mathbf{I}\right), \tag{3b}$$

$$\mathbf{T}_{21} = \left(\mathbf{A}_{12}\mathbf{A}_{12}^T + \mathbf{I}\right)^{-1} 2\mathbf{A}_{12}, \tag{3c}$$

$$\mathbf{R}_{21} = \left(\mathbf{A}_{12}^T\mathbf{A}_{12} + \mathbf{I}\right)^{-1}\left(\mathbf{I} - \mathbf{A}_{12}^T\mathbf{A}_{12}\right), \tag{3d}$$

where $\mathbf{A}_{12} = \mathcal{Z}_1^{-1}\mathcal{Z}_2$. These equations are exact at full rank, when all relevant plane waves and Bloch modes are considered, and are otherwise least-squares-style approximations. In the Appendix we show that, for the cases in this paper, five Bloch modes and five plane waves are sufficient to obtain highly accurate results.

The impedance-like matrix $\mathcal{Z}$ is the crucial quantity that we use throughout the remainder of this paper to describe how light behaves in the PC. It is defined in terms of the PC's numerically found Bloch modes, but once the Bloch modes are known, Eq. (3) holds rigorously at full rank and becomes a least-squares approximation when the set of plane waves or Bloch modes is truncated [12].

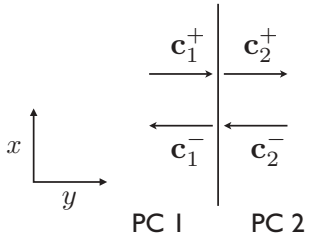

FIG. 1. Schematic of a two PC interface, with incoming and outgoing Bloch vectors.

III. SINGLE INTERFACE SURFACE MODES

We derive a necessary and sufficient condition for the existence of a PC surface mode in a similar way to how the surface plasmon condition Eq. (2) may be derived: we look for poles of the reflection matrices. We work in the PCs' Bloch bases, with notation as in Fig. 1. Poles of matrices imply infinite eigenvalues; to avoid the ensuing numerical instabilities, we instead calculate the inverse of these matrices and look for zero eigenvalues. The condition for a surface mode, in this form, is then the pair of homogenous equations

$$\mathbf{R}_{12}^{-1}\mathbf{c}_1^- = \mathbf{c}_1^+ = \mathbf{0}, \tag{4a}$$

$$\mathbf{R}_{21}^{-1}\mathbf{c}_2^+ = \mathbf{c}_2^- = \mathbf{0}. \tag{4b}$$

Equation (4) constitutes a necessary condition because a surface mode has zero incoming field (i.e., $\mathbf{c}_1^+ = \mathbf{0}$ and $\mathbf{c}_2^- = \mathbf{0}$) and nonzero outgoing field (i.e., $\mathbf{c}_1^- \neq \mathbf{0}$ and $\mathbf{c}_2^+ \neq \mathbf{0}$), so $\mathbf{R}_{12}^{-1}$ and $\mathbf{R}_{21}^{-1}$ must be singular. Possible issues of degeneracy are resolved by studying the null space, for which the singular value decomposition is a useful tool. They also constitute a sufficient condition because the null vectors of $\mathbf{R}_{12}^{-1}$ and $\mathbf{R}_{21}^{-1}$ are valid outgoing fields without incoming fields, which is the definition of a surface mode.

To find the source of the singularity, consider the expressions for $\mathbf{R}_{12}$ and $\mathbf{R}_{21}$ in Eqs. (3b) and (3d). The impedance ratio $\mathbf{A}_{12}\mathbf{A}_{12}^T$ does not have an infinite eigenvalue since that would imply that one of the Bloch modes could not be normalized and had zero or an infinite field associated with it. Therefore to satisfy Eqs. (4a) and (4b), $(\mathbf{A}_{12}\mathbf{A}_{12}^T + \mathbf{I})$ and $(\mathbf{A}_{12}^T\mathbf{A}_{12} + \mathbf{I})$ must have a zero eigenvalue. Looking again at Eq. (3), this implies that surface modes are tied to poles of the reflection and transmission matrices in both directions. This is consistent with the condition used by Enoch *et al.* [10], that of a pole in the scattering matrix determinant; and the condition of Che and Li [11], that $\det(\mathbf{S}_{11}) = \mathbf{0}$, where $\mathbf{S}_{11}$ is the submatrix of the scattering matrix that maps $\mathbf{c}_2^+$ to $\mathbf{c}_1^+$.

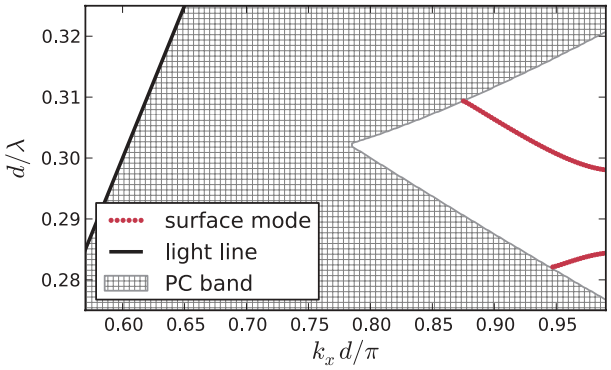

FIG. 2. (Color online) Projected band structure of surface modes at an air-PC interface. Only the region below the light line is considered.

So to find the surface modes of a structure, we scan frequency and vary k_x in search of cases where $(\mathbf{A}_{12}\mathbf{A}_{12}^T + \mathbf{I})$ has a zero eigenvalue. Thus by searching frequency-k_x space we construct the projected band structure of the interface. The eigenvector associated with each zero eigenvalue is $\mathbf{c}_1^-$ for the surface mode, as may be seen from Eq. (4a). And from Eq. (4b) we see that the amplitudes of PC 2's Bloch modes, $\mathbf{c}_2^+$, is the eigenvector corresponding to the zero eigenvalue of $(\mathbf{A}_{12}^T\mathbf{A}_{12} + \mathbf{I})$. Knowing the Bloch mode amplitudes $\mathbf{c}_1^-$ and $\mathbf{c}_2^+$ lets us find and plot the surface mode's field.

We now apply this method to find the surface modes at the interface between air and a semi-infinite PC. The PC has a triangular lattice of air holes of radius $0.25d$, with lattice constant d, in a dielectric background with $n = 2.86$. We look for surface modes in the $\mathbf{E} = E_z\hat{\mathbf{z}}$ polarization; surface plasmons do not exist in this polarization since this would require a medium with negative permeability.

Surface modes only occur where there are no propagating modes in either material; since one of the media is air, we only look for surface modes below the light line [4]. We scan over frequency and k_x for eigenvalues of $(\mathbf{A}_{12}^T\mathbf{A}_{12} + \mathbf{I})$ that have magnitudes below our accuracy goal of 10^{-12} and find two surface modes in a partial band gap. The resulting projected band structure is plotted in Fig. 2.

The real and imaginary parts of the smallest eigenvalue ψ of $(\mathbf{A}_{12}^T\mathbf{A}_{12} + \mathbf{I})$ are plotted in Fig. 3 for $d/\lambda = 0.3$. The surface mode is found where the real part crosses the x axis; within the band gap $\mathrm{Im}(\psi)$ is essentially zero. This eigenvalue appears to have no physical significance other than indicating whether $(\mathbf{A}_{12}^T\mathbf{A}_{12} + \mathbf{I})$ is singular. This result was obtained considering five Bloch modes and five plane waves; a convergence analysis presented in the Appendix shows that this approximation is highly accurate.

The field in the PC (shown in Fig. 4) is essentially a superposition of the two most slowly decaying Bloch modes; for $d/\lambda = 0.3$, the moduli of the Bloch amplitudes $\mathbf{c}_2^+$ are 0.43, 0.90, 4.4×10^{-3}, 7.7×10^{-3}, and 1.4×10^{-4}, where the corresponding Bloch factors (eigenvalues of the transfer matrix) have moduli 0.65, 0.64, 1.0×10^{-3}, 7.9×10^{-4}, and 2.7×10^{-6}, respectively. Close to the interface, the second Bloch mode dominates, but deep in the PC the first Bloch mode becomes responsible for most of the field because it decays

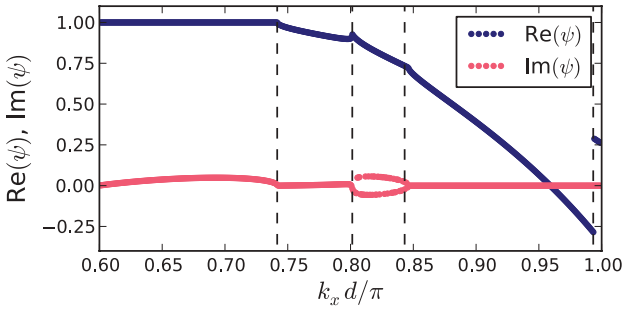

FIG. 3. (Color online) Real and imaginary parts of the smallest eigenvalue of $(\mathbf{A}_{12}^T\mathbf{A}_{12} + \mathbf{I})$, for $d/\lambda = 0.3$. Surface modes occur when this eigenvalue is exactly zero. The discontinuities in slope occur where two or more eigenvalues have equal moduli.

slightly more slowly. Similarly, on the air side of the interface most of the field is due to the two most slowly decaying plane waves; the transition region where the two plane waves are of comparable amplitude and so interference is clearly visible in Fig. 4(b). The slowest decaying plane wave has a decay length (to a factor $1/e$ amplitude) of $0.23\sqrt{3/2}d$.

Since the field on both sides of the interface is a superposition of two modes with different decay factors, the field does not exponentially decay away from the interface, and

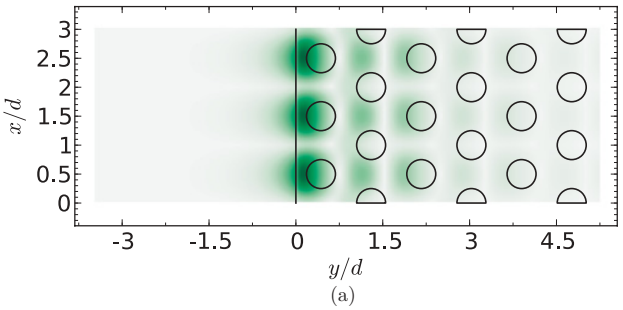

(a)

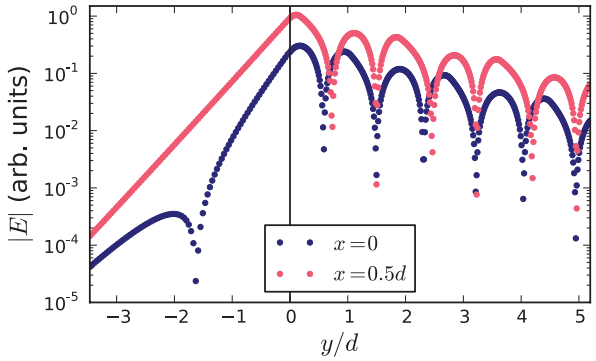

(b)

FIG. 4. (Color online) Modulus of the E field for the surface mode at $d/\lambda = 0.3$ and $k_x = 0.959\pi/d$; air is on the left of the vertical line, PC is on the right. Two horizontal cuts through (a) are shown in (b); the $x = 0$ cut is along the lower edge of (a), and the $x = 0.5d$ cut bisects one of the three PC holes nearest the interface. The $x = 0$ cut shows two exponential decay regimes in air, which is evidence that one evanescent plane wave dominates near the interface and another dominates away from it.

so the surface mode may not faithfully be approximated by a surface plasmon. In other words, this PC's behavior may not be reproduced by any uniform medium; no effective permittivity or permeability that may be ascribed to the PC could predict this surface mode.

IV. DOUBLE INTERFACE SURFACE MODES

Another much-studied configuration in the surface plasmon literature is that of thin metallic slabs in air (or another dielectric). Such structures can support surface plasmons on both faces of the metallic slab, which couple [17]. These surface states are long-range or short-range surface plasmons, depending on their symmetry. In this section we explore nonmetallic PC analogs to long- and short-range surface plasmons; we consider structures with three media and two interfaces, either of which may or may not be capable of supporting a surface mode.

Such structures have previously been studied by Enoch *et al.* [10], who investigated a dielectric-PC-dielectric structure analogous to the dielectric-metal-dielectric structures on which long- and short-range surface plasmons have been observed. Their PC region is fixed at 18 periods thick, so the coupling between interfaces is minimal. Choi *et al.* [18] investigated a PC-air-PC structure. In our examples we consider an air-PC-air structure, but the theory developed is general and also applies to other structures, including PC waveguides.

The three media, which for generality we consider to be PCs, are arranged as in Fig. 5. $\mathbf{\Lambda}_+ = \mathrm{diag}(\mu^s_{f,i})$ and $\mathbf{\Lambda}_- = \mathrm{diag}(\mu^{-s}_{b,i})$, where $\mu_{f,i}$ and $\mu_{b,i}$ are, respectively, PC 2's forward and backward Bloch factors (eigenvalues) and s is PC 2's width.

To find the condition for a surface mode, we set the incoming field vectors $\mathbf{c}_1^+$ and $\mathbf{c}_3^-$ to zero and derive

$$\mathbf{c}_2^+ = \mathbf{R}_{21}\mathbf{\Lambda}_-\mathbf{c}'^-_2, \tag{5a}$$

$$\mathbf{c}'^-_2 = \mathbf{R}_{23}\mathbf{\Lambda}_+\mathbf{c}_2^+, \tag{5b}$$

which leads to

$$(\mathbf{R}_{21}\mathbf{\Lambda}_-\mathbf{R}_{23}\mathbf{\Lambda}_+ - \mathbf{I})\mathbf{c}_2^+ = \mathbf{0}. \tag{6}$$

This expression is closely related to the familiar waveguide phase condition; it is satisfied by conventional waveguide modes. However, it is also satisfied by surface modes, which decay inside PC 2 away from the interfaces. For surface modes, the entries of the diagonal matrices $\mathbf{\Lambda}_+$ and $\mathbf{\Lambda}_-$ all have magnitude less than unity; this is balanced by reflection matrices that increase field amplitude upon reflection.

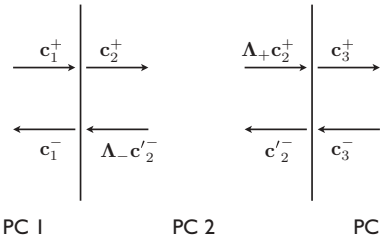

FIG. 5. Schematic of a three PC (double interface) structure, with Bloch vectors $\mathbf{c}$.

In deriving Eq. (6), we neglected terms due to the incoming field vectors $\mathbf{c}_1^+$ and $\mathbf{c}_3^-$, which both vanish for a surface mode. The more general form of Eq. (5a) is $\mathbf{c}_2^+ = \mathbf{R}_{21}\mathbf{\Lambda}_-\mathbf{c}'^-_2 + \mathbf{T}_{12}\mathbf{c}_1^+$. In Sec. III, we found surface modes occurring at poles of the reflection and transmission matrices (i.e., modes where $\mathbf{T}_{12}\mathbf{c}_1^+$ was nonzero even when $\mathbf{c}_1^+ = \mathbf{0}$). We now consider whether the possibility of a pole in the transmission matrix can invalidate Eq. (5a).

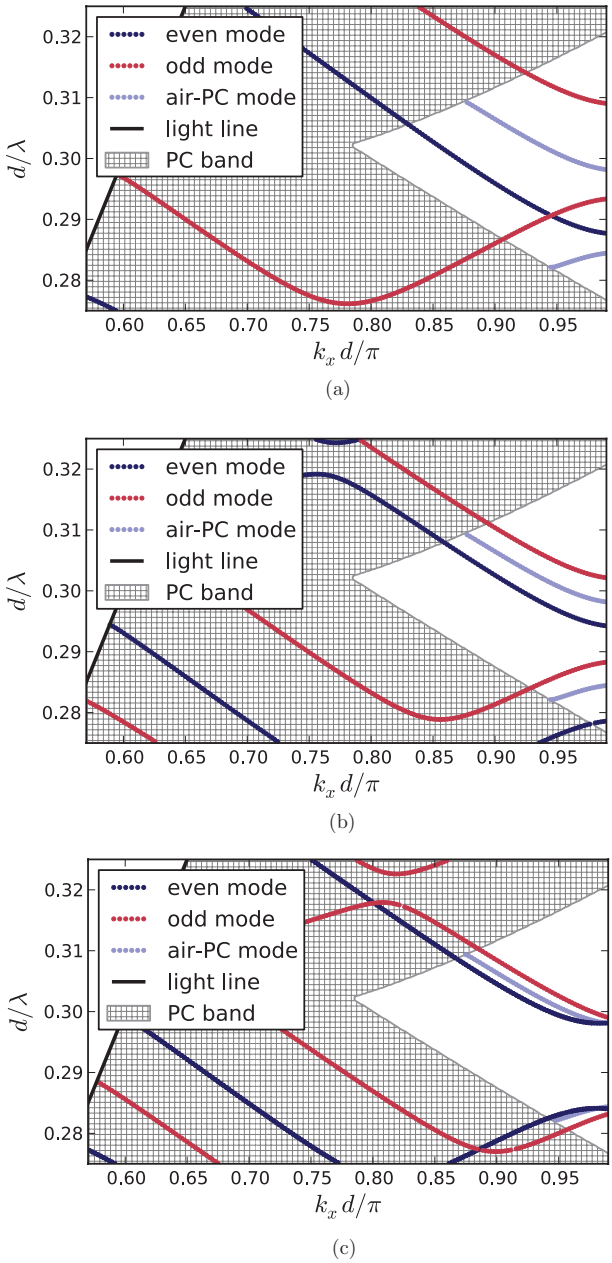

FIG. 6. (Color online) Projected band structure of surface modes (dark blue and midtone red) of an air-PC-air structure with (a) three, (b) five, and (c) six periods of PC. The projected band structure of the surface modes at the corresponding air-PC interface is shown for reference in light blue.

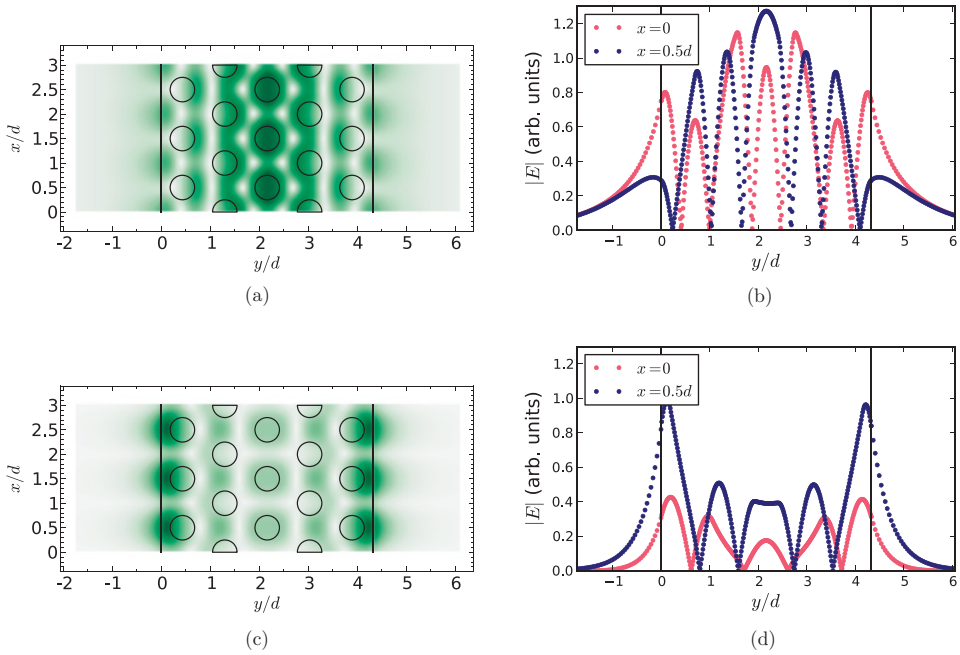

FIG. 7. (Color online) Field strength $|E|$ for an even mode of an air-PC-air structure with five periods of PC [see Fig. 6(b)]: (a) and (b) at $d/\lambda = 0.318$, $k_x = 0.715\pi/d$, in the PC's band; (c) and (d) at $d/\lambda = 0.299$, $k_x = 0.927\pi/d$, in the PC band gap.

As we saw in Sec. III, poles occur when $\mathbf{c}_1^-$ lies in the null space of $(\mathbf{A}_{12}\mathbf{A}_{12}^T + \mathbf{I})$. Considering the field at the PC 1-PC 2 interface, we may write

$$\left(\mathbf{A}_{12}\mathbf{A}_{12}^T + \mathbf{I}\right)\mathbf{c}_1^- = \left(\mathbf{A}_{12}\mathbf{A}_{12}^T - \mathbf{I}\right)\mathbf{c}_1^+ + 2\mathbf{A}_{12}\mathbf{\Lambda}_-\mathbf{c'}_2^-, \quad (7)$$

and see that if $\mathbf{c}_1^-$ is in the null space of $(\mathbf{A}_{12}\mathbf{A}_{12}^T + \mathbf{I})$, the necessary condition for a pole, then $(\mathbf{A}_{12}\mathbf{A}_{12}^T + \mathbf{I})\mathbf{c}_1^- = \mathbf{0}$. Furthermore $\mathbf{c}_1^+ = \mathbf{0}$ for a surface mode, resulting in $2\mathbf{A}_{12}\mathbf{\Lambda}_-\mathbf{c'}_2^- = \mathbf{0}$. This implies that no field from the PC 2-PC 3 interface reaches the PC 1-PC 2 interface, which is not physical. Therefore there can be no double interface surface modes when there are poles in the transmission matrices and Eq. (6) is both a sufficient and necessary condition for a double interface surface mode.

Of particular interest is the symmetric case, where PC 1 and PC 3 are the same material. Then $\mathbf{R}_{21} = \mathbf{R}_{23}$ and we can factorize Eq. (6). We use the relation $\mathbf{\Lambda}_- = e^{i\pi k_x s d}\mathbf{\Lambda}_+$, where s is the number of rows of holes in PC 2, to write

$$(\mathbf{R}_{21}\mathbf{\Lambda}_+ e^{i\pi k_x s d/2} - \mathbf{I})(\mathbf{R}_{21}\mathbf{\Lambda}_+ e^{i\pi k_x s d/2} + \mathbf{I})\mathbf{c}_2^+ = \mathbf{0}. \quad (8)$$

Comparing this to Eq. (5), two solutions are apparent: an even solution, where $\mathbf{c'}_2^- = e^{-i\pi k_x s d/2}\mathbf{c}_2^+$ and an odd solution for which $\mathbf{c'}_2^- = -e^{-i\pi k_x s d/2}\mathbf{c}_2^+$. Note that this phase shift of $\pm e^{-i\pi k_x s d/2}$ is measured between points separated by s lattice vectors, so for triangular lattices these points have different x values since that lattice vector is not parallel to the y axis.

We now apply this method to find the modes of a structure in which PC 1 and PC 3 are vacuum and PC 2 is the PC studied in Sec. III. We search for eigenvectors of $\mathbf{R}_{21}\mathbf{\Lambda}_+ e^{i\pi k_x s d/2}$ that have an eigenvalue ψ within an accuracy range 10^{-6} of ± 1, for $\mathbf{E} = E_z\hat{\mathbf{z}}$ polarized light. The modes found when PC 2 is three, five, and six rows of holes thick are shown in Fig. 6.

The striking difference between the single interface surface modes of Sec. III and the double interface modes in Fig. 6 is that the double interface modes cross the PC's band edge, as reported for the thick PC limit by Enoch *et al.* [10]. As previously discussed, single interface surface modes cannot exist in band, as energy is inevitably radiated away [4]. When a second interface is present, in-band waveguide solutions arise for Eq. (6), in addition to band-gap surface mode solutions.

The character of a mode changes across the band edge: in the band gap, the field envelope must decay toward the center of the PC slab since all its constituent Bloch modes are evanescent. In band, this restriction does not apply. Figure 7 shows two cuts through the field of an even mode of the air-5 period PC-air structure of Fig. 6(b). The difference between the in-band waveguide mode [Figs. 7(a) and 7(b)] and the band-gap surface mode [Figs. 7(c) and 7(d)] is readily apparent; the surface mode's field unambiguously decays toward the center of the PC region, whereas the waveguide mode has a large field along the middle of the PC. There is a smooth transition between these two kinds of mode: near the band edge, the waveguide mode adopts the shape of the surface mode. The moduli of the elements of $\mathbf{c}_2^+$ for each mode vary continuously, even across the band edge, and likewise there is no sudden change in the field profile as the band edge is crossed.

The introduction of a second interface splits the single interface surface mode into an even mode and an odd mode. As the thickness of PC 2 is increased, we see from Fig. 6 that these modes' dispersion relations converge, approaching that of the single interface surface mode. This behavior makes physical sense, as the interfaces become increasingly decoupled as PC 2's thickness increases. Furthermore as

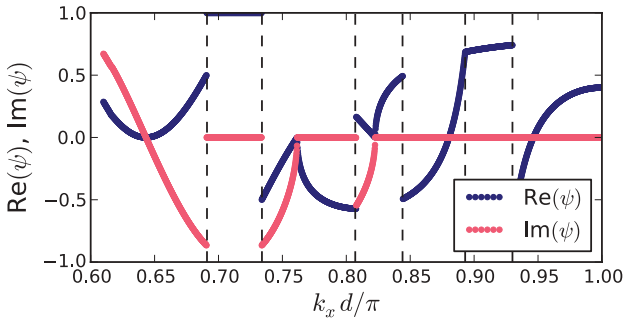

FIG. 8. (Color online) Real and imaginary parts of the smallest eigenvalue ψ of $\mathbf{R}_{21}\mathbf{\Lambda}_+ e^{i\pi k_x sd/2} \pm \mathbf{I}$ at $d/\lambda = 0.305$ for the air-PC-air structure used in Fig. 6(b). The condition for a surface mode or waveguide mode is $\psi = 0$. Discontinuities occur where two or more eigenvalues have equal moduli.

PC 2's thickness increases, the magnitude of the entries of $\mathbf{\Lambda}_+$ decrease exponentially. Since $\mathbf{R}_{21}^{-1}\mathbf{c}_2^+ = \pm e^{i\pi k_x sd/2}\mathbf{\Lambda}_+\mathbf{c}_2^+$, as PC 2's thickness becomes infinite, $\mathbf{\Lambda}_+ \to \mathbf{0}$. Therefore $\mathbf{R}_{21}^{-1}$ must become singular, which is precisely the condition for a single interface surface mode.

Unlike the PC-air-PC structure studied by Choi *et al.* [18], Fig. 6 shows that, in our case, the lower-frequency mode does not always have even parity. For our configuration, when the PC is an even number of periods thick the lowest-frequency surface mode is odd, and vice versa; we have checked this for PCs from four to eight periods thick. This behavior is equivalent to that previously observed in coupled PC waveguides [19]. For thinner structures, in which the interfaces are strongly coupled, the lower air-PC mode does not split into two surface modes.

Numerically finding solutions to Eq. (8) is sometimes more difficult than the single-mode case, because the eigenvalue ψ that must be minimized can vary strongly with frequency and k_x. For example, $\psi(k_x)$ is shown in Fig. 8 at $d/\lambda = 0.305$ for the 5 period thick PC of Fig. 6(b). This function has several discontinuities and is less well behaved than the equivalent function for the single interface, shown in Fig. 3. The discontinuities occur where the two smallest eigenvalues have equal magnitude. Discontinuities close to a zero can cause a root-finder to miss valid solutions; this manifests as a gap in the dispersion relation and can be avoided by instead searching for a zero determinant. This measure was necessary to obtain certain points on the even mode dispersion relations in Fig. 6(c). Furthermore in Fig. 8 there are cusps near $k_x = 0.76\pi/d$ and $k_x = 0.82\pi/d$, where the number of propagating Bloch modes changes. These anomalies are extremely localized—for the $k_x \simeq 0.76\pi/d$ anomaly, $|\psi| < 10^{-5}$ over a domain of size $\Delta k_x < 10^{-10}\pi/d$—so the anomalies are of no practical importance and are therefore ignored in Fig. 6.

The numerical issues in finding modes arise because to find a k_x for a given frequency (or vice versa) that supports a mode, a numerical search must be performed to find a k_x such that $|\psi| = 0$. To find a projected band structure like those in Fig. 6, we must scan over frequency and k_x, a 2D search. Our approach is to do a coarse search over the entire parameter space, then to use a root finder to check local minima for zeros. The information calculated for each PC (i.e., its impedance and Bloch factor) in the coarse search is independent of the overall PC 1-PC 2-PC 3 structure. This means that the hard work in generating Figs. 6(a), 6(b), and 6(c) only needs to be done once: with the PCs' impedances known, the coarse search becomes simply a matter of manipulating known 3×3 or 5×5 matrices.

Supercell methods [4] require only a one-dimensional (1D) search because for each frequency, all appropriate k_x may be found directly from a single FEM (or other) computation. The main downside to supercell methods is that coupling occurs between supercells; the supercell must be made large to minimize this, which adds computation time. The minimal supercell size depends on the decay rates in the outermost media, which depend on k_x and may not be known in advance. Our impedance method does not suffer from this problem: the outer media are truly semi-infinite and the computational domain is small since we compute each PC's Bloch modes using a single unit cell. Our Bloch mode method also provides additional insight into the field structure that supercell methods do not provide.

V. DISCUSSION AND CONCLUSION

In Sec. IV we generalize the principles from Sec. III to investigate modes that propagate along a three-layer structure. The results given in Sec. IV are for an air-PC-air structure, which was chosen so that in the partial band gap the surface modes are analogous to long-range surface plasmons. However, the derived equations are quite general: Eq. (6) may be used to find the modes of any three-layer structure and Eq. (8) may be applied to any structure of the form PC 1-PC 2-PC 1, which includes many PC waveguides. Unlike supercell methods, our approach allows the field of a waveguide mode to be expressed as a superposition of Bloch modes in each of the structure's constituent PCs. This allows a deeper understanding of the waveguide mode and how it decays in the confining media.

The method developed in Sec. IV may be extended to treat structures with more than three media; this simply requires further use of the transfer matrix method used in deriving Eqs. (5) and (6). Such an approach could be used to find the modes of coupled PC waveguides, or of more complicated PC waveguide structures where the rows of holes nearest the central guiding region have been modified.

In conclusion, we have developed a method of finding surface modes on two- and three-layer structures. The condition for surface modes on a single interface is that the Bloch mode reflection matrix has an infinite eigenvalue, which is analogous to the condition for a surface plasmon on an air-metal interface, and we provide an equivalent condition in terms of PC impedances. Our PC impedance condition is more numerically suitable than the reflection matrix formulation, since we isolate the matrix responsible for the zero eigenvalues that correspond to physically significant solutions. The analysis of an example shows that a single surface mode may involve two Bloch modes with different decay rates, on both sides of the interface.

The condition for surface and waveguide modes on a three-layer structure [Eq. (6)] is similar to that for a dielectric

TABLE I. k_x for a surface mode is repeatedly calculated, varying the number of Bloch modes (vertical axis) and plane waves (horizontal axis) used in the calculation. The table shows the difference of these calculated k_x from $0.957\ 765\ 360\ 815\ 104\pi/d$, the k_x for the surface mode calculated with 11 forward and 11 backward Bloch modes and plane waves.

	Number of plane waves				
	3	5	7	9	11
2	3.2×10^{-5}	1.1×10^{-4}	8.0×10^{-5}	1.1×10^{-4}	8.0×10^{-5}
3	6.1×10^{-5}	1.4×10^{-4}	1.3×10^{-5}	1.4×10^{-4}	1.3×10^{-5}
4		1.1×10^{-7}	3.6×10^{-8}	1.8×10^{-7}	3.4×10^{-8}
5		4.4×10^{-8}	1.8×10^{-7}	2.4×10^{-7}	1.8×10^{-7}
6			8.7×10^{-10}	2.8×10^{-10}	7.6×10^{-10}
7			4.8×10^{-10}	9.5×10^{-10}	1.3×10^{-9}
8				4.2×10^{-12}	4.8×10^{-12}
9				4.8×10^{-12}	3.0×10^{-12}
10					1.0×10^{-14}

TABLE II. k_x for a surface mode is repeatedly calculated, varying the number of Bloch modes and plane waves, as in Table I. The eigenvalue of $(\mathbf{A}_{12}^T\mathbf{A}_{12} + \mathbf{I})$, which should be zero for a surface mode, is then calculated for each k_x using 11 Bloch modes and 11 plane waves.

	Number of plane waves				
	3	5	7	9	11
2	2.4×10^{-4}	8.2×10^{-4}	6.0×10^{-4}	8.2×10^{-4}	6.0×10^{-4}
3	4.6×10^{-4}	1.1×10^{-3}	9.8×10^{-5}	1.1×10^{-3}	9.8×10^{-5}
4		8.1×10^{-7}	2.7×10^{-7}	1.3×10^{-6}	2.6×10^{-7}
5		3.3×10^{-7}	1.4×10^{-6}	1.8×10^{-6}	1.4×10^{-6}
6			6.6×10^{-9}	2.1×10^{-9}	5.8×10^{-9}
7			3.6×10^{-9}	7.2×10^{-9}	1.0×10^{-8}
8				3.2×10^{-11}	3.7×10^{-11}
9				3.7×10^{-11}	2.2×10^{-11}
10					8.1×10^{-14}
11					9.8×10^{-15}

waveguide. We find that some of the waveguide modes of an air-PC-air structure cross the band edge and continue into the partial band gap, becoming surface modes with mode profiles that decay toward the center of the PC region.

ACKNOWLEDGMENTS

This work was produced with the assistance of the Australian Research Council (ARC). CUDOS (the Centre for Ultrahigh-bandwidth Devices for Optical Systems) is an ARC Centre of Excellence.

APPENDIX: COMPLETENESS AND CONVERGENCE

In Sec. II we noted that for the calculations in this paper we represent the field by five forward and five backward propagating and decaying plane-wave diffraction orders. We now explore the validity of this truncation by presenting a convergence analysis for one data point of our results.

As our method is based on that of Botten *et al.* [14], there are two fundamental approximations made in representing field in the PC: the countably infinite set of plane-wave grating diffraction orders is truncated to a finite size, and the set of Bloch modes found by diagonalizing the plane-wave transfer matrix is also truncated. The total set of Bloch modes is complete [20], so without such truncations arbitrary fields in the PC could be exactly represented as superpositions of Bloch modes. We have shown in previous work [13] that there is a minimum number of Bloch modes necessary to provide realistic results for PC reflection coefficients, and that beyond this, convergence with increasing mode number is very rapid. This feature carries over to the study of surface modes, given their close connection to reflection matrices. In this Appendix we further investigate the effect of these truncations on our results for the k_x of a surface mode on an air-PC interface found at a particular frequency. There are further numerical inaccuracies arising from the calculation of plane-wave scattering, but these are comprehensively treated elsewhere [21].

As mentioned in Sec. III, we consider the interface between air and a triangular lattice PC with air holes of radius $0.25d$, where d is the lattice constant, and the background refractive index is $n = 2.86$. The air-PC interface is in the y-z plane. Light is polarized with $\mathbf{E} = E_z\hat{\mathbf{z}}$ and has the frequency $d/\lambda = 0.3$.

We repeatedly apply a root finder to determine the k_x for a surface mode, varying the number of plane-wave orders and the number of Bloch modes. Table I shows how the calculated k_x varies with these parameters. The results converge quickly as the size of the Bloch basis increases. There is negligible difference (4.4×10^{-8}) between the five plane wave and Bloch mode calculation (the approximation used throughout this paper) and the 11 plane wave and Bloch mode calculation. Since the Bloch modes are orthogonal and represented in terms of plane-wave orders, every calculation has more plane-wave orders than Bloch modes. When using a single Bloch mode, the surface mode is not found.

In Sec. III it was established that surface modes occur when $(\mathbf{A}_{12}^T\mathbf{A}_{12} + \mathbf{I})$ has a zero eigenvalue. Table II gives the magnitude of the smallest eigenvalue associated with each k_x in Table I, as calculated with 11 Bloch modes and plane waves. It shows good convergence thereby demonstrating that our work has a solid foundation.

[1] A. D. Boardman, *Electromagnetic Surface Modes* (Wiley, New York, 1982).
[2] R. Ulrich and M. Tacke, Appl. Phys. Lett. **22**, 251 (1973).
[3] M. C. Hutley, *Diffraction Gratings* (Academic Press, New York, 1982).
[4] R. D. Meade, K. D. Brommer, A. M. Rappe, and J. D. Joannopoulos, Phys. Rev. B **44**, 10961 (1991).
[5] W. M. Robertson, G. Arjavalingam, R. D. Meade, K. D. Brommer, A. M. Rappe, and J. D. Joannopoulos, Opt. Lett. **18**, 528 (1993).

[6] Y. A. Vlasov, N. Moll, and S. J. McNab, Opt. Lett. **29**, 2175 (2004).
[7] B. Wang, W. Dai, A. Fang, L. Zhang, G. Tuttle, T. Koschny, and C. M. Soukoulis, Phys. Rev. B **74**, 195104 (2006).
[8] K. Ishizaki and S. Noda, Nature (London) **460**, 367 (2009).
[9] J. M. Elson and P. Tran, Phys. Rev. B **54**, 1711 (1996).
[10] S. Enoch, E. Popov, and N. Bonod, Phys. Rev. B **72**, 155101 (2005).
[11] M. Che and Z. Y. Li, J. Opt. Soc. Am. A **25**, 2177 (2008).
[12] F. J. Lawrence, L. C. Botten, K. B. Dossou, C. M. de Sterke, and R. C. McPhedran, Phys. Rev. A **80**, 023826 (2009).
[13] F. J. Lawrence, L. C. Botten, K. B. Dossou, and C. M. de Sterke, Appl. Phys. Lett. **93**, 121114 (2008).
[14] L. C. Botten, T. P. White, A. A. Asatryan, T. N. Langtry, C. M. de Sterke, and R. C. McPhedran, Phys. Rev. E **70**, 056606 (2004).
[15] L. C. Botten, N.-A. P. Nicorovici, A. A. Asatryan, R. C. McPhedran, C. M. de Sterke, and P. A. Robinson, J. Opt. Soc. Am. A **17**, 2165 (2000).
[16] K. Dossou, M. A. Byrne, and L. C. Botten, J. Comput. Phys. **219**, 120 (2006).
[17] F. Yang, J. R. Sambles, and G. W. Bradberry, Phys. Rev. B **44**, 5855 (1991).
[18] H.-G. Choi, S. S. Oh, S.-G. Lee, M.-W. Kim, J.-E. Kim, H. Y. Park, and C.-S. Kee, J. Appl. Phys. **100**, 123105 (2006).
[19] C. M. de Sterke, L. C. Botten, A. A. Asatryan, T. P. White, and R. C. McPhedran, Opt. Lett. **29**, 1384 (2004).
[20] C. H. Wilcox, Journal d'analyse mathématique **33**, 146 (1978).
[21] R. C. McPhedran, N. A. Nicorovici, L. C. Botten, and K. A. Grubits, J. Math. Phys. **41**, 7808 (2000).

Erratum: Photonic-crystal surface modes found from impedances [Phys. Rev. A 82, 053840 (2010)]

Felix J. Lawrence,* Lindsay C. Botten, Kokou B. Dossou, R. C. McPhedran, and C. Martijn de Sterke

(Received 24 January 2011; published 23 February 2011)

DOI: 10.1103/PhysRevA.83.029907 PACS number(s): 42.70.Qs, 73.20.At, 42.79.Gn, 41.20.Jb, 99.10.Cd

We report an error in the appendix of the original article. The numbers quoted were for a different physical structure than that which was specified. The corrected versions of Tables I and II are given here and show that good convergence is also obtained for the specified physical structure. Specifically, there remains negligible difference (4.7×10^{-8}) between the approximation used throughout the paper and the 11 plane-wave and Bloch mode calculation. The conclusions of the appendix are unchanged.

TABLE I. k_x for a surface mode is repeatedly calculated, varying the number of Bloch modes (vertical axis) and plane waves (horizontal axis) used in the calculation. The table shows the difference of these calculated k_x from 0.959 110 616 739 566 π/d, the k_x for the surface mode calculated with 11 forward and 11 backward Bloch modes and plane waves.

	Number of plane waves				
	3	5	7	9	11
2	9.6×10^{-5}	1.1×10^{-4}	1.1×10^{-4}	1.1×10^{-4}	1.1×10^{-4}
3	6.2×10^{-5}	1.5×10^{-4}	1.5×10^{-4}	1.5×10^{-4}	1.5×10^{-4}
4		1.1×10^{-7}	1.8×10^{-7}	1.8×10^{-7}	1.8×10^{-7}
5		4.7×10^{-8}	2.5×10^{-7}	2.5×10^{-7}	2.5×10^{-7}
6			1.5×10^{-10}	2.8×10^{-10}	2.8×10^{-10}
7			4.8×10^{-10}	9.8×10^{-10}	1.0×10^{-9}
8				4.0×10^{-12}	6.9×10^{-12}
9				4.7×10^{-12}	7.7×10^{-12}
10					3.2×10^{-15}

TABLE II. k_x for a surface mode is repeatedly calculated, varying the number of Bloch modes and plane waves, as in Table I. The eigenvalue of $(\mathbf{A}_{12}^T \mathbf{A}_{12} + \mathbf{I})$, which should be zero for a surface mode, is then calculated for each k_x using 11 Bloch modes and 11 plane waves.

	Number of plane waves				
	3	5	7	9	11
2	7.2×10^{-4}	8.5×10^{-4}	8.4×10^{-4}	8.4×10^{-4}	8.4×10^{-4}
3	4.7×10^{-4}	1.1×10^{-3}	1.1×10^{-3}	1.1×10^{-3}	1.1×10^{-3}
4		8.5×10^{-7}	1.4×10^{-6}	1.4×10^{-6}	1.4×10^{-6}
5		3.5×10^{-7}	1.9×10^{-6}	1.9×10^{-6}	1.9×10^{-6}
6			1.2×10^{-9}	2.1×10^{-9}	2.1×10^{-9}
7			3.6×10^{-9}	7.4×10^{-9}	7.8×10^{-9}
8				3.0×10^{-11}	5.2×10^{-11}
9				3.6×10^{-11}	5.8×10^{-11}
10					4.5×10^{-15}
11					2.9×10^{-14}

*felix@physics.usyd.edu.au

The Appendix to Paper 5.1 was added to demonstrate the accuracy of the numerical technique with which we calculate the impedance matrices—in this case, the multipole method—and of the ensuing procedure to find surface modes. In the original paper, the impedance matrices for air were not calculated analytically—they were calculated using the same multipole implementation as the PCs. However this implementation of the multipole method does not support the trivial case of uniform media, and so air was approximated by a PC with a background of $n = 1$ and tiny cylinders with a different refractive index. While this approximation is sufficient for the results quoted in the main text of the paper, it affects the results of the Appendix where numbers are quoted to 15 decimal places in order to enable a convergence study. Therefore we published the Erratum, which gives the correct results, obtained with analytically calculated impedance matrices for air.

5.2 PC waveguides

In Paper 5.1, we give Eq. (6), which is the condition for a coupled surface mode. As noted in the paper, it is also the condition for a waveguide mode, and is directly analogous to Eq. (1.12). This method can also be used to calculate the dispersion relations of conventional PC waveguides, which typically consist of two bandgap PCs that act as mirrors, either side of a uniform dielectric channel. If the matrix $\mathbf{R}$ gives not the reflection off a single PC, but the reflection off a stack of PCs, then the modes of more complicated structures can be found, e.g. the modes of a PC waveguide where the innermost rows of holes have been shifted transversely. Such structures are commonly employed to obtain slow light with low dispersion, which is useful for enhancing nonlinear effects.

There are many other ways to calculate the dispersion relations of PC waveguides. Most of these require a computational domain that includes the waveguiding region and several periods of the barrier PC in the x–direction.

Our impedance-based method instead only requires simulation of one unit cell of each PC in the problem: the PCs that comprise the barrier, and the PC in the waveguiding region (in the rare case that the waveguiding region is not just a uniform dielectric [5, 8]). However, our impedance-based method has a critical disadvantage in efficiency compared to other methods, which scan over frequency, and the propagation constant k_x of the waveguide mode is found directly from each simulation (e.g. transfer matrix supercell methods [108])—or vice versa (e.g. the frequency-domain methods used by the popular MIT Photonic-Bands package). Using our impedance method, we must scan both over frequency and k_x, running separate simulations to determine whether a mode exists at each point: we must scan a 2D parameter space to obtain the dispersion relation, whereas other methods need only scan a 1D parameter space.

However, Blown *et al.* [7] showed that this extra dimension of scanned parameters need not be wasted. Having calculated the PC mirror's reflection matrix at a particular frequency and k_x, it is possible to solve a simple transcendental equation (Eq. (5) in Ref. [7]) for a waveguide thickness that supports a mode. Another equation (Eq. (6) in Ref. [7]) gives the waveguide's group velocity in terms of the mirror's reflection matrix and the waveguide's thickness. Therefore, when scanning the 2D parameter space, rather than asking at each frequency and k_x "is there a mode here?", we can ask "what waveguide thickness would support a mode here?", at minimal additional computational expense. This insight allows efficient calculation of dispersion relations for many PC waveguides simultaneously: when dis-

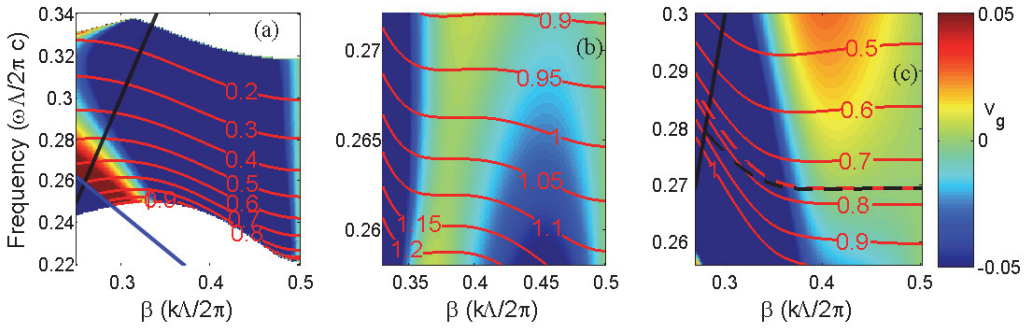

Figure 5.1: Group velocities and thicknesses of PC waveguides based around three different PC mirrors. The PC mirror in (c) was obtained by modifying the radii of the first and second rows of holes. The black line is the light line, and the blue line is the first Wood anomaly. For full details, see Ref. [7], from which this figure was taken.

persion engineering, the waveguide width becomes a parameter that costs almost nothing to explore. The contours in Fig. 5.1 are individual waveguides' dispersion relations found in this way. Using this method it was not difficult to find a PC waveguide with a quartic point on its dispersion relation that has zero group velocity and zero first and second order dispersion (Fig. 5.1). Note that almost all points of interest lie above the first Wood anomaly, and so reflection matrices, not coefficients, are required.

Dispersion engineering can be done by modifying hole radius, as in Ref. [7], or by modifying hole position; typically the latter degree of freedom is preferred for ease of accurate fabrication. If dispersion engineering is performed only by shifting rows of holes in the transverse direction and by changing the waveguide thickness, then the dispersion engineering could be done extremely efficiently using the methods described in Ref. [7], combined with the trick mentioned at the end of Chapter 2. That is, rows of holes could be transversely shifted by inserting dielectric padding layers—which does not require further simulations. Doing this would mean that at each frequency and k_x only one PC unit cell would need to be simulated: using this PC's impedance and Bloch factors the entire parameter space could be mapped out analytically and extremely efficiently.

5.3 Coupled PC waveguide arrays

A similar approach, albeit one in which waveguide thickness was not varied, has been used to calculate dispersion relations and supermodes of coupled PC waveguides [5, 164] and of large arrays of coupled PC waveguides [8]. In the former references, reflection matrices in the plane wave basis are calculated using the work of Botten *et al.* [108], which underpins the impedance method. In Ref. [8], which poses the problem in terms of Bloch mode amplitudes, impedance matrices are used to calculate the reflection and transmission matrices.

Figure 5.2, taken from Ref. [8], shows the dispersion relation of an array of 31 PC waveguides. Although such a system is not especially difficult to fabricate, simulating it with most methods would require a prohibitively large computational domain. Propagation through the array, which involves discrete diffraction, is easily modelled using this dispersion relation and the supermode profiles.[1] Figure 5.3 shows how light propagates through many

[1] In the tight-binding approximation, the supermode profiles may analytically be writ-

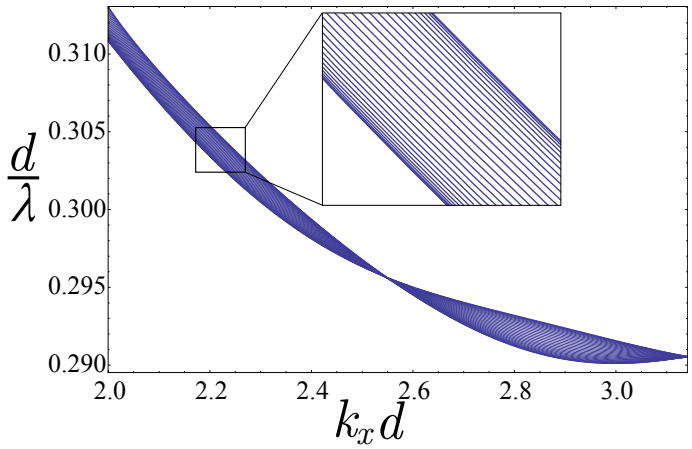

Figure 5.2: Dispersion relation of an array of 31 coupled PC waveguides [8].

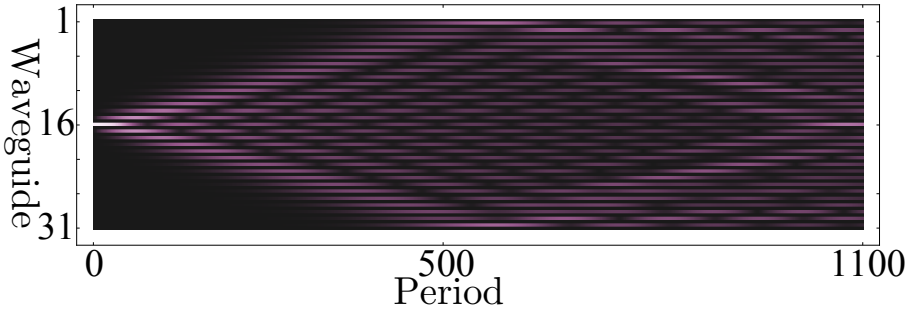

Figure 5.3: Light incident from one waveguide into an array of 31 coupled PC waveguides [8].

periods of the 31 PC waveguide array, diffracting outwards until it reaches the edge waveguides, then reflecting back in.

Using impedances to calculate the waveguide modes and the coupling between waveguides allows efficient dispersion engineering of PC waveguide arrays. Furthermore, the method described in Sec. 5.3 and Ref. [7] could be employed to perform this search even more efficiently, enabling the discovery of PC waveguide arrays with unusual discrete diffraction properties. This is a current area of investigation.

ten in terms of the individual waveguide modes [8, 81]

Chapter 6

Concluding remarks

In the preceding chapters I described a framework that can be used to calculate reflection and transmission properties of PC stacks in terms of the PCs' Bloch modes, accurately and efficiently. The propagative characteristics of each PC's modes are encapsulated in Bloch factors: by Bloch's theorem these govern how a mode propagates or decays. The reflective properties of each PC are encapsulated in a new quantity, the PC impedance matrix, defined in Chapter 2. We presented two ways to calculate Bloch factors and PC impedances: either by transfer matrix methods based on specialised FEM or multipole methods (Chapter 2), or by using generic field solvers with a mode extraction algorithm (Chapter 3). We inspected some PC impedance matrix elements and Bloch factors in Chapter 4, and explored their behaviour in a few cases, as well as their possible relation at low frequency to familiar effective material parameters such as n and Z_c—albeit parameters that vary strongly with frequency, incident angle and polarisation.

We applied this PC impedance framework to a number of problems. In Chapters 2 and 3 we used it to design antireflection coatings for PCs in an efficient manner: in Paper 3.1 we give an example where, once the PCs' impedances were calculated, 13 million coatings were evaluated on a 16 core workstation, taking 80 minutes per polarisation. Other applications of the PC impedance framework were demonstrated in Chapter 5: single and double interface PC surface modes were modelled, and we briefly described work that applies PC impedances to engineer PC waveguides' dispersion efficiently, and to analyse large arrays of coupled PC waveguides.

6.1 Context

We developed the PC impedance framework to describe coupling between bulk PCs, and its first application was to design antireflection coatings that aid coupling into bulk PCs. In Sec. 1.1.1 we described the most prominent applications of bulk PCs: superprisms, and self-collimation. In the last few years these applications have not garnered a great deal of attention: photonic crystal research has mostly focussed on PC waveguides and cavities; and as a whole, photonic crystals have been pushed somewhat out of the limelight by metamaterials. Partially this is due to the maturing of photonic crystals as a research field—they have largely moved out of the exploration stage into the application stage and are now studied less for their intrinsic properties and more for what can be done with them.

For example, PC waveguides receive attention for their slow light modes; as light slows down its intensity increases, along with the associated nonlinear effects. There is strong demand for waveguide modes with low group velocity

and dispersion, and this continues to drive research into PC waveguides. PC cavities have also received sustained interest as they can achieve large quality factors, which is useful for all-optical switching or modifying spontaneous emission rates (cavity quantum electrodynamics). In both cases, the research into PCs is now being driven by its applications.

In Sec. 1.1.1, we stated that superprisms could have applications as frequency demultiplexers and spectrometers. Superprism-based *spectrometers* have received waning levels of attention; for example Momeni *et al.* in 2010 abandoned these in favour of grating spectrometers, citing superprism-based spectrometers' large insertion losses [165]. Several superprism-based *demultiplexers* have been demonstrated, e.g. by Momeni *et al.* [166] in 2006 and Matsumoto *et al.* [30], with others recently proposed by Khorshidahmad and Kirk [167, 168]. It has long been known that the superprism effect is usually masked by broadening of the incident beam due to diffraction [169]. Efforts have been made to overcome this by using a superlens [30] or a very long preconditioning region [166]. Some authors also cite coupling loss as a limiting factor for their devices [30, 168].

Even with the countermeasures used in these papers, the demonstrated performance of superprisms is not spectacular. The superprism in Ref. [166] is designed for the C band, 1525–1565 nm. This band is relatively narrow; wavelength demultiplexers working in the C band need high spectral resolution to be able to separate many narrowly-spaced channels. The demultiplexer demonstrated by Momeni *et al.* [166] supports only four channels with a spacing of 8 nm. Including the preconditioning region, their device has a footprint of about $90\,\mu\text{m} \times 1150\,\mu\text{m}$. The $80\,\mu\text{m} \times 100\,\mu\text{m}$ demultiplexer demonstrated by Matsumoto *et al.* [30] has a larger bandwidth, supporting light between 1.50–1.63 μm, but only six channels were demonstrated, and the spacings were uneven due to their superprism's dispersion properties. By comparison, almost ten years earlier, a C band grating-based WDM demultiplexer in a slab waveguide was demonstrated with 120 channels separated by 0.29 nm [170], although this demultiplexer is considerably larger, fitting on a 10 mm × 34 mm chip.

It appears that this uncompetitive performance is due to two related problems: coupling loss at the PC interfaces, and the excitation of several outgoing plane waves. The first problem can be solved by an antireflection coating: indeed, Matsumoto *et al.* [30] did exactly this. In principle, the second problem might also be solved by blazing, designing a coating that at each frequency couples the superprism's propagating Bloch mode to only one plane wave in the output dielectric, thus avoiding the diffractive effects that Matsumoto *et al.* [30] tried to counteract using a superlens. The design of such a coating (albeit one where each layer has up-down symmetry) is inherently suited to methods such as ours that represent transmission by a matrix in the Bloch mode basis—in fact we did this for a single frequency in Sec. IV C of Paper 3.1. However it is unclear whether there would exist such a coating that is simultaneously effective at all superprism/multiplexing frequencies.

Research into self-collimation has also reached an awkward position—it is no longer particularly novel to present a self-collimating PC as an end in itself, yet the most advanced demonstration of self-collimating devices was presented in 2007 by Prather *et al.* [39]. This *tour de force*, experimentally demonstrating a range of exciting devices and proposing several more, might have been expected to mark the field's coming of age. Since this paper, there have been a few more demonstrations of Mach-Zender interferometers in self-collimating PCs, and some proposals of PCs that support self-collimation in both polarisations simultaneously. But sadly there has not been the ex-

pected flurry of engineering papers boasting designs with ever-larger figures of merit; indeed the "currently in progress" experimental validation of the reconfigurable optical switch that was promised in Ref. [39] seems never to have been published.

Perhaps the reason for the loss of interest in self-collimation is that, as a light-guiding mechanism, it competes with PC waveguides. While it is exciting to see light guided by a structure that does not appear to contain a waveguide, the advantages of guiding light in this way are few—Prather *et al.* [39] cite ease of alignment, and the possibility of propagating perpendicular beams across one another without crosstalk. PC waveguides, on the other hand, can be substituted for self-collimating PCs in most of the cited applications. Furthermore, PC waveguides support a range of parameters that may be tuned to engineer the group velocity of the guided light. Finally, in a self-collimating PC, much of the field's intensity is in the air-holes, where it is not confined in the out-of-plane direction. Therefore the loss of such devices could be expected to be higher, and the fabrication tolerances more stringent, than for similar devices designed with PC waveguides.

As the in-band applications of PCs fade in popularity, we have considered how our work on PC impedance may be applied to PC waveguides; this resulted in the efficient method for dispersion-engineering described in Sec. 5.2. Further steps that could be taken in this direction are discussed in the next section.

6.2 Future directions

Slab PC impedance

So far, we have only developed the PC impedance framework for 2D photonic crystals. 2D photonic crystals are most often idealised structures used to model slab PCs: the background index of the 2D PC is chosen to be the effective index of the background slab, which depends on the slab's refractive index and its thickness. In this way, efficient 2D calculations can model PC slabs with some success; however, direct 3D simulations of PC slabs remain the gold standard, albeit a gold standard that is significantly slower and more memory intensive and thus is typically run with coarser resolution.

Therefore, a logical next step would be to extend the impedance framework to treat slab PCs and their modes in 3D. This would require the inclusion of all field components, since, unlike in 2D, the problem cannot be exactly decoupled into E_z and H_z polarisations. It would also require a new reference medium and a basis to go with it. An obvious choice for the reference medium would be an unpatterned dielectric slab of equal thickness to the PC. In the thin-film framework (Sec. 1.2.1), the basis was a pair of forward and backward plane waves in each medium: this basis was complete under reflection and transmission at parallel interfaces. In the 2D PC framework (Sec. 1.5.2), we again used plane waves as a basis, but had to include the infinite set of grating diffraction orders, which is closed under grating scattering—we then truncated this set to a more manageable handful of orders. For slab PCs, the obvious way to extend the 2D method is to use slab modes instead of plane waves—specifically, to use the slab modes diffracted from a grating embedded in the slab. By the grating equation, which also applies to slab modes, this set is closed under scattering by other gratings with the same period, and thus is complete enough to model PC scattering. I anticipate that the mode finding algorithm described in Chapter 3 would require few changes to find the Bloch modes of slab PCs.

The main challenge therefore lies in defining slab PC impedances in terms

of the modal fields. Our impedance definition heavily relies on a rigorous set of Bloch mode orthogonality relations (Eqs. (2.14)). To apply our method to slab PCs, we would need to use 3D orthogonality relations, such as those given by Lecamp *et al.* [64] or Dossou *et al.* [171]. An impedance formalism could then be built up rigorously around these orthogonality relations. While waiting for the formalism to be rigorously developed, it may be possible simply to recast the overlap integrals in Sec. 3.2 in terms of these new orthogonality relations and use them to calculate "impedance matrices". Doing so has no rigour and is essentially guessing the outcome of a rigorous derivation, but it would be easy to check the results numerically, and if such matrices are successful then this could inform the derivation.

PC waveguide impedance

It would also be of interest to define impedance for PC waveguides, which are more widely used than bulk PCs (as discussed in Sec. 6.1). While we have applied the PC impedance framework to find the propagating modes of PC waveguides, and to tailor their dispersion, we neither found the impedances of these waveguides nor calculated the reflection and transmission at an interface between them. Our numerical methods require that k_x be real, and therefore we cannot find evanescent waveguide modes using the techniques of Sec. 5.2. As we have seen, evanescent modes play a critical role in reflection and transmission between bulk PCs and so need to be represented in the impedance matrix—they also play an important role in coupling between PC waveguides [172].

I see three approaches for calculating PC waveguide impedance matrices. The first is to simulate the PC waveguide using a supercell transfer matrix method: Bloch mode reflection and transmission matrices for PC waveguides have previously been obtained in this way [49], and it should be straightforward to apply the impedance definition for square lattice PCs to these supercells. The second way is to find the important propagating and evanescent modes of the PC waveguide by a Chapter 3–style mode extraction. The third is an improved version of the Sec. 5.2 method that also finds evanescent modes, which would require a numerical method that finds transfer matrices across half-gratings when k_x is complex, which is a difficult, perhaps insoluble problem.

Regardless of how the impedance matrices are found, as discussed in Sec. 3.3 some thought needs to go into the representation of the modes and the choice of reference medium—air may well prove to be a less suitable reference medium for PC waveguides than it does for the bulk PCs we studied. In related work [49], the modes of a PC waveguide were represented along the supercell edge by supercell grating orders, and the number of these that had to be included in the calculation scaled with the supercell's size. The supercell's grating orders are also the modes of air, and so if air is the reference medium then the number of reference modes needed to represent the waveguide modes, and thus the dimension of the PC impedance matrix, also scales with the supercell size. This is undesireable. In principle, the number of modes required to characterise a PC waveguide should not scale with the size of the supercell used to simulate it. Perhaps a wisely chosen reference PC would allow each PC waveguide's important modes to be characterised by a smaller subset of modes in the reference PC, allowing a smaller impedance matrix. Speculatively, the input or output PC waveguide might be a good reference medium for coating applications, since its modes are inherently related to the problem.

More-efficient dispersion engineering

At the end of Sec. 5.2 we discussed how a single set of simulations of a single PC unit cell, over a range of frequencies and k_x, can be used to dispersion engineer a PC waveguide extremely efficiently. Using no further numerical simulations, it is possible to apply the PC impedance framework to find the reflectance of many PC mirrors, by shifting the rows of holes towards or away from the mirror's surface. The key to this is that the PC impedance and Bloch factors of a uniform dielectric can be calculated analytically, which leads to a number of extra degrees of freedom being made available for dispersion engineering, with little associated computational expense.

This could be taken one step further: rows of holes could also be shifted parallel to the mirror's surface, also without further simulations. This would be done by converting into the plane wave basis (e.g. by using impedance matrices to calculate the transmission into an infinitesimal layer of uniform dielectric) and applying a method presented by White *et al.* [173] to transform the reflection and transmission matrices across this interface to account for the shift. The opposite shift would occur on the other side of the row of holes, to restore the lattice to its original origin. Doing so, three continuous degrees of freedom per row of holes are available for dispersion engineering: longitudinal shifts, transverse shifts, and hole radius; using the proposed method, only the last of these must be explored using numerical simulations—the impedances and Bloch factors for each radius would be stored and repeatedly reused for each mirror configuration.

6.3 Strengths and weaknesses of our method

The key strength of our method is that it allows reuse of computationally expensive simulations, by characterising each PC. Therefore it is most suited to applications requiring simulation of many PC stacks constructed from a smaller pool of PCs. The PC impedance framework is thus particularly suited to designing antireflection coatings and dispersion engineering.

The impedance framework that we describe only applies to a subset of possible PCs (albeit a subset that includes the most commonly-applied 2D PCs). The PC lattice must be rectangular or triangular, that is, each row of holes must either be in line with the last or shifted by half a period,[1] and its unit cell must be up-down symmetric. These two restrictions, which rule out the treatment of arbitrary 2D lattices and arbitrary unit cells, allow the forward and backward Bloch modes to be related (Eq. (6) vs. Eq. (7) in Paper 2.3), and the impedance matrix to be defined. If Eq. (6) is not simplified to Eq. (7), then it might be possible to derive *two* impedance matrices, one for forward modes and one for backward modes, that (together) characterise a non-symmetric PC's reflection and transmission properties.

We have not yet applied our impedance method to unit cells that cut across inclusions. Rectangular-lattice supercells for triangular lattice PC waveguides with hole radii $r > a/4$ cannot be defined without supercell edges cutting through some holes. As long as the unit cells are up-down symmetric, our method should be valid for these structures—indeed, the method upon which ours is based has been successfully applied to such structures [110].

Our method applies both to lossless and lossy PCs, because we use mode orthogonality relations based on reciprocity (Eqs. (2.14)) instead of the more common form based on energy conservation. However, we have not yet

[1] The shifts described in the previous section do not fall foul of this restriction because they are applied at the interfaces of a PC layer, rather than after every row in a semi-infinite bulk PC.

applied the method to lossy PCs. For the above reason, our method does not apply to PCs containing non-reciprocal media, such as that proposed by Wang *et al.* [174]; for such PCs, impedance matrices might be derived in a similar way using energy conservation mode orthogonality relations [108]. Such PCs are unlikely to have up-down symmetry.

The above weaknesses mainly restrict the domain of applicability of our method; therefore for a given problem they either preclude our method's use, or do not apply and are not weaknesses. To provide a more nuanced view, we now directly compare our method to alternative methods of simulating structures to which our method may be applied.

vs. Field scattering calculations

Our impedance method is particularly effective for simulating many PC stacks composed from a smaller set of PCs. Methods such as FEM and FDTD may be used to simulate each PC stack directly, but this requires one slow simulation per stack. The larger the ratio between the number of stacks and number of PCs, the greater the intrinsic advantage of our impedance method over these methods. For problems where each PC is used only once at a given frequency, incident angle and polarisation, our method has no intrinsic advantage over field scattering methods other than that it gives reflection and transmission matrices rather than coefficients.

vs. Transfer/scattering matrix methods

Even when applied to a suitable problem, is our impedance framework better than the scattering and transfer matrix methods upon which it is based? The most efficient form of our method, described in Chapter 2, works by first calculating the transfer matrix, which is the most computationally-intensive step in calculating a PC impedance. The transfer matrix, or the scattering matrix that may be derived from it to avoid instabilities [106], could be stored in place of an impedance, giving rise to similar efficiencies. These matrices too can calculate plane wave scattering through a stack of PCs, and at interfaces with semi-infinite PCs [108]: does the impedance framework have any advantages over such methods?

In my opinion, the PC impedance method does not have a large computational advantage over scattering matrix methods, but it requires little additional effort and is conceptually preferable. The main computational advantage of the PC impedance method is that the stored quantities, the impedance and Bloch factors, are smaller than the transfer matrix $\mathcal{T}$ and the scattering matrix $\mathbf{S}$. If as many Bloch modes as plane waves are used (a full rank calculation, of equal accuracy to a scattering matrix calculation), then the impedance matrix has one quarter as many elements as the transfer or scattering matrices; if fewer Bloch modes are used, then this fraction is even smaller. Half this efficiency is gained by relating forward and backward modes (Eq. (7) in Paper 2.3), the other half is intrinsic to the concept of impedance. Therefore, impedance matrices consume at most one quarter the RAM of a transfer matrix, and a database of impedance matrices needs one quarter the storage size of a transfer matrix database. But usually neither matrix contains particularly many elements, computer memory is cheap, and the cost of operations with these 5×5 impedance matrices or 10×10 transfer matrices is minimal in comparison to other numerical methods.

The more significant difference is the conceptual one. Transfer and scattering matrix methods work in one fixed reference basis across all PC layers, e.g. the plane wave grating orders in free space. Using the impedance framework, one works only with each PC's Bloch modes, which provide more phys-

ical insight—the amplitude vectors are for modes that do not couple upon propagation, and reflection and transmission matrices relate the eigenmodes in the adjacent PCs. I found this physical insight useful to analyse uncoupled modes, potential for homogenisation, and surface modes, and it informed the design of antireflection coatings. For example, an antireflection coating could be designed specifically to couple one superprism Bloch mode to one plane wave, and vice-versa. Bloch mode amplitudes and reflection/transmission matrices can be obtained from scattering matrix methods using extra steps [108], but it is arguably simpler to do so using impedances, just as it is simpler to use the Fresnel equations instead of calculating reflection coefficients from first principles each time.

Microwave engineers analysing a two-port network can represent its properties by any of the five 2×2 matrices discussed in Sec. 1.3.2: the scattering, ABCD, or transfer matrices, or what they define as impedance and admittance matrices. However, when a signal is only incident from one of the ports, frequently the other port and everything behind it is described by an input impedance—one number—as opposed to a matrix that contains four; when describing such a system our impedance matrix reduces to a scalar.

It is not clear whether much value would be generated by generalising our PC impedance matrices to calculate properties of N–port networks such as junctions between multiconductor transmission lines and metallic waveguides. The PC impedance framework was developed to calculate reflection and transmission matrices for the interface between two PCs, where each PC has $N/2$ modes. The N–port network formalism is more general than this—it characterises a junction between N ports, and does not distinguish between input ports and output ports, tying half the ports to one object and the other half to another. For a given frequency, incident angle, and k_x, a PC has a fixed set of Bloch modes: this set may be truncated but one Bloch mode cannot be somehow removed and replaced by another PC's. The PC's impedance matrix is defined for this fixed set of modes. At a junction between N transmission lines, however, the transmission lines are not inherently separable into two bound halves—typically one line could be replaced independently of the others—and so the value of characterising that half of the lines by one matrix is lost.

6.4 Concluding remarks

PCs are more complicated than uniform dielectrics because many PC modes couple at each interface, requiring the field to be represented by the amplitudes of a set of propagating and evanescent modes instead of one forward wave and one backward wave. This means that vectors and matrices must be used instead of scalar amplitudes and reflection coefficients. We have shown that in bulk PCs, wave impedances may be generalised to matrices which can be used to calculate the reflection and transmission matrices between the Bloch modes of adjacent PCs. By including a sufficient (but still small) number of Bloch modes, even single-period PC layers can be modelled accurately, enabling the efficient design of antireflection coatings, and efficient dispersion engineering. The fact that impedance often needs to be represented as a matrix rather than a scalar indicates that the physics is richer, and raises the possibility of counter-intuitive effects (such as efficient direct coupling between modes with very different field profiles [45]) that one would not expect to be possible were the impedance able to be represented by a scalar. While PC impedance is unlikely to enjoy the ubiquity enjoyed by electrical impedances, the PC impedance framework is a useful, efficient, accurate and conceptually satisfying method to simulate stacks of bulk PCs.

Appendix A

E and H matrices for uniform media

The **E** and **H** matrices are defined in Paper 2.3, by Eq. (9) for light with E_z polarisation, and by Eq. (10) for light with H_z polarisation. The relevant Bloch modes/eigenstates of uniform media are the grating orders, so it is easy to write down the matrix

$$\mathcal{F} = \begin{pmatrix} \mathbf{F}_+ & \mathbf{Q}\mathbf{F}_- \\ \mathbf{F}_- & \mathbf{Q}\mathbf{F}_+ \end{pmatrix} \tag{A.1}$$

that maps the Bloch modes to (propagating and evanescent) plane waves, and arrive at an analytic expression for such media's **E** and **H** matrices. We do so in this Appendix, then remark on some consequences of this close link between Bloch modes and the grating orders.

Since the Bloch modes of uniform media are grating orders, one could simply choose the matrix $\mathcal{F}$ to be the identity matrix **I** (with sign adjustments **Q** for backward odd grating orders for triangular lattice PCs). However, there exists a sensible and unique way to enumerate the grating orders, namely sorting by each wave's order s. This is different to the sorting of Bloch modes, which are typically ordered for ease of truncation: the propagating modes first, then the evanescent modes from least to fastest-decaying. Therefore, in practice we choose $\mathbf{F}_+$ to be in most cases a permutation of **I**. Since forward grating orders have no backward component, $\mathbf{F}_- = \mathbf{0}$.

For positive incident angles $\theta > 0$, with 5 forward plane waves and 5 forward Bloch modes, a sensible choice of $\mathbf{F}_+$ is

$$\mathbf{F}_+ = \begin{pmatrix} 0 & 0 & 0 & 1 & 0 \\ 0 & 1 & 0 & 0 & 0 \\ 1 & 0 & 0 & 0 & 0 \\ 0 & 0 & 1 & 0 & 0 \\ 0 & 0 & 0 & 0 & 1 \end{pmatrix}, \tag{A.2}$$

because it can be shown from the grating equation Eq. (1.24) and Eq. (1.25) that an evanescent plane wave with positive diffraction order s decays faster than its counterpart with order $-s$ (the vector of plane wave amplitudes is ordered from most negative s to most positive s). At normal incidence, the grating orders $\pm s$ are degenerate, so it is useful to write them in even and

odd superpositions:

$$\mathbf{F}_+ = \begin{pmatrix} 0 & 0 & 0 & 1/\sqrt{2} & 1/\sqrt{2} \\ 0 & 1/\sqrt{2} & 1/\sqrt{2} & 0 & 0 \\ 1 & 0 & 0 & 0 & 0 \\ 0 & 1/\sqrt{2} & -1/\sqrt{2} & 0 & 0 \\ 0 & 0 & 0 & 1/\sqrt{2} & -1/\sqrt{2} \end{pmatrix}. \tag{A.3}$$

Thus for uniform media, Eq. (9) of Paper 2.3 yields for E_z polarisation

$$\mathbf{E} = \mathbf{Y}^{-1/2}\mathbf{F}_+, \tag{A.4a}$$

$$\mathbf{H} = \mathbf{Y}^{+1/2}\mathbf{F}_+, \tag{A.4b}$$

where

$$\mathbf{Y} = \mathrm{diag}(\sqrt{\epsilon/\mu}\, k_\perp^{(s)}/k) \tag{A.5}$$

is a diagonal matrix of wave admittances. For H_z polarisation, Eq. (10) from the same paper yields

$$\mathbf{E} = -\mathbf{Z}^{+1/2}\mathbf{F}_+, \tag{A.6a}$$

$$\mathbf{H} = \mathbf{Z}^{-1/2}\mathbf{F}_+, \tag{A.6b}$$

where

$$\mathbf{Z} = \mathrm{diag}(\sqrt{\mu/\epsilon}\, k_\perp^{(s)}/k) \tag{A.7}$$

is the corresponding matrix of wave impedances. The $-$ sign in Eq. (A.6a) occurs because of how the plane wave amplitudes $f^\pm$ are defined in Paper 2.3, in a way consistent with Eq. (3) of Ref. [108].

Truncating the set of Bloch modes involves removing columns of $\mathbf{E}$ and $\mathbf{H}$, and reduces the dimension of the (always square) impedance matrix $\mathcal{Z}$. At non-normal incidence, by inspecting Eq. (A.2) we see that removing a column always removes the only nonzero entry from a row of $\mathbf{E}$ and $\mathbf{H}$; in other words by truncating the set of Bloch modes, perhaps unsurprisingly we are also implicitly truncating the set of grating diffraction orders. This means that if the reference medium 0 against which impedances are calculated (using Eq. (26a) of Paper 2.3) is a uniform medium, then there is no point in using rectangular $\mathbf{E}$ and $\mathbf{H}$ matrices and having a larger set of diffraction orders than of Bloch modes. At normal incidence, if symmetry allows it is sometimes possible to discard the modes corresponding to odd superpositions of grating orders, leading to smaller impedance matrices that give results equivalent to those found with larger matrices, as long as all incident fields are evenly symmetric. This technique is applied in Secs. IV A and IV C of Paper 3.1.

Appendix B

Effect of choice of reference medium

PC impedance (Eq. (26a) in Paper 2.3) is defined with respect to a reference material, which throughout this thesis we have taken to be vacuum. Aside from a speculative discussion about PC waveguides at the end of Sec. 3.2, which is recapitulated in the concluding Chapter 6, we did not consider in detail the choice of this reference medium, which might be a PC instead of free space. In this Appendix we consider a few example problems and determine whether additional accuracy may be gained by choosing a reference material other than free space.

The $\mathbf{E}_0$ and $\mathbf{H}_0$ matrices of the reference medium are the quantities used to calculate a given PC's impedance. If these $\mathbf{E}_0$ and $\mathbf{H}_0$ matrices have deleterious properties, such as zero rows, then when calculating the impedance we miss some information that is present in the PC's $\mathbf{E}$ and $\mathbf{H}$ matrices. Therefore the choice of reference medium might affect the calculated reflection and transmission matrices at an interface. There are three classes of potential reference medium; increasing in generality they are: vacuum, another dielectric, or a PC.

As noted in Appendix A, $\mathbf{E}$ and $\mathbf{H}$ for uniform media have zero rows when the matrices are rectangular, i.e., when the set of Bloch modes is more strongly truncated than the set of grating orders (although as noted the story is slightly more complicated at normal incidence, due to degeneracies).

Appendix A gives analytic expressions for the $\mathbf{E}$ and $\mathbf{H}$ matrices of uniform media, in terms of the medium's refractive index and the light's frequency, polarisation and angle of incidence. From these equations A.4 and A.6, we see that the matrices representing different uniform media are intimately related. In fact, for square lattices, by inserting Eqs. A.4 or A.6 into Eq. (26a) in Paper 2.3, and substituting this equation into the expressions for the transmission and reflection matrices (Eqs. (27) in Paper 2.3), it can be shown that if the reference medium is uniform then any calculated reflection and transmission matrices are independent of the reference medium's refractive index. A numerical experiment for a triangular lattice PC shows that every element in the calculated reflection matrix between it and vacuum is also essentially independent of whether the reference medium's refractive index is 1 or 3: each element of the reflection matrix differs from its equivalent by less than 1×10^{-15}, comparable to machine precision. Since the calculated quantities are not affected, I can see no reason to prefer any uniform dielectric over vacuum as the reference PC.

We now investigate whether using a PC as the reference can improve accuracy beyond that obtained with vacuum as a reference. While any PC

may be chosen as the reference, the most obvious candidates are the PCs involved in the simulations. I see no convincing mathematical reason to select one of these PCs over any other PC, other than that no additional simulation is required to calculate $\mathbf{E}_0$ and $\mathbf{H}_0$ since the PC is already going to be simulated, and that perhaps some of the mathematics might simplify because the impedance matrix $\mathcal{Z}_0$ of the reference PC is by definition $\mathcal{Z}_0 = \mathbf{I}$. So, in the absence of any other obvious candidate PCs, in this Appendix we compare the use of vacuum as a reference material to the use of one of the PCs already involved in the problem.

For our first example, we consider the reflectance at a vacuum-PC interface. The photonic crystal has a triangular lattice with lattice constant a of vacuum holes with radius $0.35\ a$ in a background with refractive index $n = 3$. Light is normally incident polarised with E out of plane, in the PC's second band, at frequencies $a/\lambda \in [0.26, 0.39]$. We calculate $\mathbf{E}_{\text{vacuum}}$ and $\mathbf{H}_{\text{vacuum}}$ analytically and $\mathbf{E}_{\text{PC}}$ and $\mathbf{H}_{\text{PC}}$ with the multipole method for each frequency, considering 9 plane wave orders and 9 Bloch modes. We use the resulting 9×9 impedance matrices (with vacuum as the reference medium) to calculate the reflectances at the interface; we take these reflectances to be our standard against which we measure the others. Then, truncating the set of Bloch modes to 1, 3, 5 and 7 modes, we calculate vacuum's and the PC's impedance matrices first using vacuum as a reference medium, then using the PC. From these impedance matrices we calculate the interface's reflectance, and we compare these to those found directly from the 9×9 matrices.

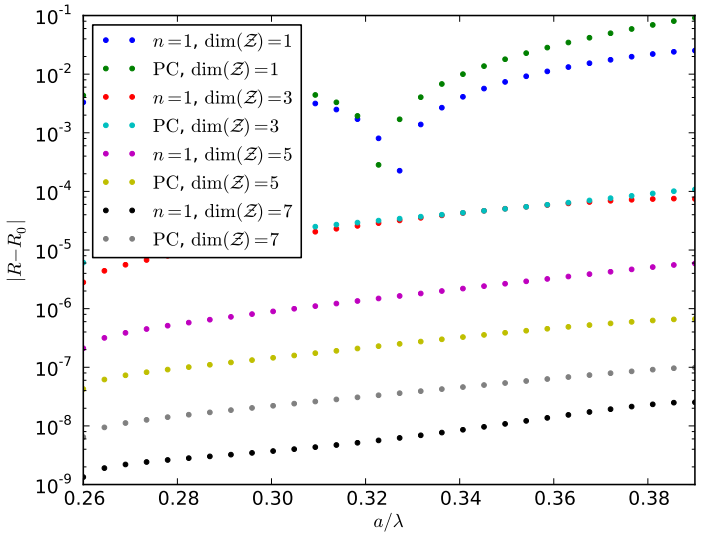

Figure B.1: Absolute difference between reflectances R_0 calculated by an accurate calculation with $\dim(\mathcal{Z}) = 9$, and reflectances R calculated with vacuum or a PC as the reference medium and smaller $\dim(\mathcal{Z})$. All reflectances are calculated for an air-PC interface at various frequencies a/λ.

In Fig. B.1 we plot the absolute value of the difference between each of the truncated reflectances and the standard value. The most apparent feature is that impedance matrices of larger dimension (which thus contain information about more modes) give more accurate results, exactly as expected. In this example, for 1×1 impedance matrices, the PC is a slightly better reference medium in most cases—but the results are inaccurate for both references at frequencies above the Wood anomaly at $d/\lambda = 1/3$. For

$\dim(\mathcal{Z}) = 3$, air is slightly better for the examined frequencies $a/\lambda < 0.35$, and the PC is slightly better at higher frequencies. For $\dim(\mathcal{Z}) = 5$ impedance matrices, the PC is a better reference material at all simulated frequencies. For $\dim(\mathcal{Z}) = 7$, air is a better reference material at all simulated frequencies. For 9×9 impedance matrices, the $\mathbf{E}$ and $\mathbf{H}$ matrices are not truncated and identical results are obtained regardless of the reference medium. These results do not consistently indicate that either vacuum or PC is better as a reference material.

If we denote vacuum by 1, and PC by 2, then when vacuum is the reference medium, the impedance matrix of vacuum $\mathcal{Z}_1^{\text{ref}=1} = \mathbf{I}$ and the impedance matrix of the PC is $\mathcal{Z}_2^{\text{ref}=1} = \mathbf{A}_{12}$, where $\mathbf{A}_{12}$ is defined in Eq. (28a) of Paper 2.3. If the PC is taken to be the reference material, then instead $\mathcal{Z}_2^{\text{ref}=2} = \mathbf{I}$, and $\mathcal{Z}_1^{\text{ref}=2} = \mathbf{A}_{21}$. By Eqs. (23) and (24) in Paper 2.3, at full rank $\mathbf{A}_{21}\mathbf{A}_{12} = \mathbf{A}_{22} = \mathbf{I}$, so $\mathbf{A}_{21} = \mathcal{Z}_1^{\text{ref}=2}$ and $\mathbf{A}_{12} = \mathcal{Z}_2^{\text{ref}=1}$ are inverses of each other. Inspecting Eqs. (27) in Paper 2.3, this means that the same $\mathbf{R}$ and $\mathbf{T}$ are calculated with $\mathcal{Z}_i = \mathbf{I}$ and $\mathcal{Z}_j = \mathcal{Z}_2^{\text{ref}=1}$, as with $\mathcal{Z}_i = \mathcal{Z}_1^{\text{ref}=2}$ and $\mathcal{Z}_j = \mathbf{I}$. Therefore at full rank the choice of reference medium is irrelevant, and Fig. B.1 is essentially a measure of how well the transitivity approximation Eq. (25a) in Paper 2.3 holds.

In the above example, both trialled reference media are present at the interface simulated. It might be thought that vacuum may be a less-effective reference for calculating reflectances at interfaces that do not involve vacuum. Therefore we now investigate a set of PC-PC interfaces, where the first PC is fixed and the second is varied, and calculate reflectances using either vacuum or the first PC as a reference medium. The input PC is a triangular lattice of $r = 0.3\,a$ air holes in an $n = 3$ background dielectric. The 30 target PCs differ from the input PC in that one of their lattice vectors is stretched in the direction of propagation y; the y components of their lattice vectors are $a_y \in (1, 1.6]\,\sqrt{3}/2$. We simulate these interfaces for normally incident light polarised with H out of plane, for light at the frequency $a/\lambda = 0.35$. Again, we vary the reference medium and the dimension of $\mathcal{Z}$, and compare the calculated reflectances with those calculated using 9 plane wave orders and 9 Bloch modes.

The absolute error in the calculated reflectances are shown in Fig. B.2. For $a_y \in [1.26, 1.34]\sqrt{3}/2$, the target PC has no propagating modes and so all light is reflected; thus all simulations are able to give accurate values for the reflectance. Again, there is a broad trend that the results become more accurate with larger $\dim(\mathcal{Z})$, although here $\dim(\mathcal{Z}) = 3$ and $\dim(\mathcal{Z}) = 5$ are of comparable accuracy. With $\dim(\mathcal{Z}) = 1$ and $\dim(\mathcal{Z}) = 3$, the PC reference gives slightly better results in most of the simulations, although the results for both simulations with $\dim(\mathcal{Z}) = 1$ are insufficiently accurate to be useful in most circumstances. For $\dim(\mathcal{Z}) = 5$ and $\dim(\mathcal{Z}) = 7$, there is no appreciable difference in accuracy between the two reference media. Again it can be concluded that for these bulk PCs, it does not matter much whether vacuum or the input PC is the reference medium.

For simplicity, the above discussion concerns only the reflectance, not the whole reflection matrix, which also includes phase information, or the transmission matrix. I have directly inspected a handful of reflection matrices involved in the above simulations, and their accuracy seems to broadly align with that of the reflectances.

The two examples presented here fall far short of the randomised statistical study (considering many PCs, types of light and reference materials) that would be required to definitively say whether there is a general advantage to be gained by using a PC (and which PC) as a reference medium instead of air. However, in these two cases there appears to be little or no

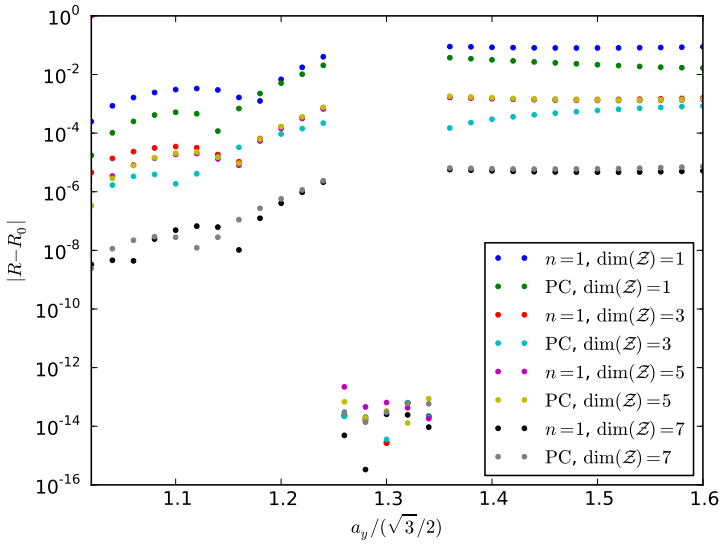

Figure B.2: Same as Fig. B.1, but for PC-PC interfaces at a single frequency. The x axis here gives a_y, the spacing between rows of holes in the second (target) photonic crystal.

consistent difference in accuracy due to the choice of reference medium. If a trend existed that were strong enough to lead to a useful rule of thumb, I would expect this trend to manifest itself in the above results, which it has not. Therefore, when studying bulk PCs such as those used in this thesis, I would not bother varying the reference medium in search of accuracy unless I noticed that results converged unacceptably slowly when increasing $\dim(\mathcal{Z})$.

Bibliography

1. F. J. Lawrence, L. C. Botten, K. B. Dossou and C. M. de Sterke. "Antireflection coatings for two-dimensional photonic crystals using a rigorous impedance definition". *Appl. Phys. Lett.* **93,** 121114 (2008).
2. F. J. Lawrence, L. C. Botten, K. B. Dossou, C. M. de Sterke and R. C McPhedran. "Impedance of square and triangular lattice photonic crystals". *Phys. Rev. A* **80,** 023826 (2009).
3. F. J. Lawrence, L. C. Botten, K. B. Dossou, R. C McPhedran and C. M. de Sterke. "Photonic-crystal surface modes found from impedances". *Phys. Rev. A* **82,** 053840 (2010).
4. F. J. Lawrence, K. B. Dossou, L. C. Botten, R. C McPhedran and C. M. de Sterke. "Bloch-mode based homogenisation of photonic crystals". *Optical Fibre Technology (ACOFT), 2010 35th Australian Conference on,* 1–3 (2010).
5. J. S. Brownless, S. Mahmoodian, K. B. Dossou, F. J. Lawrence, L. C. Botten and C. M. de Sterke. "Coupled waveguide modes in hexagonal photonic crystals". *Opt. Express* **18,** 25346–25360 (2010).
6. F. J. Lawrence, L. C. Botten, K. B. Dossou, R. C McPhedran and C. M. de Sterke. "A flexible Bloch mode method for computing complex band structures and impedances of two-dimensional photonic crystals". *J. Appl. Phys.* **111,** 013105 (2012).
7. P. Blown, C. Fisher, F. J. Lawrence, N. Gutman and C. M. de Sterke. "Semi-analytic method for slow light photonic crystal waveguide design". *Photon. Nanostruct.: Fundam. Appl.* **10,** 478–484 (2012).
8. J. S. Brownless, F. J. Lawrence, S. Mahmoodian, K. B. Dossou, L. C. Botten and C. M. de Sterke. "Supermodes of hexagonal lattice waveguide arrays". *J. Opt. Soc. Am. B* **29,** 1338–1346 (2012).
9. E. Yablonovitch. "Inhibited Spontaneous Emission in Solid-State Physics and Electronics". *Phys. Rev. Lett.* **58,** 2059–2062 (1987).
10. R. D. Meade, A Devenyi, J. D. Joannopoulos, O. Alerhand, D. Smith and K Kash. "Novel applications of photonic band gap materials: Low-loss bends and high Q cavities". *J. Appl. Phys.* **75,** 4753–4755 (1994).
11. A. Mekis, J Chen, I Kurland, S. Fan, P. R. Villeneuve and J. D. Joannopoulos. "High Transmission through Sharp Bends in Photonic Crystal Waveguides". *Phys. Rev. Lett.* **77,** 3787–3790 (1996).
12. S.-Y. Lin, E Chow, V Hietala, P. R. Villeneuve and J. D. Joannopoulos. "Experimental demonstration of guiding and bending of electromagnetic waves in a photonic crystal". *Science* **282,** 274 (1998).
13. A. Chutinan and S. Noda. "Waveguides and waveguide bends in two-dimensional photonic crystal slabs". *Phys. Rev. B* **62,** 4488–4492 (2000).

14. J. Yonekura, M. Ikeda and T. Baba. "Analysis of Finite 2-D Photonic Crystals of Columns and Lightwave Devices Using the Scattering Matrix Method". *J. Lightwave Technol.* **17,** 1500– (1999).

15. S. Fan, S. G. Johnson, J. D. Joannopoulos, C Manolatou and H. A. Haus. "Waveguide branches in photonic crystals". *J. Opt. Soc. Am. B* **18,** 162–165 (2001).

16. S. Boscolo, M. Midrio and T. F. Krauss. "Y junctions in photonic crystal channel waveguides: high transmission and impedance matching". *Opt. Lett* **27,** 1001–1003 (2002).

17. W. Bogaerts, R. Baets, P. Dumon, V. Wiaux, S. Beckx, D. Taillaert, B. Luyssaert, J. V. Campenhout, P. Bienstman and D. V. Thourhout. "Nanophotonic Waveguides in Silicon-on-Insulator Fabricated With CMOS Technology". *J. Lightwave Technol.* **23,** 401– (2005).

18. J. Joannopoulos, S. Johnson, R. Meade and J. Winn. *Photonic Crystals: Molding the Flow of Light.* 2nd (Princeton University Press, Princeton, 2008).

19. M. Notomi, K Yamada, A Shinya, J Takahashi, C Takahashi and I Yokohama. "Extremely Large Group-Velocity Dispersion of Line-Defect Waveguides in Photonic Crystal Slabs". *Phys. Rev. Lett.* **87,** 253902 (2001).

20. T. Baba. "Slow light in photonic crystals". *Nature Photonics* **2,** 465 (2008).

21. S. A. Schulz, L. O'Faolain, D. M. Beggs, T. P. White, A Melloni and T. F. Krauss. "Dispersion engineered slow light in photonic crystals: a comparison". *J. Opt.* **12,** 104004 (2010).

22. T. F. Krauss. "Planar photonic crystal waveguide devices for integrated optics". *phys. stat. sol. (a)* **197,** 688–702 (2003).

23. K. Busch, G von Freymann, S Linden, S. F. Mingaleev, L Tkeshelashvili and M Wegener. "Periodic nanostructures for photonics". *Physics Reports* **444,** 101 (2007).

24. H. Kosaka, T. Kawashima, A. Tomita, M. Notomi, T. Tamamura, T. Sato and S. Kawakami. "Superprism phenomena in photonic crystals". *Phys. Rev. B* **58,** R10096–R10099 (1998).

25. H. Kosaka, T. Kawashima, A Tomita, M. Notomi, T Tamamura, T. Sato and S. Kawakami. "Superprism phenomena in photonic crystals: Toward microscale lightwave circuits". *J. Lightwave Technol.* **17,** 2032 (1999).

26. S.-Y. Lin, V. M. Hietala, L. Wang and E. D. Jones. "Highly dispersive photonic band-gap prism". *Opt. Lett* **21,** 1771–1773 (1996).

27. H. Kosaka, T. Kawashima, A. Tomita, M. Notomi, T. Tamamura, T. Sato and S. Kawakami. "Photonic crystals for micro lightwave circuits using wavelength-dependent angular beam steering". *Appl. Phys. Lett.* **74,** 1370 (1999).

28. L. Wu, M Mazilu, T Karle and T. F. Krauss. "Superprism phenomena in planar photonic crystals". *IEEE Journal of Quantum Electronics* **38,** 915–918 (2002).

29. L. Wu, M Mazilu and T. F. Krauss. "Beam steering in planar-photonic crystals: from superprism to supercollimator". *J. Lightwave Technol.* **21,** 561 (2003).

30. T. Matsumoto, T Asatsuma and T. Baba. "Experimental demonstration of a wavelength demultiplexer based on negative-refractive photonic-crystal components". *Appl. Phys. Lett.* **91,** 091117 (2007).

31. S. Enoch, G Tayeb and D Maystre. "Numerical evidence of ultrarefractive optics in photonic crystals". *Opt. Commun.* **161,** 171–176 (1999).

32. M. Notomi. "Theory of light propagation in strongly modulated photonic crystals: Refractionlike behavior in the vicinity of the photonic band gap". *Phys. Rev. B* **62,** 10696–10705 (2000).

33. B. Gralak, S. Enoch and G. Tayeb. "Anomalous refractive properties of photonic crystals". *J. Opt. Soc. Am. A* **17,** 1012–1020 (2000).

34. H. Kosaka, T. Kawashima, A. Tomita, M. Notomi, T. Tamamura, T. Sato and S. Kawakami. "Self-collimating phenomena in photonic crystals". *Appl. Phys. Lett.* **74,** 1212 (1999).

35. J. Witzens, M. Lončar and A. Scherer. "Self-collimation in planar photonic crystals". *IEEE Journal of Selected Topics in Quantum Electronics* **8,** 1246–1257 (2002).

36. D. Chigrin, S. Enoch, C. S. Torres and G. Tayeb. "Self-guiding in two-dimensional photonic crystals". *Opt. Express* **11,** 1203–1211 (2003).

37. D. Tang, L. Chen and W. Ding. "Efficient beaming from photonic crystal waveguides via self-collimation effect". *Appl. Phys. Lett.* **89,** 131120–131120–3 (2006).

38. D. W. Prather, S. Shi, D. M. Pustai, C. Chen, S. Venkataraman, A. Sharkawy, G. J. Schneider and J. Murakowski. "Dispersion-based optical routing in photonic crystals". *Opt. Lett* **29,** 50–52 (2004).

39. D. W. Prather, S. Shi, J. Murakowski, G. J. Schneider, A. Sharkawy, C. Chen, B. L. Miao and R. Martin. "Self-collimation in photonic crystal structures: a new paradigm for applications and device development". *J. Phys. D: Appl. Phys.* **40,** 2635 (2007).

40. Z. H. Wu, K Xie, H Yang, P Jiang and X. J. He. "All-angle self-collimation in two-dimensional rhombic-lattice photonic crystals". *J. Opt.* **14,** 015002 (2012).

41. J. Li, T. P. White, L. O'Faolain, A. Gomez-Iglesias and T. F. Krauss. "Systematic design of flat band slow light in photonic crystal waveguides". *Opt. Express* **16,** 6227–32 (2008).

42. Y. Ruan, M.-K. Kim, Y.-H. Lee, B. Luther-Davies and A. Rode. "Fabrication of high-Q chalcogenide photonic crystal resonators by e-beam lithography". *Appl. Phys. Lett.* **90,** 071102–071102–3 (2007).

43. F. G. Omenetto and D. L. Kaplan. "A new route for silk". *Nature Photonics* **2,** 641 (2008).

44. B. Momeni and A. Adibi. "Adiabatic matching stage for coupling of light to extended Bloch modes of photonic crystals". *Appl. Phys. Lett.* **87,** 171104 (2005).

45. T. P. White, L. C. Botten, C. M. de Sterke, K. B. Dossou and R. C McPhedran. "Efficient slow-light coupling in a photonic crystal waveguide without transition region". *Opt. Lett* **33,** 2644–2646 (2008).

46. S. G. Johnson, P. Bienstman, M Skorobogatiy, M. Ibanescu, E. Lidorikis and J. D. Joannopoulos. "Adiabatic theorem and continuous coupled-mode theory for efficient taper transitions in photonic crystals". *Phys. Rev. E* **66,** 066608 (2002).

47. M Palamaru and P. Lalanne. "Photonic crystal waveguides: Out-of-plane losses and adiabatic modal conversion". *Appl. Phys. Lett.* **78,** 1466 (2001).

48. T. D. Happ, M. Kamp and A. Forchel. "Photonic crystal tapers for ultracompact mode conversion". *Opt. Lett* **26,** 1102–1104 (2001).

49. K. B. Dossou, L. C. Botten, C. M. de Sterke, R. C McPhedran, A. A. Asatryan, S Chen and J Brnovic. "Efficient couplers for photonic crystal waveguides". *Opt. Commun.* **265,** 207–219 (2006).

50. S. Kuchinsky, V. Golyatin and A. Kutikov. "Coupling in PBG material with high group index". *Proc. of SPIE* **5000,** 59–70 (2003).

51. A Talneau, P. Lalanne, M Agio and C. M. Soukoulis. "Low-reflection photonic-crystal taper for efficient coupling between guide sections of arbitrary widths". *Opt. Lett* **27,** 1522–1524 (2002).

52. A Talneau, M Mulot, S Anand and P. Lalanne. "Compound cavity measurement of transmission and reflection of a tapered single-line photonic-crystal waveguide". *Appl. Phys. Lett.* **82,** 2577–2579 (2003).

53. M Dinu, R. L. Willett, K Baldwin, L. N. Pfeiffer and K. W. West. "Waveguide tapers and waveguide bends in AlGaAs-based two-dimensional photonic crystals". *Appl. Phys. Lett.* **83,** 4471–4473 (2003).

54. P. Pottier, I. Ntakis and R. M. D. L. Rue. "Photonic crystal continuous taper for low-loss direct coupling into 2D photonic crystal channel waveguides and further device functionality". *Opt. Commun.* **223,** 339–347 (2003).

55. P. Sanchis, J Marti, J Blasco, A Martinez and A Garcia. "Mode matching technique for highly efficient coupling between dielectric waveguides and planar photonic crystal circuits". *Opt. Express* **10,** 1391–1397 (2002).

56. P. Sanchis, J Garcia, J Marti, W. Bogaerts, P Dumon, D Taillaert, R. Baets, V. Wiaux, J Wouters and S. Beckx. "Experimental demonstration of high coupling efficiency between wide ridge waveguides and single-mode photonic Crystal waveguides". *IEEE Photonics Technology Letters* **16,** 2272–2274 (2004).

57. A. Håkansson, P. Sanchis, J. Sánchez-Dehesa and J. Martí. "High-Efficiency Defect-Based Photonic-Crystal Tapers Designed by a Genetic Algorithm". *J. Lightwave Technol.* **23,** 3881– (2005).

58. P. Sanchis, J Marti, P. Bienstman and R. Baets. "Semianalytic approach for analyzing coupling issues in photonic crystal structures". *Appl. Phys. Lett.* **87,** 203107 (2005).

59. S.-G. Lee, J. sun Choi, J.-E. Kim, H. Y. Park and C.-S. Kee. "Reflection minimization at two-dimensional photonic crystal interfaces". *Opt. Express* **16,** 4270–4277 (2008).

60. T Kim, S.-G. Lee, M Kim and H. Y. Park. "Experimental demonstration of reflection minimization at two-dimensional photonic crystal interfaces via antireflection structures". *Appl. Phys. Lett.* **95,** 011119 (2009).

61. C. M. de Sterke, J Walker, K. B. Dossou and L. C. Botten. "Efficient slow light coupling into photonic crystals". *Opt. Express* **15,** 10984–10990 (2007).

62. M. Miri, A. Khavasi, K. Mehrany and B. Rashidian. "Transmission-line model to design matching stage for light coupling into two-dimensional photonic crystals". *Opt. Lett* **35,** 115–7 (2010).

63. J. P. Hugonin, P. Lalanne, T. P. White and T. F. Krauss. "Coupling into slow-mode photonic crystal waveguides". *Opt. Lett* **32,** 2638–2640 (2007).

64. G Lecamp, J. P. Hugonin and P. Lalanne. "Theoretical and computational concepts for periodic optical waveguides". *Opt. Express* **15,** 11042–11060 (2007).

65. Z. Li, E. Ozbay, H. Chen, J. Chen, F. Yang and H. Zheng. "Resonant cavity based compact efficient antireflection structures for photonic crystals". *J. Phys. D: Appl. Phys.* **40,** 5873 (2007).

66. T. Baba, T. Matsumoto and M. Echizen. "Finite difference time domain study of high efficiency photonic crystal superprisms". *Opt. Express* **12,** 4608–4613 (2004).

67. T. Baba and D. Ohsaki. "Interfaces of Photonic Crystals for High Efficiency Light Transmission". *Jpn. J. Appl. Phys.* **40,** 5920–5920 (2001).

68. F Ramos-Mendieta and P Halevi. "Surface electromagnetic waves in two-dimensional photonic crystals: Effect of the position of the surface plane". *Phys. Rev. B* **59,** 15112–15120 (1999).

69. J Ushida, M Tokushima, M Shirane, A Gomyo and H Yamada. "Immittance matching for multidimensional open-system photonic crystals". *Phys. Rev. B* **68,** 155115 (2003).

70. P. Sanchis, J Marti, B. Luyssaert, P. Dumon, P. Bienstman and R. Baets. "Analysis and design of efficient coupling in photonic crystal circuits". *Optical and Quantum Electronics* **37,** 133–147(15) (2005).

71. Y. A. Vlasov and S. J. McNab. "Coupling into the slow light mode in slab-type photonic crystal waveguides". *Opt. Lett* **31,** 50–52 (2006).

72. B. Momeni, A. A. Eftekhar and A. Adibi. "Effective impedance model for analysis of reflection at the interfaces of photonic crystals". *Opt. Lett* **32,** 778 (2007).

73. A. D. Falco, L. O'Faolain and T. F. Krauss. "Dispersion control and slow light in slotted photonic crystal waveguides". *Appl. Phys. Lett.* **92,** 083501–083501–3 (2008).

74. W. Śmigaj and B. Gralak. "Semianalytical design of antireflection gratings for photonic crystals". *Phys. Rev. B* **85,** 035114 (2012).

75. B Zhang and M. Li. "A new anti-reflection surface structure for photonic crystal slab lens". *Eur. Phys. J. D* **45,** 321 (2007).

76. W. Śmigaj, B. Gralak, R Pierre and G. Tayeb. "Antireflection gratings for a photonic-crystal flat lens". *Opt. Lett* (2009).

77. G. Scherrer, M. Hofman, W. Śmigaj, B. Gralak, X. Melique, O. Vanbésien, D. Lippens, C. Dumas, B. Cluzel and F. de Fornel. "Interface engineering for improved light transmittance through photonic crystal flat lenses". *Appl. Phys. Lett.* **97,** 071119 (2010).

78. J. Witzens, M. Hochberg, T. Baehr-Jones and A. Scherer. "Mode matching interface for efficient coupling of light into planar photonic crystals". *Phys. Rev. E* **69,** 046609 (2004).

79. O. Heavens. *Optical properties of thin solid films* (Dover Publications, Mineola, 1991).

80. E. Wolf and M. Born. *Principles of optics* 6th (Pergamon, New York, 1980).

81. P. Yeh. *Optical waves in layered media* (John Wiley & Sons, Inc, 1988).

82. P. Lorrain, D. R. Corson and F. Lorrain. *Electromagnetic fields and waves* (1988).

83. R. E. Collin. *Field Theory of Guided Waves* 2nd (IEEE, New York, 1991).

84. H. A. Macleod. *Thin Film Optical Filters* (2001).

85. V. G. Veselago. "Electrodynamics of materials with negative index of refraction". *Physics Uspekhi* **46,** 764 (2003).

86. V. G. Veselago. "Some remarks regarding electrodynamics of materials with negative refraction". *Appl. Phys. B* **81,** 403–407 (2005).

87. P. Rouard. "Étude des propriétés optiques des lames métalliques très minces". *Ann. d. Physique* **7,** 291 (1937).

88. E. Palik and G. Ghosh. *Handbook of optical constants of solids* 3rd ed. (Academic press, 1998).

89. L. A Catalán. "Some computed optical properties of antireflection coatings". *J. Opt. Soc. Am.* **52,** 437 (1962).

90. J. H. Apfel. "Graphics in Optical Coating Design". *Appl. Opt.* **11,** 1303–1312 (1972).

91. W. M. Robertson, G Arjavalingam, R. D. Meade, K. D. Brommer, A. M. Rappe and J. D. Joannopoulos. "Observation of surface photons on periodic dielectric arrays". *Opt. Lett* **18,** 528–30 (1993).

92. Y. A. Vlasov, N. Moll and S. J. McNab. "Observation of surface states in a truncated photonic crystal slab". *Opt. Lett* **29,** 2175–7 (2004).

93. B Wang, W Dai, A Fang, L Zhang, G Tuttle, T. Koschny and C. M. Soukoulis. "Surface waves in photonic crystal slabs". *Phys. Rev. B* **74,** 195104 (2006).

94. K. Ishizaki and S. Noda. "Manipulation of photons at the surface of three-dimensional photonic crystals". *Nature* **460,** 367–70 (2009).

95. J. M. Elson and P Tran. "Coupled-mode calculation with the R-matrix propagator for the dispersion of surface waves on a truncated photonic crystal". *Phys. Rev. B* **54,** 1711 (1996).

96. S. Enoch, E Popov and N Bonod. "Analysis of the physical origin of surface modes on finite-size photonic crystals". *Phys. Rev. B* **72,** 155101 (2005).

97. M. Che and Z.-Y. Li. "Analysis of surface modes in photonic crystals by a plane-wave transfer-matrix method". *J. Opt. Soc. Am. A* **25,** 2177 (2008).

98. D. Pozar. *Microwave Engineering* 3rd (John Wiley & Sons, Inc, 2005).

99. R Ulrich. "Far-infrared properties of metallic mesh and its complementary structure". *Infrared Physics* **7,** 37–55 (1967).

100. L. C. Botten, R. C McPhedran and J. M Lamarre. "Inductive grids in the resonant region: Theory and experiment". *Int J Infrared Milli Waves* **6,** 511–575 (1985).

101. J Brown. "Propagation in coupled transmission line systems". *Quart. Journ. Mech. and Applied Math.* **11,** 235–243 (1958).

102. L. Li. "Formulation and comparison of two recursive matrix algorithms for modeling layered diffraction gratings". *J. Opt. Soc. Am. A* **13,** 1024–1035 (1996).

103. L. C. Botten, N.-A. P. Nicorovici, R. C McPhedran, C. M. de Sterke and A. A. Asatryan. "Photonic band structure calculations using scattering matrices". *Phys. Rev. E* **64,** 046603 (2001).

104. D. M. Whittaker. "Inhibited emission in photonic woodpile lattices". *Opt. Lett* **25,** 779–781 (2000).

105. A Modinos, N Stefanou and V. Yannopapas. "Applications of the layer-KKR method to photonic crystals". *Opt. Express* **8,** 197–202 (2001).

106. B. Gralak, S. Enoch and G. Tayeb. "From scattering or impedance matrices to Bloch modes of photonic crystals". *J. Opt. Soc. Am. A* **19,** 1547 (2002).

107. R. Smaâli, D. Felbacq and G Granet. "Bloch waves and non-propagating modes in photonic crystals". *Physica E* **18,** 443–451 (2003).

108. L. C. Botten, T. P. White, A. A. Asatryan, T. N Langtry, C. M. de Sterke and R. C McPhedran. "Bloch mode scattering matrix methods for modeling extended photonic crystal structures. I. Theory". *Phys. Rev. E* **70,** 56606 (2004).

109. *Electromagnetic theory of gratings* (ed R. Petit) (Springer-Verlag Berlin, 1980).

110. K. B. Dossou, M. A. Byrne and L. C. Botten. "Finite element computation of grating scattering matrices and application to photonic crystal band calculations". *Journal of Computational Physics* **219,** 120 –143 (2006).

111. R. C McPhedran, N.-A. P. Nicorovici, L. C. Botten and K. A Grubits. "Lattice sums for gratings and arrays". *J. Math. Phys.* **41,** 7808 (2000).

112. R. W. Wood. *Philos. Mag.* **4,** 396 (1902).

113. L. Rayleigh. "On the dynamical theory of gratings". *Proceedings of the Royal Society of London. Series A* **79,** 399–416 (1907).

114. A Hessel and A. A. Oliner. "A New Theory of Wood's Anomalies on Optical Gratings". *Appl. Opt.* **4,** 1275–1297 (1965).

115. C. Kittel. *Introduction to Solid State Physics* 3rd ed. (John Wiley & Sons, Inc, 1966).

116. J. Callaway. *Quantum theory of the solid state* (Academic Press New York, 1974).

117. V Heine. "On the general theory of surface states and scattering of electrons in solids". *Proc. Phys. Soc.* **81,** 300 (1963).

118. V Heine. "Some theory about surface states". *Surface Science* **2,** 1 (1964).

119. N. W. Ashcroft and N. D. Mermin. *Solid State Physics* (Holt, Rinehart and Winston, New York, 1976).

120. Y.-C. Hsue and T.-J. Yang. "Applying a modified plane-wave expansion method to the calculations of transmittivity and reflectivity of a semi-infinite photonic crystal". *Phys. Rev. E* **70,** 016706 (2004).

121. Z.-Y. Li and K.-M. Ho. "Light propagation in semi-infinite photonic crystals and related waveguide structures". *Phys. Rev. B* **68,** 155101 (2003).

122. C. R. Simovski, S. A. Tretyakov and A. Schuchinsky. in. *Nanostructured Metamaterials* (ed A. F. de Baas) 96–122 (Publications Office of the European Union, Luxembourg, 2010). ISBN: 978-92-79-07563-6.

123. A. Fallahi and C. Hafner. "Analysis of semi-infinite periodic structures using a domain reduction technique". *J. Opt. Soc. Am. A* **27,** 40 (2010).

124. A. Andryieuski, R. Malureanu and A. V. Lavrinenko. "Wave propagation retrieval method for metamaterials: Unambiguous restoration of effective parameters". *Phys. Rev. B* **80,** 193101 (2009).

125. W. Śmigaj, P. Lalanne, J Yang, T. Paul, C. Rockstuhl and F. Lederer. "Closed-form expression for the scattering coefficients at an interface between two periodic media". *Appl. Phys. Lett.* **98,** 111107 (2011).

126. S. Ha, A. A. Sukhorukov, K. B. Dossou, L. C. Botten, C. M. de Sterke and Y. S. Kivshar. "Bloch-mode extraction from near-field data in periodic waveguides". *Opt. Lett* **34,** 3776 (2009).

127. A. A. Sukhorukov, S. Ha, I. V. Shadrivov, D. A. Powell and Y. S. Kivshar. "Dispersion extraction with near-field measurements in periodic waveguides". *Opt. Express* **17,** 3716 (2009).

128. S. Ha, M. Spasenović, A. A. Sukhorukov, T. P. White, C. M. de Sterke, L. K. Kuipers, T. F. Krauss and Y. S. Kivshar. "Slow-light and evanescent modes at interfaces in photonic crystal waveguides: optimal extraction from experimental near-field measurements". *J. Opt. Soc. Am. B* **28,** 955 (2011).

129. S. Fan, I. Appelbaum and J. D. Joannopoulos. "Near-field scanning optical microscopy as a simultaneous probe of fields and band structure of photonic crystals: A computational study". *Appl. Phys. Lett.* **75,** 3461–3463 (1999).

130. S. Boscolo, C. Conti, M. Midrio and C. G. Someda. "Numerical Analysis of Propagation and Impedance Matching in 2-D Photonic Crystal Waveguides With Finite Length". *J. Lightwave Technol.* **20,** 304 (2002).

131. Z. Lu and D. W. Prather. "Calculation of effective permittivity, permeability, and surface impedance of negative-refraction photonic crystals". *Opt. Express* **15,** 8340–8345 (2007).

132. W. Śmigaj and B. Gralak. "Validity of the effective-medium approximation of photonic crystals". *Phys. Rev. B* (2008).

133. R Biswas, Z.-Y. Li and K.-M. Ho. "Impedance of photonic crystals and photonic crystal waveguides". *Appl. Phys. Lett.* **84,** 1254 (2004).

134. K. Sakoda. *Optical Properties of Photonic Crystals* (Springer-Verlag, Berlin, 2001).

135. B. Momeni, M. Badieirostami and A. Adibi. "Accurate and efficient techniques for the analysis of reflection at the interfaces of three-dimensional photonic crystals". *J. Opt. Soc. Am. B* **24,** 2957 (2007).

136. C. Caloz and T. Itoh. *Electromagnetic metamaterials: transmission line theory and microwave applications: the engineering approach* (Wiley-IEEE Press, 2006).

137. N. Faché, F. Olyslager and D. De Zutter. *Electromagnetic and circuit modelling of multiconductor transmission lines* (Clarendon Press, 1993).

138. C. R. Simovski and S. A. Tretyakov. "Local constitutive parameters of metamaterials from an effective-medium perspective". *Phys. Rev. B* **75,** 195111 (2007).

139. C. R. Simovski. "Bloch material parameters of magneto-dielectric metamaterials and the concept of Bloch lattices". *Metamaterials* **1,** 62 (2007).

140. T. Paul, C. Menzel, W. Śmigaj, C. Rockstuhl, P. Lalanne and F. Lederer. "Reflection and transmission of light at periodic layered metamaterial films". *Phys. Rev. B* **84,** 115142 (2011).

141. C. Croënne, N. Fabre, D. Gaillot, O. Vanbésien and D. Lippens. "Bloch impedance in negative index photonic crystals". *Phys. Rev. B* **77,** 125333 (2008).

142. C Tserkezis and N Stefanou. "Retrieving local effective constitutive parameters for anisotropic photonic crystals". *Phys. Rev. B* **81,** 115112 (2010).

143. D. R. Smith, S Schultz, P Markoš and C. M. Soukoulis. "Determination of effective permittivity and permeability of metamaterials from reflection and transmission coefficients". *Phys. Rev. B* **65,** 195104 (2002).

144. M Mazilu and K Dholakia. "Optical impedance of metallic nanostructures". *Opt. Express* **14,** 7709 (2006).

145. C Tserkezis. "Effective parameters for periodic photonic structures of resonant elements". *J. Phys.: Condens. Matter* **21,** 155404 (2009).

146. C. R. Simovski. "On electromagnetic characterization and homogenization of nanostructured metamaterials". *J. Opt.* **13,** 013001 (2011).

147. K. Sakoda. "Symmetry, degeneracy, and uncoupled modes in two-dimensional photonic lattices". *Phys. Rev. B* **52,** 7982 (1995).

148. D. A. Hill. "Electromagnetic Wave Propagation along a Pair of Rectangular Bonded Wire Meshes". *Electromagnetic Compatibility, IEEE Transactions on* **EMC-21,** 114–122 (1979).

149. C. E. Baum. "Interaction of electromagnetic fields with an object which has an electromagnetic symmetry plane". *Interaction Note 63.* Air Force Weapons Laboratory (1971).

150. J Park, S.-G. Lee, H Park and M Lee. "Self-collimating photonic crystal antireflection structure for both TE and TM polarizations". *Opt. Express* **18,** 13083 (2010).

151. A. Andryieuski, S. Ha, A. A. Sukhorukov, Y. S. Kivshar and A. V. Lavrinenko. "Bloch-mode analysis for unambiguous retrieval of metamaterial effective parameters". *eprint arXiv* (2010).

152. S Foteinopoulou. "Photonic crystals as metamaterials". *Physica B* (2012).

153. J Yang, C Sauvan, T. Paul, C. Rockstuhl, F Lederer and P. Lalanne. "Retrieving the effective parameters of metamaterials from the single interface scattering problem". *Appl. Phys. Lett.* **97,** 061102 (2010).

154. Z. Ruan, M. Qiu, S. Xiao, S. He and L. Thylén. "Coupling between plane waves and Bloch waves in photonic crystals with negative refraction". *Phys. Rev. B* **71,** 045111 (2005).

155. E. H. Lock. "The properties of isofrequency dependences and the laws of geometrical optics". *Phys.-Usp.* **51,** 375 (2008).

156. D Schurig, J. J Mock, B. J Justice, S. A Cummer, J. B Pendry, A. F Starr and D. R Smith. "Metamaterial Electromagnetic Cloak at Microwave Frequencies". *Science* **314,** 977–980 (2006).

157. N Fang. "Sub-Diffraction-Limited Optical Imaging with a Silver Superlens". *Science* **308,** 534–537 (2005).

158. L. H. Gabrielli, J. Cardenas, C. B. Poitras and M. Lipson. "Silicon nanostructure cloak operating at optical frequencies". *Nature Photonics* **3,** 461 (2009).

159. J. Valentine, J. Li, T. Zentgraf, G. Bartal and X. Zhang. "An optical cloak made of dielectrics". *Nature Materials* **8,** 568 (2009).

160. D. H. Spadoti, L. H. Gabrielli, C. B. Poitras and M. Lipson. "Focusing light in a curved-space". *Opt. Express, OE* **18,** 3181–3186 (2010).

161. T Ergin, N Stenger, P Brenner, J. B Pendry and M Wegener. "Three-Dimensional Invisibility Cloak at Optical Wavelengths". *Science* **328,** 337–339 (2010).

162. Y. A. Urzhumov and D. R. Smith. "Transformation Optics with Photonic Band Gap Media". *Phys. Rev. Lett.* **105,** 163901 (2010).

163. Z. Liang and J. Li. "Scaling two-dimensional photonic crystals for transformation optics". *Opt. Express, OE* **19,** 16821–16829 (2011).

164. C. M. de Sterke, L. C. Botten, A. A. Asatryan, T. P. White and R. C McPhedran. "Modes of coupled photonic crystal waveguides". *Opt. Lett* **29,** 1384–6 (2004).

165. B. Momeni, M Askari, E. S. Hosseini, A Atabaki and A. Adibi. "An on-chip silicon grating spectrometer using a photonic crystal reflector". *J. Opt.* **12,** 035501 (2010).

166. B. Momeni, J. Huang, M. Soltani, M. Askari, S. Mohammadi, M. Rakhshandehroo and A. Adibi. "Compact wavelength demultiplexing using focusing negative index photonic crystal superprisms". *Opt. Express* **14,** 2413–2422 (2006).

167. A. Khorshidahmad and A. G. Kirk. "Composite superprism photonic crystal demultiplexer: analysis and design". *Opt. Express* **18,** 20518–20528 (2010).

168. A. Khorshidahmad and A. G. Kirk. "Reflective Heterostructure Photonic Crystal Superprism Demultiplexer". *IEEE Photonics Technology Letters* **24,** 303 (2012).

169. T. Baba and T. Matsumoto. "Resolution of photonic crystal superprism". *Appl. Phys. Lett.* **81,** 2325 (2002).

170. Z. J. Sun, K. A. McGreer and J. N. Broughton. "Demultiplexer with 120 Channels and 0.29-nm Channel Spacing". *IEEE Photonics Technology Letters* **10,** 90 (1998).

171. K. B. Dossou, L. C. Botten, A. A. Asatryan, B. P. C. Sturmberg, M. A. Byrne, C. G. Poulton, R. C. McPhedran and C. M. de Sterke. "Modal formulation for diffraction by absorbing photonic crystal slabs". *J. Opt. Soc. A.* Doc. ID: 156881 (2012). In press.

172. C. M. de Sterke, K. B. Dossou, T. P. White, L. C. Botten and R. C McPhedran. "Efficient coupling into slow light photonic crystal waveguide without transition region: role of evanescent modes". *Opt. Express* **17,** 17338 (2009).

173. T. P. White, L. C. Botten, C. M. de Sterke, R. C McPhedran, A. A. Asatryan and T. N Langtry. "Bloch mode scattering matrix methods for modeling extended photonic crystal structures. II. Applications". *Phys. Rev. E* **70,** 056607 (2004).

174. Z. Wang, Y. D. Chong, J. D. Joannopoulos and M. Soljacic. "Reflection-Free One-Way Edge Modes in a Gyromagnetic Photonic Crystal". *Phys. Rev. Lett.* **100,** 013905 (2008).